

NASA/CP-1999-209520



1995 NASA High-Speed Research Program Sonic Boom Workshop

Volume II—Configuration Design, Analysis, and Testing

*Edited by
Daniel G. Baize
Langley Research Center, Hampton, Virginia*



December 1999

The NASA STI Program Office . . . in Profile

Since its founding, NASA has been dedicated to the advancement of aeronautics and space science. The NASA Scientific and Technical Information (STI) Program Office plays a key part in helping NASA maintain this important role.

The NASA STI Program Office is operated by Langley Research Center, the lead center for NASA's scientific and technical information. The NASA STI Program Office provides access to the NASA STI Database, the largest collection of aeronautical and space science STI in the world. The Program Office is also NASA's institutional mechanism for disseminating the results of its research and development activities. These results are published by NASA in the NASA STI Report Series, which includes the following report types:

- **TECHNICAL PUBLICATION.** Reports of completed research or a major significant phase of research that present the results of NASA programs and include extensive data or theoretical analysis. Includes compilations of significant scientific and technical data and information deemed to be of continuing reference value. NASA counterpart of peer-reviewed formal professional papers, but having less stringent limitations on manuscript length and extent of graphic presentations.
- **TECHNICAL MEMORANDUM.** Scientific and technical findings that are preliminary or of specialized interest, e.g., quick release reports, working papers, and bibliographies that contain minimal annotation. Does not contain extensive analysis.
- **CONTRACTOR REPORT.** Scientific and technical findings by NASA-sponsored contractors and grantees.

- **CONFERENCE PUBLICATION.** Collected papers from scientific and technical conferences, symposia, seminars, or other meetings sponsored or co-sponsored by NASA.
- **SPECIAL PUBLICATION.** Scientific, technical, or historical information from NASA programs, projects, and missions, often concerned with subjects having substantial public interest.
- **TECHNICAL TRANSLATION.** English-language translations of foreign scientific and technical material pertinent to NASA's mission.

Specialized services that complement the STI Program Office's diverse offerings include creating custom thesauri, building customized databases, organizing and publishing research results . . . even providing videos.

For more information about the NASA STI Program Office, see the following:

- Access the NASA STI Program Home Page at <http://www.sti.nasa.gov>
- Email your question via the Internet to help@sti.nasa.gov
- Fax your question to the NASA STI Help Desk at (301) 621-0134
- Telephone the NASA STI Help Desk at (301) 621-0390
- Write to:
NASA STI Help Desk
NASA Center for Aerospace Information
7121 Standard Drive
Hanover, MD 21076-1320

NASA/CP-1999-209520



1995 NASA High-Speed Research Program Sonic Boom Workshop

Volume II—Configuration Design, Analysis, and Testing

Edited by
Daniel G. Baize
Langley Research Center, Hampton, Virginia

Proceedings of a workshop held at
Langley Research Center,
Hampton, Virginia
September 12–13, 1995

National Aeronautics and
Space Administration

Langley Research Center
Hampton, Virginia 23681-2199

December 1999

Available from:

NASA Center for AeroSpace Information (CASI)
7121 Standard Drive
Hanover, MD 21076-1320
(301) 621-0390

National Technical Information Service (NTIS)
5285 Port Royal Road
Springfield, VA 22161-2171
(703) 605-6000

PREFACE

The High-Speed Research Program and NASA Langley Research Center sponsored the NASA High-Speed Research Program Sonic Boom Workshop on September 11-13, 1995. The workshop was designed to bring together NASA's scientists and engineers and their counterparts in industry, other Government agencies, and academia working in the sonic boom element of NASA's High-Speed Research Program. Specific objectives of this workshop were to: (1) report the progress and status of research in sonic boom propagation, acceptability, and design; (2) promote and disseminate this technology within the appropriate technical communities; (3) help promote synergy among the scientists working in the Program; and (4) identify technology pacing the development of viable reduced-boom High-Speed Civil Transport concepts.

The Workshop was organized in four sessions as follows:

Session I	Sonic Boom Propagation (Theoretical)
Session II	Sonic Boom Propagation (Experimental)
Session III	Acceptability Studies - Human and Animal
Session IV	Configuration Design, Analysis and Testing

Sessions I to III are published in NASA Conference Publication 3335, July 1996.

Session IV is published in this publication.

Conference Chairman Daniel G. Baize, NASA Langley Research Center

**NASA HIGH SPEED RESEARCH PROGRAM
1995 SONIC BOOM WORKSHOP**

ATTENDEES

**SESSION 4 - CONFIGURATION DESIGN,
ANALYSIS, AND TESTING**

Daniel G. Baize
NASA Langley Research Center
Mail Stop 248
Hampton, VA 23681-0001

Robert L. Calloway
NASA Langley Research Center
Mail Stop 119
Hampton, VA 23681-0001

Aditi Chattopadhyay
Mechanical & Aerospace Engineering Dept.
Arizona State University
Tempe, AZ 85287-6106

Samson H. Cheung
McDonnell Douglas
Mail Code 71-35
Box 22608
Long Beach, CA 90801-5608

Christine M. Darden
NASA Langley Research Center
Mail Stop 119
Hampton, VA 23681-0001

Kamran Fouladi
Lockheed Engineering and Sciences Co.
Mail Stop 248
NASA Langley Research Center
Hampton, VA 23681-0001

William P. Gilbert
NASA Langley Research Center
Mail Stop 119
Hampton, VA 23681-0001

George T. Haglund
Boeing Commercial Airplane Group
P. O. Box 3707
Seattle, WA 98124-2207

Robert J. Mack
NASA Langley Research Center
Mail Stop 248
Hampton, VA 23681-0001

John M. Morgenstern
McDonnell Douglas Aerospace
2401 E. Wardlow Road
Long Beach, CA 90807-4418

Johnny R. Narayan
Aerospace Research Center
Arizona State University
Tempe, AZ 85287-8006

Michael J. Siclari
Northrop Grumman
Mail Stop K01-14
Bethpage, NY 11714

Eugene L. Tu
NASA Ames Research Center
MS 258-1
Moffett Field, CA 94035

SESSION IV

CONFIGURATION DESIGN, ANALYSIS, AND TESTING

CONTENTS

PREFACE.....	iii
ATTENDEES.....	v

SESSION IV

1. A WHITHAM-THEORY SONIC-BOOM ANALYSIS OF THE TU-144 AIRCRAFT AT A MACH NUMBER OF 2.2.....	1
Robert J. Mack	
2. DEVELOPMENT OF A MULTIOBJECTIVE OPTIMIZATION PROCEDURE FOR SONIC BOOM MINIMIZATION.....	18
J. R. Narayan, A. Chattopadhyay, and N. Papalapati	
3. LANGLEY'S COMPUTATIONAL EFFORTS IN SONIC-BOOM SOFTENING OF THE BOEING HSCT.....	47
Kamran Fouladi	
4. SONIC BOOM MINIMIZATION EFFORTS ON BOEING HSCT BASELINE.....	73
Samson Cheung, Kamran Fouladi, George Haglund, and Eugene Tu	
5. POTENTIAL FOR SONIC BOOM REDUCTION OF THE BOEING HSCT.....	96
George T. Haglund	
6. BOOM SOFTENING AND NACELLE INTEGRATION ON AN ARROW-WING HIGH-SPEED CIVIL TRANSPORT CONCEPT.....	121
Robert J. Mack	
7. SONIC BOOM PREDICTION AND MINIMIZATION OF THE DOUGLAS REFERENCE OPT5 CONFIGURATION.....	138
Michael J. Siclari	
8. POTENTIAL FOR SONIC BOOM REDUCTION OF THE 2.4-H5085 ARROW WING HSCT.....	162
John M. Morgenstern	



A WHITHAM-THEORY SONIC-BOOM ANALYSIS OF THE TU-144

AIRCRAFT AT A MACH NUMBER OF 2.2

Robert J. Mack

NASA Langley Research Center

Hampton, Virginia

SUMMARY

NASA became interested in the Tu-144 aircraft when it was offered for use as a "flying testbed" to study operating characteristics of a supersonic-cruise commercial airplane. In addition to the other operational tests being conducted on the Tu-144 aircraft, it was proposed that two sets of sonic-boom pressure signature measurements be made. One set of tests would consist of ground-level pressure measurements. The second set would be measurements of pressures under the Tu-144 aircraft in cruise. Pressure gages would be required for this second set of tests: measuring ambient and differential pressures in the flow field of a Tu-144 cruising at supersonic speeds. The range of these gages had to be determined well in advance of the scheduled flights so that they could be installed and calibrated.

To satisfy these requirements, Whitham theory was used to obtain predictions of the Tu-144 sonic-boom characteristics. At a separation distance of 500 feet below the aircraft, the nose-shock overpressure was estimated to be about 8.8 psf. For pressure gage selection purposes, a safety factor of 10-percent, increasing the nose-shock strength to 9.7 psf, was considered prudent because the separation distance was only about 5.3 span lengths and the nose shock was fairly strong. This nose-shock strength dropped to about 5.4 psf at a separation distance of 1000 feet, almost 10.6 span lengths, below the aircraft. The ground-level pressure signature was also predicted in this study. It was estimated that an N-wave pressure signature would be generated with a nose shock strength of about 2.0 psf when the Tu-144 aircraft cruised at a Mach number of 2.2, an altitude of 61,000 feet, and a weight of 350,000 pounds.

It was found, from an examination of the aircraft's F-function, that the predicted pressure signatures at distances 500 and 1000 feet below the cruising aircraft as well as on the ground were strongly influenced by the size and location of the engine nacelle inlets. These components generated volume and interference-lift disturbances that rivaled the magnitude of the disturbances from the aircraft's nose, fuselage-wing junction, and wing leading-edge crank at a cruise Mach number of 2.2 and a cruise weight of 350,000 pounds. This observation explained why the predicted signatures were almost N-wave in shape at 500 and 1000 feet separation distances, and completely N-wave in shape on the ground.

After this analysis was under way, the in-flight sonic-boom pressure measurement segment of the Tu-144 tests was cancelled. However, these Whitham-theory pressure-signature predictions could be useful as comparisons with pressure-signature predictions obtained from *Computational Fluid Dynamics (CFD)* or other methods.

INTRODUCTION

Officially, the Tu-144 was the first supersonic-cruise, passenger-carrying aircraft to enter commercial service. Design, construction, and testing were carried out by the Soviet Union, flight certification was by the Soviet Union, and the only regular passenger flights were scheduled and flown across the territory of the Soviet Union. Although it was not introduced to international passenger service, there were many significant engineering accomplishments achieved in the design, production, and flight of this aircraft.

Development of the aircraft began with a prototype stage. Systematic testing and redesign led to a production aircraft in discrete stages that measurably improved the performance of the aircraft from the starting concept to final aircraft certification. It flew in competition with the English-French Concorde for a short time, but was withdrawn from national commercial service due to a lack of interest by airlines outside the Soviet Union.

NASA became interested in the Tu-144 aircraft when it was offered for use as a flying "testbed" in the study of operating characteristics of a supersonic-cruise commercial airplane. Since it had been in supersonic-cruise service, the Tu-144 had operational characteristics similar to those anticipated in the conceptual aircraft designs being studied by the United States aircraft companies.

In addition to the other operational tests being conducted on the Tu-144 aircraft, it was proposed that two sets of sonic-boom pressure signature measurements be made. The first set would be made on the ground, using techniques and devices similar to those in reference 1 and many other subsequent studies. A second set would be made in the air with an instrumented aircraft flying close under the Tu-144 in supersonic flight. Such in-flight measurements would require pressure gages that were capable of accurately recording the flow-field overpressures generated by the Tu-144 at relatively close distances under the vehicle. Therefore, an analysis of the Tu-144 was made to obtain predictions of pressure signature shape and shock strengths at cruise conditions so that the range and characteristics of the required pressure gages could be determined well in advance of the tests.

Cancellation of the sonic-boom signature measurement part of the tests removed the need for these pressure gages. Since *CFD* methods would be used to analyze the aerodynamic performance of the Tu-144 and make similar pressure signature predictions, the relatively quick and simple Whitham-theory pressure signature predictions presented in this paper could be used for comparisons.

Pressure signature predictions of sonic-boom disturbances from the Tu-144 aircraft were obtained from geometry derived from a three-view description of the production aircraft, reference 2. The geometry was used to calculate aerodynamic performance characteristics at supersonic-cruise conditions. These characteristics and Whitham/Walkden sonic-boom theory, references 3 and 4, were employed to obtain F-functions and flow-field pressure signature predictions at a Mach number of 2.2, at a cruise altitude of 61,000 feet, and at a cruise weight of

350,000 pounds. Near-field pressure signatures at separation distances of 500 and 1000 feet (5.3 and 10.6 span lengths) below the aircraft at supersonic-cruise conditions were also predicted. These pressure signatures would have provided data for the estimation of pressure gage sizes.

SYMBOLS

A_E	equivalent area, ft ²
C_L	lift coefficient
$C_{L,I}$	nacelle-wing interference-lift coefficient
$C_{L,W}$	wing-alone lift coefficient
$F(y)$	Whitham F-function with parameter y , ft ^{1/2}
h	altitude, ft
l	effective length of the aircraft, ft
M	Mach number
Δp	overpressure due to aircraft pressure disturbances, psf
t	time duration of the pressure signature measured relative to the arrival of a Mach wave from the nose, sec
W	aircraft weight, lb
x_e	effective distance in the longitudinal direction, ft
y	Whitham F-function effective-length parameter, ft
α	aircraft angle of attack at cruise, deg

MODEL DESCRIPTION

A three view of the production Tu-144 aircraft, reference 2, is shown in figure 1. It differed from the prototype aircraft in that it had retractable canard control surfaces, noticeable wing anhedral, separated two-engine nacelle pods, and landing gear main struts that retracted into the engine nacelles. Like the British-French Concorde, the nose sections could be drooped during takeoff and landing to provide improved visibility for the pilot and co-pilot. The English-French

Concorde relied entirely on trailing-edge surfaces for takeoff and landing control, while the Tu-144 had canards with leading- and trailing-edge flaps for improved takeoff and landing performance on relatively low-technology runways.

In figure 2, a numerical description of the Tu-144 aircraft is provided using the format of reference 5. Several simplifications were made to the description of the wing, fuselage, and the nacelles to fit the input format of the analysis codes as well as to reduce component definition time. These simplifications are discussed in the following paragraphs.

Wing. The wing description was obtained from the three view and a communication from the Rockwell Corporation, which had made initial contacts with engineers from the Tupelov Design Bureau. It had twist and very modest camber, including some inboard trailing-edge reflexing, that was simplified to just spanwise twist in the wave-drag model. The aircraft's inboard airfoils had slightly-blunted leading edges and parabolic-arc airfoils on the outboard wing panels. On the wave-drag model, the airfoils were defined with a 2.5 percent thickness along with a sharp, parabolic-arc airfoil shape from root to tip. A small, constant (leading-edge radius)/chord ratio was included in the wing-analysis description so that leading-edge thrust effects accruing from modest leading-edge bluntness could be assessed.

Vertical Tail. The airfoil thickness ratio put on the panels of the wing, 2.5 percent, was used also on the vertical tail. However, the airfoil on the vertical tail had a slab center section with a parabolic-arc leading- and trailing-edge. No leading-edge blunting was included in the wave-drag code description of the vertical tail.

Fuselage. The fuselage was described by circular cross sections from nose to tail. Nose-down (not the nose droop used during takeoff and landing) and tail-up camber was included in the fuselage description. This improved the numerical model's fidelity, the predicted wave-drag accuracy, and the area-ruling required for sonic-boom analysis. To keep the body description as simple as possible, a straight line through the cabin and center section was used as part of the fuselage camber description. A careful check of the Tu-144 aircraft side view, figure 1, showed that this simplified fuselage camber curve was a reasonably good representation.

Nacelles. Although the engine nacelles on the Tu-144 aircraft have two-dimensional inlets and rectangular cross sections along most of their length, the wave-drag code description and the nacelle-wing interference-lift analysis code inputs need axisymmetric nacelles because of code limitations. Cylindrical engine exhausts were extended aft from the nacelles nozzles (to provide tail-shock prediction data) because precise engine operating conditions and engine-exhaust plume shapes during supersonic cruise were not known.

In figure 3, a "wire-frame" three-view representation of the Tu-144 wave-drag model, obtained from the numerical description in figure 2, is shown for comparison with the aircraft's three-view picture presented in figure 1. The overall similarity between figures 1 and 3 is reasonably good considering the fidelity of the original three-view picture and the limitations in wave-drag code input format.

ANALYSIS

Wing analysis comparison. Preliminary wing performance data, calculated from the simplified numerical wing model with the method of reference 6, agreed well with the preliminary wing-performance data supplied by Rockwell. These similarities in wing performance data and the fairly close physical similarity between the numerical model and the Tu-144 aircraft in the three-view picture suggested that meaningful, but limited, sonic-boom pressure signature data could be obtained.

Methodology. The methods and techniques for predicting the sonic-boom characteristics of the Tu-144 are described in references 7 and 8. Equivalent areas, A_E , due to the aircraft volume contributions (excluding the nacelles) were obtained from the area-ruling output of the wave drag code, reference 9. This summation of select aircraft component volume equivalent areas is based on the first and second derivative continuity of the wing, fuselage, and fin areas.

Equivalent areas due to lift came from both the wing lift and the nacelle-wing interference lift codes. First, the method of reference 10 was used to estimate the nacelle-wing interference lift portion of the total lift. Then, the method of reference 6 was used to calculate equivalent areas from the wing lift coefficient, $C_{L,W}$ ($C_{L,W} = C_L - C_{L,I}$) and the wing planform area. Since both the equivalent area contributions from the aircraft volume (minus the engine nacelles) and the wing lift met first- and second-derivative continuity criteria, they were summed and used to compute the first half of the total Tu-144 aircraft Whitham F-function.

The engine nacelles are analyzed separately since their equivalent areas did not satisfy first- or second-derivative continuity at the inlet lips. The method of reference 10 was employed to: (1) calculate the magnitude of the interference lift coefficient, $C_{L,I}$; (2) supply the equivalent area distributions due to nacelle-wing interference lift; and (3) compute the nacelle volume F-function. An additional set of F-functions, calculated from the interference-lift equivalent areas, completed the second half of the aircraft's F-function requirements. A final summation of F-functions from: (1) aircraft volume minus nacelles; (2) engine nacelle volumes (inboard and outboard); (3) wing lift; and (4) nacelle-wing interference lifts (inboard and outboard) provided the combined F-function input to the ARAP code, reference 11, for the prediction of the sonic-boom pressure signatures.

DISCUSSION

As previously noted in the model description section, the wave-drag model of the Tu-144, figure 3, was a reasonably good representation of the actual Tu-144 aircraft, figure 1, so the area-ruled volume was assumed to be at least first-order accurate for wave-drag and sonic-boom calculations. Also, the theoretical performance data for the wing of the numerical model, obtained from reference 6 methodology, agreed fairly well with the preliminary estimated performance data supplied by Rockwell. However, during the analysis of nacelle-wing interference lift, it was noted that, at the cruise Mach number of 2.2, disturbances from the engine inlets would "spill over" the wing leading-edge and affect the upper-wing lifting pressures. The amount of inlet-shock spill-over was found to be small at Mach 2.2, so its effects on wing lift, drag, and pitching moment were ignored.

On the Tu-144 aircraft, a low-wing mounting is employed, but the fuselage forebody area and camber were not included in the wing camber-and-twist description to simplify the analysis. The resulting wing analysis data could have been corrected by calculating fuselage-wing interference effects and obtaining an additional F-function to be summed with the other F-function contributions. However, the wing was situated well aft of the nose where the fuselage becomes cylindrical. Since first-order effects only were being considered, this fuselage-wing interference contribution, like the nacelle-shock spill-over contribution, was also ignored. It should be noted that in an analysis of the aircraft at Mach numbers less than the design point of 2.2, these effects cannot be ignored and must be included.

In figure 4, the "Mach-sliced" equivalent areas from both the wing lift and the aircraft volume (without engine nacelles) are shown, and in figure 5, the sum of the wing lift and volume (without engine nacelles) equivalent areas are presented. The summed equivalent areas in figure 5, which met the previously-mentioned continuity criteria, were used to compute the F-function shown in figure 6.

The F-functions calculated from the nacelle volumes and the contributions of the nacelle-wing interference lift are presented in figure 7. Since the engine nacelle representations are side by side and start at about the same distance from the nose, their volume effects and interference-lift effects have been combined into two summed F-functions. Interference-lift effects were different from, and clearly larger in magnitude than, the nacelle-volume effect, though they are similar in shape and influence distance.

The Tu-144's F-function was computed from a summation of the F-functions from the aircraft volume (minus nacelles), nacelle volume, wing lift, and nacelle-wing interference-lift as shown in figure 8. A comparison of figures 6 to 8 readily shows how influential the nacelle volume and interference-lift disturbance effects are relative to the fuselage-wing-fin volume plus wing-lift disturbance contributions. The one exception is at station $x_e/l = 0.56$ on figure 6. There, the sum of the aircraft volume (excluding nacelles) equivalent areas and the wing-lift equivalent areas gives a distinct F-function "spike." This "spike" is caused by the pronounced change in local second derivatives in the "dog leg", at x_e of about 130 feet, on the summed equivalent area curve in figure 5.

Three predicted sonic-boom pressure signatures, calculated from the summed Tu-144 aircraft F-function, given in figure 8, are presented in figure 9. The N-wave ground-level pressure signature contains a reflection factor of 1.90, while the other two pressure signatures, at altitudes 500 and 1000 feet below the cruising aircraft, were disturbances superimposed on the ambient pressure (reflection factor of 1.0).

A predicted pressure signature nose-shock strength of 8.6 psf at a distance of 500 feet cannot be considered as more than first-order accurate because the separation distance below the aircraft is only about 5.3 span lengths (2.5 body lengths). It was included in the predictions to permit estimation of pressure-gage size and provide information on the rate of N-wave development. With the correction derived in reference 8, this predicted nose-shock strength was increased to 8.8 psf. A better estimate of this pressure signature nose-shock strength would be about 9.7 psf; a value with a 10-percent safety factor included. This larger value is more useful toward sizing pressure gage limits because of practical considerations stemming from cruise Mach number, the crudeness of the analytical model, and the lack of high aerodynamic finesse in the shape of the aircraft.

At a separation distance of 1000 feet below the aircraft, the predicted nose-shock strength is about 5.3 psf; with the reference 8 correction, it is 5.4 psf. This overpressure nose-shock strength

was predicted at a distance of about 10.6 span lengths which should make it more accurate than the shock strength prediction at 500 feet.

With the exception of the small shock in the expansion segment of the two free-stream signatures, the overall shape of the overpressure signatures was an N-wave. When the strengths of the nacelle inlet shocks and the reflected shocks, as indicated by the nacelle volume and the interference-lift F-functions are considered, the tendency for the rapid formation of an N-wave pressure signature from the Tu-144 aircraft was not surprising.

The predicted nose-shock strength of 2.0 psf on the ground-level signature again showed the result of the strong nacelle-pressure disturbances, the aircraft weight of 350,000 pounds, the cruise altitude of 61,000 feet, and the Mach 2.2 cruise speed. Since the arrangement of fuselage, wing, and engine nacelles tended to force the early formation of N-wave or almost N-wave pressure signatures, a somewhat heavier or lighter Tu-144 aircraft would still generate an N-wave pressure signature at the 5000 and 1000 foot separation distances as well as on the ground. Either overpressure level would not excessively high and would cause no difficulties for conventional overpressure measuring and recording devices.

CONCLUDING REMARKS

Whitham theory has been used to obtain a prediction of the Tu-144 aircraft's sonic boom characteristics for the purpose of estimating pressure gage range. The ground-level pressure signature was predicted to be an N-wave with a 2.0 psf nose-shock strength when the Tu-144 aircraft cruised at a Mach number of 2.2, an altitude of 61,000 feet, and a weight of 350,000 pounds. At a separation distance of 500 feet below the aircraft, the pressure-signature nose-shock strength was estimated to be about 8.8 psf. For pressure gage selection purposes, a 10-percent increase in shock strength (safety factor) to 9.7 psf could be considered a better estimate because the separation distance is only about 5.3 span lengths below the aircraft. The nose-shock strength dropped to about 5.4 psf at a separation distance of 1000 feet, almost 10.6 span lengths, below the aircraft.

It was found, from an examination of the aircraft's F-function, that the predicted pressure signatures at distances 500 and 1000 feet below the cruising aircraft and on the ground were strongly influenced by the size and location of the engine-nacelle inlets. These components generated volume and interference-lift disturbances that easily equalled the disturbances from the aircraft's nose, fuselage-wing junction, and wing leading-edge crank at a cruise Mach number of 2.2 and a cruise weight of 350,000 pounds. This explained why the predicted signature shapes were almost N-waves at the 500 and 1000 feet separation distances, and completely N-wave on the ground.

REFERENCES

1. Maglieri, Domenic J.; and Hubbard, Harvey H.: *Ground Measurements Of The Shock-Wave Noise From Supersonic Bomber Airplanes In The Altitude Range From 30,000 To 50,000 Feet*. NASA TN D-880, 1961.

2. Gunston, Bill: *Aircraft of the Soviet Union*. pp. 345-349, Osprey Publishing Limited, 1983.
3. Whitham, G. B.: *The Flow Pattern Of A Supersonic Projectile*. Communication on Pure and Applied Mathematics, vol. V, no. 3, August 1952, pp. 301 - 348.
4. Walkden, F.: *The Shock Pattern Of A Wing-Body Combination, Far From The Flight Path*. Aeronautical Quarterly, vol. IX, pt. 2, May 1958, pp. 164 - 194.
5. Craidon, Charlotte B.: *Description Of A Digital Computer Program For Airplane Configuration Plots*. NASA TM X-2074, 1970.
6. Carlson, Harry W.; and Mack, Robert J.: *Estimation Of Wing Nonlinear Aerodynamic Characteristics At Supersonic Speeds*. NASA TP-1718, 1980.
7. Mack, Robert J.; and Needleman, Kathy: *A Methodology For Designing Aircraft To Low Sonic Boom Constraints*. NASA TM-4246, 1991.
8. Mack, Robert J.: *Some Considerations On The Integration Of Engine Nacelles Into Low-Boom Aircraft Concepts*. High-Speed Research: Sonic Boom, Volume II, NASA Conference Publications 3173, 1992.
9. Harris, Roy V., Jr.: *A Numerical Technique For Analysis Of Wave Drag At Lifting Conditions*. NASA TN D-3586, 1966.
10. Mack, Robert J.: *A Numerical Method For Evaluation And Utilization Of Supersonic Nacelle-Wing Interference*. NASA TN D-5057, 1969.
11. Hayes, Wallace D.; Haefeli, Rudolph C.; and Kulsrud, H. E.: *Sonic Boom Propagation In A Stratified Atmosphere, With Computer Program*. NASA CR-1299, 1969.

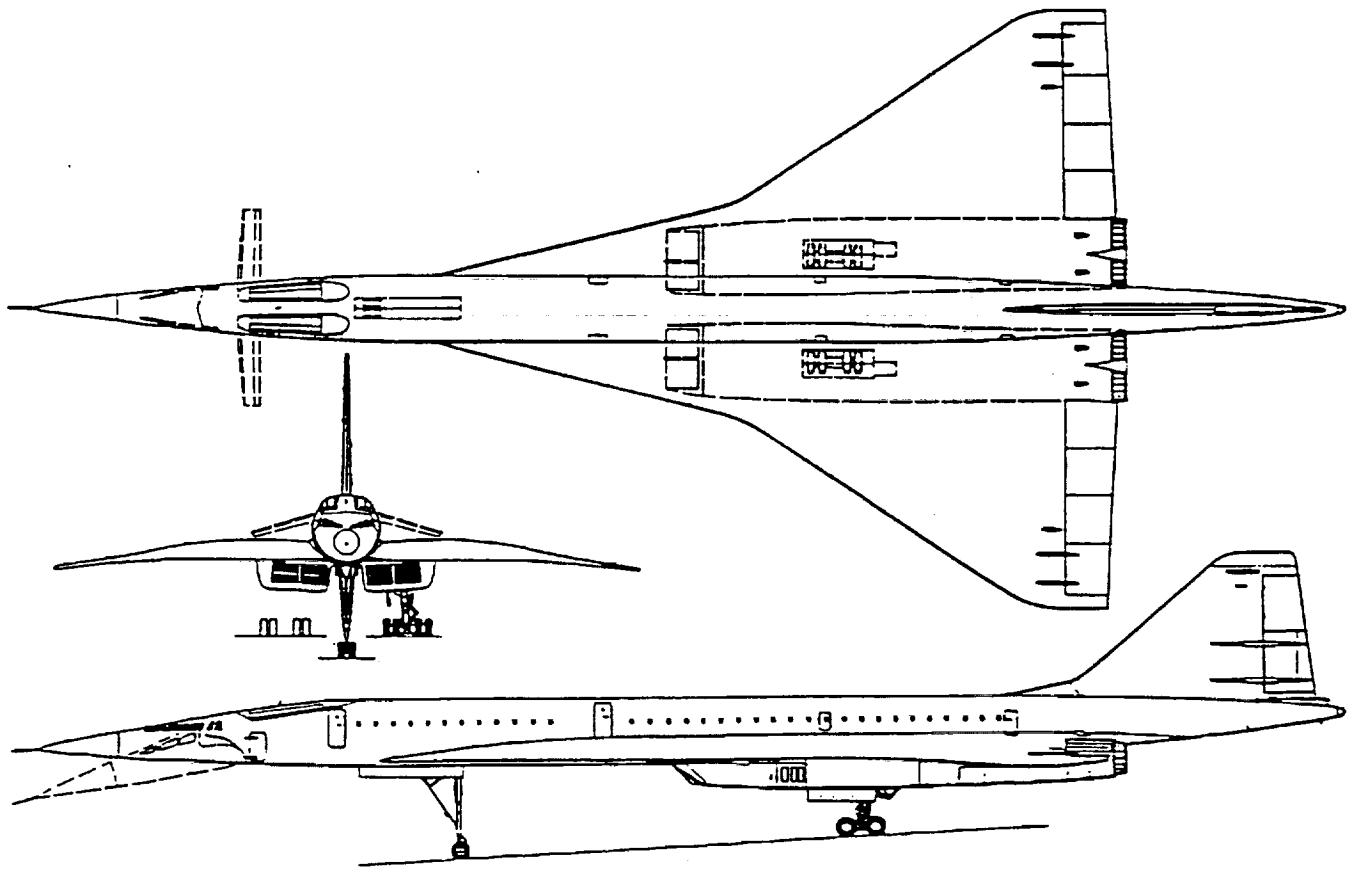


Figure 1. Three view of the Tu-144 supersonic-cruise aircraft.

TU-144 aircraft, wing with twist and dihedral, M = 2.2
 1 1 -1 1 1 0 0 6 17 2 19 30 19 17 2 10 3 10
 5457.17
 0.0 2.5 5.0 10.0 15.0 20.0 30.0 40.0 50.0 60.0
 70.0 80.0 85.0 90.0 95.0 97.5 100.0
 64.94 5.14 -1.257 107.20
 101.8 14.3 -1.715 70.34
 110.30 16.42 -1.821 61.73
 114.30 18.09 -1.95 57.65
 157.76 46.24 -4.88 12.74
 161.99 47.244 -5.000 8.46
 0.0 .442 .0884 .1769 .2653 .3538 .5306 .7075 .8844 1.0613
 1.2382 1.4150 1.5035 1.5919 1.6804 1.7246 1.7688
 0.0 .06893 .13787 .27573 .41360 .55147 .82720 1.1029 1.3787 1.6544
 1.9301 2.2059 2.3437 2.4816 2.6195 2.6884 2.7573
 0.0 .06852 .13704 .27408 .41112 .54816 .82224 1.0963 1.3704 1.6445
 1.9186 2.1926 2.3297 2.4667 2.6038 2.6723 2.7408
 0.0 .06918 .13836 .27672 .41508 .55344 .83016 1.1069 1.3836 1.6603
 1.9370 2.2138 2.3521 2.4905 2.6288 2.6980 2.7672
 0.0 .03140 .06281 .12562 .18842 .25123 .37685 .50247 .62808 .75370
 .87931 1.0049 1.0677 1.1305 1.1934 1.2248 1.2562
 0.0 .02115 .04230 .08460 .12690 .16920 .25380 .33840 .42300 .50760
 .59220 .67680 .71910 .76140 .80370 .82485 .84600
 0.0 .12188 .2375 .450 .6375 .800 1.050 1.20 1.25 1.20
 1.050 .800 .6375 .450 .2375 .12188 0.0
 0.0 .12188 .2375 .450 .6375 .800 1.050 1.20 1.25 1.20
 1.050 .800 .6375 .450 .2375 .12188 0.0
 0.0 .12188 .2375 .450 .6375 .800 1.05 1.20 1.25 1.20
 1.05 .800 .6375 .450 .2375 .12188 0.0
 0.0 .12188 .2375 .450 .6375 .800 1.05 1.20 1.25 1.20
 1.05 .800 .6375 .450 .2375 .12188 0.0
 0.0 .12188 .2375 .450 .6375 .800 1.05 1.20 1.25 1.20
 1.05 .800 .6375 .450 .2375 .12188 0.0
 0.0 .14625 .285 .540 .765 .960 1.26 1.44 1.50 1.44
 1.26 .960 .765 .540 .285 .14625 0.0
 0.0 2.5 5.0 7.5 10.0 15.0 20.0 25.0 30.0 35.0
 40.0 45.0 50.0 55.0 60.0 62.5 65.0 70.0 75.0 80.0
 85.0 90.0 95.0 100.0 105.0 110.0 115.0 120.0 125.0 130.0
 0.0 .1429 .2857 .4286 .5714 .8571 1.1429 1.4286 1.7143 1.7660
 1.9682 2.0 2.0 2.0 2.0 2.0 2.0 2.0 2.0 2.0
 2.0 2.0 2.0 2.0 2.0 2.0 2.0 2.0 2.0 2.0
 0.0 .3848 1.8146 4.0828 7.2583 14.387 23.758 34.420 44.888 55.418
 65.039 73.290 78.540 81.713 82.355 82.355 82.355 82.355 82.355 82.355
 82.355 82.355 82.355 82.355 82.355 82.355 82.355 82.355 82.355 82.355
 130.0 135.0 140.0 145.0 150.0 155.0 160.0 165.0 170.0 175.0
 180.0 185.0 190.0 195.0 200.0 205.0 209.0
 2.0 2.0 2.0 2.0 2.0206 2.0823 2.1852 2.3704 2.5556 2.7407
 2.9259 3.1111 3.2963 3.4815 3.6667 3.8519 4.0
 82.355 81.713 81.073 78.854 76.356 71.780 65.325 58.223 51.149 43.592
 35.785 28.274 21.237 13.987 7.8427 2.4053 0.0
 103.60 4.50 -5.30
 0.0 5.0 10.0 15.0 20.0 25.0 30.0 40.0 60.0 70.0
 2.46 2.69 2.85 2.98 3.088 3.156 3.184 3.166 2.98 2.46
 103.60 11.00 -4.95
 0.0 5.0 10.0 15.0 20.0 25.0 30.0 40.0 60.0 70.0
 2.46 2.69 2.85 2.98 3.088 3.156 3.184 3.166 2.98 2.46
 155.39 0.0 6.78 48.60 165.63 0.0 9.191 38.201
 0.0 20.0 30.0 40.0 45.0 55.0 60.0 70.0 80.0 100.0
 0.0 .75 1.125 1.5 1.5 1.5 1.5 1.125 .75 0.0
 155.39 0.0 6.78 48.60 204.5 0.0 2.90 0.0
 0.0 20.0 30.0 40.0 45.0 55.0 60.0 70.0 80.0 100.0
 0.0 .75 1.125 1.5 1.5 1.5 1.5 1.125 .75 0.0
 165.6 0.0 9.191 38.201 190.35 0.0 27.475 10.787
 0.0 20.0 30.0 40.0 45.0 55.0 60.0 70.0 80.0 100.0
 0.0 .75 1.125 1.5 1.5 1.5 1.5 1.125 .75 0.0
 12200 611 44 36

Figure 2. Wave-drag format description of the Tu-144 aircraft.

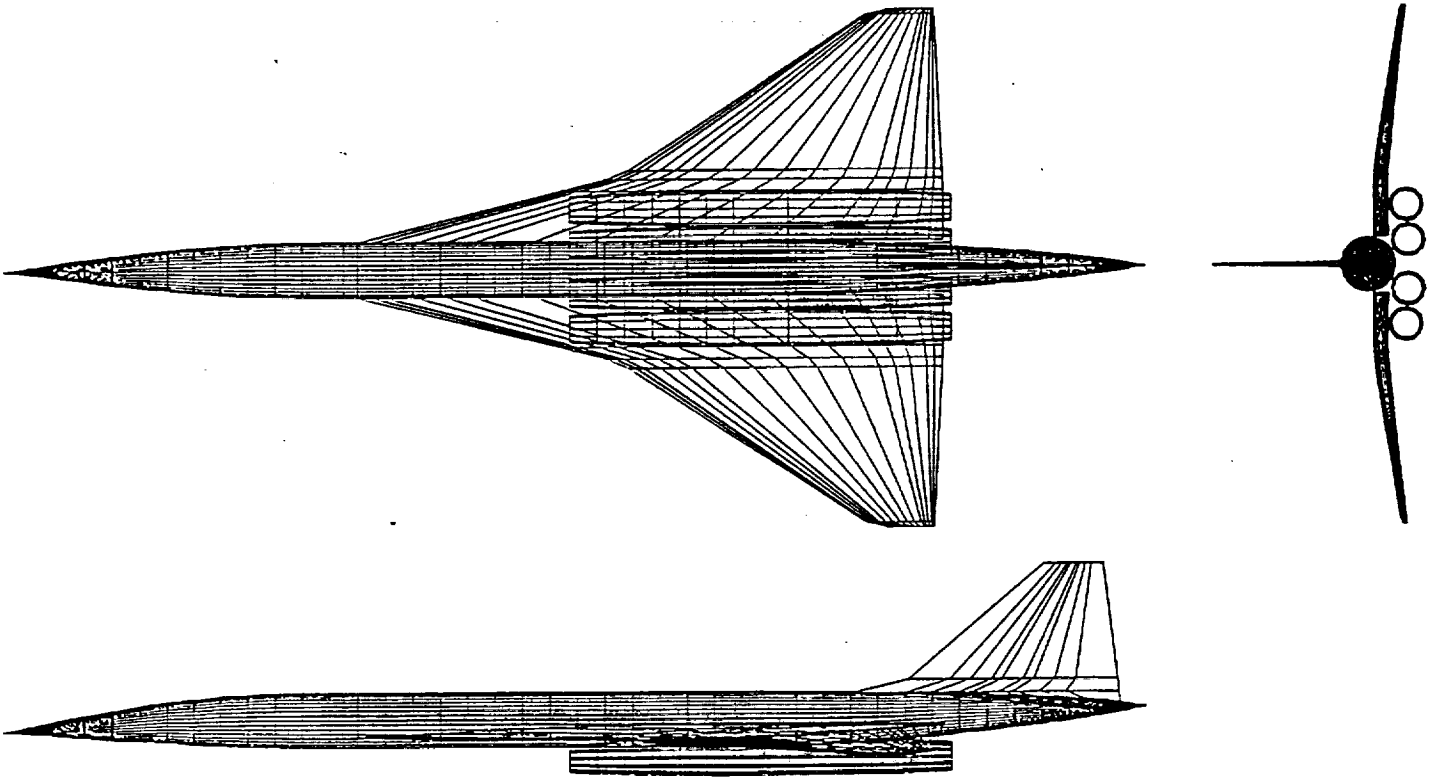


Figure 3. "Wire frame" three view of the Tu-144 obtained from the figure 2 description.

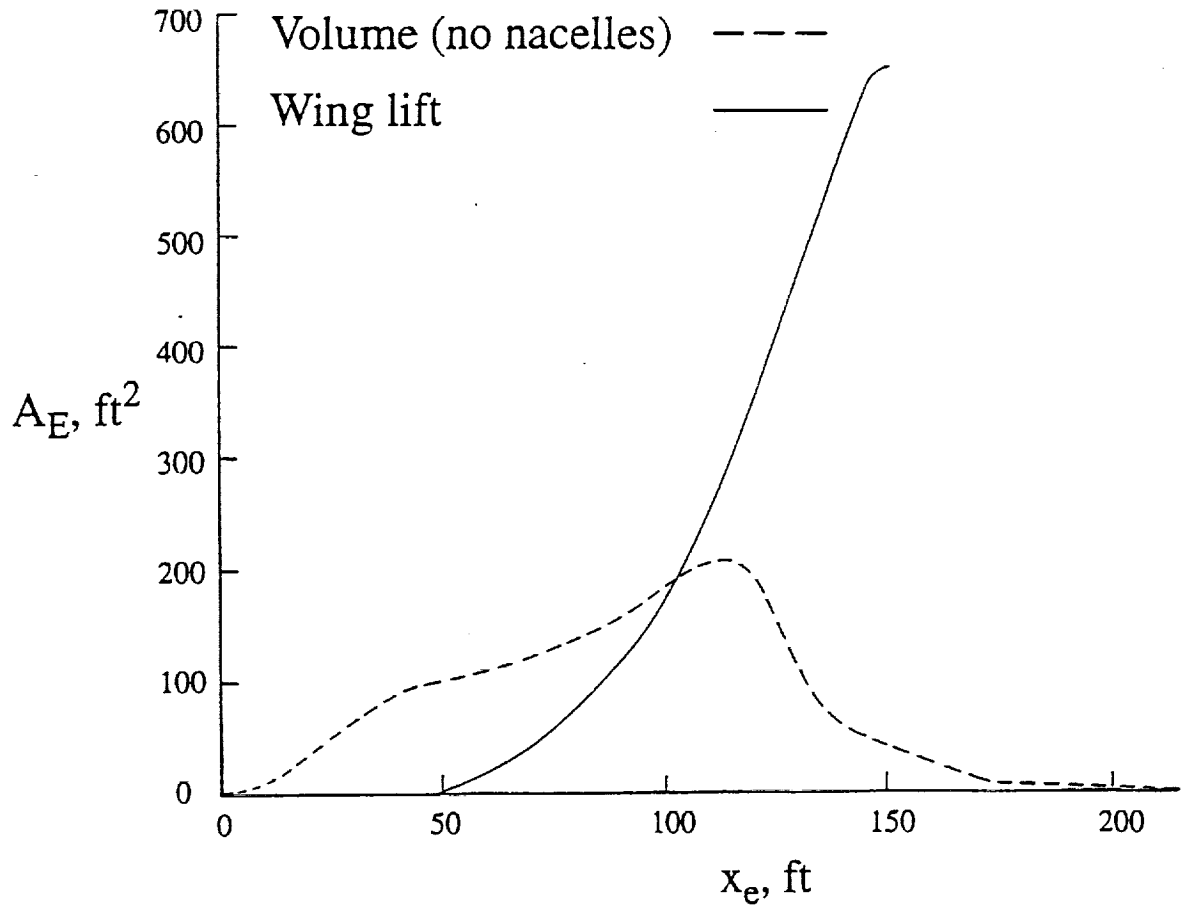


Figure 4. Equivalent areas of the volume (without nacelles) and the wing lift.
 $M = 2.2$, $W = 350,000$ lb, $\alpha = 6.11$ deg

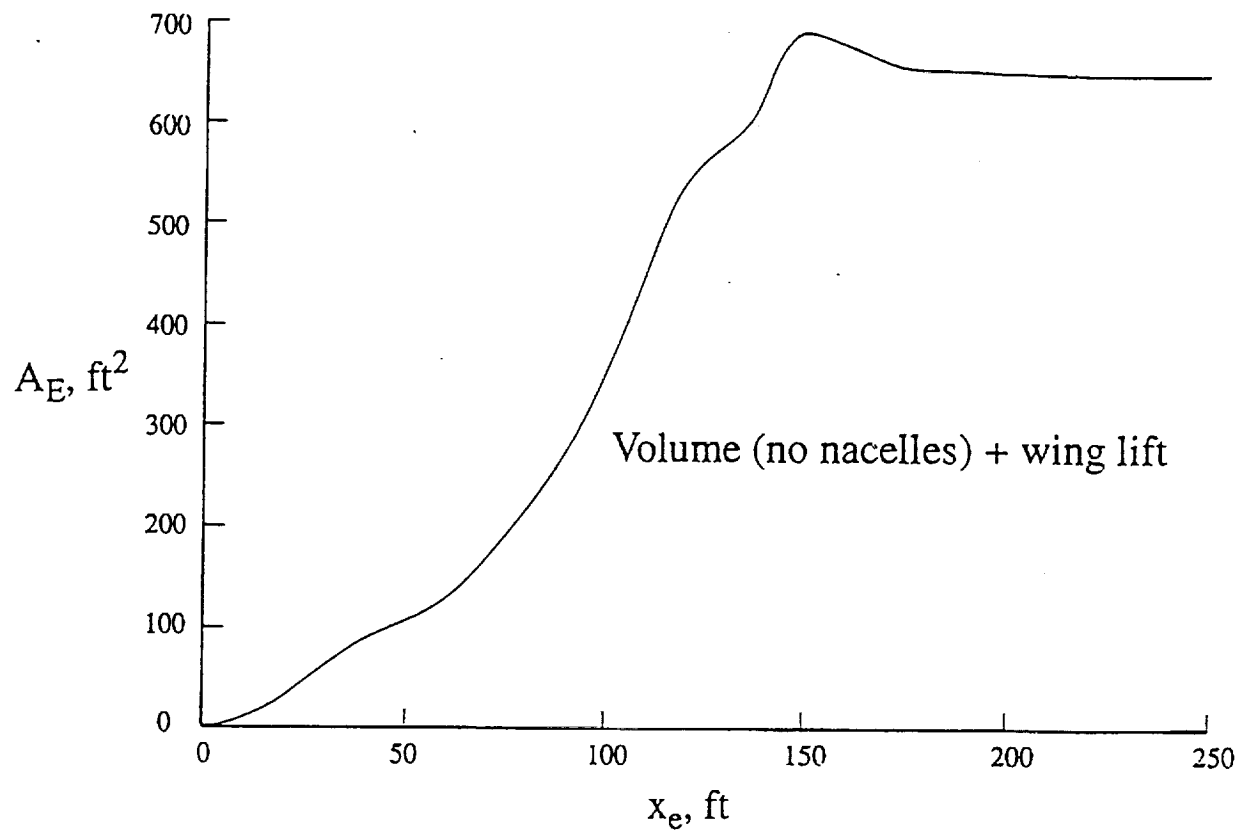


Figure 5. Sum of the equivalent areas given in figure 4.
 $M = 2.2$, $W = 350,000$ lb, $\alpha = 6.11$ deg

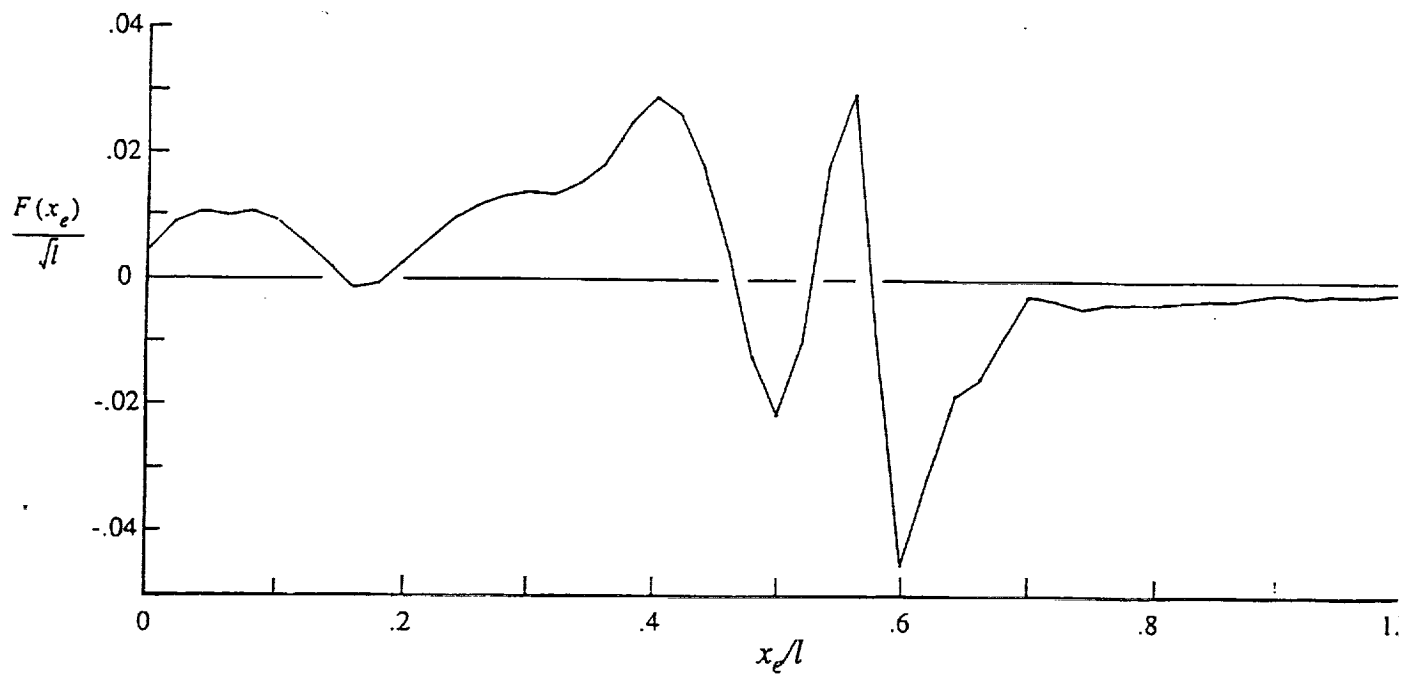


Figure 6. Whitham F-function of the volume (without nacelles) and the wing lift.
 $M = 2.2$, $W = 350,000$ lb, $\alpha = 6.11$ deg, $l = 250.0$ ft

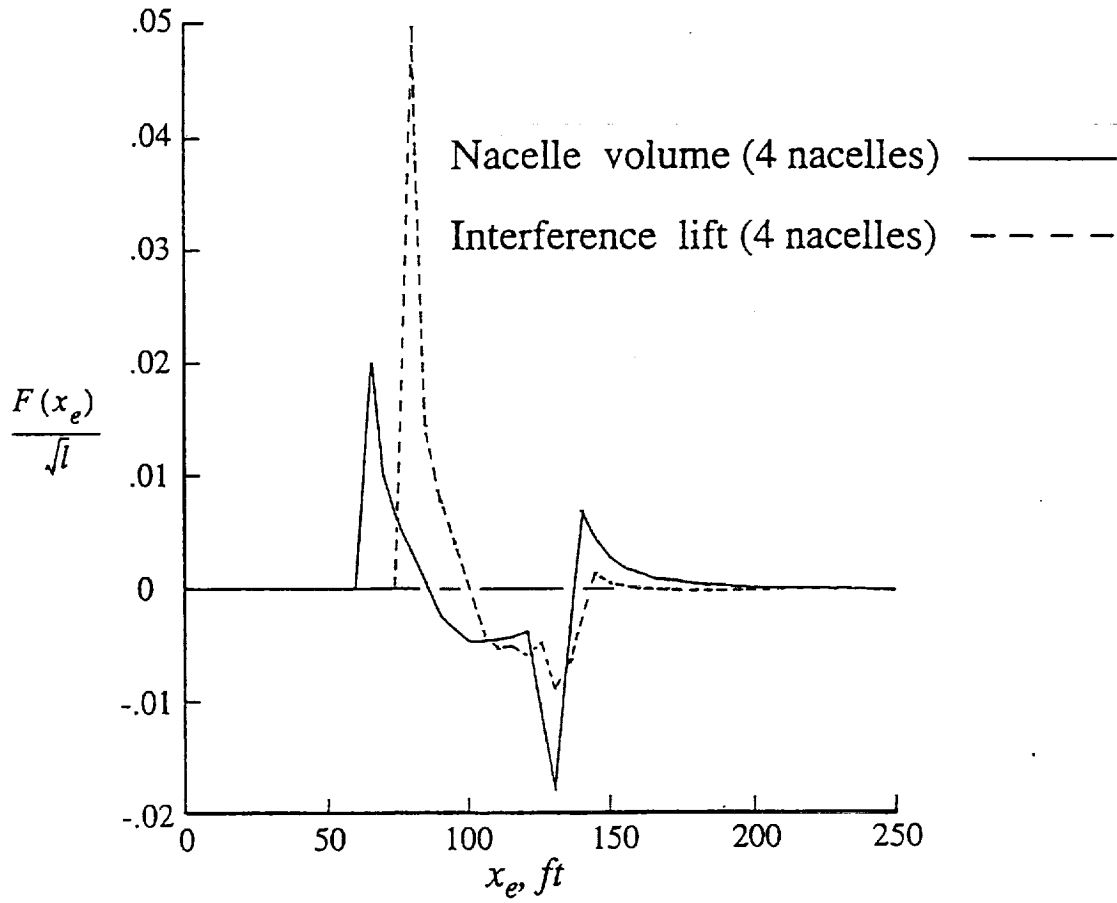


Figure 7. Whitham F-functions of the nacelle volumes and the nacelle-wing interference lift.
 $M = 2.2, l = 250.0$ ft

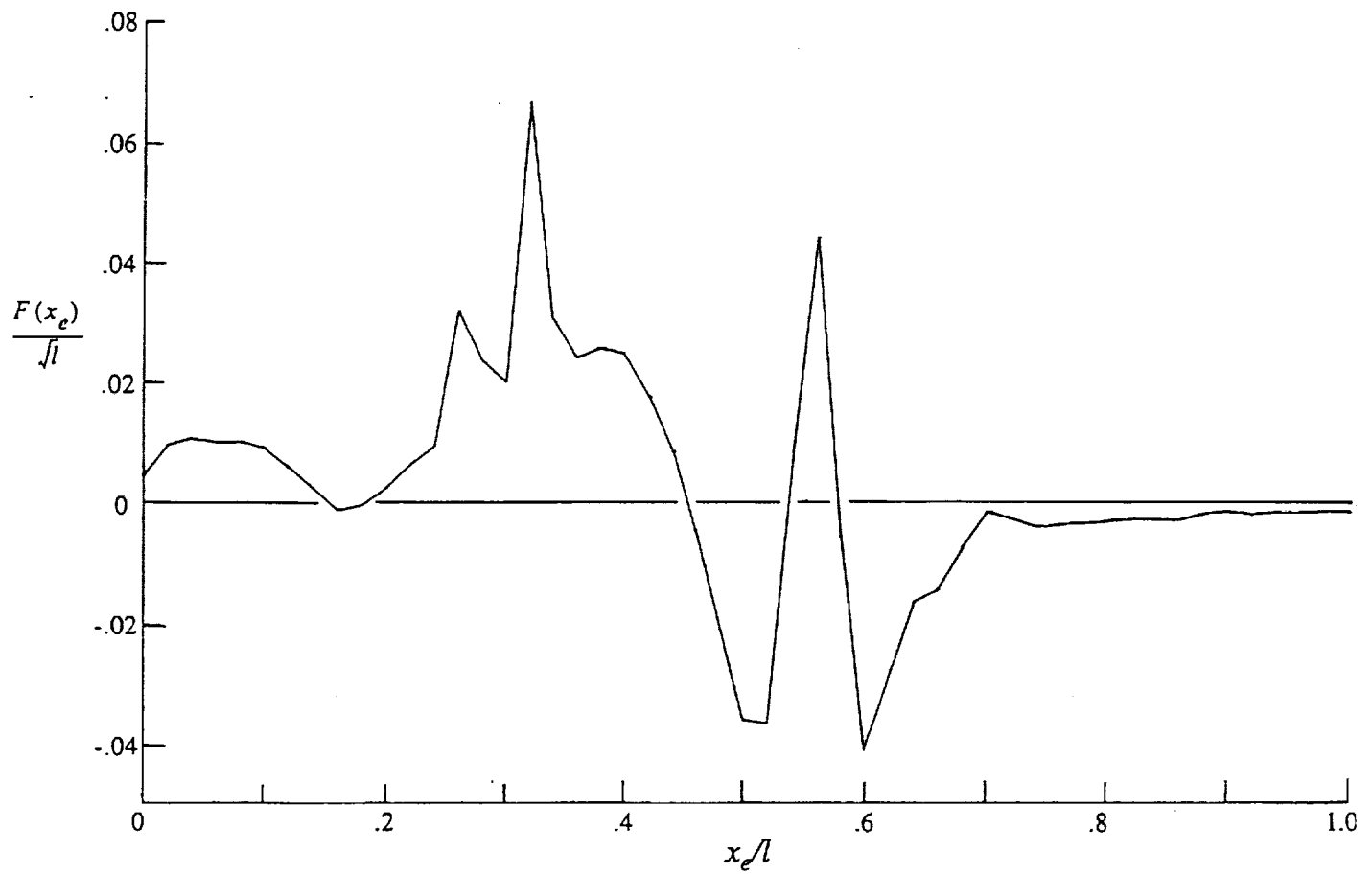


Figure 8. Complete Whitham F-function of the Tu-144 aircraft.
 $M = 2.2$, $W = 350,000$ lb, $\alpha = 6.11$ deg, $l = 250.0$ ft

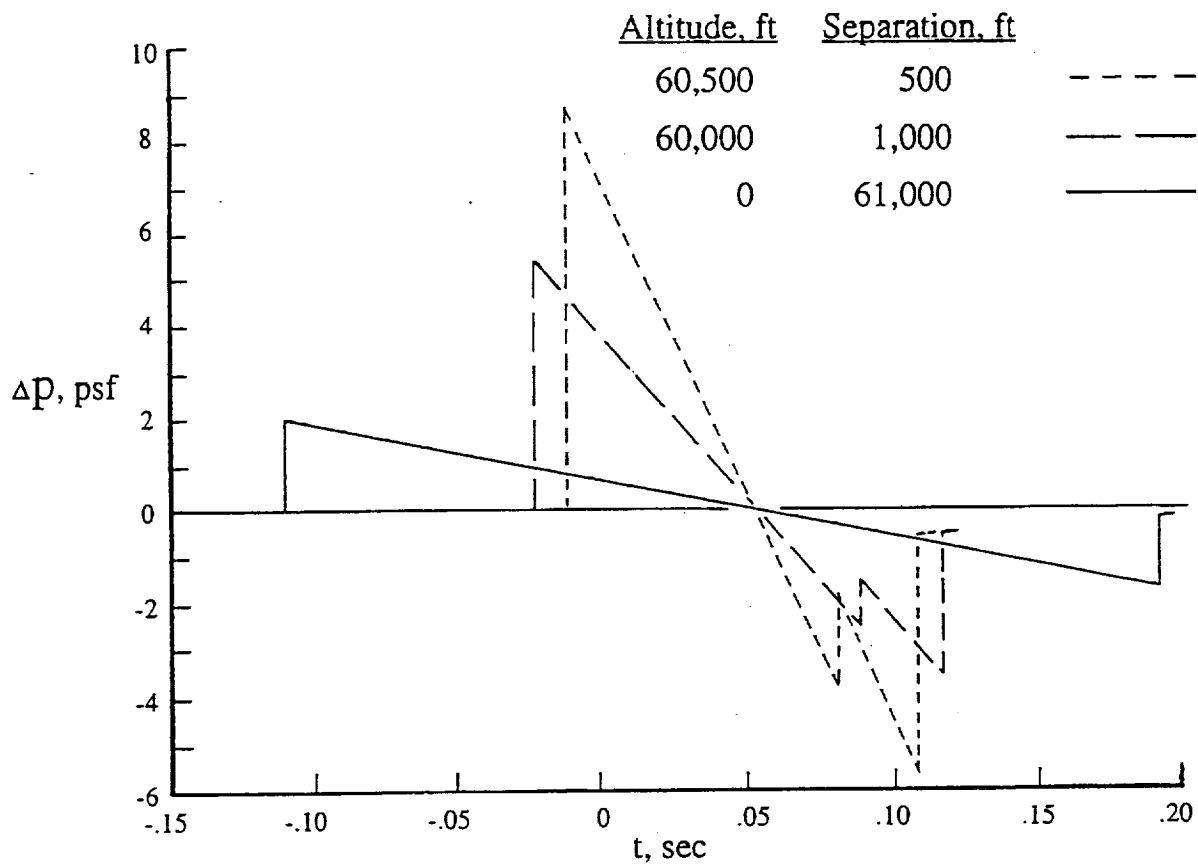


Figure 9. Predicted pressure signatures from the Tu-144 cruising at 61,000 feet.
 $M = 2.2$, $W = 350,000$ lb, $\alpha = 6.11$ deg

**DEVELOPMENT OF A MULTIOBJECTIVE OPTIMIZATION
PROCEDURE FOR SONIC BOOM MINIMIZATION**

J. R. Narayan
Aerospace Research Center

and

A. Chattopadhyay and N. Pagaldipti
Department of Mechanical and Aerospace Engineering
Arizona State University, Tempe, AZ

NASA HSR Program Sonic Boom Workshop
NASA Langley Research Center, Hampton, VA
September 12-13, 1995

Research Supported by NASA Ames Research Center
Grant NCC2-5064

DEVELOPMENT OF A MULTIOBJECTIVE OPTIMIZATION PROCEDURE FOR SONIC BOOM MINIMIZATION

J. R. Narayan, A. Chattopadhyay and N. Pagaldipti
Arizona State University, Tempe, AZ

ABSTRACT

A design optimization procedure for improved sonic boom and aerodynamic performance of high speed aircraft is presented. The multiobjective optimization procedure simultaneously minimizes the sonic boom at a given distance from the aircraft and the drag-to-lift ratio (C_D/C_L) of the aircraft. Upper and lower bounds are also imposed on the lift coefficient. The Kreisselmeier-Steinhauser function is used for the multiobjective optimization formulation. A discrete semi-analytical aerodynamic sensitivity analysis procedure coupled with an analytical grid sensitivity analysis technique is used for evaluating design sensitivities. The use of the semi-analytical sensitivity analysis techniques results in significant computational savings. The flow equations are solved using a three-dimensional parabolized Navier-Stokes solver. Sonic boom analysis is performed using an extrapolation procedure. A nonlinear programming technique and an approximate analysis procedure are used for the optimization. The optimization procedure developed is applied to the design of two high speed configurations, namely, a doubly swept wing-body configuration and a delta wing-body configuration. For the two sweep case only, minimization of the first peak in the pressure signature is performed first by optimizing only the nose radius and length of the aircraft. Minimization of the second peak in the pressure signature is performed next by optimizing only the wing geometric parameters. Significant improvements are obtained in the sonic boom characteristics and the aerodynamic performance of the wing-body configurations.

INTRODUCTION

Sonic boom prediction and minimization are important issues in the design of high speed aircraft. In the past, Hague and Jones [1] used optimization techniques to obtain body shapes with low sonic boom. Darden [2] developed equivalent area distributions for low boom configurations at given cruise conditions based on Whitham's F-function theory. Recently, Computational Fluid Dynamics (CFD) based techniques have been developed for accurate prediction of the sonic boom pressure signatures at mid-field and far-field regions from the aircraft [3,4]. Accuracy of these techniques has been established by comparison with wind tunnel test data. Due to the recent advances in optimization methods and the development of semi-analytical sensitivity analysis techniques [5], it is now possible to achieve low sonic boom levels by including them in the optimization formulation. Low boom configurations often correspond to blunt nose designs which degrade the aerodynamic efficiency by increasing drag. Therefore, it is necessary to study the trade-offs associated with low boom and aerodynamically efficient configurations and optimization is an efficient tool that aids in such a study. Narayan et al. [5,6] developed an integrated sonic boom/aerodynamic performance optimization procedure for wing-body configurations. The optimization procedure demonstrated the trade-off between low boom and high lift configurations.



BACKGROUND

- **Hague and Jones, 1970**
Design of low sonic boom overpressure body shapes using multivariable search techniques
- **Darden, 1979**
Equivalent area distribution for low boom configurations for given cruise conditions
- **Siclari and Darden, 1991**
Prediction of sonic boom using CFD for high Mach number flows
- **Cheung et al., 1992**
Prediction of mid-field solution from near-field solution through extrapolation
- **Narayan et al., 1995**
Integrated sonic boom/aerodynamic optimization

OBJECTIVES OF THE PRESENT WORK

The objective of the present work is to develop a multidisciplinary design optimization procedure for improved sonic boom and aerodynamic performance of high speed aircraft. The aim is to simultaneously minimize the sonic boom overpressure peaks and the drag-to-lift ratio of the aircraft. A semi-analytical sensitivity analysis technique has been developed and integrated with the above optimization strategy for computational savings.



OBJECTIVES

Development of efficient multiobjective optimization procedure for simultaneous minimization of sonic boom at designated distances from aircraft and improvements in aerodynamic performance.

Use of semi-analytical sensitivity analysis technique for design sensitivity analysis.

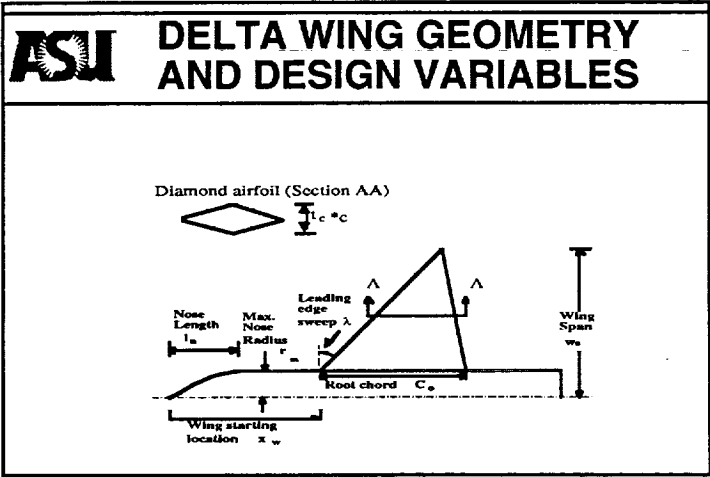
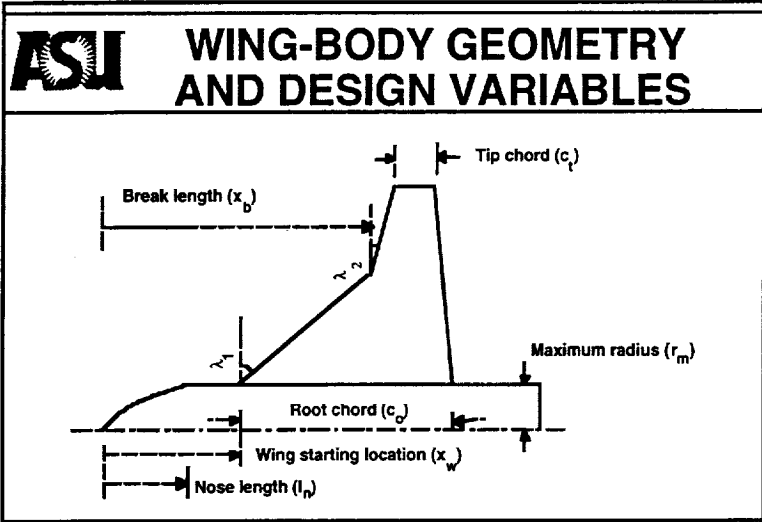
OPTIMIZATION FORMULATION

The objective of this paper is to develop an optimization procedure that simultaneously improves the aerodynamic and sonic boom characteristics of wing-body configurations. From a sonic boom perspective, it is of interest to minimize the peaks in the overpressure signal at a given distance, d_1 , from the axis of the aircraft. From aerodynamics point of view, it is of interest to minimize the ratio of aerodynamic drag coefficient to lift coefficient while maintaining the lift coefficient at a desired level. The multiobjective optimization problem can be stated in the nonlinear programming format as follows.

ASU	OPTIMIZATION FORMULATION
Minimize Δp_{\max}	overpressure peak
Minimize C_D/C_L	drag to lift ratio
subject to $C_{L\min} \leq C_L \leq C_{L\max}$ $\Phi_l \leq \Phi \leq \Phi_u$	lift constraint side constraints on design variables


AIRCRAFT CONFIGURATION


The optimization procedure is applied to two wing-body configurations illustrated in the following figures. For the doubly swept wing-body configuration, the design variables used in the optimization include maximum radius of the nose section (r_m), nose length (l_n), wing root chord (c_o), wing tip chord (c_t), two leading edge sweeps (λ_1 and λ_2), break length (x_b) and the longitudinal location of the wing tip (x_w). For the delta wing configuration, the design variables included are the leading edge sweep, root chord, nose length, maximum radius, wing span (w_s) and the wing thickness-to-chord ratio (t_c).



OPTIMIZATION STRATEGY


Since the optimization problem involves multiple objective functions, a multiobjective optimization technique based on the Kreisselmeier-Steinhauser (K-S) function [8,9] is used in the present work. The K-S function reduces the optimization problem to an unconstrained minimization problem. This unconstrained problem is solved using the Broyden-Fletcher-Goldfarb-Shanno (BFGS) algorithm [10]. A semi-analytical approach [7] is used to calculate the sensitivities of the objective functions during the optimization. Since the optimizer requires several evaluations of the objective functions and constraints and such evaluations are computationally expensive, a two-point exponential approximate analysis procedure [12] is used within the optimizer to approximate these functions. The K-S function approach is illustrated by first considering a general, multiobjective optimization problem of the following form.

 OPTIMIZATION STRATEGY
<ul style="list-style-type: none">• Multiobjective optimization technique• Unconstrained BFGS algorithm for optimization• Semi-analytical discrete sensitivity analysis procedure• Approximate analysis for function evaluation within optimizer

 MULTIOBJECTIVE OPTIMIZATION PROBLEM
Minimize $F_i(\Phi) \quad i = 1, \dots, \text{NOBJ}$
subject to $g_j(\Phi) \leq 0 \quad j = 1, \dots, \text{NCON}$
Side constraints $\phi_k^l \leq \phi_k \leq \phi_k^u \quad k = 1, \dots, \text{NDV}$

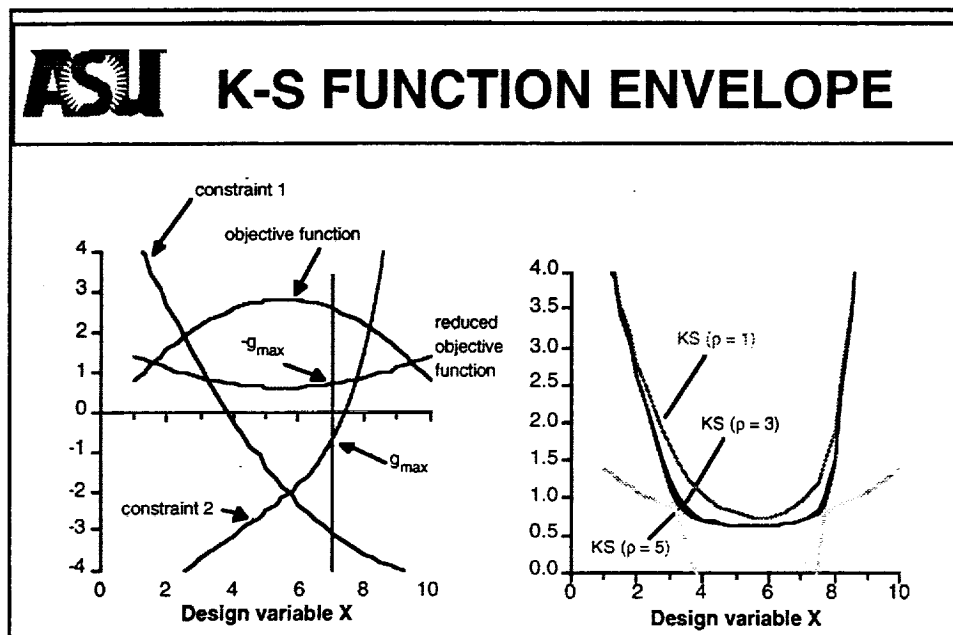
KREISSELMEIER-STEINHAUSER (K-S) MULTIOBJECTIVE FORMULATION

The first step in forming the composite (K-S) function involves transformation of the original objective functions into reduced objective functions [8,9]. These reduced objective functions assume the following form where F_{k_0} represents the value of the original objective function F_k , calculated at the beginning of each optimization cycle. The quantity NOBJ denotes the total number of objective functions in the original optimization problem. The quantity g_{\max} is the value of the largest constraint of the original optimization problem and is held constant during each cycle. Since the reduced objective functions assume the form of constraints, a new constraint vector $f_m(\Phi)$ ($m = 1, 2, \dots, \text{NCON} + \text{NOBJ}$, NCON being the total number of constraints in the original optimization problem) is introduced which includes the original constraints and the constraints introduced by the reduced objective functions. The new objective function to be minimized is then defined using the K-S function as follows.

	KREISSELMEIER-STEINHAUSER FUNCTION APPROACH
MINIMIZE	
$\text{KS}(\phi) = \frac{1}{\rho} \ln \left(\sum_{i=1}^{\text{NCON} + \text{NOBJ}} e^{\rho \hat{f}_i(\phi)} \right)$	
ρ = user-specified draw down factor	
Reduced objective functions:	
$\hat{f}_i(\phi) = \frac{F_i(\phi)}{F_{i_0}} - 1 - g_{\max}$	
F_{i_0} - i^{th} objective function (F_i) at beginning of each optimization cycle	


K-S FUNCTION FORMULATION (CONTINUED)

The multiplier ρ , which is analogous to the draw-down factor of penalty function formulation, controls the distance from the surface of the K-S envelope to the surface of the maximum constraint function. When ρ is large, the K-S function will closely follow the surface of the largest constraint function and when ρ is small, the K-S function will include contributions from all violated constraints. The new unconstrained optimization problem is solved using the Broyden-Fletcher-Goldfarb-Shanno (BFGS) algorithm [10]. This algorithm approximates the inverse of the Hessian of the composite objective function using a rank-two update and guarantees both symmetry and positive definiteness of the updated inverse Hessian matrix. The K-S formulation coupled with the BFGS algorithm has been successfully applied to a variety of rotary wing aircraft by Chattopadhyay et al. [11].



Approximation Technique

The optimizer requires several evaluations of the objective functions and the constraints during each optimization cycle. The use of exact analysis to evaluate them at each iteration during an optimization cycle is computationally expensive. Therefore, an approximation technique known as the two-point exponential approximation [12], is used within the optimizer for approximating the objective functions and the constraints. This technique takes its name from the fact that the exponent used in the approximation is based on gradient information from the previous and current design cycles and is formulated as follows. Here $\hat{F}(\Phi)$ is the approximation of the function $F(\Phi)$ in the neighborhood of the current design variable vector, Φ_1 . The quantity ϕ_n represents the n^{th} design variable and NDV is the total number of design variables. The approximate values for the constraints, $\hat{g}_j(\Phi)$, are similarly calculated. The exponent, p_n , is defined below. Here Φ_1 refers to the design variable vector from the current cycle and Φ_0 denotes the design variable vector from the previous cycle. The two point exponential approximation indicates that in the limiting case of $p_n = 1$, the expansion is identical to the traditional first order Taylor series and when $p_n = -1$, the two-point exponential approximation reduces to the reciprocal expansion form. Therefore, the exponent (p_n) can be interpreted as a "goodness of fit" parameter which explicitly determines the trade-offs between traditional and reciprocal Taylor series based expansions and is defined to lie within the interval, $-1 \leq p_n \leq 1$. This results in a hybrid approximation technique.

 <h2 style="margin: 0; display: inline-block; vertical-align: middle;">TWO-POINT EXPONENTIAL ANALYSIS</h2>
$\hat{F}(\Phi) = F(\Phi_1) + \sum_{n=1}^{NDV} \left[\left(\frac{\phi_n}{\phi_{1n}} \right)^{p_n} - 1.0 \right] \frac{\phi_{1n}}{p_n} \frac{\partial F(\Phi_1)}{\partial \phi_n}$ $p_n = \frac{\log_e \left\{ \frac{\frac{\partial F(\Phi_0)}{\partial \phi_n}}{\frac{\partial F(\Phi_1)}{\partial \phi_n}} \right\}}{\log_e \left\{ \frac{\phi_{0n}}{\phi_{1n}} \right\}} + 1.0$
<p>• move limits used to control design variable movement</p>

SEMI-ANALYTICAL AERODYNAMIC SENSITIVITY ANALYSIS

Sensitivity analysis is an essential part of a gradient-based, design optimization procedure. In the present study, the aerodynamic performance parameters (lift and drag coefficients) are of primary interest. Therefore, it is necessary to evaluate the sensitivities of these parameters to changes in the design variables. Since a CFD-based, 3D Navier Stokes solver is used for aerodynamic analysis, the use of standard finite difference techniques for calculation of the design sensitivities can be computationally prohibitive. Therefore, in this paper, a previously developed discrete semi-analytical sensitivity analysis procedure [7] is used to calculate the aerodynamic design sensitivities and is briefly described next. The term $\left\{ \frac{\partial Q^*}{\partial \phi_i} \right\}$, which represents the sensitivity of the steady state flow variables with respect to the i^{th} design variable, is calculated using the direct differentiation technique.



SEMI-ANALYTICAL AERODYNAMIC SENSITIVITY ANALYSIS

$C_j = C_j(Q^*(\phi), X(\phi), \phi)$ - derivative w.r.t. ϕ required

ϕ = vector of aerodynamic design variables

X = vector of grid point coordinates


Q^* = vector of steady state flow variable

$$\frac{dC_j}{d\phi_i} = \left[\frac{\partial C_j}{\partial Q^*} \right]^T \left[\frac{\partial Q^*}{\partial \phi_i} \right] + \left[\frac{\partial C_j}{\partial X} \right]^T \left[\frac{\partial X}{\partial \phi_i} \right] + \frac{\partial C_j}{\partial \phi_i}$$

$\frac{\partial C_j}{\partial \phi_i}$, $\left[\frac{\partial C_j}{\partial Q^*} \right]$, $\left[\frac{\partial C_j}{\partial X} \right]$ - from explicit dependence of C_j
on ϕ_i , Q^* and X

AERODYNAMIC SENSITIVITY ANALYSIS (CONTINUED)

In the discrete sensitivity approach, the discretized flow equations are directly differentiated, as described below. The coefficient matrix for the linear system in $\left\{ \frac{\partial Q^*}{\partial \phi_i} \right\}$ is a block pentadiagonal matrix. The coefficient matrix is L-U decomposed to obtain the solution of the linear system.



AERODYNAMIC SENSITIVITY ANALYSIS (CONT'D)

- **Discretized governing equations:**

$$R = R(Q^*(\phi), X(\phi), \phi) = [0]$$
- **Sensitivity**

$$\left[\frac{dR}{d\phi_i} \right] = \left[\frac{\partial R}{\partial Q^*} \right]^T \left[\frac{\partial Q^*}{\partial \phi_i} \right] + \left[\frac{\partial R}{\partial X} \right]^T \left[\frac{\partial X}{\partial \phi_i} \right] + \left[\frac{\partial R}{\partial \phi_i} \right] = [0]$$
- **Linear system of equations in** $\left[\frac{\partial Q^*}{\partial \phi_i} \right]$
 $\left[\frac{\partial R}{\partial \phi_i} \right], \left[\frac{\partial R}{\partial Q^*} \right], \left[\frac{\partial R}{\partial X} \right]$ - **calculated from explicit dependence of R on ϕ_p , Q^* and X**

SONIC BOOM ANALYSIS

For isentropic flow past smooth axisymmetric bodies, the pressure disturbances (sonic boom) at large distances from the aircraft can be evaluated by using the Whitham F-function [14], which is based on the Abel integral of the equivalent area distribution of the aircraft. Lighthill [15] developed an alternate formulation of the F-function which was shown to be suitable for sonic boom prediction of smooth and non smooth projectile shapes. Walkden [16] extended Whitham's theory for application to wing-body configurations. The asymptotic form of the equations used in developing the sonic boom overpressure signature ($\Delta p/p_\infty$), is shown. Here $F(y)$ is the Whitham F-function, Δp is $(p_{local} - p_\infty)$, $\gamma = 1.4$ for air, M_∞ is the freestream Mach number, R is the radius (or equivalent radius) of the flying object, S' is the derivative of the area distribution of the flying object and h is the Heaviside unit step function. $y(x, d_0) = \text{constant}$, is a characteristic curve, x is the streamwise distance and d_0 is the distance normal to the flight axis. The first integral of $F(y)$ is associated with the volume of the flying object, the second integral is associated with the lift and the third integral is associated with the interference lift for a winged body [16].




SONIC BOOM ANALYSIS

Whitham's F-function (quasi-linear) theory

$$\begin{aligned}
 F(y) = & \frac{1}{2\Pi} \int_0^\infty \sqrt{\frac{2}{\beta R_{vol}(t)}} h \left[\frac{y-t}{\beta R_{vol}(t)} \right] dS'_{vol}(t) \\
 & + \frac{1}{2\Pi} \int_0^\infty \sqrt{\frac{2}{\beta R_{lift}(t)}} h \left[\frac{y-t}{\beta R_{lift}(t)} \right] dS'_{lift}(t) \\
 & + \frac{1}{2\Pi} \int_0^\infty \sqrt{\frac{2}{\beta R_{int}(t)}} h \left[\frac{y-t}{\beta R_{int}(t)} \right] dS'_{int}(t)
 \end{aligned}$$

SONIC BOOM ANALYSIS (CONTINUED)

Since these models are based on linearized theory, they fail to agree with wind-tunnel data in highly nonlinear flows such as the flow at angle-of-attack at high Mach numbers ($M_\infty > 2$). Reference 17 describes an F-function extrapolation method that is used to extrapolate the pressure signature at d_0 to a distance d_1 ($d_1 > d_0$). First, a pressure signature at distance d_0 , where the flowfield is assumed to be locally axisymmetric, is directly measured in the wind-tunnel and the value of the F-function (at d_0) is evaluated. Since the pressure signal propagates at the local speed of sound and each point of the signal advances according to its amplitude, the signal is distorted as it propagates away from the aircraft and the F-function becomes multivalued. The new F-function at d_1 is obtained by placing discontinuities (shocks) in such a way that the discontinuities divide the multivalued regions with equal areas on either side of them. This new F-function gives the overpressure signature at d_1 .

	SONIC BOOM ANALYSIS (CONT'D)
$\frac{\Delta p}{P_\infty} = \gamma M_\infty^2 F(y) / \sqrt{2\beta d_0}$	(Sonic boom overpressure)
$\beta = (M_\infty^2 - 1)^{0.5}$	
Extrapolation used to obtain signature at d_1 from d_0	

SONIC BOOM ANALYSIS (CONTINUED)

Cheung et al. [4] have used a three-dimensional parabolized Navier-Stokes (PNS) code in combination with Whitham's quasilinear theory for sonic boom prediction. The CFD code used in this study, UPS3D [18], solves the PNS equations governing the flow using an implicit, approximately factored, finite volume algorithm. The flow field associated with wing-body configurations is evaluated and the drag, lift and moment coefficients are computed. Three different approaches have been used in Ref. 4 to obtain the overpressure signal at mid- and far-fields from the near-field CFD solution of various configurations such as a cone-cylinder, a low aspect-ratio rectangular wing and a delta wing-body. In the first approach (for nonlifting cases), the UPS3D code is modified so that it has an axisymmetric version that provides a propagation capability incorporating all nonlinear effects. In the second approach (for both lifting as well as nonlifting cases), the near field three-dimensional solution provides the overpressure signal at a distance d_0 . The sonic boom at a far-field distance d_1 , is then obtained using the extrapolation technique of Ref. 17. In the third approach (for lifting cases), the equivalent area distribution due to lift is generated by the surface pressure coefficients calculated by the UPS3D code. The equivalent area distribution due to volume is calculated directly from the geometry of the flying object. Summation of the two equivalent area distributions gives the total equivalent area distribution which is used to evaluate the F-function of the body. In the present work, a solution procedure for sonic boom analysis based on the second approach is used in conjunction with the CFD code, within the multidisciplinary optimization procedure to achieve the objectives of minimum sonic boom and improved aerodynamic performance.




SONIC BOOM ANALYSIS (CONT'D)

- **Integration of Whitham's theory with CFD (Cheung et al.)**
- **3D parabolized Navier Stokes code, UPS3D**
 - **PNS equations integrated using implicit, approximately factored, finite volume algorithm**
 - **Inviscid option currently used**

SONIC BOOM SENSITIVITIES

The sonic boom pressure signature is obtained using an extrapolation procedure [4]. This procedure takes as input, a near-field pressure signature at a distance d_0 directly beneath the aircraft. This near-field pressure signature is calculated by the UPS3D code and is passed on to the sonic boom procedure as input. The sensitivity of this near-field pressure signature is a part of the aerodynamic sensitivities calculated using the semi-analytical procedure described in the previous section. Knowing the near-field pressure signature sensitivity, the sensitivity of the extrapolated signatures can be obtained as explained below.

	SONIC BOOM SENSITIVITIES
<ul style="list-style-type: none">• Near field pressure signature input to sonic boom extrapolation procedure• Sensitivities of near field pressure signature from semi-analytical aerodynamic sensitivity analysis• Perturbed near field signatures input to sonic boom procedure to generate perturbed extrapolated signatures• Sonic boom sensitivities using forward finite differences	

RESULTS

The multiobjective optimization procedure and sensitivity analysis techniques are applied to the design optimization of a doubly swept wing-body configuration and a delta wing configuration. The flight conditions under which the optimization is performed are described below.




RESULTS

- Design Mach number = 2.5
- Angle of attack = 5 degrees
- Grid: 80 (normal) x 75 (circumferential)
- Sonic boom: compute pressure at d_0 , extrapolate to d_1
 - $d_0 = 0.5$ lb
 - $d_1 = 3.61$ lb

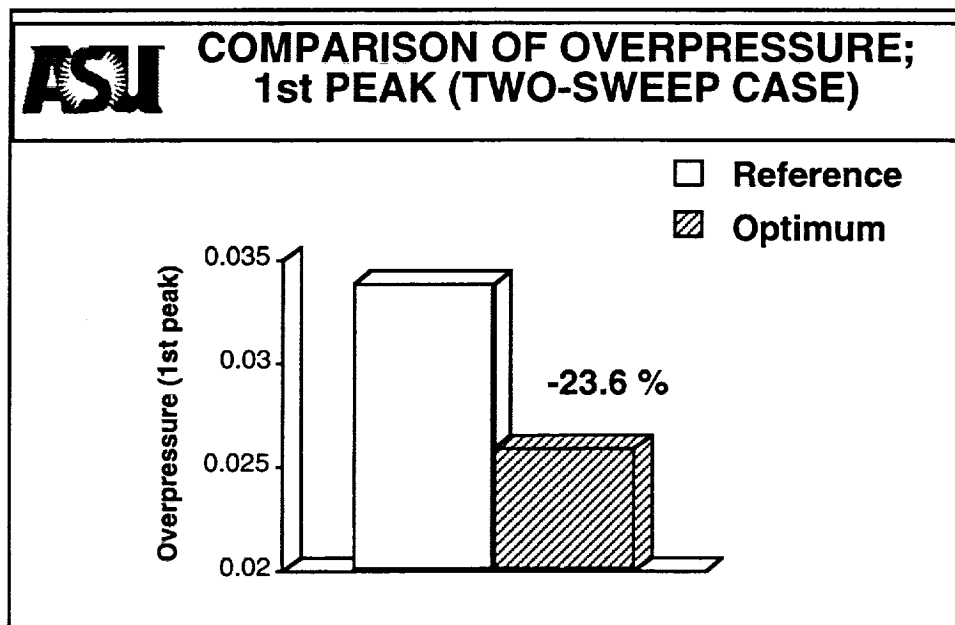
RESULTS (Continued)

First, the design optimization of the doubly swept wing-body configuration is considered. The overpressure signature of the wing-body configuration has two peaks, the first corresponding to the nose of the aircraft and the second corresponding to the wing. The first peak is affected primarily by the nose dimensions of the wing-body configuration. The second peak is affected primarily by the wing geometric parameters. Therefore, in the present study, the optimization is carried out in two steps. In the first step, the body radius and the nose length are used as design variables to minimize the first peak in the sonic boom pressure signature. In the second step, the wing geometric parameters are used as design variables to minimize the second peak in the sonic boom pressure signature, while the nose dimensions are maintained at their optimum values obtained from the first optimization.

	RESULTS (TWO-SWEEP CASE)
Step 1:	Minimization of 1st peak in overpressure signature
	Design variables:
	<ul style="list-style-type: none">• Maximum radius (r_m)• Nose length (l_n)
Step 2:	Minimization of 2nd peak in overpressure signature
	Design variables:
	<ul style="list-style-type: none">• First leading edge sweep (λ_1)• Root chord (c_o)• Second leading edge sweep (λ_2)• Tip chord (c_t)• Break length (x_b)• Wing starting location (x_w)

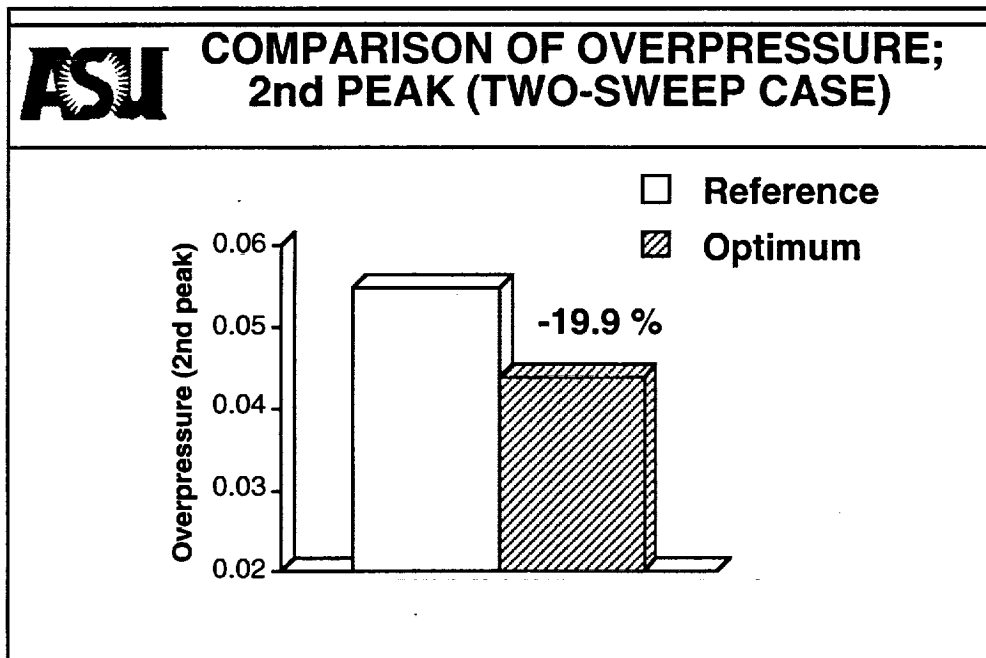
COMPARISON OF OVERPRESSURE (FIRST PEAK) - TWO SWEEP CASE

The following figure compares the reference and the optimum values of the first peak in the sonic boom pressure signature. The optimization procedure yields a significant reduction of 23.6 percent in the first peak of the sonic boom pressure signature. The maximum radius decreases and the nose length increases resulting in a optimum configuration more slender than the reference design. The slender nose has a smaller equivalent area distribution for the nose region yielding a reduced sonic boom pressure peak.



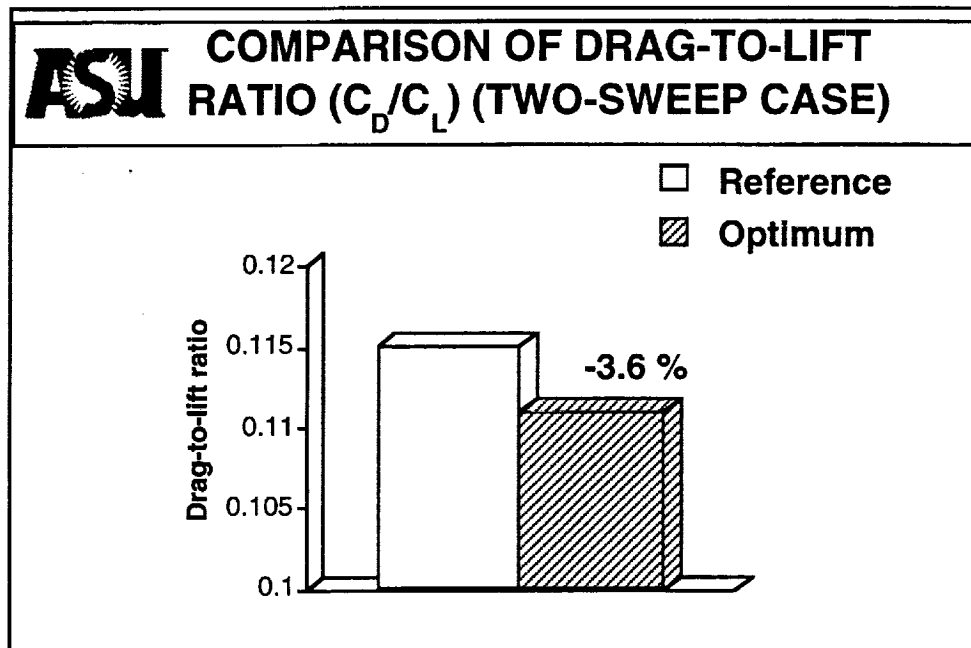
COMPARISON OF OVERPRESSURE (SECOND PEAK) - TWO SWEEP CASE

The following figure compares the reference and the optimum values of the second peak in the sonic boom pressure signature. The optimization procedure yields a very significant reduction of 19.9 percent in the second peak of the sonic boom pressure signature. Significant increases are observed in the first leading edge sweep, the root chord and the break length of the optimum wing. These increases coupled with the decreases in the wing tip chord and starting location result in a smaller planform area for the optimum wing. The smaller planform area has a smaller equivalent area and lift distribution that account for the reduction in the second sonic boom pressure peak.



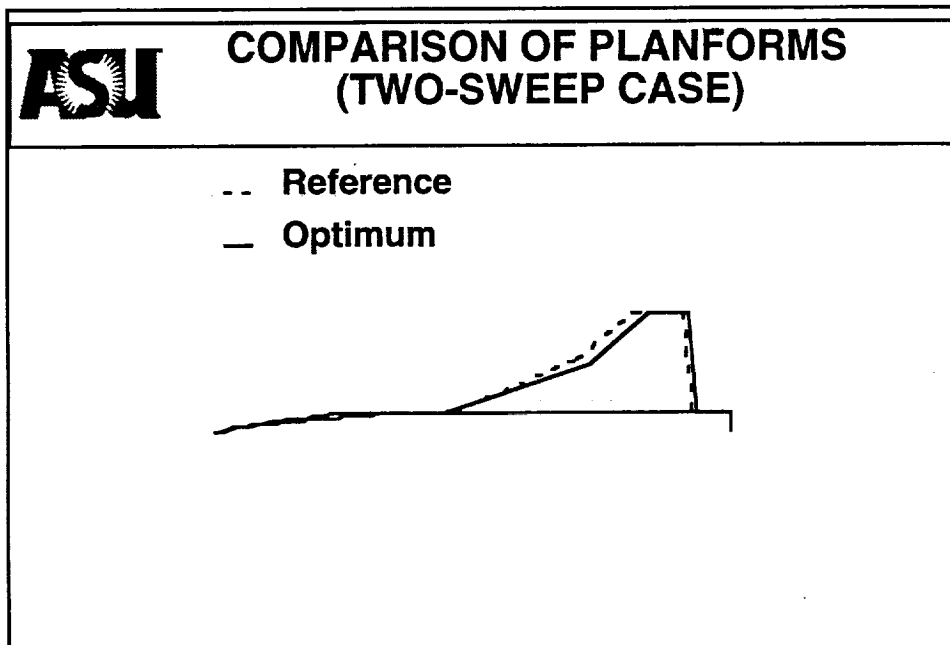
COMPARISON OF DRAG-TO-LIFT RATIO

The drag-to-lift ratio is included as an objective function to be minimized during the optimizations. The following chart compares the reference and the optimum values of the drag-to-lift ratios. As shown, there is a small reduction of 3.6 percent in the drag-to-lift ratio of the optimum configuration. This is because, while the drag has reduced due to the reduction in the body radius and wing planform area, the lift has also reduced due to the reduction in the wing planform area. These reductions in the drag and the lift seem to offset each other in the optimum configuration, yielding only a net 3.6 percent reduction in the drag-to-lift ratio.



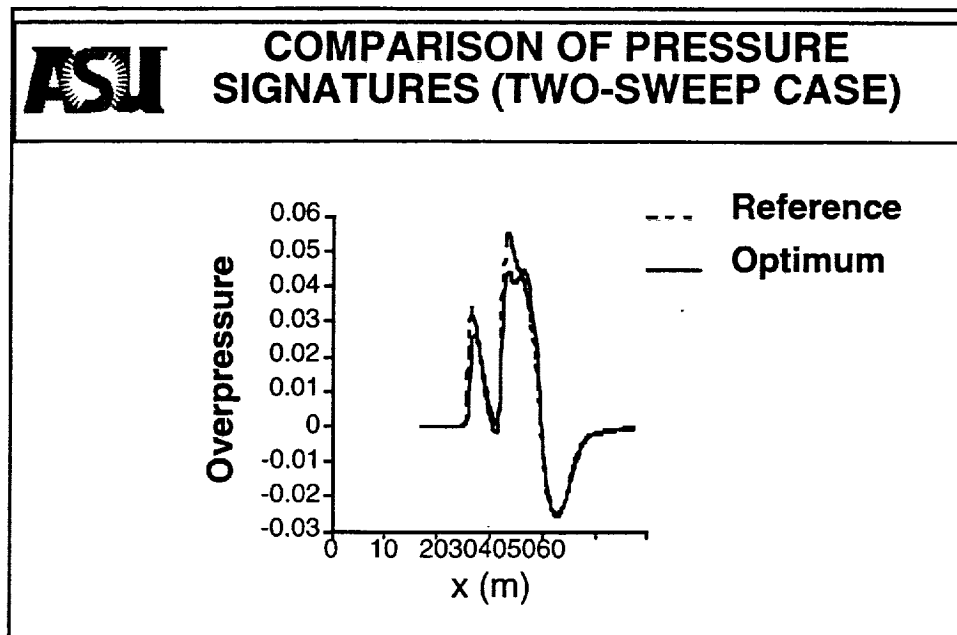
COMPARISON OF PLANFORMS - TWO SWEEP CASE

The significant changes in the aircraft nose and planform variables are illustrated in the following figure. As mentioned earlier, there are significant reductions in the maximum radius, nose length, tip chord and the wing starting location. However, this is also accompanied by significant increases in the first leading edge sweep, root chord and the wing break length. The result is a smaller planform area of the optimum configuration as shown in the figure.



COMPARISON OF PRESSURE SIGNATURES - TWO SWEEP CASE

A comparison of the reference and optimum sonic boom pressure signatures is made in the following chart. As seen, significant reductions occur in both the sonic boom pressure peaks. This illustrates that the multiobjective optimization procedure effectively modifies the airplane geometry to achieve these reductions while maintaining aerodynamic efficiency.



COMPARISON OF DESIGN VARIABLES AND PERFORMANCE FUNCTIONS - TWO SWEEP CASE

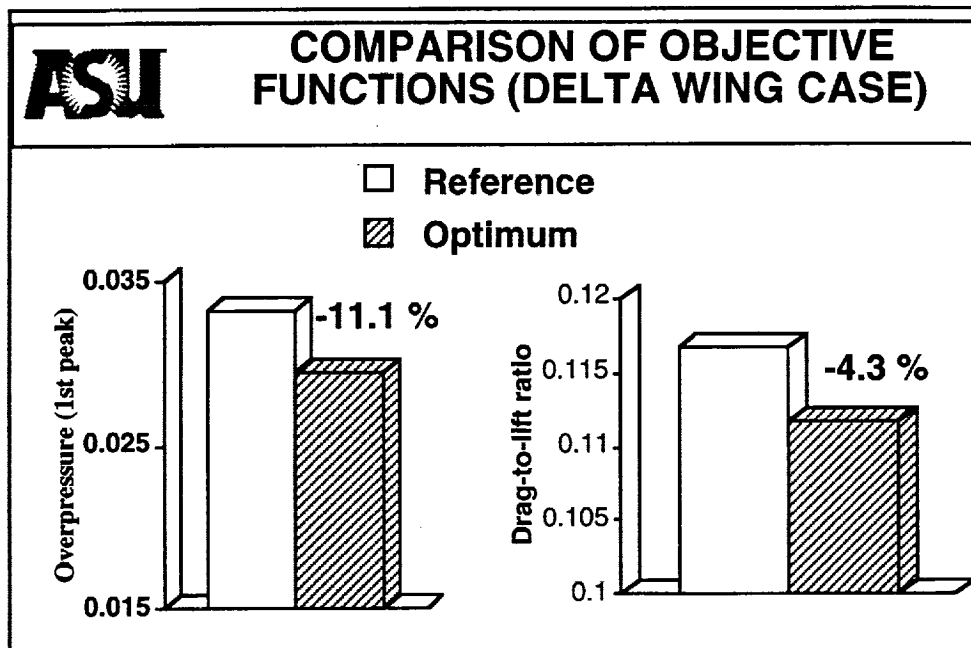
The reference and the optimum values of the design variables and the objective functions are tabulated below. The percentage changes in the performance functions are also indicated.

COMPARISON OF DESIGN VARIABLES (TWO-SWEEP CASE)		
Design variable	Reference	Optimum
Maximum radius (r_m)	0.570 m	0.513 m
Nose length (l_n)	6.01 m	6.611 m
1st leading edge sweep (λ_1)	70.16 deg.	74.25 deg.
Root chord (c_o)	8.12 m	8.60 m
2nd leading edge sweep (λ_2)	54.93 deg.	52.51 deg.
Tip chord (c_t)	1.62 m	1.39 m
Break length (x_b)	12.28 m	12.76 m
Wing starting location (x_w)	8.13 m	7.75 m

COMPARISON OF PERFORMANCE FUNCTIONS (TWO-SWEEP CASE)		
Function	Reference	Optimum
Overpressure (Peak 1)	0.03389	0.02590 (-23.6%)
Overpressure (Peak 2)	0.05483	0.04394 (-19.9%)
Drag-to-lift ratio (C_D/C_L)	0.11510	0.11099 (-3.6%)
Lift coefficient (C_L)	0.19441	0.19221 (-1.1%)

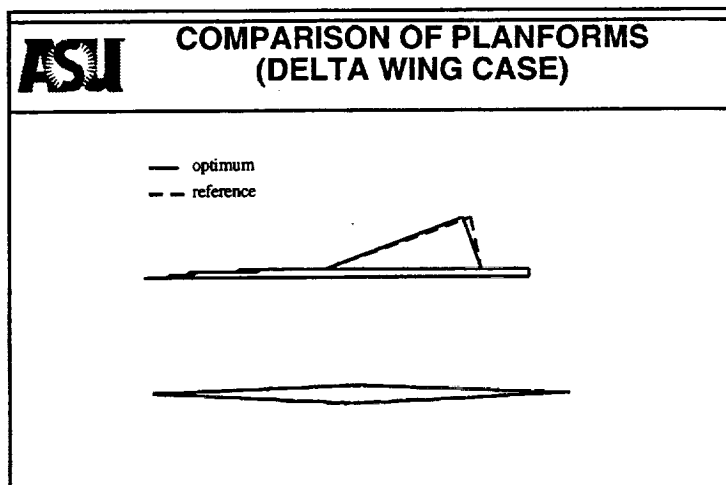
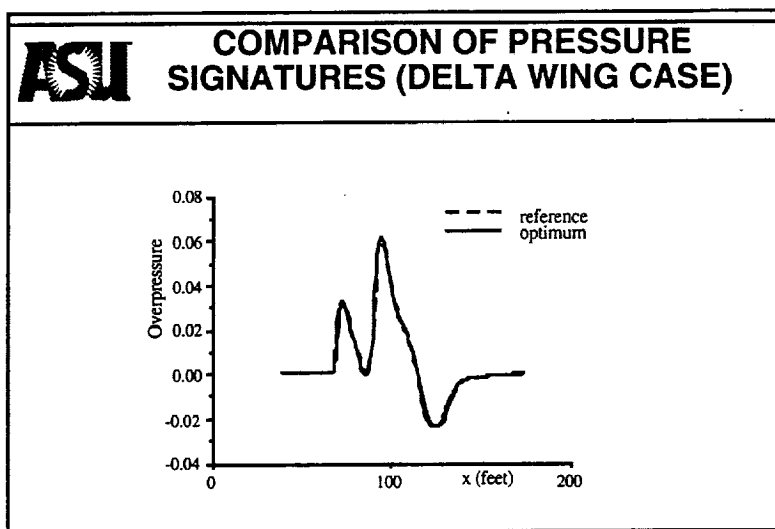
COMPARISON OF OBJECTIVE FUNCTIONS - DELTA WING CASE

Results from the optimization of the delta wing-body configuration are presented next. It is to be noted that during this optimization, the first peak in the overpressure signature and the drag-to-lift ratio are included as objective functions whereas the second peak in the overpressure signature is constrained to be below the reference value. The following figure compares the overpressure peaks (first peaks) and the drag-to-lift ratio for the reference and the optimum configurations. There is a significant reduction of 11.1 percent in the first pressure peak of the optimum configuration. The optimum configuration is more slender than the reference configuration and this is indicated by the reduction in the maximum radius and the increase in the nose length of the optimum configuration. This results in the reduction in the pressure peak and the drag-to-lift ratio. The drag-to-lift ratio decreases by 4.3 percent for the optimum configuration. The optimum design has a lower wing thickness-to-chord ratio which helps reduce the drag-to-lift ratio.



COMPARISON OF PRESSURE SIGNATURES AND AIRCRAFT GEOMETRY - DELTA WING BODY CASE

The pressure signatures and the planforms of the reference and the optimum configurations are presented in the following figures. As shown, the changes in the geometry of the delta wing-body configuration are small compared to the changes in the geometry of the doubly swept wing-body configuration. This explains the smaller percentage reduction in the pressure peak of the optimum delta wing configuration.



COMPARISON OF DESIGN VARIABLES AND OBJECTIVE FUNCTIONS - DELTA WING CASE


The following tables compare the reference and the optimum values of the design variables and objective functions used in the optimization of the delta wing-body. The percentage changes in the performance functions are also indicated.

ASU COMPARISON OF DESIGN VARIABLES (DELTA WING CASE)		
Design variable	Reference	Optimum
Maximum radius (r_m)	0.570 m	0.536 m
Nose length (l_n)	6.01 m	6.379 m
Leading edge sweep (λ)	66.00 deg.	64.80 deg.
Root chord (c_r)	7.08 m	7.11 m
Wing span (w_s)	3.530 m	3.496 m
Thickness-to-chord ratio (t_c)	0.0520	0.0489

ASU COMPARISON OF PERFORMANCE FUNCTIONS (DELTA WING CASE)		
Function	Reference	Optimum
Overpressure (Peak 1)	0.03319	0.02951 (-11.1%)
Drag-to-lift ratio (C_D/C_L)	0.11681	0.11179 (-4.3%)

CONCLUDING REMARKS

A multidisciplinary optimization procedure has been developed for the design of high speed aircraft. The objective is to simultaneously minimize sonic boom and the aircraft drag-to-lift ratio. A multiobjective function formulation technique based on the K-S function approach has been used to model the optimization problem. An efficient semi-analytical sensitivity analysis technique is coupled with the optimization procedure. A nonlinear programming technique is used for solving the optimization problem and an approximate analysis procedure is used within the optimizer for computational economy. The developed optimization procedure is applied to two high speed configurations namely, a doubly swept wing-body configuration and a delta wing-body configuration. The following observations are made on the results from the optimization procedure.

	<h2>CONCLUDING REMARKS</h2>
<ul style="list-style-type: none">• Multiobjective optimization procedure very efficient; yields significant reduction in sonic boom overpressure peaks of both configurations.• Semi-analytical sensitivity analysis very efficient over finite difference sensitivity analysis; yields computational savings.• Procedure demonstrates definite trade-off between low boom and aerodynamically efficient designs.• Reduction in first peak through changes to nose dimensions; reduction in second peak through changes to wing dimensions.	

REFERENCES

1. Hague, D. S. and Jones, R. T., "Application of Multivariable Search Techniques to the Design of Low Sonic Boom Overpressure Body Shapes," *Third Conference on Sonic Boom Research*, NASA Head Quarters, Washington, D. C., October, 1970.
2. Darden, C. M., "Minimization of Sonic-Boom Parameters in Real and Isothermal Atmospheres," NASA TN D-7842, 1975.
3. Siclari, M. and Darden, C. M., "CFD Predictions of the Near-Field Sonic-Boom Environment for Two Low Boom HSCT Configurations," AIAA Paper 91-1631, *AIAA 22nd Fluid Dynamics, Plasma Dynamics and Lasers Conference*, Honolulu, Hawaii, June, 1991.
4. Cheung, S. H., Edwards, T. A. and Lawrence, S. L., "Application of Computational Fluid Dynamics to Sonic Boom Near- and Mid-Field Prediction," *Journal of Aircraft*, Vol. 29, No. 5, 1992, pp. 920-926.
5. Narayan, J. R., Chattopadhyay, A., Pagaldipti, N. and Cheung, S. H., "Optimization Procedure for Improved Sonic Boom and Aerodynamic Performance Using a Multiobjective Formulation Technique," AIAA Paper 95-0127, *33rd Aerospace Sciences Meeting and Exhibit*, Reno, Nevada, January 1995.
6. Narayan, J. R., Chattopadhyay, A., Pagaldipti, N., Wensheng, X. and Cheung, S. H., "Optimization Procedure for Reduced Sonic Boom in High Speed Flight," AIAA Paper 95-2156, *26th AIAA Fluid Dynamics Conference*, San Diego, California, June 1995.
7. Pagaldipti, N. and Chattopadhyay, A., "A Discrete Semi-Analytical Procedure for Aerodynamic Sensitivity Analysis Including Grid Sensitivity," AIAA Paper 94-4268, *5th AIAA/USAF/NASA/ISSMO Symposium on Multidisciplinary Analysis and Optimization*, Panama City, Florida, September, 1994.
8. Kreisselmeier, A. and Steinhauser, R., "Systematic Control Design by Optimizing a Vector Performance Index," *Proceedings of the IFAC Symposium on Computer Aided Design of Control Systems*, Zurich, Switzerland, 1979, pp. 113.-117.
9. Wrenn, G. A., "An Indirect Method for Numerical Optimization Using the Kreisselmeier-Steinhauser Function," AIAA Paper 87-1112, June 1987.
10. Haftka, R. T., Gurdal, Z. and Kamat, M. P., "Elements of Structural Optimization," Kluwer Academic Publishers, Dordrecht, The Netherlands, 1990.
11. McCarthy, T. R., Chattopadhyay, A. and Zhang, S., "A coupled Rotor/Wing Optimization Procedure for High Speed Tilt-Rotor Aircraft," *51st Annual Forum of the American Helicopter Society*, Fort Worth, Texas, May, 1995.
12. Fadel, G. M., Riley, M. F. and Barthelemy, J. F. M., "Two-point Exponential Approximation Method for Structural Optimization," *Structural Optimization 2*, 1990, pp. 117-124.
13. Hoffmann, K. A., "Computational Fluid Mechanics for Engineers," *A Publication of Engineering Education System*, Austin, Texas, 1989.
14. Whitham, G. B., "The Flow Pattern of a Supersonic Projectile," *Communications on Pure and Applied Mathematics*, Vol. 5, No. 3, 1952, pp. 301-348.
15. Lighthill, M. J., "General Theory of High Speed Aerodynamics, Sec. E; see also High Speed Aerodynamics and Propulsion," Vol. 6, Princeton University Press, Princeton, NJ, 1954, pp. 345-389.
16. Walkden, F., "The Shock Pattern of a Wing-Body Combination, Far From the Flight Path," *Aeronautical Quarterly*, Vol. 9, Pt. 2, May 1958, pp. 164-194.
17. Hicks, R. and Mendoza, J., "Prediction of Aircraft Sonic Boom Characteristics from Experimental Near-Field Results," NASA TMX1477, November 1967.
18. Lawrence, S., Chaussee, D. and Tannehill, J., "Application of an Upwind Algorithm to the 3-D Parabolized Navier-Stokes Equations," AIAA Paper 87-1112, June 1987.

LANGLEY'S COMPUTATIONAL EFFORTS IN SONIC-BOOM SOFTENING OF THE BOEING HSCT

Kamran Fouladi

Lockheed Martin Engineering & Sciences

ABSTRACT

NASA Langley's computational efforts in the sonic-boom softening of the Boeing high-speed civil transport are discussed in this paper. In these efforts, an optimization process using a higher order Euler method for analysis was employed to reduce the sonic boom of a baseline configuration through fuselage camber and wing dihedral modifications. Fuselage modifications did not provide any improvements, but the dihedral modifications were shown to be an important tool for the softening process. The study also included aerodynamic and sonic-boom analyses of the baseline and some of the proposed "softened" configurations. Comparisons of two Euler methodologies and two propagation programs for sonic-boom predictions are also discussed in the present paper.

INTRODUCTION

During Phase I of the High Speed Research (HSR) program, low-boom conceptual designs were pursued by NASA and industry. The designers involved in this study began working on a series of High-Speed Civil Transport (HSCT) configurations with several objectives. The major objective was to design configurations which generate ground pressure signatures other than typical N-wave signatures, such as "ramped," "flat-top," and multiple-shock signatures. Other objectives were correct integration of the nacelle and improved performance of the low-boom concepts. While much progress was achieved during this phase of design work, many significant difficulties were also encountered as detailed in Ref. 1. The radical configuration changes required to "shape" the sonic-boom signature were judged to have unacceptable risks. Therefore, configuration design studies have recently been redirected toward reducing or "softening" of the sonic-boom of the baseline configuration.

Earlier this year, two NASA/industry teams were established to study ways to reduce the sonic boom levels of the baseline configurations; one team was to concentrate on the Boeing Reference-H baseline configuration and the other on the Douglas Arrow Wing baseline configuration. The Boeing team proposed a set of guidelines for the softening task under which the analysis and optimization of the configuration using higher-order computational fluid dynamics (CFD) methods were assigned to NASA LaRC and ARC. This paper discusses the LaRC's CFD efforts in the softening task.

Three separate categories of modifications to the Boeing HSCT configuration were proposed in the set of guidelines for the softening efforts. The first category involves modifications which result in negligible adverse effects on the performance of the aircraft. The second and the third categories, however, entail modifications which result in moderate and significant aircraft performance penalties, respectively. The current effort to investigate the reduction of the sonic-boom level by modifying the fuselage camber and the wing dihedral falls under the first category.

To track the reduction in sonic-boom level and changes in aircraft performance, it was first necessary to analyze the sonic-boom characteristics of the baseline configuration. The baseline study was extended to examine the nacelle and pylon integration for better understanding of the nacelle-pylon-wing interference and its effect on the ground sonic-boom level. The study also included comparisons of two Euler methodologies and two propagation codes for the assessment of these methodologies on the sonic-boom predictions.

ANALYSIS METHODS

NASA Langley's current sonic-boom analysis capabilities are based on two different numerical schemes. The first scheme is based on the Euler unstructured grid methodology of USM3D/VGRID (Refs. 2-4), and the second on the Euler structured grid marching code of MIM3D-SB (Refs. 5-7).

The flow solver code, USM3D (Ref. 2), is a NASA Langley developed finite volume, upwind code which solves Euler equations on unstructured tetrahedral meshes. USM3D uses the three dimensional unstructured tetrahedral inviscid grid generated by VGRID3D (Ref. 3).

The code MIM3D-SB (Refs. 5-7) is an Euler marching code specifically tailored for prediction of near-field pressure signatures of supersonic configurations. MIM3D-SB uses a simple Harris wave drag geometry input data format to describe the input geometry and then internally enhances this geometry to generate smooth, continuous surfaces. MIM3D-SB then utilizes the internally generated grid for marching techniques. MIM3D-SB code is an efficient technique which has been

used extensively for the sonic-boom analysis of HSCT configurations.

The MDBOOM (Ref. 8) and Thomas Wave Propagation (Ref. 9) programs are propagation codes which compute sonic-boom characteristics of a supersonic aircraft in a horizontally stratified atmosphere. The overpressure ratio is computed using a higher order CFD code and is directly input into each code. MDBOOM input requires that the pressure ratio to be interpolated on the surface of a cylinder with a specified radius and azimuth, whereas input to the Thomas code is the pressure ratio on a line at a specified distance below the aircraft. It is assumed that the pressure ratio input to the Thomas code is axisymmetric. The propagation portion of MDBOOM is based on the Thomas wave propagation theory; however, MDBOOM allows the pressure ratios to be extracted at smaller separation distances since it uses a matching technique based on an acoustic multipole formulation and accounts for diffraction effects in the flow field near the aircraft. This feature allows for flow-field solutions to be calculated at distances practical for most CFD schemes.

OPTIMIZATION METHODOLOGY

The design optimization methodology utilized in the present study is the newly developed code, MIM3DES (Ref. 10). This method couples the numerical optimization technique NPSOL (Ref. 11) with the CFD Euler code MIM3D-SB (Refs. 5-7). The NPSOL method is a tool designed to solve the nonlinear programming problem for the minimization of a smooth nonlinear function subject to a set of constraints on the variables. The working details of the present system are presented in Ref. 10. A subroutine in the CFD code calls the Thomas code (Ref. 9) to extrapolate the near-field pressure signatures through the atmosphere down to the ground.

In the present optimization process, a parameter such as the initial overpressure peak of the ground pressure signature is designated as the objective function and the aim of the process is to reduce this function. The Euler code MIM3D-SB is used to evaluate the objective function and any other nonlinear aerodynamic constraints. Cubic splines with matched first and second derivatives are used for simplicity to describe the geometric design variables. A new set of design variables is used to regenerate the portion of the configuration which is being modified to reduce the objective function. The process of the generating a new geometry with the new design variables and evaluation of the objective function using a new grid for the new configuration is performed automatically within this optimization process. An initial guess for the design variables and proper upper and lower bounds for these variables are the inputs by the user. The computational time required for each optimization process is highly dependent to the number of design variables (Ref. 10). Therefore, care must be taken to utilize the minimize number of design variables needed.

RESULTS AND DISCUSSIONS

The Boeing 1080-1122 (Fig. 1) is the Reference-H baseline configuration considered for the softening task. The components of the configuration include wings, fuselage, nacelles, pylons, and empennage. The geometrical details of 1080-1122 were available in both the standard Harris Wave-Drag format and the Initial Graphics Exchange Standard (IGES) format. Although, it was possible to include the empennage in the CFD analysis and optimization, the empennage was omitted from the configuration. This was justified since the softening efforts in the present study was focused on reducing the initial overpressure peak (nose shock) in the ground signature and the effects of empennage on the ground boom level is mainly manifested in the tail shock of the ground signature.

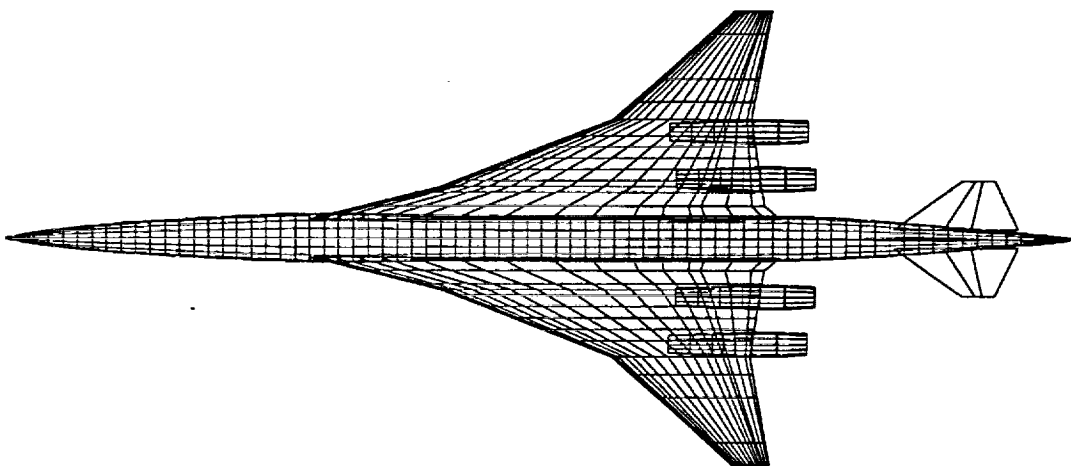


Fig. 1 - Top-View of the Boeing 1080-1122 baseline configuration.

The aircraft was designed to transport payload of 63,800 lbs (304 passengers) with start-cruise-conditions of freestream Mach number (M)=2.4, flight altitude=54,850 ft., gross weight=684,000 lbs, and coefficient of lift (C_L) = 0.115. The wing reference area and the wing span are 7700 ft.² and 134.84 ft., respectively. The length of the fuselage is 314 ft.

For the CFD analyses, several preliminary runs were required to obtain the correct angle of attack (α) corresponding to the designed C_L . For the baseline analysis, $\alpha=4.5^\circ$ was determined to correspond to $C_L=0.115$. It should be noted that for a meaningful comparison, the analyses of the modified configurations must also be made at the same lift.

Euler Marching Analysis of the Baseline

The sonic-boom analysis of the baseline configuration with nacelles off (REFH_WB) and nacelles on (REFH_WBN) at $M=2.4$ and $\alpha=4.5^\circ$ using the Euler Marching Code MIM3D-SB are considered here.

The multi-block computational grid used by MIM3D-SB is generated internally and is comprised of crossflow grids stacked in the streamwise direction. Due to its marching nature, MIM3D-SB is computationally efficient and uses very little memory for large grids. Hence, grid blocks with fine resolutions with small marching steps may be constructed where necessary. The finer grid resolution is particularly required near the wing leading and trailing edges and the nacelle inlet and exit planes. For both cases, the grid densities vary from 69×68 in the coarse grid block to 147×120 in the fine grid block and the marching steps vary from 2.0 ft. in the forebody to 0.25 ft. near the nacelle exit. The details of grid topology used in MIM3D-SB are presented in Refs. 5-7.

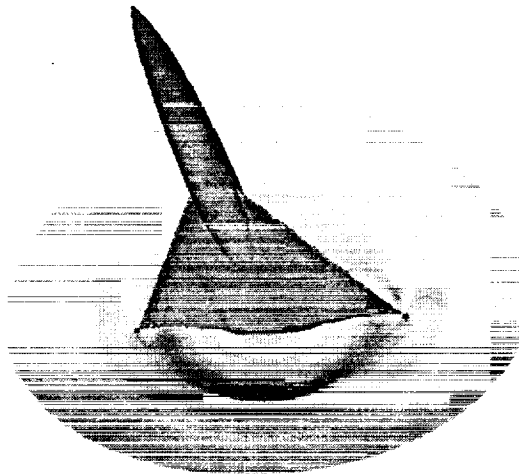


Fig. 2 - Computed pressure contours at axial station 180 ft.

The computed pressure contours on a plane perpendicular to the wing at axial station 180 ft. are presented in Fig. 2. The darker shades represent the higher pressure regions. The near-field centerline pressure signature at $h/l=1.5$, where (h) is the separation distance below the aircraft and (l) is the aircraft length, is presented in Fig. 3. The main differences between the two signatures are the higher pressure in the expansion region and the stronger tail shock in the ground signature of the REFH_WBN configuration. The extrapolation of this signature to the ground using Thomas code is also shown in Fig. 3. The predicted overpressure peaks for the REFH_WBN and REFH_WB configurations are 2.82 psf and 2.68 psf, respectively.

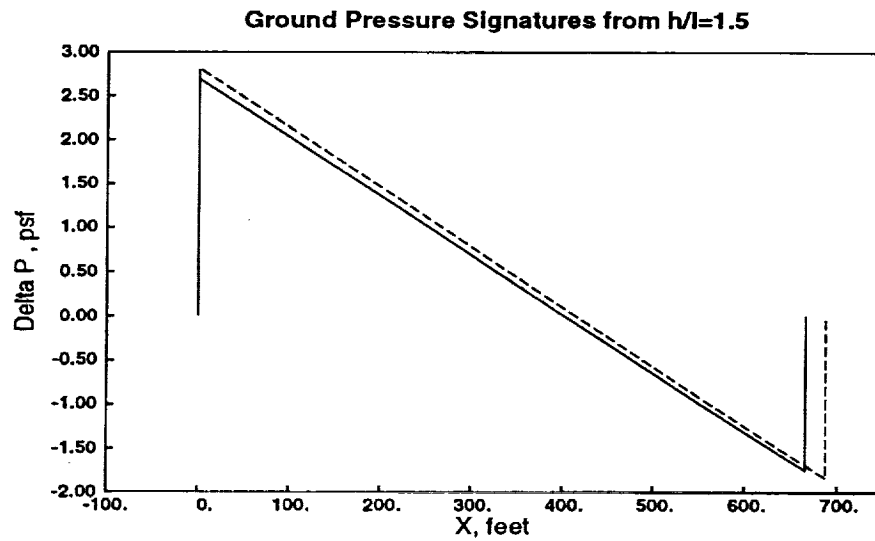
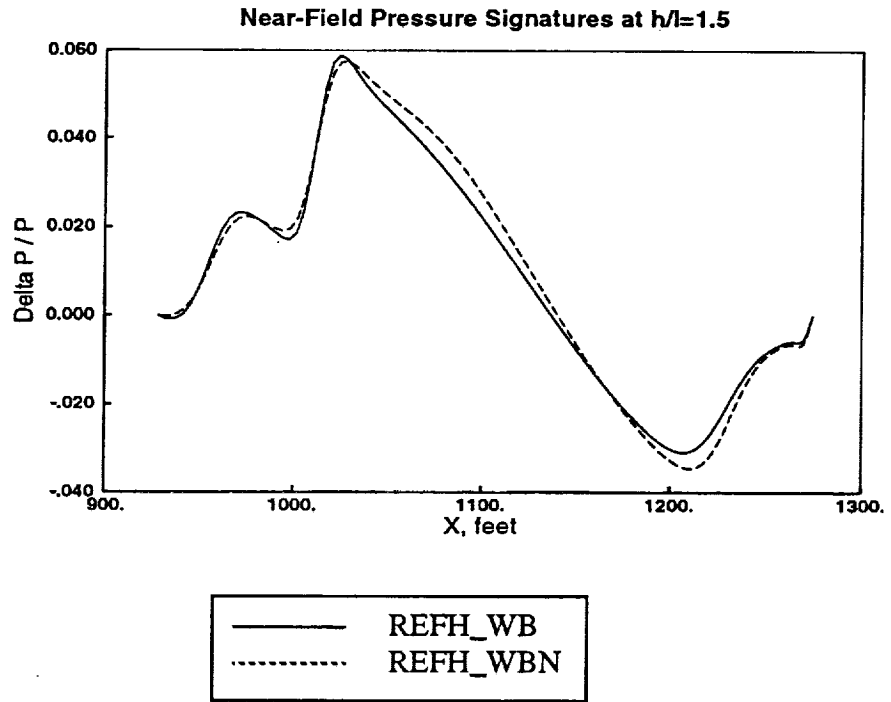


Fig. 3- Near-field and ground pressure signatures of the baseline configuration using MIM3D-SB.

Euler/Unstructured Grid Analysis of the Baseline

The sonic-boom analysis of the baseline configuration at $M=2.4$ and $\alpha=4.5^\circ$ with nacelles/pylons off (REFH_WB) and nacelle/pylons on (REFH_WBNP) using the unstructured grid methodology of USM3D/VGRID3D are considered here. The pylons in the REFH_WBNP configuration are represented as flow diverters as designed in the baseline configuration, however, both configurations are without an empennage for the sake of simplicity. Separate grids about each of the baseline configurations were generated from the IGES geometrical definition of the configurations. The grids are similar in the surface geometry, the size of the flow field, and the grid resolution. A representative surface grid of each configuration is shown in Fig. 4.

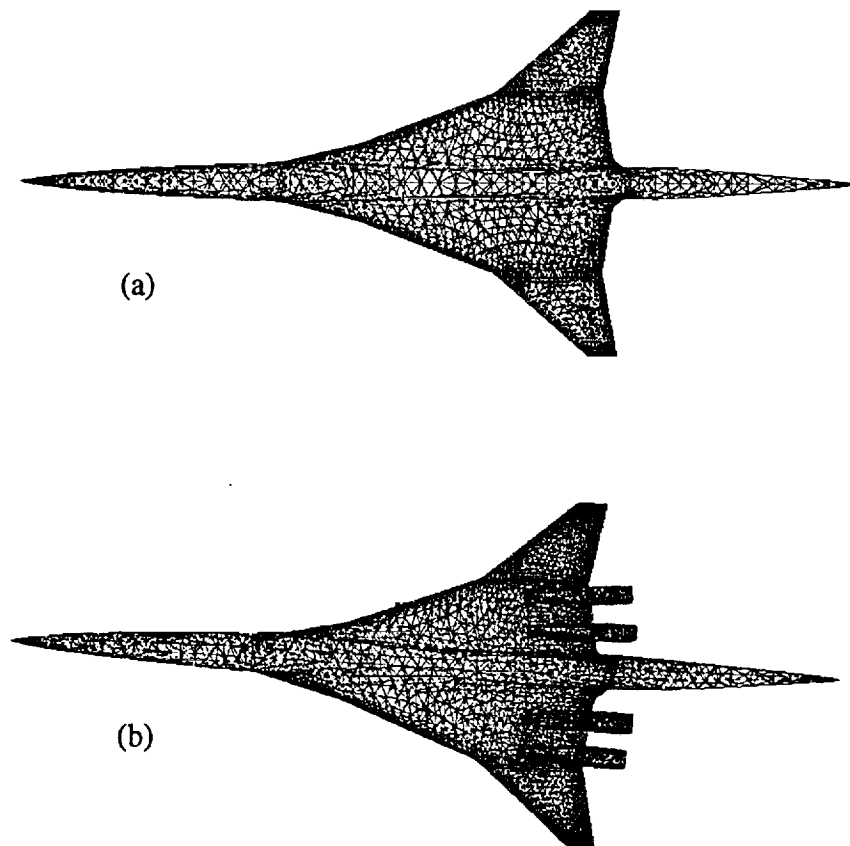


Fig. 4 - Surface grid of the baseline 1080-1122, (a) top view of REFH_WB, (b) bottom view of REFH_WBNP.

Sonic-boom grid topology which mimics the method of characteristics, with both upstream and downstream boundaries flaring out at free stream Mach angles, is used for this case. The implementation of sonic-boom grid topology in unstructured grid analysis is presented in Ref. 4. Table 1 lists the details of the grids used for each configuration.

Table 1: Grid size specifications

	REFH_WB Grid	REFH_WBNP Grid
No. of Cells	264,321	378,693
No. of Nodes	50,492	71,339
No. of Boundary Faces	20,888	26,182
No. of Boundary Nodes	10,446	13,093

The near-field pressure signatures of the REFH_WB and REFH_WBNP configurations at $h/l=0.37$ below the aircraft are compared in Fig. 5. The computed near-field pressure signatures are extracted from the three-dimensional solutions. The comparisons of the two signatures indicate a third shock (in the expansion region) and a larger magnitude tail shock for the REFH_WBN configuration. The computed near-field pressure signatures are extrapolated down to impingement on the ground using the MDBOOM code. Comparisons of the ground pressure signatures, also shown in Fig.5, indicate the effects of nacelle/pylon on the of ground boom level. as listed in Table 2.

Table 2: Predicted shock strength on the ground.

	REFH_WB	REFH_WBNP	Difference
Bow shock, psf	2.82	3.07	8.1%
Tail shock, psf	-2.51	-2.80	10.3%

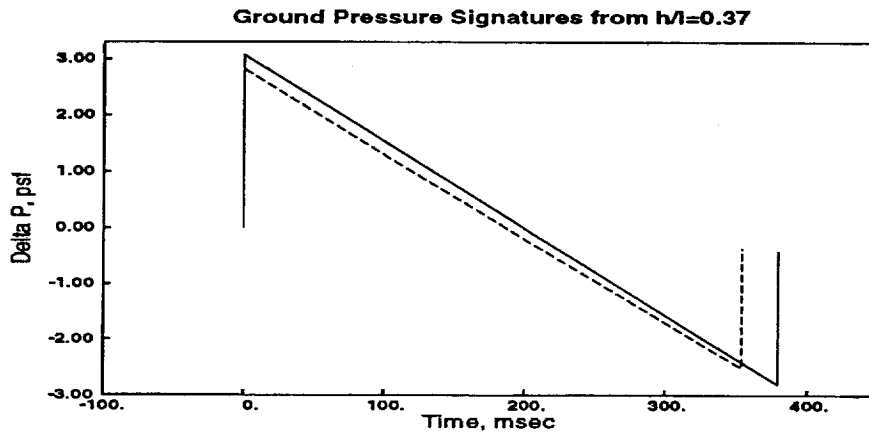
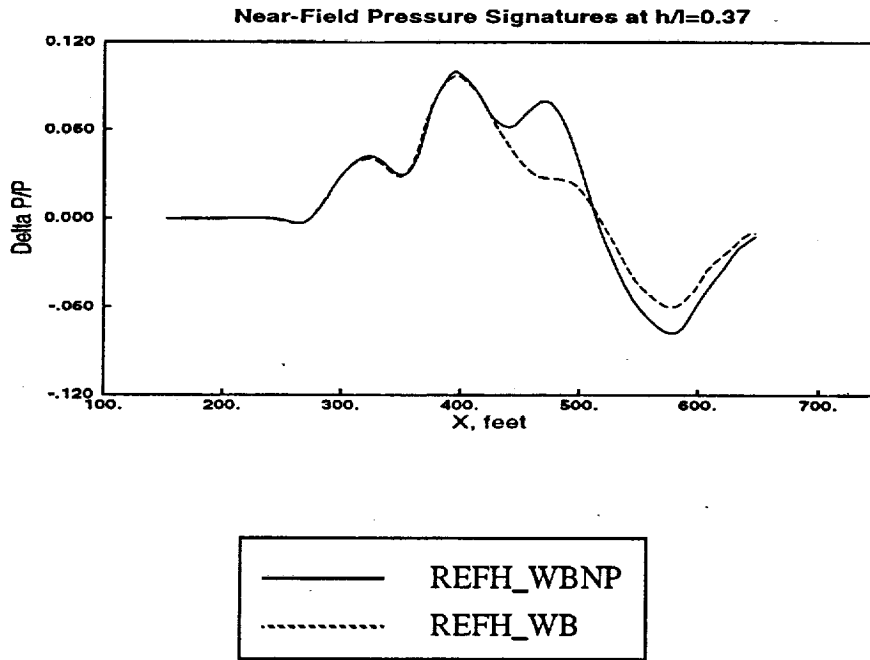


Fig. 5- Near-field and ground pressure signatures of the baseline configuration using USM3D.

The effect of pylons on the sonic-boom level on the ground was also investigated using the unstructured grid methodology. An unstructured grid was generated about the 1080-1122 baseline configuration without pylons (REFH_WBN). The grid about the REFH_WBN configuration is similar to the grid generated for the REFH_WBNP configuration and has the same grid resolution characteristics. The comparison of sonic-boom analyses of the REFH_WBNP and REFH_WBN configurations indicated a slight difference in the expansion region of the near-field pressure signatures, but similar ground pressure signatures (Fig. 6). The predicted values of the bow and the tail shocks for the REFH_WBN configuration is about 2% less than the values predicted for REFH_WBNP configuration.

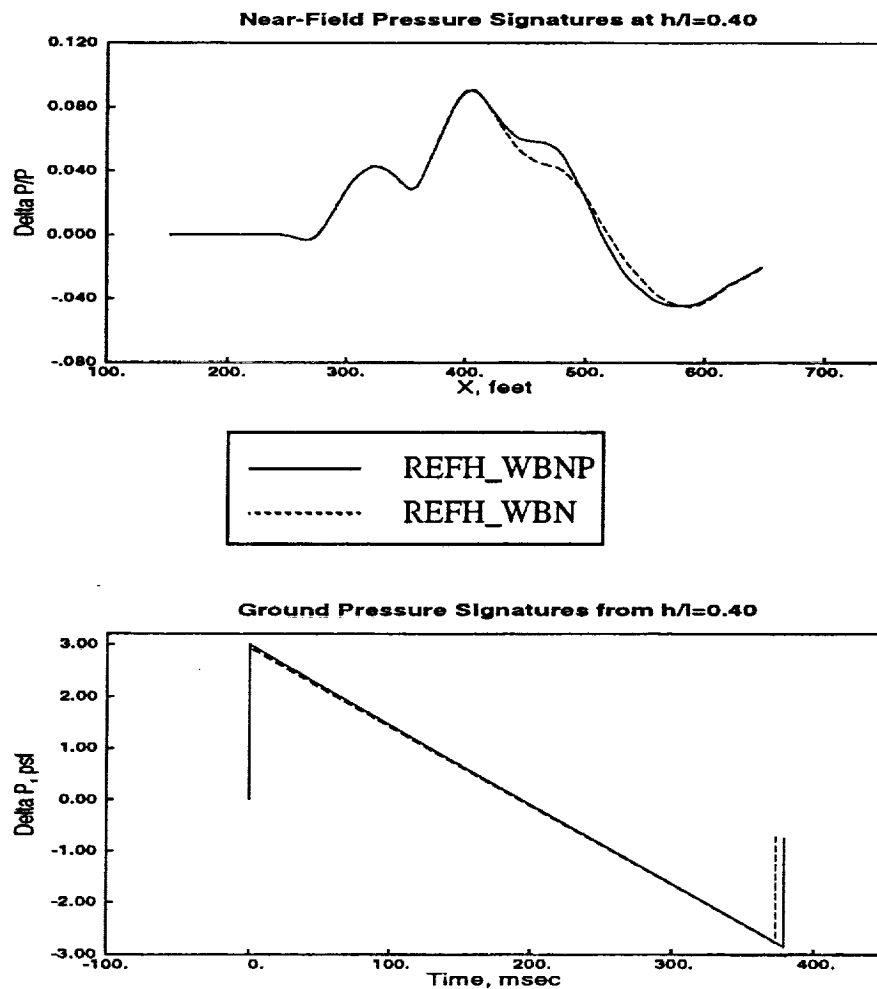


Fig. 6- Near-field and ground pressure signatures of REFH_WBNP vs. REFH_WBN.

Due to the small change in the boom level on the ground, it may be beneficial to exclude the pylons from the configuration in the sonic-boom optimization cycle. The omission of the pylons from the configuration may result in significant savings in labor connected to grid generation which may not cause a substantial alteration in the predicted values. It should be noted that the small effects of the pylon on the ground signature may be a configuration dependent phenomenon and should be investigated further.

Comparisons of Analyses form Two Euler Codes

Similar sonic-boom analyses of the baseline configuration with and without nacelles/pylons were performed using both MIM3D-SB and USM3D. The major differences between the two analyses are as follows: (1) MIM3D-SB requires the geometry input in form of the Harris Wave-Drag format which is a more coarse representation than the IGES format used by USM3D; (2) Due to the marching nature of MIM3D, a finer grid can be generated and utilized by this method than the grid used by USM3D; (3) Engine integration capability of MIM3D-SB currently only allows for axisymmetric nacelles and a thin plate in place of the pylon; (4) The configuration used in MIM3D-SB is modified to represent a sting-mounted model for the ease of grid generation and analysis (Ref. 5-7).

Comparisons of the pressure signatures of the REFH_WB and REFH_WBNP configurations are presented in Fig. 8 (a-c). The comparisons of signatures in Fig. 7 include the near-field pressure signatures of REFH_WB at the distance of $h/l=0.37$ where the signatures are extracted directly from the three-dimensional solutions. The comparison of the two signatures indicates more shock smearing by USM3D and the values of the overpressure peaks slightly underpredicted as compared with values computed by MIM3D-SB. On the other hand, a bigger pressure expansion and a small flat section in the expansion regions is predicted by USM3D. The comparisons of the ground pressure signatures extrapolated using MDBOOM indicate that initial overpressure peaks of similar magnitude are predicted by both codes while MIM3D-SB predicted signature has a smaller tail shock and a shorter length. This may be due to the sting-mounted model used for MIM3D-SB analysis. It is apparent from these comparisons that adequate sonic-boom predictions are possible from both codes. MIM3D-SB analysis is well-suited for configurations which only the Wave-Drag format definition of the geometry is available; when detailed modeling of the configuration such wing-nacelle-pylon interference is required, the analysis may call for USM3D.

The nose and wing shocks predictions by USM3D may be improved using better surface modeling in the grid generation process. Other improvements to minimize the shock smearing by USM3D should also be investigated.

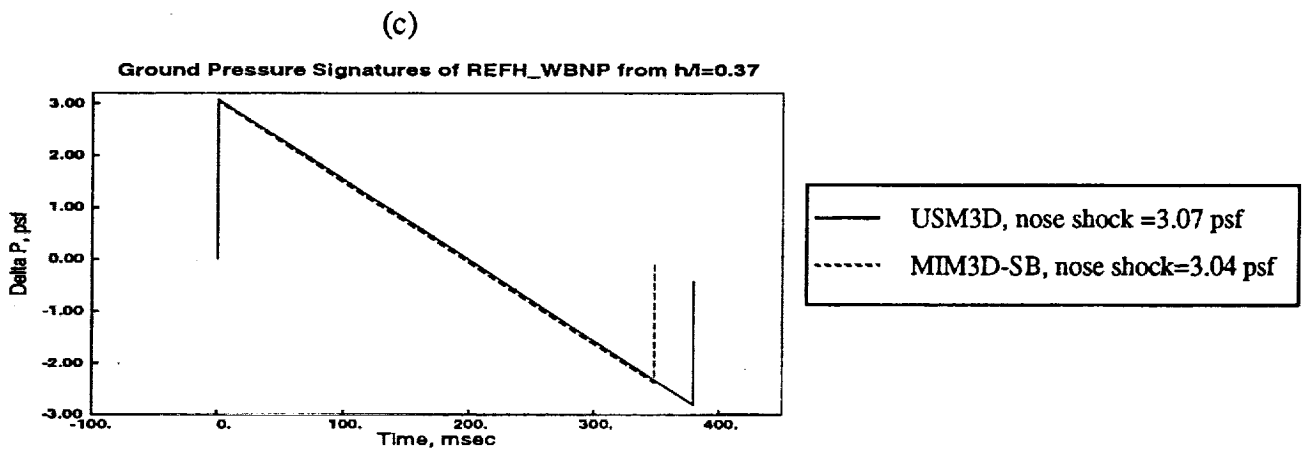
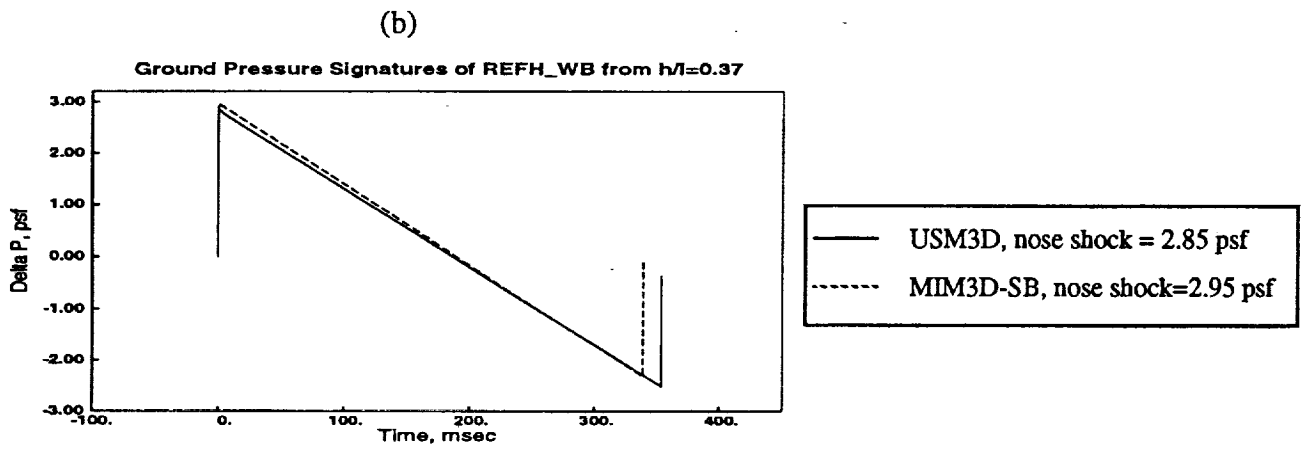
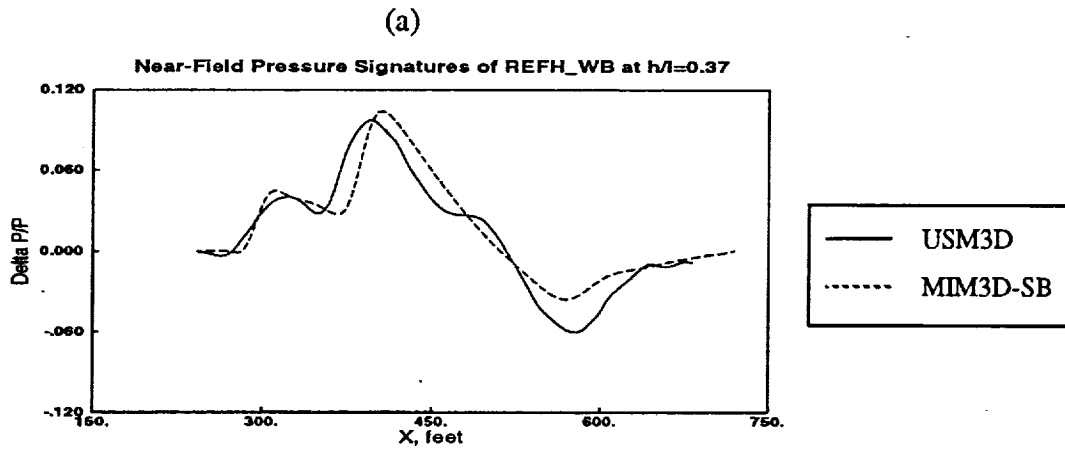


Fig. 7- Comparisons of pressure signatures of obtained using USM3D and MIM3D-SB.

Comparison of Two Propagation Codes

In propagation codes, near-field pressure signatures which are extracted from the three-dimensional solutions are extrapolated to the ground using modified linear theory. An attempt was made here to investigate the effect of the propagation code in sonic boom analysis by examining the two widely used methods of MDBOOM and THOMAS codes. In the present study, the near-field pressure field of the baseline HSCT configuration obtained using MIM3D-SB code is extrapolated to the ground using MDBOOM and THOMAS codes.

The computations were performed for a cruise Mach number of 2.4 and cruise angle of attack of 4.5° . The near-field pressure fields were extracted at four different separation distances of $h/l=0.25, 0.5, 1.0,$ and 2.0 and extrapolated to the ground. The comparisons of the ground signatures using both codes are presented in Fig. 8.

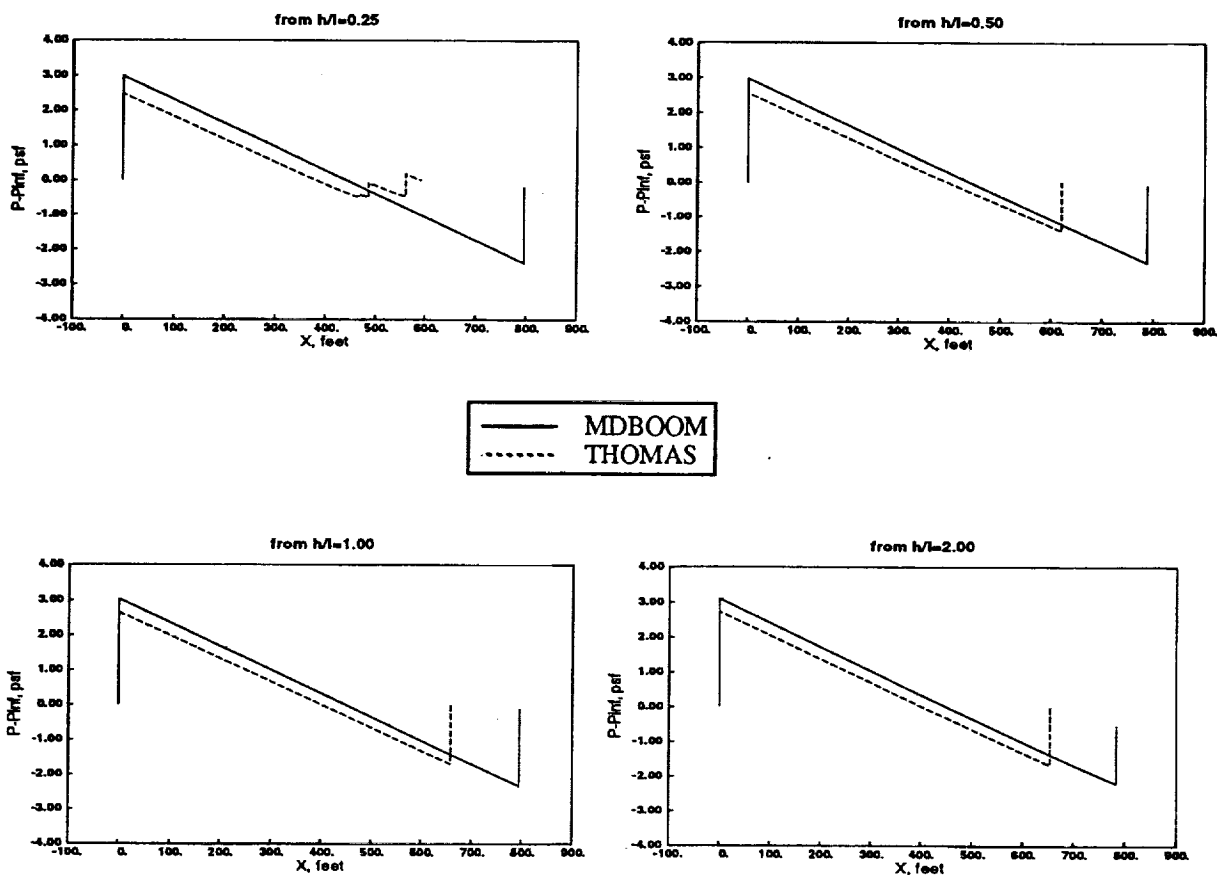


Fig. 8- Comparison of the ground pressure signatures of the baseline configuration, MDBOOM vs. THOMAS.

The comparisons show that the Thomas code extrapolated signatures are shorter in duration and have smaller pressure shock magnitude than signatures extrapolated by MDBOOM. The values of the overpressure shocks and the length of the ground signatures are listed in Table 3. The comparison of ground signatures using MDBOOM shows that the lowest initial overpressure peak was predicted when extrapolated from $h/l=0.25$ and the highest from $h/l=2.0$ with the difference between the two shocks about 3.8%. The comparison of the signatures using the Thomas code also shows the same trend but with a difference of 9.5%. Hence, as expected, the Thomas code shows greater sensitivity to separation distance than MDBOOM.

Table 3 - Comparison of ground pressure signatures using two propagation codes.

(a) Bow shock level, psf

	$h/l=0.25$	$h/l=0.5$	$h/l=1.0$	$h/l=2.0$
MDBOOM	2.97	2.98	3.03	3.09
THOMAS	2.47	2.55	2.65	2.73

(b) Tail shock level, psf

	$h/l=0.25$	$h/l=0.5$	$h/l=1.0$	$h/l=2.0$
MDBOOM	-2.3	-2.30	-2.32	-2.20
THOMAS	-0.47	-1.39	-1.69	-1.67

(c) Signature length, feet

	$h/l=0.25$	$h/l=0.5$	$h/l=1.0$	$h/l=2.0$
MDBOOM	796.1	787.3	795.3	783.3
THOMAS	591.1	620.0	659.0	653.0

Softening Through Fuselage Camber Modification

Sonic-boom softening solely based on modifications of the fuselage camber of the baseline configuration is discussed in this section. Two different sets of modifications to the fuselage were considered in the present study. The first modification set, Case 1, is focused primarily on the forebody camber; the focus of the second set, Case 2, is concentrated on the fuselage segment from the nose to the wing trailing edge-fuselage junction. The main objective for both cases is to reduce or “soften” the sonic boom level on the ground by minimizing the initial overpressure peak on the ground, P_{\max} . This objective is achieved by varying the camber distributions of the fuselage which is described herein by a cubic spline with a number of control points and with matched first and second derivatives. In the present optimization study and for both cases, the maximum overpressure in the ground signature, P_{\max} , is considered the objective function and the control points in the cubic spline which describes the fuselage camber are designated as the design variables (Fig. 9). Each set of variables results in a new cubic spline, hence, a new forebody camber. With each new camber, the new geometry is generated automatically in MIM3DES and then analyzed to obtain P_{\max} of the new configuration. The new P_{\max} is compared with the value of the previous configuration. If the new P_{\max} is lower then the changes to the configuration continues in the same direction until the P_{\max} or the objective becomes less than a preset value. For Case 1, several attempts were made at modifying the camber distributions by specifying different cubic spline control points or design variables with different constraints on variations of these variables. None of the forebody camber distributions generated in Case 1 provided any significant reduction in the sonic boom level on the ground without adversely affecting the drag coefficient; therefore, forebody camber modification was abandoned as a tool for the sonic-boom minimization.

In the second case, which involved the fuselage from nose to wing trailing edge junction, care was taken in specifying the constraints so as not to allow the fuselage camber to grow unbounded and to keep the wing roots within the fuselage. For the second case, P_{\max} and the control points of the cubic spline were designated as the objective function and the design variables, respectively (Fig. 9). From a number of attempts at modifying the fuselage, two candidate camber distributions emerged which showed improvement in the sonic boom level. The camber distribution of the baseline and the two new candidate configurations dubbed FUSE_MOD1 and FUSE_MOD2 are presented in Fig. 9. The comparison of the ground pressure signatures for all three configurations are shown in Fig. 10. The two candidate configurations show reductions of about 3% in the P_{\max} value over the baseline configuration along with lower lift coefficients. The reductions in P_{\max} are achieved only at the reduced lift coefficients listed in Table 4. These improvements were nullified when the angle of attack was increased to achieve the original lift coefficient.

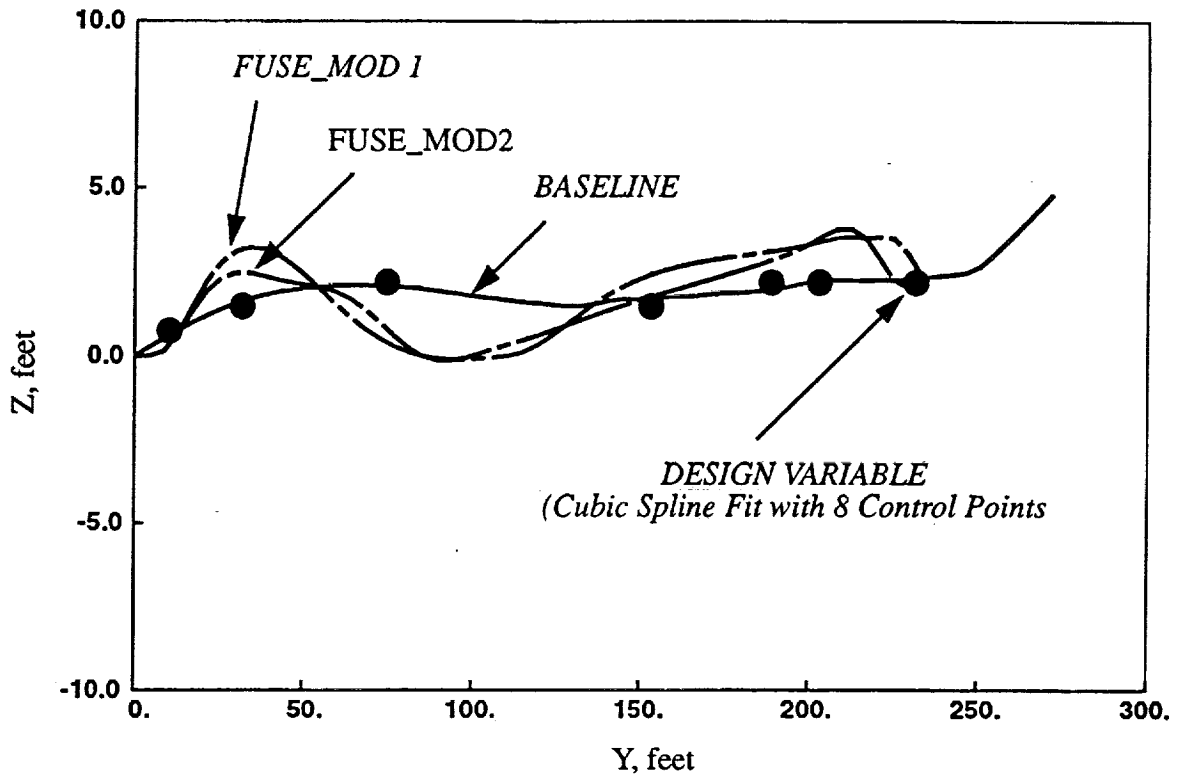


Fig. 9- Fuselage camber distributions of baseline and modified configurations of Case 2.

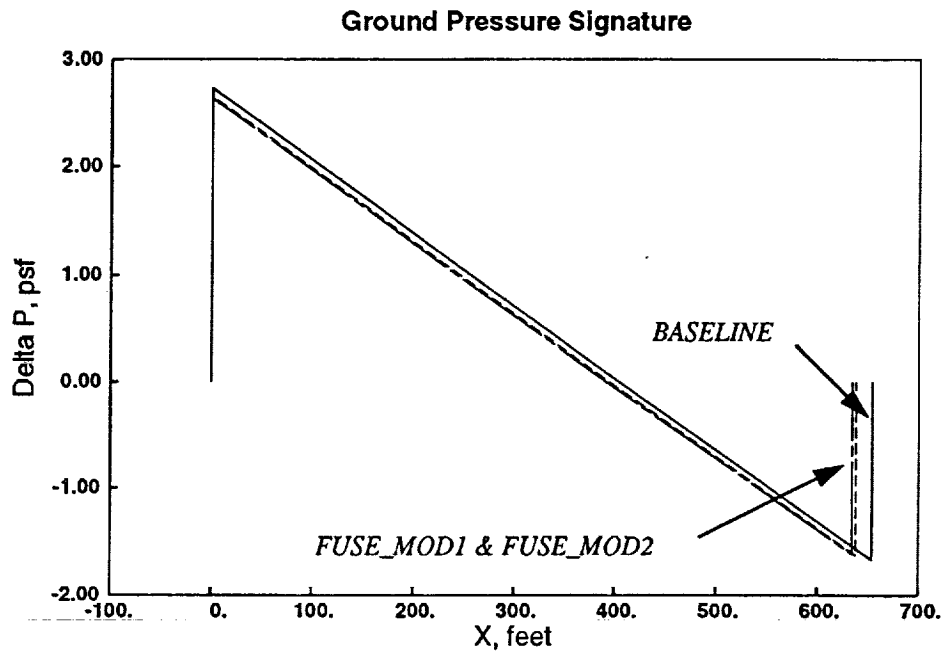


Fig. 10- Comparisons of the ground pressure signatures of baseline with two fuselage-modified candidates

Table 4 - Comparisons of P_{max} and force coefficients of the baseline with two fuselage-modified configurations.

CONFIGURATION	P_{max} , psf	C_L	C_D
BASELINE	2.73	0.1134	0.0097
FUSE_MOD1	2.64	0.1053	0.0097
FUSE_MOD2	2.63	0.1025	0.0097

Based on results presented in Fig. 10 and Table 4, it is apparent that softening through fuselage camber modifications should not be pursued further for this particular configuration.

Softening Through Wing Dihedral Modification

The procedure for softening attempts through wing dihedral modifications is similar to the one described in the previous section. The initial overpressure peak, P_{max} , is once again chosen as the objective function. In the present study, the modification to the wing dihedral is initially performed on the wing leading edge and then extended to the entire wing. The wing in the Harris wave-drag geometry definition is defined by a number of airfoils stacked in the spanwise direction. Also listed in this definition are the coordinates of the leading edge point of each airfoil along with the chord length of that airfoil. Therefore, a cubic spline fit with several control points can be used to describe the wing leading edge curve. For the present optimization process, the control points with given upper and lower limits in the vertical direction are the design variables with limits as their constraints. From each set of design variables, a new cubic spline fit is obtained from which the new position of leading edge points can be interpolated. Due to the constraints placed on the dihedral modification, the new position of each wing leading edge point should indicate the translation of that point only in the vertical direction. All the other points on the airfoil positioned at the same spanwise location of each leading edge point are then translated vertically along with the leading edge point. This type of dihedral modification allows for no change in the thickness and camber of the airfoils.

The leading edge curve of baseline_1122 along with the design variables are shown in Fig. 11. Also, presented in Fig. 11 is the leading edge curve of the modified configuration dubbed here as DIH_MOD. The comparisons of ground pressure signatures of the baseline and DIH_MOD is presented in Fig. 12.

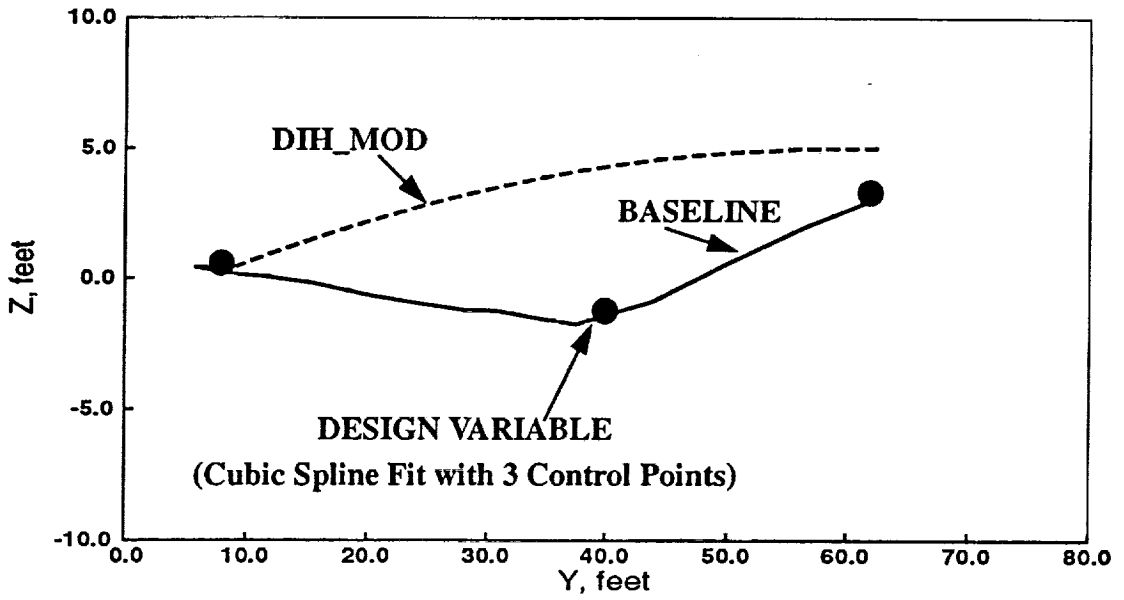


Fig. 11- Wing dihedral distributions of baseline and modified configuration.

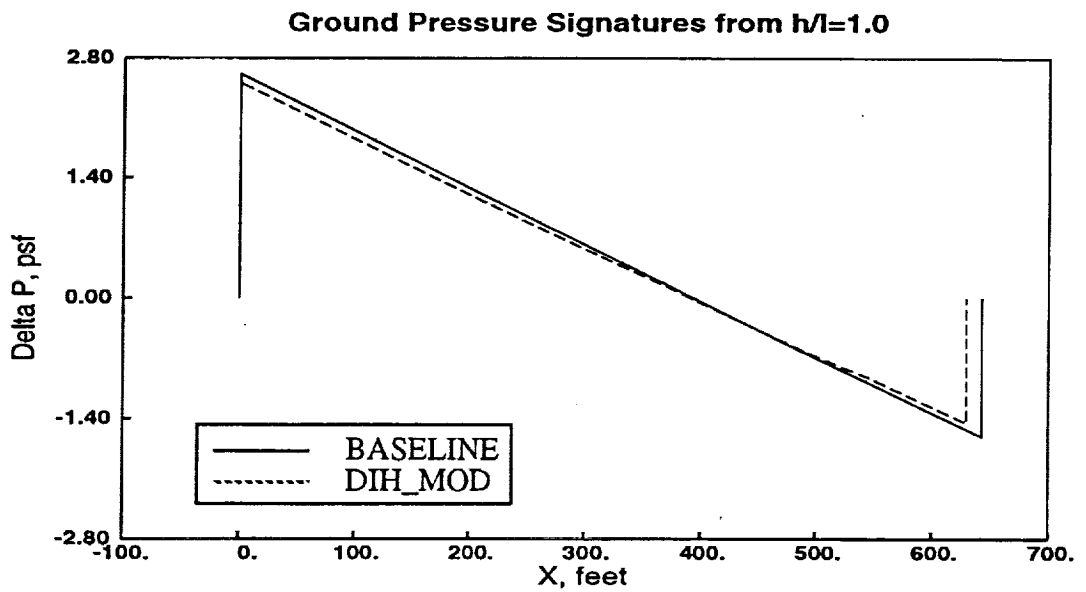


Fig. 12- Comparisons of the ground pressure signatures of baseline and the modified configuration.

The angle of attack for the aerodynamic and sonic-boom analyses of the baseline configuration is set to 4.0 °. The values of the bow and tail shocks of the ground pressure signatures of the baseline configuration is listed in Table 5. Also listed in Table 5 are the computed force coefficients of the baseline configuration. The angle of attack for DIH_MOD configuration, however, was increased to 4.04 ° to obtain the same lift coefficient as the baseline configuration. The levels of bow and tail shocks and the force coefficients for DIH_MOD configurations are also listed in Table 5. The comparisons of the results indicate that for conditions that produce similar force coefficients, the DIH_MOD is predicted to produce a ground signature which is about 4% lower in bow shock than the baseline configuration.

Table 5 - Comparisons of baseline and DIH_MOD.

CONFIGURATION	Bow Shock, psf	C _L	C _D
BASELINE	2.61	0.1056	0.0092
DIH_MOD	2.50	0.1058	0.0091

There were several other dihedral shapes designed by the softening team which the sonic-boom analysis of the corresponding softened configurations indicated similar or even more significant improvement in the ground sonic-boom level compared to the baseline configuration (Refs. 12-13). Therefore, it becomes apparent that the dihedral modification can be an important tool for the softening purposes.

It is important to further investigate the physical phenomena behind the dihedral modification which produces such significant sonic boom improvements. The comparisons of crossflow-normalized pressure contours on the wing at several axial stations of the baseline and DIH_MOD configurations are presented in Fig. 13. The darker shades represent the higher pressure regions. The lower magnitude of the ground sonic boom level of the modified configuration compared to the baseline may be explained by the lower pressure region on the lower side of the wing. The propagation of the shock below the aircraft is clearly shown at Stations X=170 ft. and X=190 ft.; however, the pressure is also lower on the upper side of the modified configuration which may explain why both configurations have similar lift coefficients.

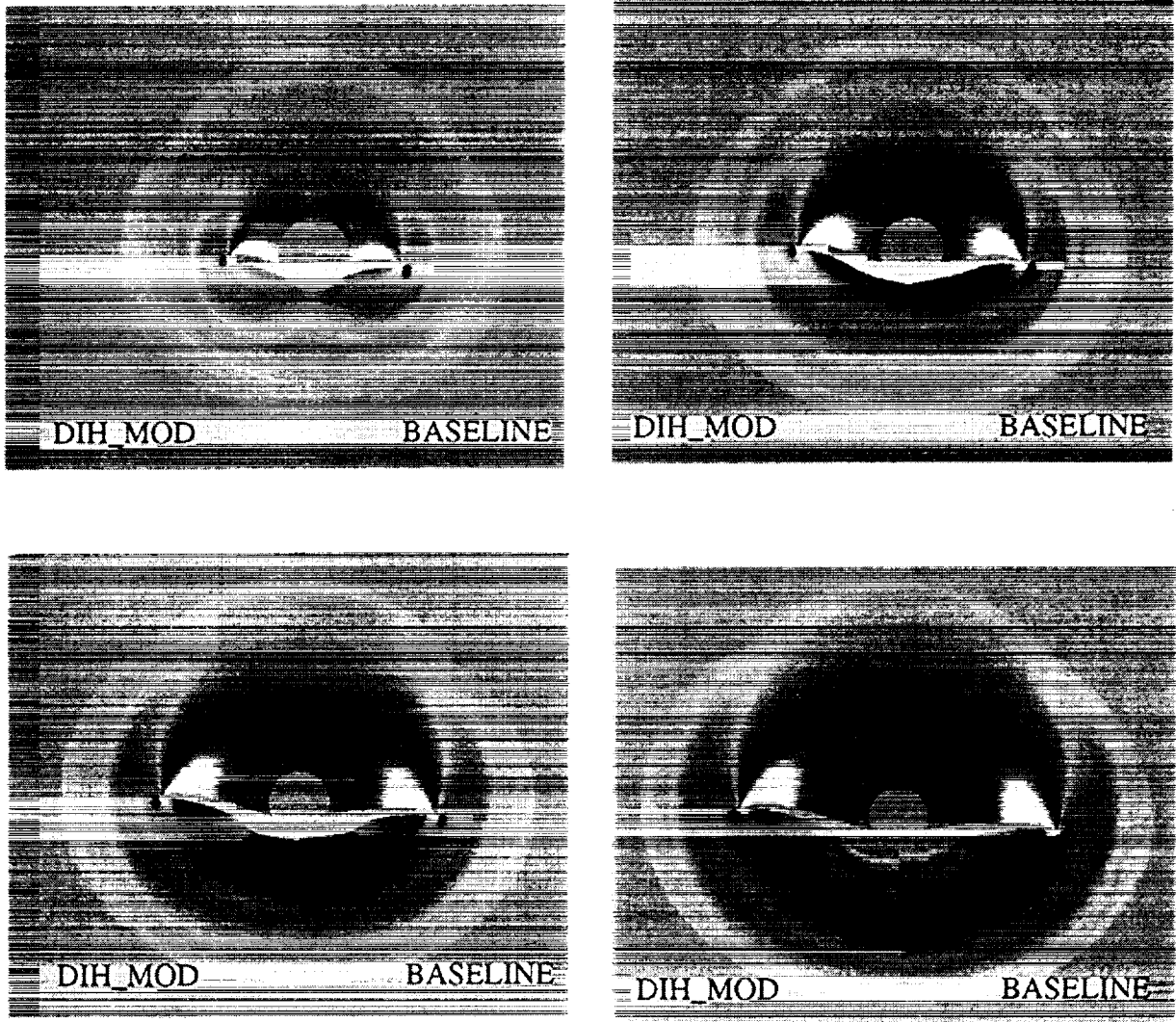


Fig. 13- Normalized pressure contours of the baseline and DIH_MOD configurations.

The crossflow Mach number contours for both configurations are presented in Fig. 14. The darker shades represent higher Mach number regions. The comparisons of the contours in Fig. 14 indicate the higher flow speed near the wing of the modified configuration which is mainly due to higher spanwise components of the velocity near the wing. It is believed that the shape of wing in the modified configuration allows for the flow to accelerate toward the outboard direction, resulting in the higher Mach number. The higher Mach number region is primarily responsible for the lower pressure region near the wing.

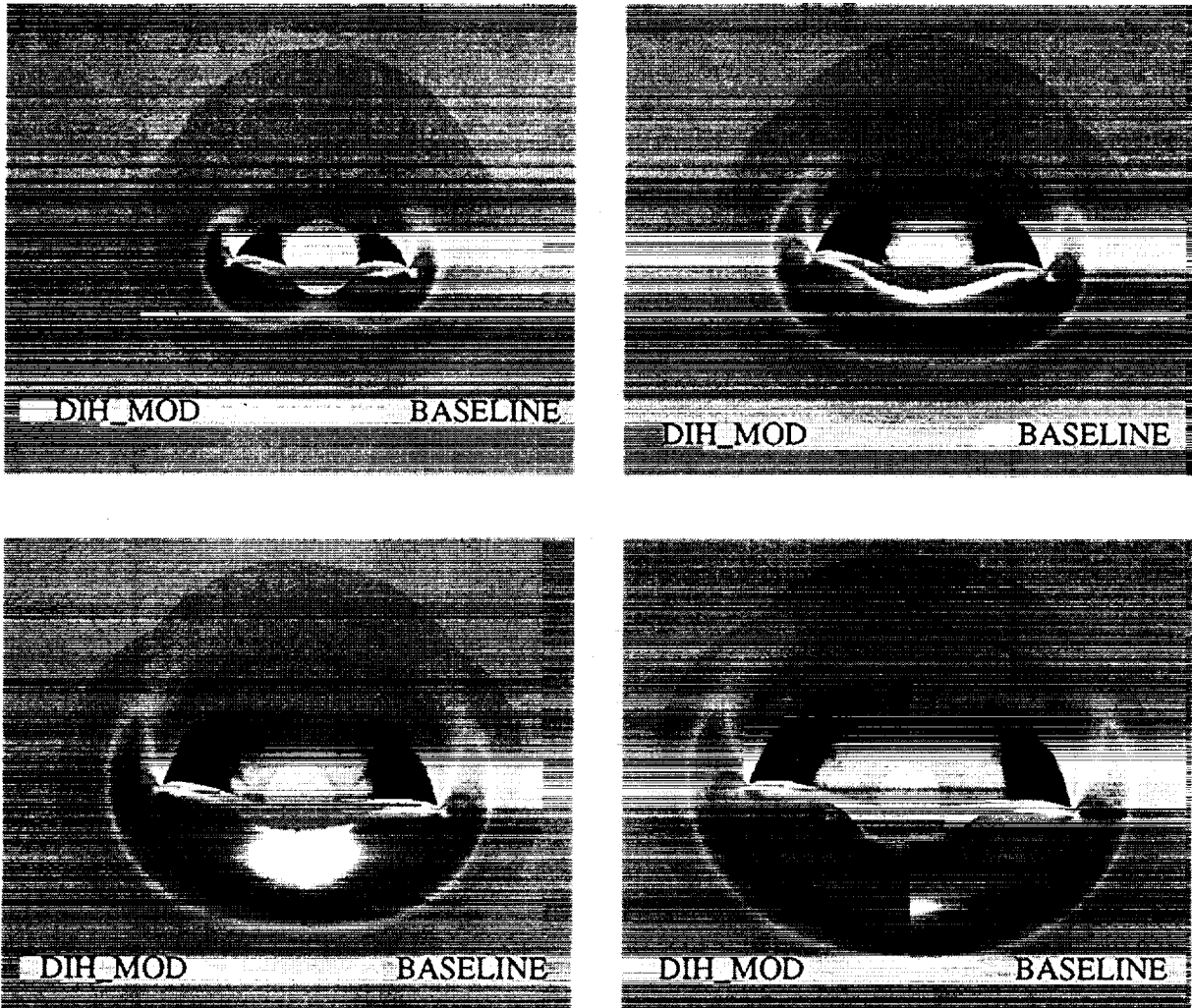


Fig. 14- Mach number contours of the baseline and DIH_MOD configurations.

It should be noted that the wing dihedral optimization was performed on the wing-body alone configuration since analysis of wing-body-nacelle configuration is more computational intensive and at this time cost prohibitive. The important effects of the nacelle-wing interference on the ground signature is not included in the redesign process until the subsequent analysis of the wing-body-nacelle configuration. This makes the process cumbersome and less than optimum. Further improvement to the efficiency of the analysis code is therefore needed for a more automated optimization process.

Sonic-Boom Analysis of the Proposed Softened Configuration

A set of geometric modifications for the sonic-boom softening of the Boeing HSCT was established based on the efforts of the present study and the efforts of the other members of the Boeing Softening Team. The details of the modifications performed on the Boeing HSCT baseline (1080-1405) are presented in Ref. 12. The modified-linear theory sonic-boom analyses of the baseline 1080_1405 and its sonic-boom softened version 1080_1444, proposed by the Boeing Softening Team, are also presented in Ref. 12. The schematics of both configurations are presented in Fig. 15.

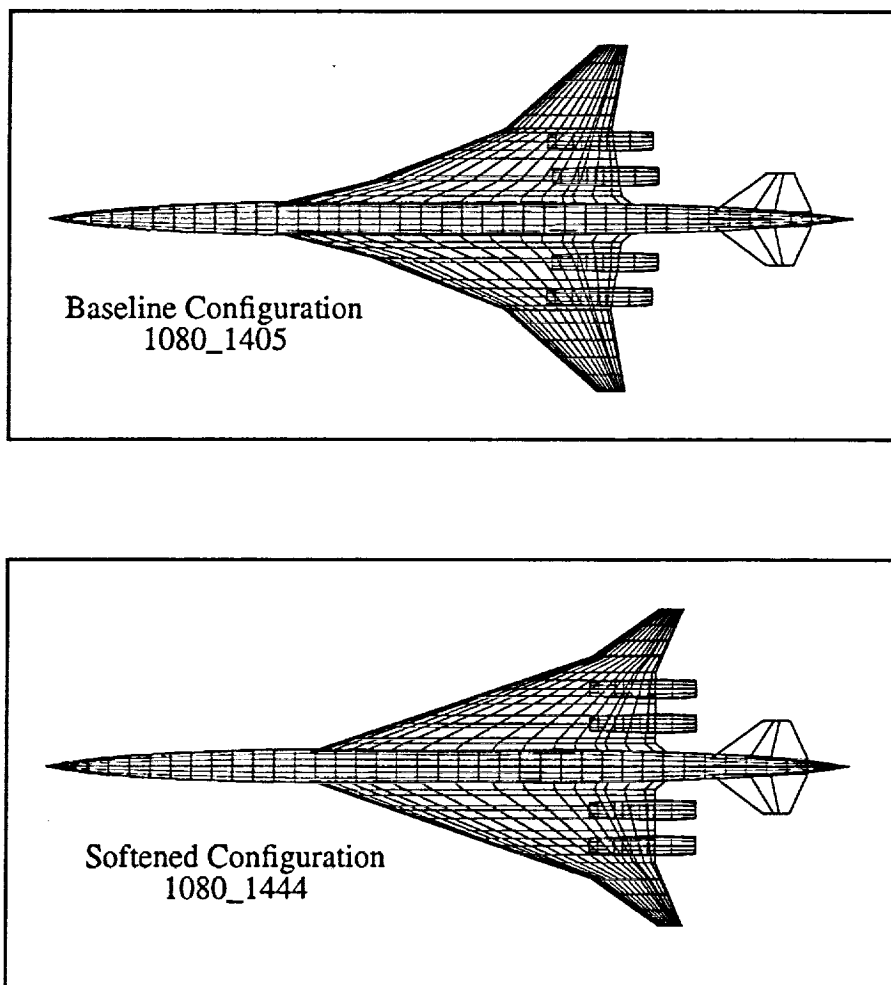


Fig. 15 - Top views of the Boeing 1080_1405 baseline and 1080_1444 softened configurations

The baseline and the softened configurations are designed for start-cruise condition of freestream Mach number 2.4. The flight altitude for 1080_1405 and 1080_1444 are 53,590 ft. and 55,300 ft., respectively. Both aircraft are 314 ft. long with the wing reference area of 8500 ft.². The design lift coefficients are 0.0903 for baseline configuration and 0.1026 for the softened configuration.

Preliminary aerodynamic analysis runs to obtain the correct angle of attack corresponding to the designed C_L yielded $\alpha = 4.1^\circ$ for the baseline configuration and $\alpha = 4.0^\circ$ for the softened configuration. The sonic-boom analyses of the both configurations using MIM3D-SB code were then performed and the ground pressure signatures compared in Fig. 16. The computed near-field pressure signatures were extrapolated from $h/l=1.0$ to the ground using MDBOOM code. The levels of bow shock on the ground are listed in Table 6.

Table 6 - Comparisons of the baseline 1080_1405 and the softened 1080_1444 configurations.

	1080_1405	1080_1444	Reduction
Bow Shock	2.93	2.60	11.2%

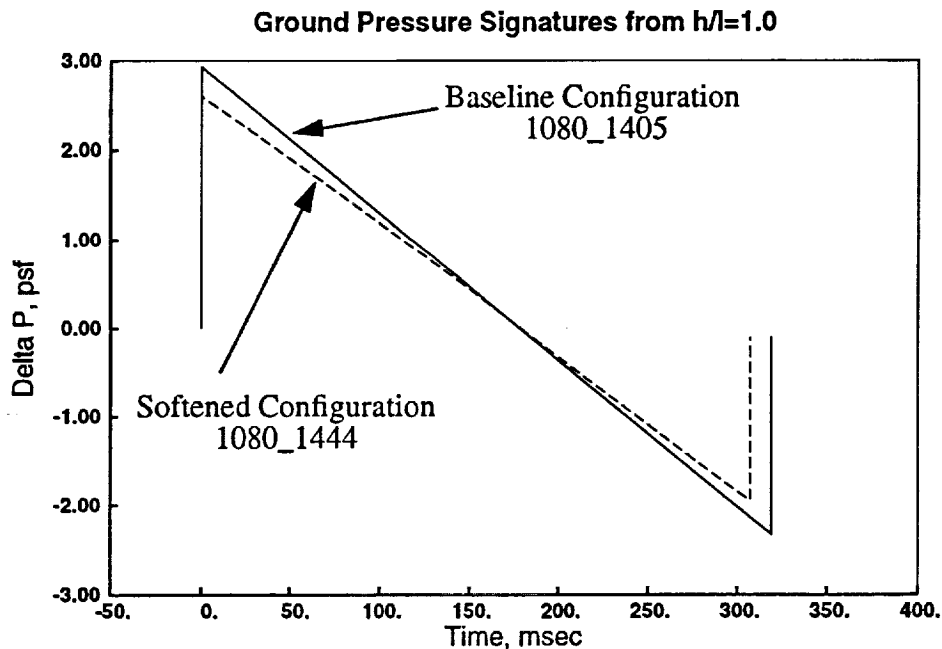


Fig. 16 - Comparisons of the ground pressure signatures of the final baseline and the softened configurations.

CONCLUDING REMARKS

NASA Langley's computational efforts in sonic-boom softening of the Boeing 1080-1122 baseline concept were presented. In these efforts, an optimization process using an Euler CFD method was employed to reduce the ground boom of the baseline through fuselage camber and wing dihedral modifications. The study also included aerodynamic and sonic-boom analyses of the baseline and some of the proposed "softened" configurations.

The comparisons of two Euler methodologies, USM3D and MIM3D-SB, for sonic-boom analysis were presented. The comparisons of the near-field signatures indicate differences in the shock magnitudes and in the expansion region; however, the two codes demonstrated 1% precision in the far-field for this configuration.

Two different wave propagation codes, MDBOOM and Thomas, were also compared. The comparison indicated that shorter length signatures and smaller pressure shock magnitudes on the ground are predicted by the Thomas code. As expected, the Thomas code shows a great deal of sensitivity to the separation distance. On the other hand, the separation distance plays a minor role on the sonic-boom level on the ground predicted by MDBOOM. Therefore, with MDBOOM, smaller separation distances and reasonable size computational fields can be used for the sonic-boom analysis. Further comparisons of signatures extrapolated by the propagation codes and flight test measured data are needed for the accuracy assessment of these codes.

The study was also extended to investigate the effects of the pylons on the sonic-boom level on the ground. The study showed that for the present baseline configuration, pylon has a small effect on the ground signature. Therefore, one may be persuaded to exclude the pylons from the configuration in the optimization cycle. The omission of pylon may result in significant reduction in labor connected to grid generation which may not cause a substantial alteration in the optimum values. The effects of pylon on ground signatures may be a configuration dependent phenomena and should be investigated further.

A CFD optimization technique was used for the sonic-boom minimization of the baseline configuration through fuselage camber and wing dihedral modifications. For fuselage camber modification cases, the softened candidates showed a reduction in the initial overpressure peak on the ground at lower lift coefficients but no reduction was achieved when a constraint was placed to maintain the lift. The optimization process worked better for wing dihedral modification cases where the study resulted in a softened configuration with a lower ground boom and without any aerodynamics penalties. The optimization process can be improved by addition of the MDBOOM propagation capability. Also, efficient nacelle integration is also needed to reduce the complexity of the design optimization process by deleting the step where sonic-boom analysis of the wing-body-nacelle configuration is performed after the configuration is optimized.

Finally, sonic-boom analyses of the final baseline configuration selected by the Boeing softening team and the softened configuration proposed by that team were performed. The softened configuration was predicted to produce a bow shock about 11.2% lower than the baseline configuration.

ACKNOWLEDGMENT

This work is supported under NASA Contract No. NAS1-19000. The technical monitor is D. Baize. Helpful discussions with the Boeing Softening Team members G. Haglund (Boeing), D. Baize (NASA Langley), S. Cheung (MCAT Institute), and E. Tu (NASA Ames) are appreciated. The author would also like to thank M. Siclari (Northrup-Grumman), J. Samareh (CSC-NASA Langley) and N. Bean (CSC-NASA Langley) for helpful discussions and their assistance with surface geometry and grid generation.

REFERENCES

1. Darden, C.: Progress in Sonic-Boom Understanding: Lessons Learned and Next Steps, High Speed Research: 1994 Sonic Boom Workshop, NASA/CP-1999-209699, December 1999.
2. Frink, N., Parikh, P., and Pirzadeh, S.: A Fast Upwind Solver for the Euler Equations on Three-Dimensional Unstructured Meshes, AIAA Paper No. 91-0102, January 1991.
3. Pirzadeh, S.: Recent Progress in Unstructured Grid Generation, AIAA Paper No. 92-0445, January 1992.
4. Fouladi, K.: Unstructured Grids for Sonic-Boom Analysis Applications, AIAA Paper No. 2929, July, 1993.
5. Siclari, M. J. and Darden, C. M.: CFD Predictions of the Near-Field Sonic Boom Environment for Two Low-Boom HSCT configuration, AIAA Paper No. 91-1631, June 1991.
6. Fouladi, K.: CFD Predictions of Near-Field Pressure Signatures of a Low-Boom Aircraft, High-Speed Research: Sonic Boom, NASA CP 3173, February 1992.
7. Siclari, M., Fouladi, K.: A CFD Study of Component Configuration Effects on the Sonic Boom of Several High-Speed Civil Transport Concepts, NASA High-Speed Research:

Sonic Boom workshop, NASA CP-10132, May 1993.

8. Plotkin, K.: Calculation of Sonic Boom From Numerical Flow Field Solutions: MDBOOM Version 2.2, Wyle Research Report WR 92-14, July 1992.
9. Thomas, C.: Extrapolation of Sonic Boom Pressure Signature by the Waveform Parameter Method. NASA TN D-6832, June 1972.
10. Siclari, M. J.: The Analysis and Design of Low Boom Configurations Using CFD and Numerical Optimization Techniques, High Speed Research: 1994 Sonic Boom Workshop, NASA/CP-1999-209699, December 1999.
11. Gill, P.M., et. al.: User's Guide for NPSOL; A Fortran Package for Nonlinear Programming, Technical Report SOL 86-2, Stanford University, January 1986.
12. Haglund, G. T.: Potential for Sonic Boom Reduction of the Boeing HSCT, High Speed Research: 1995 Sonic Boom Workshop, NASA/CP-1999-209520, December 1999.
13. Cheung, S., et. al: Sonic boom Minimization Efforts on Boeing HSCT, High Speed Research: 1995 Sonic Boom Workshop, NASA/CP-1999-209520, December 1999.

Introduction

A team was formed to tackle the sonic boom softening issues of the current Boeing HSCT design. The team consisted of personnels from NASA Ames, NASA Langley, and Boeing company. The work described in this paper was done when the first author was at NASA Ames Research Center.

This paper presents the sonic boom softening work on two Boeing HSCT baseline configurations, Ref-H and Boeing-1122. This presentation can be divided into two parts: parametric studies and sonic boom minimization by CFD optimization routines.

Although Mr. Dan Baize is not in the author list, he provides valuable suggestions and leadership during the period of the study.

■ SAMSON CHEUNG ■

Sonic Boom Minimization Efforts on Boeing HSCT Baseline

**Samson Cheung (MDA), Kamran Fouladi (NASA Langley),
George Haglund (Boeing), and Eugene Tu (NASA Ames)**

**Sonic Boom Workshop
NASA Langley Research Center
September 12-13, 1995**

The outline of this paper is shown below. First is the objectives of this paper. Then a brief description of the CFD tools that used in this study followed by the results from parametric studies of wing sweeps and wing dihedral. The results of sonic boom minimization on a wing/body configuration will be presented followed by a conclusion.

■ SAMSON CHEUNG ■

Outline

- **Objectives**
- **CFD Tools and Methodology**
- **Inboard Leading-Edge Sweep Study**
- **Outboard Leading-Edge Sweep Study**
- **Wing Dihedral Study**
- **Wing Dihedral Optimization**
- **Conclusion**

The objectives of this study are stated in the viewgraph below.

In this presentation, the results of nose camber study will not be shown. Those results are presented in the paper titled "Langley's Computational Efforts in Sonic-Boom Softening of the Boeing 1080-1122 Concept."

■ SAMSON CHEUNG ■

Objectives

- **Study effects on HSCT sonic boom with different wing geometric parameters**
 - Wing sweep, Nose camber, Wing dihedral...
- **Make use of the CFD optimization tools to explore better methods for sonic boom softening**

Most of the CFD tools and methodology used in this paper have been developed in the previous year and also presented in the previous workshops. For sonic boom prediction, only inviscid calculations are needed. A space-marching scheme would be ideal for sonic boom calculation for its efficiency and due to the nature of supersonic flow. However, the geometry complicity and the occurrence of subsonic flow near the wing/body/nacelle region require a time-iterative scheme that is normally less efficient than a space-marching scheme.

Combining the two CFD codes, a space-march code (UPS3D) and a time-iterative code (OVERFLOW), developed at NASA Ames Research Center, can provide an efficient and accurate sonic boom prediction code complex. The code complex is supported by the overset grid method and a hyperbolic grid generator. The force integration routine, OVERINT, can provide accurate force and moment calculation for this type of hybrid calculation.

While the CFD code complex calculation provides the near-field solution, the mid-field solution is calculated by a very efficient axisymmetric Euler solver (WPSYM) based on method of characteristics. The sonic boom at the ground (far-field) is calculated by linear method based on Whitham F-function developed a couple of decades ago.

An optimization routine, NPSOL, is used for sonic boom minimization.

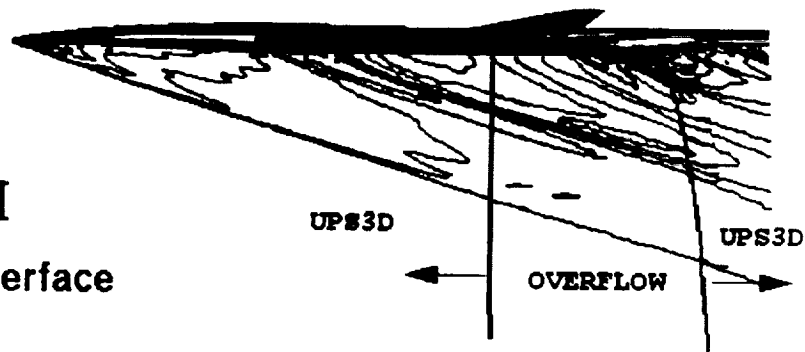
■ SAMSON CHEUNG ■

CFD Tools and Methodology

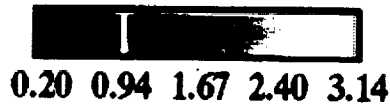
- **OVERFLOW / UPS3D code complex (hybrid)**
 - time- iterative and space-marching Euler calculations
- **Overset Grid / Hyperbolic grid generator**
- **Zip-Grid: OVERINT**
- **Boom extrapolation:**
 - WPSYM (Mid-field axisymmetric Euler solver)
 - F-Function (Far-field extrapolation code)
- **Optimizer NPSOL**

The figure below shows the CFD code complex (UPS3D/OVERFLOW) applied to solve the Boeing Ref-H wing/body/nacelle configuration. The continuity of the pressure contour lines indicates the UPS3D/OVERFLOW interface routine performed correctly.

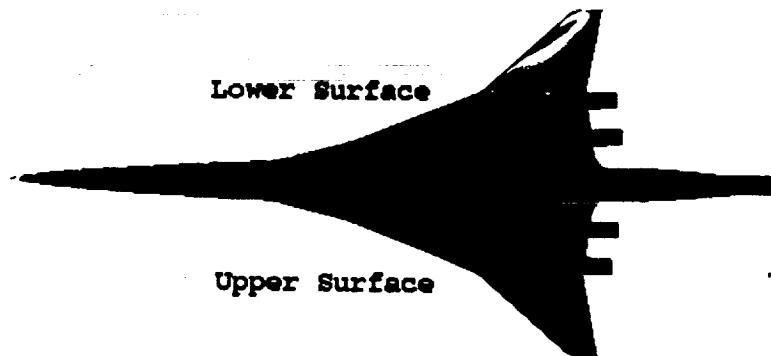
Reference-H
UPS/OVERFLOW Interface



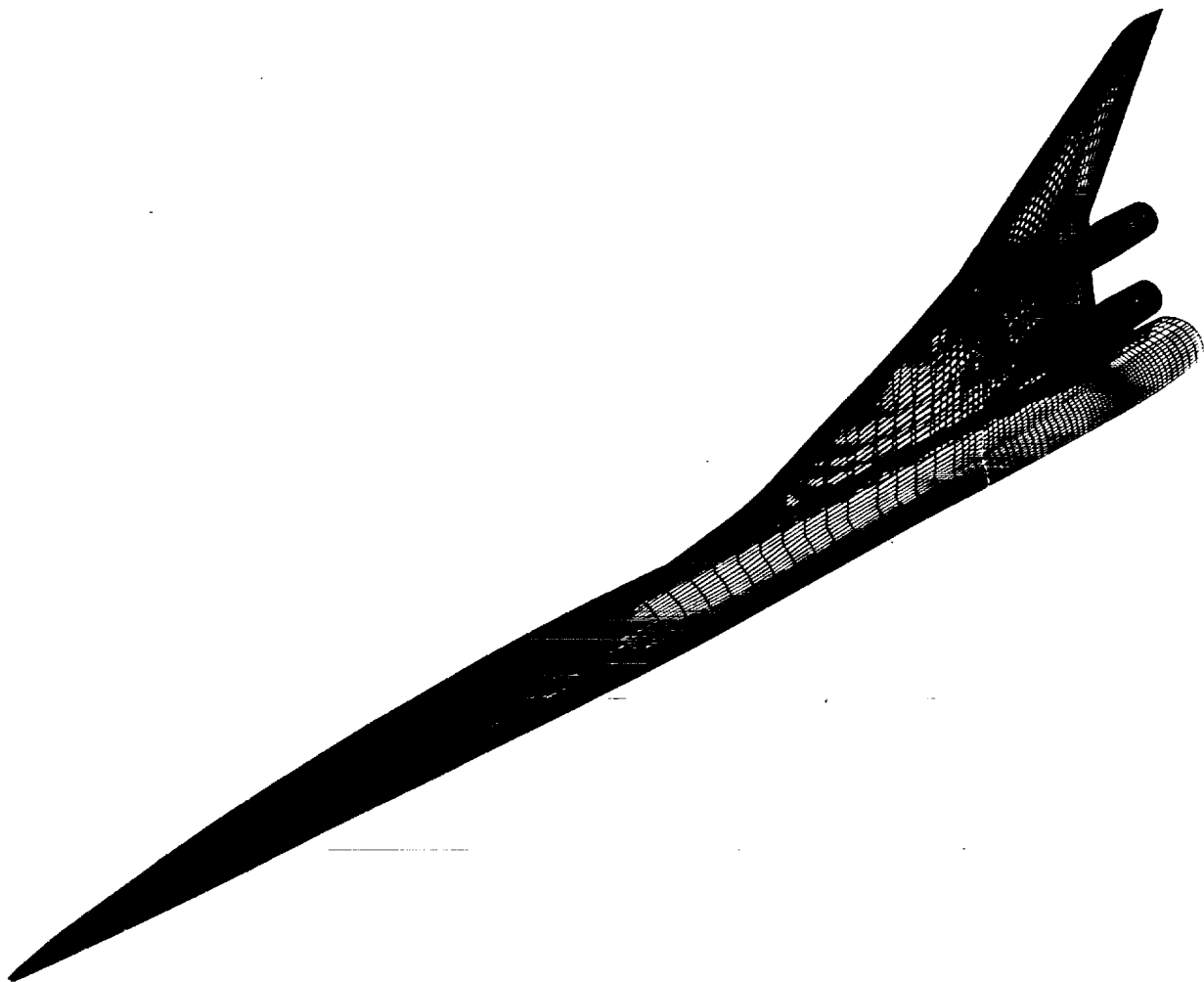
Pressure



Mach 2.4
 $\alpha = 4.5$ degrees

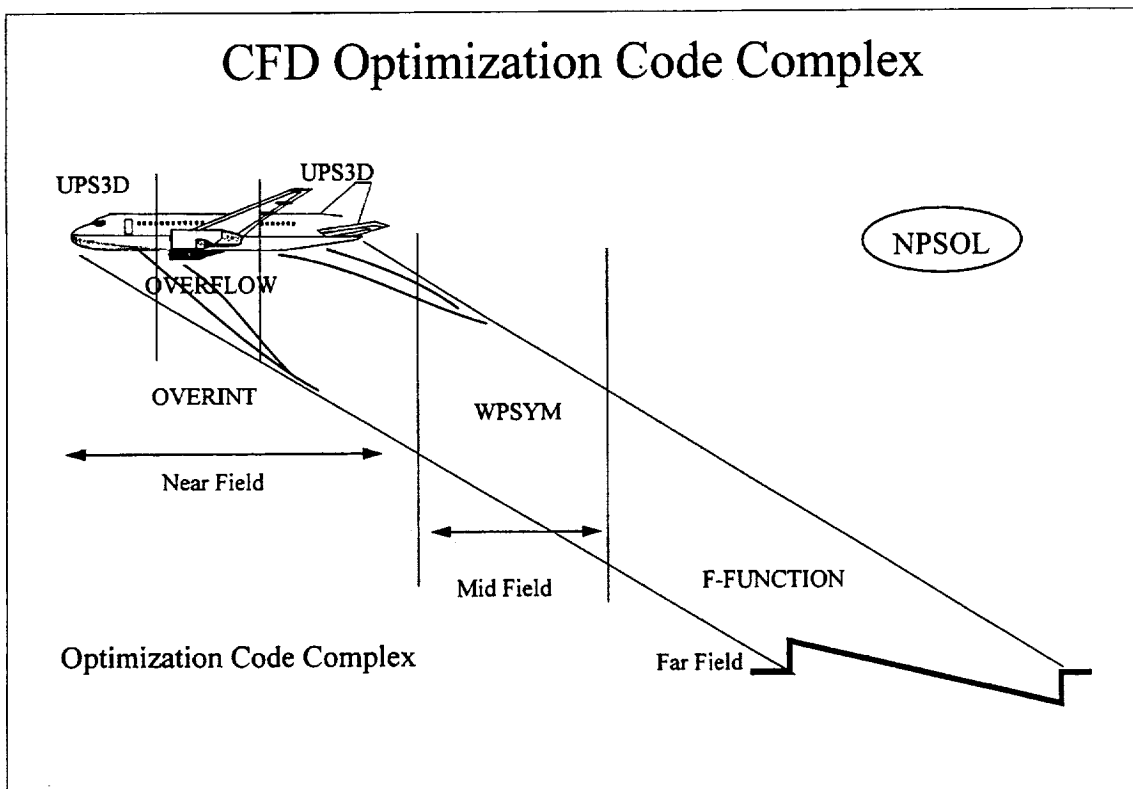


The figure below shows how OVERINT works. The code takes the surface grids and solutions from UPS3D code and OVERFLOW code, and replace the interface region by a triangular zip grid. The forces and moments are calculated on these surfaces one-by-one.



All the codes described in the previous viewgraphs are combined together with the numerical optimization routine (NPSOL) to perform sonic boom softening optimization. The viewgraph below shows schematically how these codes are combined together.

■ SAMSON CHEUNG ■



Inboard Leading-Edge Sweep Study

First presented here is the inboard leading-edge sweep study. This is inspired by the results obtained from the previous year. The reason to change the leading-edge sweep of Ref-H is to “smooth” out the total equivalent area of the aircraft which is related to the sonic boom according to the supersonic theory.

■ SAMSON CHEUNG ■

Inboard Leading-Edge Sweep Study

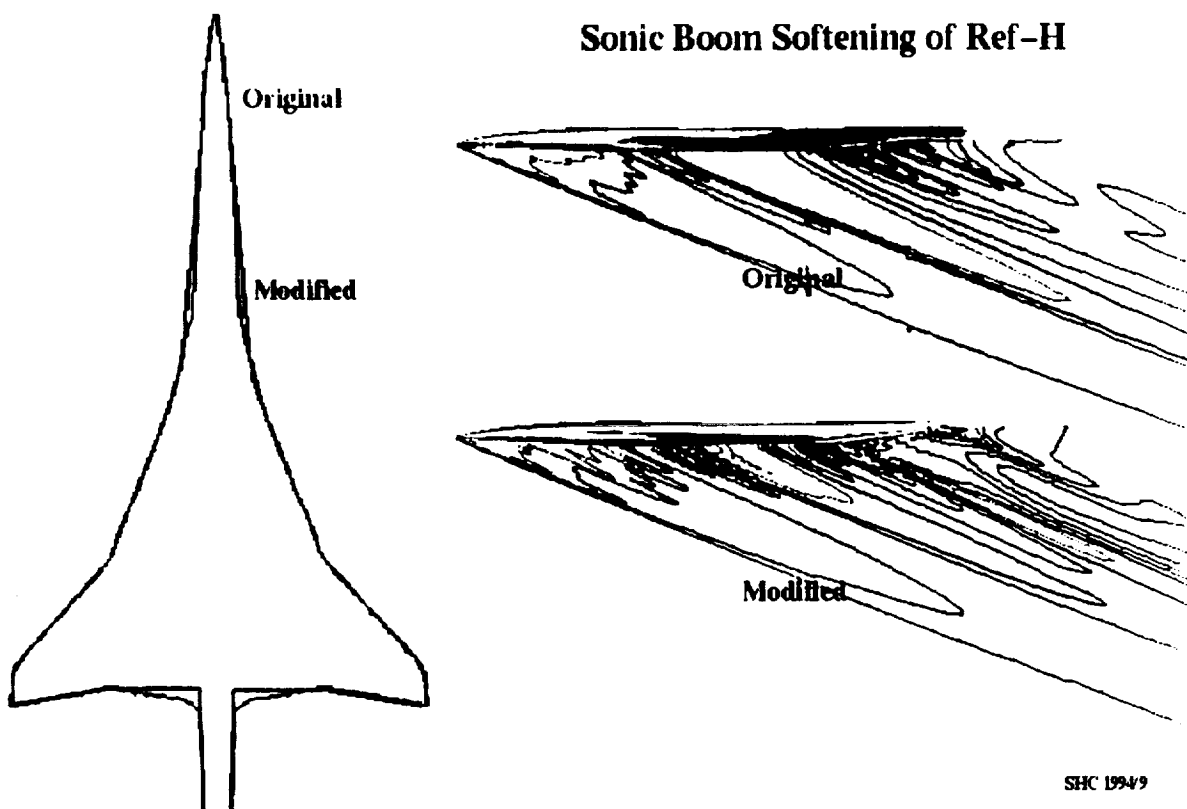
Configuration: Reference-H

Aim: Reduce the rate of change of the slope in the Ae-curve

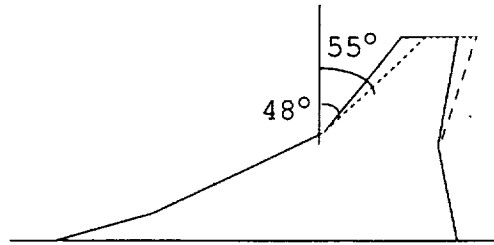
Solution: Change the inboard leading-edge sweep angle

The figure below shows the pressure contours of the Ref-H with and without leading-edge sweep modification. From the contour lines, we can see the wing shock contours are thinner in the modified case. This indicates the modification weakened the shock although there are some complicated structures right under the modified aircraft.

However, since the leading-edge of the Ref-H is round, the modification shown here has a significant drag penalty. At that point in time, the team decided to study the outboard-wing sweep of Ref-H. No further investigation of the leading-edge sweep was done.

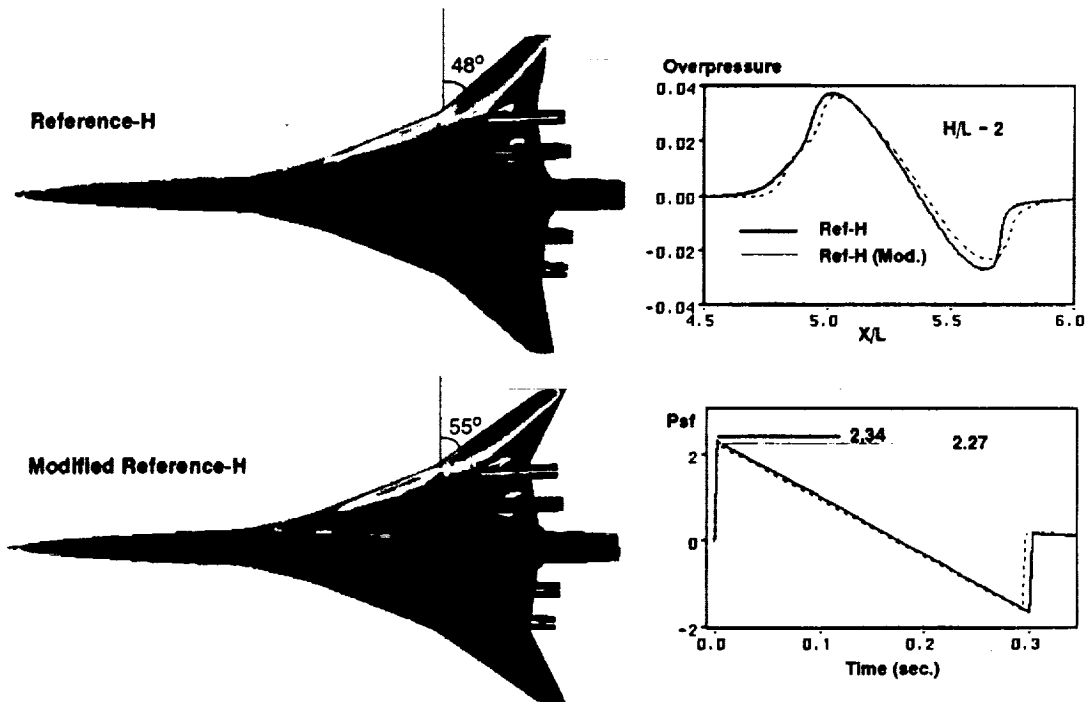


Boeing had studied a series of outboard-wing sweeps on the Ref-H using linear method. The job now is to verify the effect of the outboard-wing sweeps by the CFD tools. The case chosen to be studied is a modified sweep of 55 degrees. The sketch below shows the outboard-wing sweeps of the original Ref-H (48°) and the modified sweep (55°).



The verification was done using the CFD code complex (UPS3D/OVERFLOW) on the two wing/body/nacelle configurations. The results of sonic boom at the near and far fields are shown in the viewgraph below. The decrease in percentage of the overpressure psf is as it was predicted by the linear theory.

Pressure Field Variation of Ref-H by Wing Sweep



The viewgraph below shows the computational results of the original Ref-H and the Ref-H with modification in the outboard-wing sweep.

■ SAMSON CHEUNG ■

Outboard-Wing Sweep Study (Cont.)

- UPS3D/OVERFLOW code complex: Inviscid calculations
- Overpressure obtained at one and two body lengths under the flight track ($H/L = 1$ and 2)
- Sonic Boom Extrapolated from the near-field overpressure
- Aerodynamic Forces obtained by OVERINT

Inviscid Lift and Drag Comparison

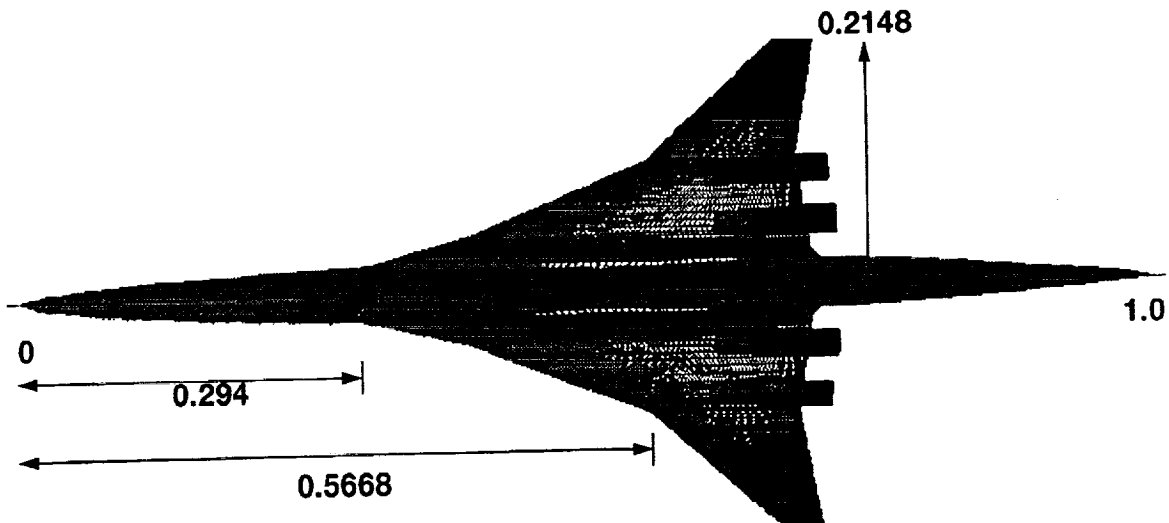
	C_L	C_D	L/D
Ref-H	0.1252	0.01188	11.29
Ref-H(mod)	0.1281	0.01050	12.74

Boeing-1122 Configuration

At this point in time a new configuration called Boeing-1122, whose has a planform very similar to the Ref-H but different nacelle concept, was introduced. The viewgraph below shows the planform and the nacelle locations of the new configuration.

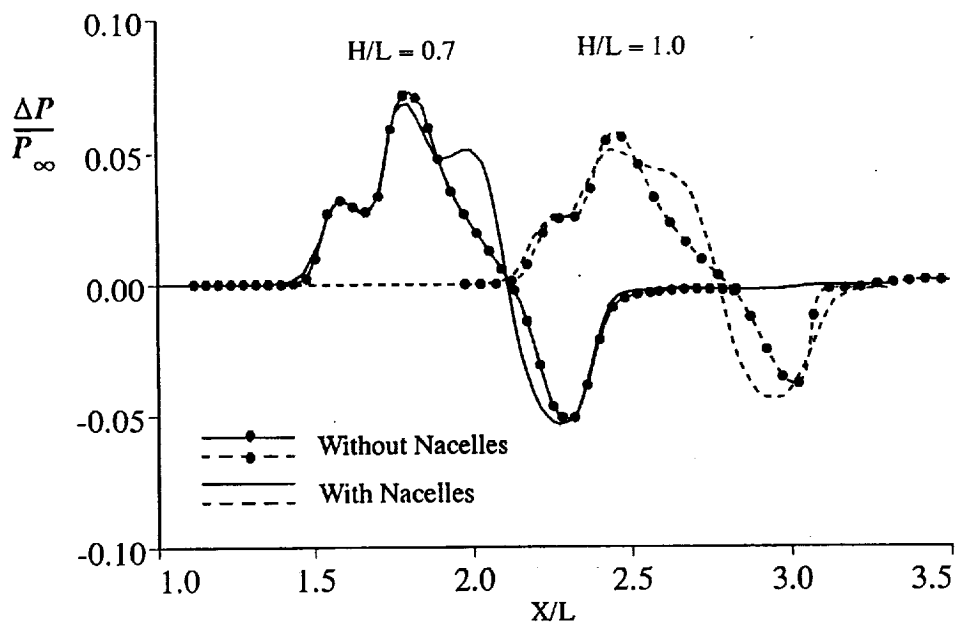
HSCT Boeing-1122

Mach = 2.4
 $C_L = 0.115$
 $L = 314$ ft.
Ref. Area = 7700 sq. ft.

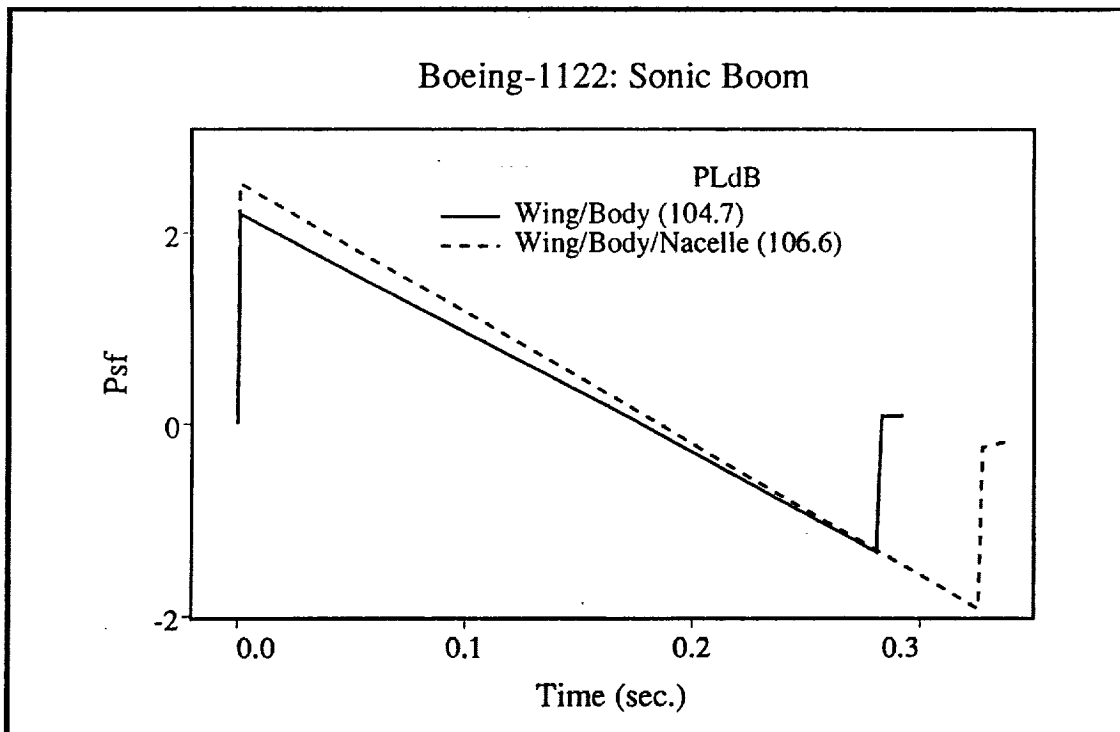


The following viewgraph shows the near-field pressure signals of the Boeing-1122 configuration with and without nacelle at 0.7 and 1 body lengths (H/L=0.7 and 1) under the aircraft. It is clear that the nacelle integration of the HSCT has a major boom contribution because of the lift and volume generated.

Pressure Signals of Boeing-1122



This viewgraph give a feel of the nacelle effect on the sonic boom.



The team decided to apply a hyperbolic tangent to the wing dihedral of the Boeing-1122 configuration. As a first step of the study, only the wing/body is considered. The viewgraph below shows the hyperbolic tangent dihedral verses the original dihedral.

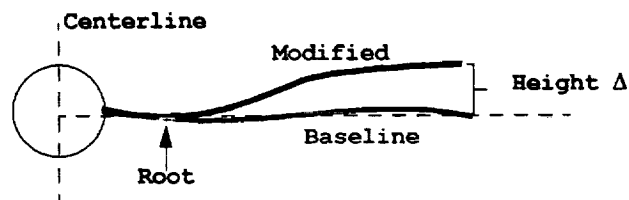
In this study, a dihedral means that at a certain spanwise location the wing is “bent” up according to the hyperbolic tangent. The hyperbolic tangent started at a distance “Root” away from the centerline and ended at the maximum wing-tip location (0.2148 body lengths).

There are three cases to be studied. The third case has a height Δ of 102 inches which is may not be realistic for HSCT, but it is worthwhile to study its effect on the boom.

■ SAMSON CHEUNG ■

Wing Dihedral Study

Parametric Study of Wing Dihedral: Hyperbolic Tangent



Case 1 (R100_D42): Root at 100 inches from centerline. Height Δ is 42 inches.

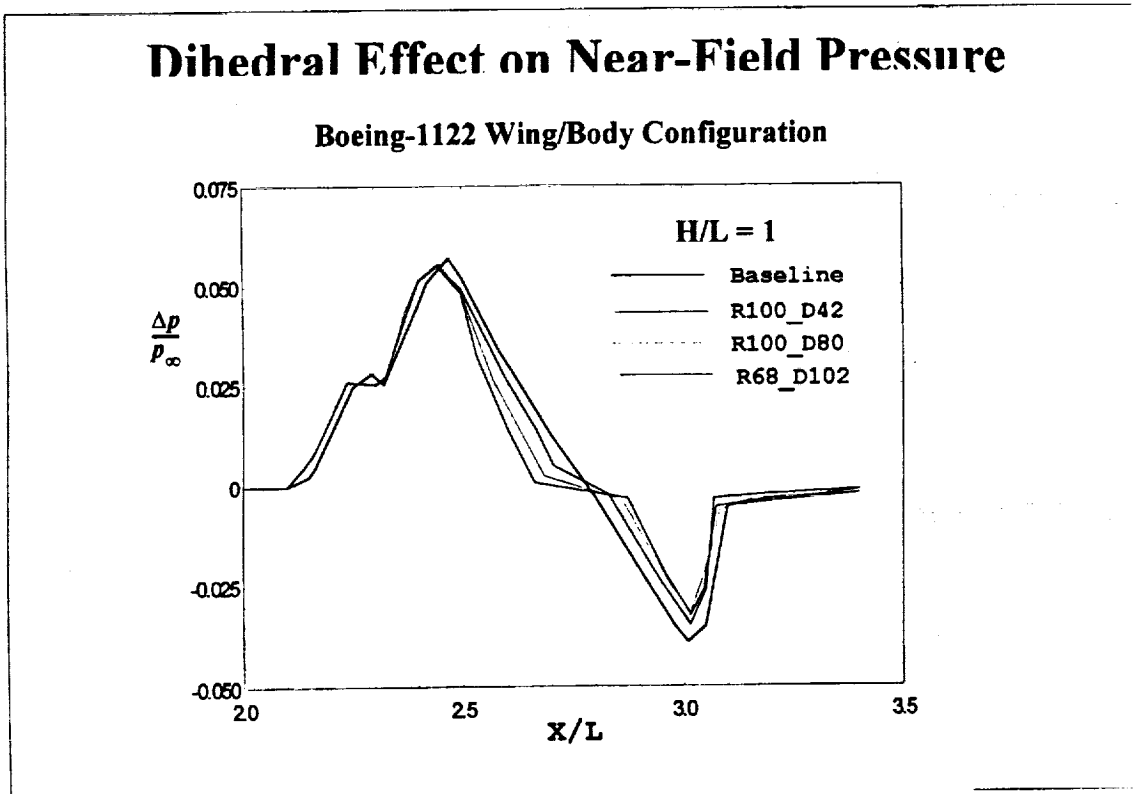
Case 2 (R100_D84): Root at 100 inches from centerline. Height Δ is 84 inches.

Case 3 (R68_D102): Root at 68 inches from centerline. Height Δ is 102 inches.

The effect of wing dihedral is shown in this viewgraph below. These are the near-field pressure signals from different wing dihedrals at one body length ($H/L=1$) under the configuration. As shown in the viewgraph, the larger the height Δ , the larger a flat region in the expansion. This flat region alleviates the steepness of the wing shock and reduce the overpressure at the ground when the wing shock coalesces the bow shock. The resulting psf of the overpressure is reduced as the height Δ goes up.

From the parametric study of wing dihedral, it seems that larger the height Δ , smaller the overpressure of the boom.

■ SAMSON CHEUNG ■



As a first step of sonic boom minimization, only wing/body configuration is considered. All the CFD tools and numerical optimization routine are linked together to form an optimization code complex as shown in the previous viewgraphs. Since nacelles are not modelled, OVERFLOW is not employed to save computational time.

We took the third dihedral case, R68_D102, as the initial configuration. It should be noticed that this dihedral with height Δ of 102 inches may not be realistic in the first place. The purpose of the optimization run is not to produce a viable HSCT configuration. Instead, we try to modify the wing dihedral, with lift constrained, to explore any possibility that we might miss in the parametric study.

A series of Fourier Sine curve is chosen to modified the hyperbolic tangent. Details of the sine curves are shown in the next viewgraph.

■ SAMSON CHEUNG ■

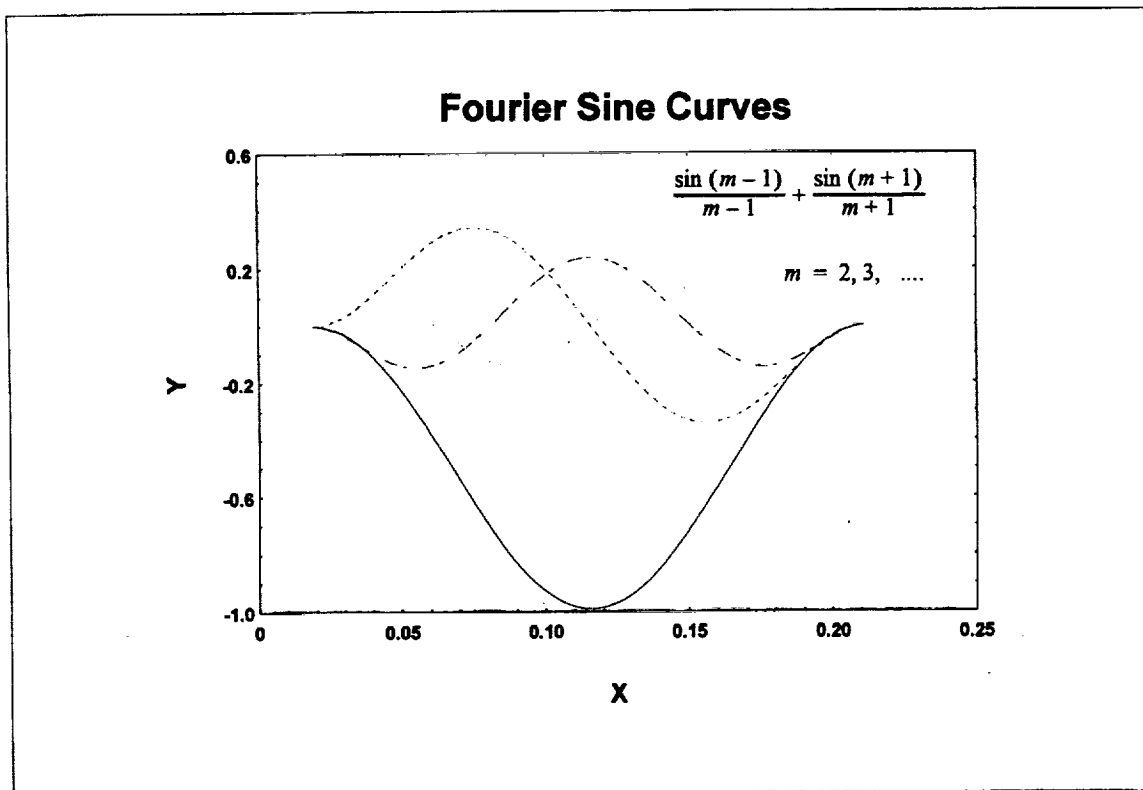
Sonic Boom Minimization

- **Boeing-1122 Wing/Body Configuration**
- **Optimization Routine: NPSOL**
- **Lift Constraint**
- **Wing Dihedral**
- **Fourier Sine Curves as Shape Functions**

A series of Fourier sine curves is shown below. These sine curves are chosen for two reasons:

- 1) they will conserve the area under the original hyperbolic curve.
- 2) more curves are chosen (i.e., higher the value m) means higher the Fourier frequencies included. This means that if the optimal solution exists, this will give the global optimum.

■ SAMSON CHEUNG ■



This viewgraph shows some data of the optimization process. The optimization routine took 4 iterations, that consists of 33 CFD/extrapolation analyses, to converge. This is equivalent to 5 CPU hours on the CRAY C-90. The table in the viewgraph indicates the overpressure of boom is reduced with the lift fixed. However, the drag is increased.

■ SAMSON CHEUNG ■

Sonic Boom Minimization Result

- **Lift Constraint**
- **33 CFD evaluations**
- **17917 sec. (5 hrs.) on CRAY C-90**
- **N-wave overpressure (psf) reduction**

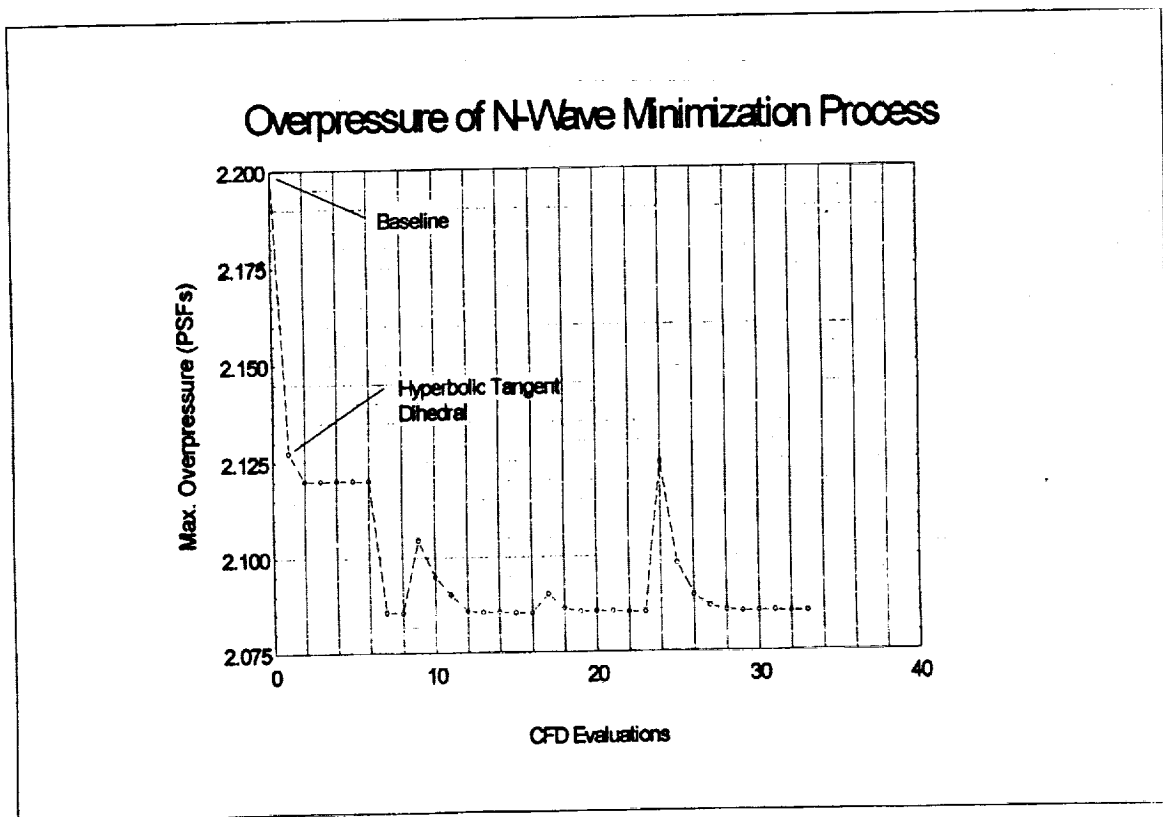
Wing Dihedral Optimization Comparison

	C_L	C_D	PSF
Initial	0.1231	0.01175	2.1274
Optimized	0.1234	0.01223	2.0852

This viewgraph shows the overpressure psf of the sonic boom during the optimization process. Initially, the optimization starts from the hyperbolic tangent dihedral (as shown). The ups and downs of the psf's indicate the "path" that the optimizer took in the search of the optimum.

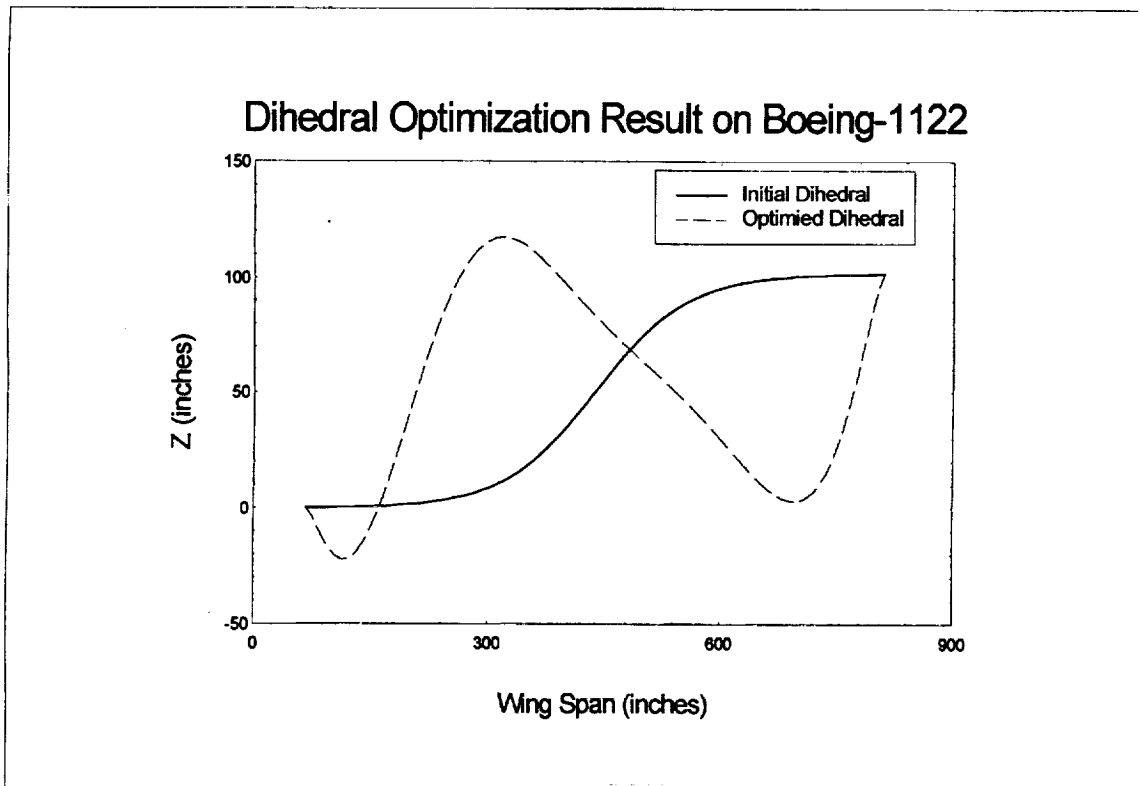
At the end, the optimization process gives a lowest boom with 0.1 psf smaller than the baseline.

■ SAMSON CHEUNG ■



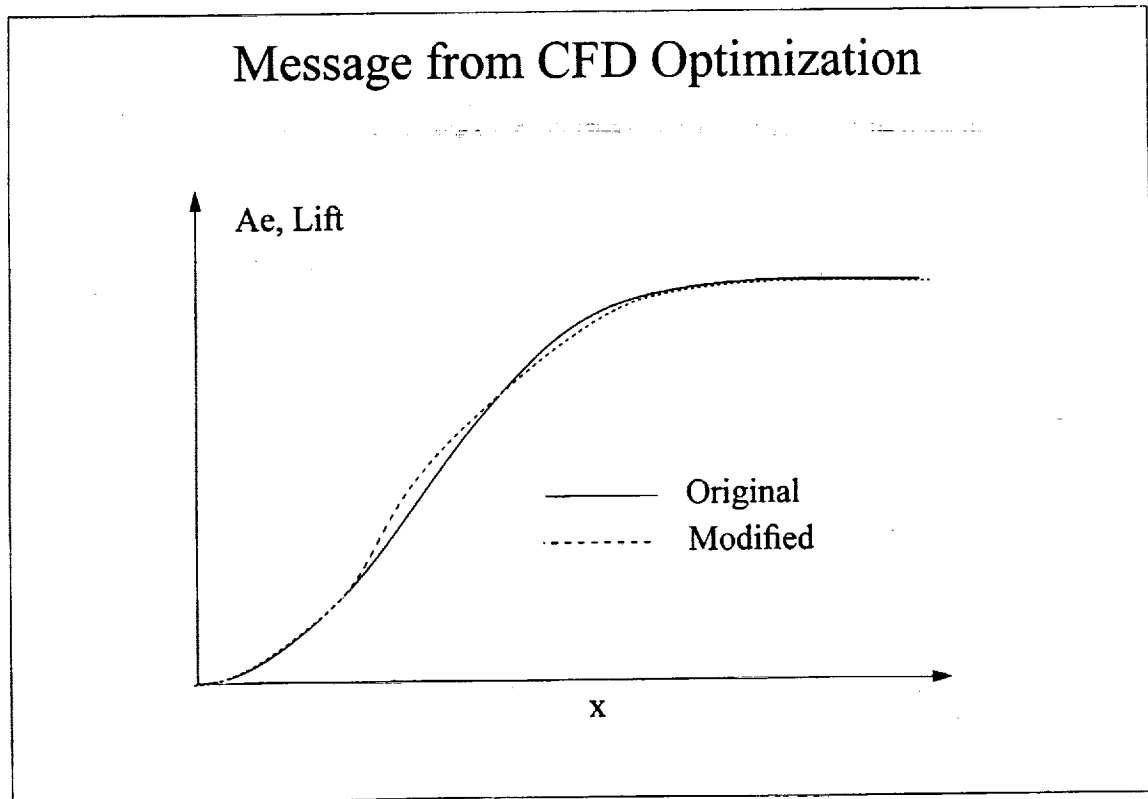
This viewgraph below shows the initial dihedral (hyperbolic tangent) and the optimized dihedral. They are very much different. The optimization result shows that the wing should be bent upward at the spanwise location 150 inches to 320 inches from the centerline. Then bend down at the mid-span. Since the configuration is an arrow wing. This figure indicates that more lift should be generated near the inboard leading edge followed by a reduction of lift from the aft. If we plot the lift or the area distribution of the wing/body configuration, it would look like the next viewgraph.

■ SAMSON CHEUNG ■



This sketch shows that the optimization routine modifies the wing dihedral such that the lift is shifted forward with the total lift fixed. In fact, it makes a lot of sense! For the HSCT, the majority of the lift is generated at the middle and downstream parts of the wing. According to the sonic boom theory, higher lift generates bigger shock (bigger boom). If the lift is distributed in such a way that the shock generated from the aft wing is lower, then, this will alleviate the steepness of the wing shock. As a result, a smaller N-wave is generated.

■ SAMSON CHEUNG ■



The viewgraph below summaries the effort of this study.

■ SAMSON CHEUNG ■

Conclusion

- **CFD Optimization Code Complex has been exercised**
 - NPSOL, UPS3D/OVERFLOW, OVERINT, WPSYM...
- **To soften the boom of an aircraft, one may consider:**
 - A modified inboard leading-edge sweep (to smooth Ae)
 - A higher outboard wing sweep
 - A significant wing dihedral
 - Lift shifted upstream on the wing

POTENTIAL FOR SONIC BOOM REDUCTION OF THE BOEING HSCT*

By George T. Haglund
Boeing Commercial Airplane Group
P.O. Box 3707
Seattle, WA 98124-2207

INTRODUCTION

The HSR sonic boom technology program includes a goal of reducing the objectionable aspects of sonic boom. Earlier HSCT sonic boom studies considered achieving significant sonic boom reduction by the use of arrow-wing planforms and detailed shaping of the airplane to produce shaped waveforms (non N-waves) at the ground (Refs 1, 2). While these design efforts were largely successful, the added risk and cost of the airplanes were judged to be unacceptable. The objective of the current work is to explore smaller configuration refinements that could lead to reduced sonic boom impact, within design and operational constraints. A somewhat modest target of 10% reduction in sonic boom maximum overpressure was selected to minimize the effect on the configuration performance.

This work was a joint NASA/Industry effort, utilizing the respective strengths of team members at Boeing, NASA Langley, and NASA Ames. The approach used was to first explore a wide range of modifications and airplane characteristics for their effects on sonic boom and drag, using classical Modified Linear Theory (MLT) methods. CFD methods were then used to verify promising modifications and to analyze modifications for which the MLT methods were not appropriate. The team produced a list of configuration changes with their effects on sonic boom and, in some cases, an estimate of the drag penalty. The NASA Langley results are reported by Fouladi (Ref. 3) and the NASA Ames results by Cheung (Ref. 4).

The most promising modifications were applied to produce a boom-softened derivative of the baseline Boeing HSCT configuration. This boom-softened configuration was analyzed in detail for the reduced sonic boom impact and also for the effect of the configuration modifications on drag, weight, and overall performance relative to the baseline.

The Boeing baseline configuration (often called the "Reference H") was initially designated as the 1080-1122 (as in Refs. 3 and 4), but was updated to the 1080-1405 late in the study. These two Reference H baselines differ only in details and in rules used in performance sizing. The -1405 baseline was a more recent baseline used in the Task 11 Planform Study. The boom-softened configuration is designated as the 1080-1444 (or simply the -1444), and is closely related to the -1407 configuration, also of the Task 11 Planform Study.

* This work was done under Task 5 of Contract NAS1-20220.

AIRPLANE LIFT AND VOLUME EFFECTS

As a starting point in sonic boom reduction, it is instructive to consider the relative importance of lift and volume on maximum overpressure. Figure 1 shows typical results during cruise for the baseline configuration. Throughout cruise, the maximum overpressure due to lift dominates over volume by a factor of 2.3. Interestingly, the ratio of maximum equivalent areas due to lift and volume is close to the same factor ($B_{\max} / A_{\max} = 827/327 = 2.5$)*. This lift dominance is a direct result of the heavy airplane weight and high altitude cruise condition. The sonic boom from a light-weight fighter aircraft at low altitude, on the other hand, is dominated by volume effects (size and shape).

The lift contribution to maximum overpressure is so dominating that the volume effect is almost negligible in comparison. For example, at the start of cruise the volume contribution to maximum overpressure is 1.16 psf, while the lift contribution is 2.71 psf. If it were possible to miraculously eliminate the volume contribution, the lift contribution of 2.71 psf would still remain, which is only a 0.24 psf reduction from the total maximum overpressure of 2.95 (and only an 8% reduction). In this formulation where lift and volume effects are considered separately, the two maximum overpressures must be combined using the following equation:

$$\Delta P_{\text{total}} = [(\Delta P_{\text{vol}})^2 + (\Delta P_{\text{lift}})^2]^{1/2} \quad 1)$$

It is clear that efforts to reduce sonic boom must focus on lift effects, or more specifically, on the wing planform and size. In the trade studies described below, we were not limited to wing effects alone, since the baseline airplane may have a particular problem that could be corrected to reduce sonic boom. However, wing planform studies formed the bulk of the trade studies since that is where the greatest gains can be made.

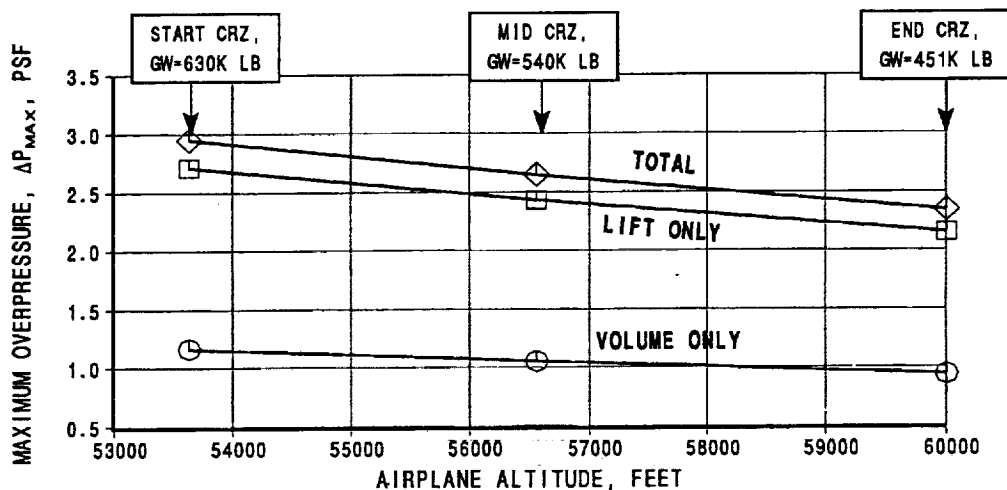


Figure 1. Relative Importance of Lift and Volume to Total Sonic Boom Overpressure.

* The maximum equivalent area due to volume is the maximum area as cut by the Mach lines in the standard manner and is about 327 ft². The maximum area of the equivalent body due to lift can be calculated as

$$B_{\max} = (\beta/2) (C_L) S_{\text{ref}} = (\beta/2) (W/q) = 827 \text{ ft}^2$$

BASELINE CONFIGURATION

The 1080-1405 is a Mach 2.4 commercial transport designed to carry 304 passengers in mixed-class seating over a distance of 5000 nm. The interior of the cabin is based on current 737/757 comfort levels. The fuselage is area-ruled for low wave drag, and the wing is positioned low on the fuselage for safe emergency egress and to allow the primary wing structure to run beneath the cabin floor. The main landing gear is a three-post design that is housed in the fuselage and wing. The most recent engine concept is used, the mixed-flow turbofan, which provides improved noise on takeoff and landing, and better overall fuel consumption. The engine is designated as the 3765.100 "Best" DSM, which features a Down Stream Mixer (DSM) nozzle with aspirated exhaust flow for reduced noise.

The -1405 baseline is a recent "Reference H" design. The performance sizing chart (or "thumbprint") is shown below in Figure 2, which indicates the minimum takeoff gross weight that satisfies the design constraints, such as required fuel for the mission and climb time. The -1405 needs a relatively large wing to carry enough fuel for the mission. Figure 3 displays the uncycled (or "point design") configuration, from which estimates are made of airplane empty weight, installed engine performance, and aerodynamics. This baseline airplane was the basis for boom softening and served as a reference point in terms of sonic boom and overall performance.

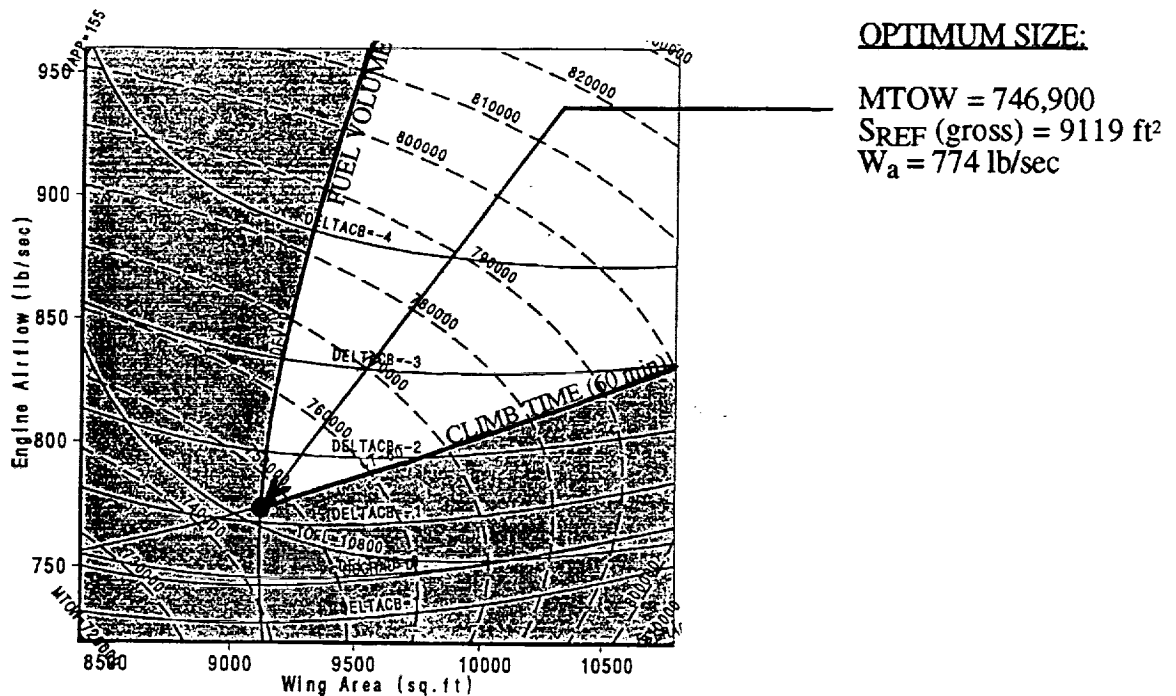


Figure 2. Performance-sizing chart for the Baseline "Reference H" 1080-1405.

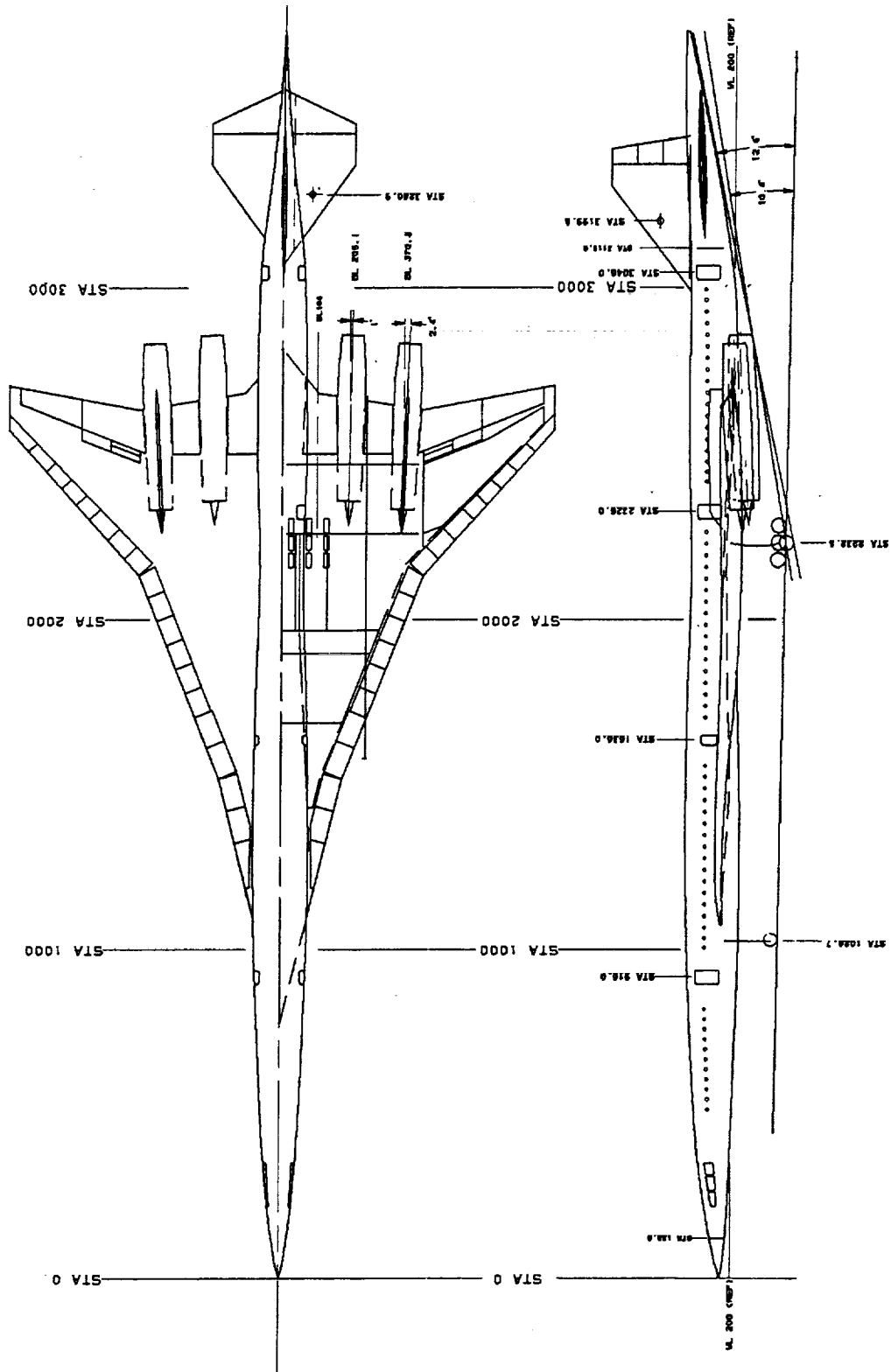


Figure 3. Configuration drawing of the Baseline Configuration, 1080-1405.

BOOM-SOFTENING OPTIONS EXPLORED

Sonic boom reduction is a challenge for vehicles flying at Mach 2.4 and with severe limits imposed by design and operational constraints. Previous studies (Refs 1, 2) had the advantage of being able to "shape" the sonic boom signature at the ground, by slowing the coalescence of shock waves through reduced Mach number and altitude, arrow-wing planforms, and detailed airplane shaping. In these latest studies, however, concepts to achieve non-coalescence of shock waves or long rise time were not explored. Thus, the rules of the game are changed considerably, since our boom reduction must occur for flight at high Mach number and altitude when N-wave pressure signatures at the ground are produced. In this case, sonic boom reduction is a little bit like trying to fool Mother Nature. Indeed, we have reason to be humble when we consider that turbulence and air absorption have greater influences on sonic boom than the airplane designer.

Nevertheless, it's clear that sonic boom can be reduced by careful configuration design, and the "Reference H" Team began with that prospect in January, 1995. The Team consisted of the following members:

REFERENCE H BOOM-SOFTENING TEAM

<u>Boeing</u>	George Haglund (Team Leader) Reggie Abel
<u>Langley R. C.</u>	Dan Baize Kamran Fouladi (Lockheed)
<u>Ames R. C.</u>	Eugene Tu Samson Cheung (MCAT)

The first order of business was to identify possible boom-softening modifications for study. About 30 candidates were identified and prioritized according to their estimated effect on drag and performance, as shown in Figure 4. We focused on modifications in Group A, which are items with probable drag reduction. Group B (small drag penalty) and Group C (significant drag penalty) had lower priority.

The approach taken was to study as many -1405 modifications as possible as individual trade studies. Boeing (Haglund and Abel) used the Modified Linear Theory (MLT) methods to quickly explore a wide range of modifications and parameters for their effects on sonic boom and drag. Selected promising modifications and studies were given to Langley or Ames for CFD analysis, verification, or optimization. This division of labor made the best use of our respective strengths. An example of this procedure was the study of outboard wing sweep completed in January. Boeing analyzed the full range of outboard leading edge sweep (48, 55, 62, and 68.5 deg). Cheung at Ames R. C. verified the MLT results with a CFD method for the most promising sweep angle of 55 deg (most promising from sonic boom and overall performance, considering wing weight, etc.).

In the time available, most of the items in Group A were examined, as shown in Figure 4. The MLT results are summarized in the next paragraphs, and the CFD results are reported separately by Fouladi (Ref. 3) and Cheung (Ref. 4). Wing dihedral is discussed in somewhat greater detail in a later section.

ID	Parameter	Range	Group A -- Drag Improvement Items			Status	Boom-Softening Potential
			Boeing	LaRC	Ames		
A-0	Baseline Analysis	None, basic config. only	FULL	FULL	FULL	Done, 4-28	---
A-1	Trim/C.G. location	no tail, 50, 54, 58% MAC					
A-2	Low GW, Opt. Alt.	GW= 680, 630, 580	FULL			Done, 1-18	Good
A-3	Wing Dihedral	0, 4, 8 deg dihedral	FULL	Part*	Part*	Done, 7-12	Good
A-4	Forebody Camber	nose Δα and camber	FULL*		Part	Done, 3-15	Poor
A-5	Outboard Wing Sweep	48, 55, 62, 68.5 deg	FULL			Done, 1-27	Good
A-6	Nacelle Forecowl	lip angle = , , ,	FULL			Done, 6-6	Fair
A-7	Wing Tip Chord	+20, +40 inches					
A-8	Extended L.E. Strake	Δ SREF = + 500 ft ²	FULL			Done, 3-6	Fair
A-9	Planform Study A/P's	Ten planforms	FULL			Done, 3-6	Good
A-10	Nacelle/Diverter Effect	Nac./div. on & off	FULL			Done, 5-1	Small
A-11	Smooth L.E. Break	Planform L.E. Radius	FULL			Done, 5-31	Small to Fair
A-12	T.E. Yehudi						
A-13	T. E. Sweep						
A-14	Increased Wing Area	7700, 8400, 9000 ft ²	FULL			Done, 4-11	Good
A-15	Thrust Vectoring	0, 5, 10 deg					
A-16	Fuselage Camber	Nose to wing i.e.		FULL*		Done, 5-22	Small
A-17	LCAP Study (canard)	Three-surface A/P					
A-18	Better Engine Match	CRZ. / TO Thrust	FULL			Done, 5-10	Good
A-19	Final Softened Config.	As defined	FULL	FULL		Done, 8-28	---
Group B -- Small Drag Penalty							
B-1	Fuselage Area Dist.						
B-2	Engine Location	aft					
B-3	Nacelle Boat-tail	exit area					
B-4	Canard	forward lift					
B-5	Forebody shape	conical or linear area					
B-6	Outb'd Wing Flaps						
B-7	Extended Forebody						
B-8	Extended Aftbody						
Group C -- Significant Drag Penalty							
C-1	Number of Engines						
C-2	Increased Cruise Alt.						
C-3	Wing Camber & Twist						
C-4	Reduced Nacelle Amax						

NOTE: "FULL" indicates prime responsibility for exploring the full range of the parameter of interest. "Part" indicates verification of the final parametric value, or an optimization; an * indicates optimization methods were used.

Figure 4. Summary of parametric trade studies for boom-softening of the Reference H configuration.

Effect of Airplane Gross Weight (A-2)

Since the HSCT sonic boom is lift dominated, any reduction in airplane weight will reduce the sonic boom accordingly. However, the sonic boom dependence with gross weight is fairly weak, as shown in Figure 5. For a 100,000 lb reduction in gross weight, the maximum overpressure is reduced from 2.89 to 2.57 psf (about 11% reduction). This analysis was for a fixed wing size with the lift coefficient held constant (and therefore higher altitude at the lighter weight). The higher altitude gives an additional boom reduction.

Improved structural or propulsion efficiencies will help to reduce gross weight, however, boom reduction will only occur if that weight reduction shows up as reduced wing loading. The tendency will be to reduce the wing size and keep a high wing loading for optimum performance, which would give little sonic boom reduction.

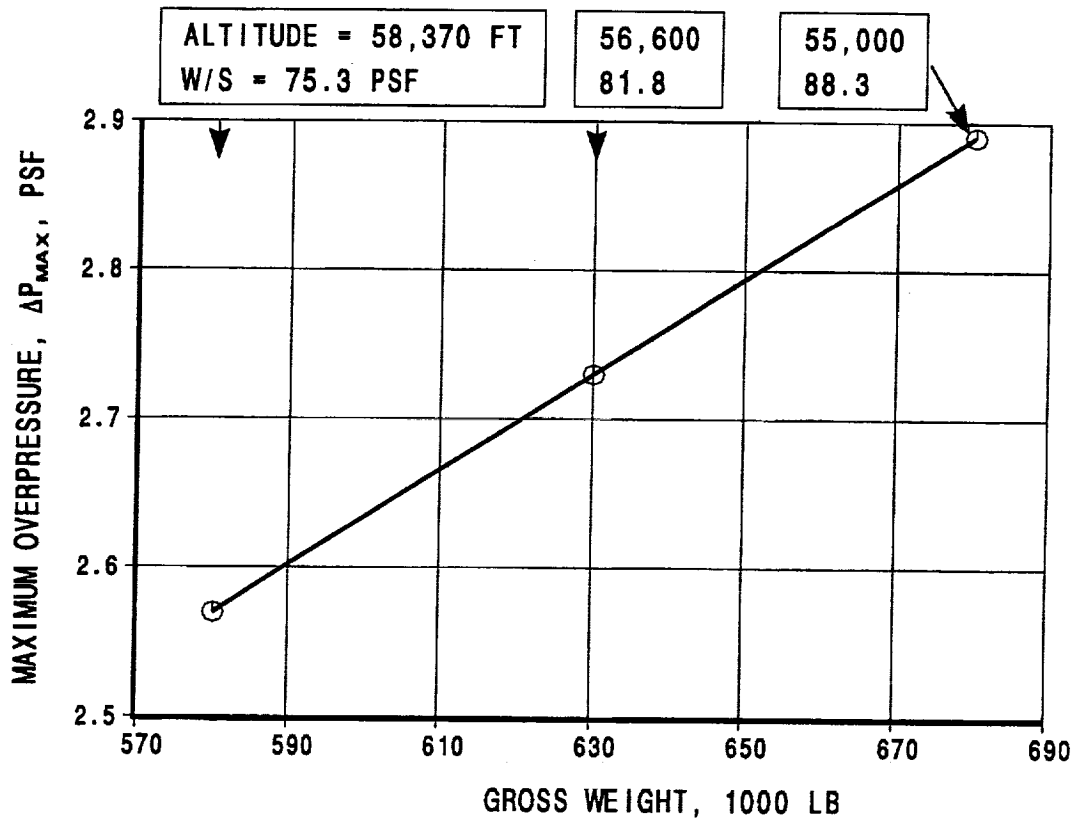


Figure 5. Sonic boom variation with airplane gross weight (fixed wing size).

Effect of Wing Area (A-14)

The baseline planform was used to evaluate the effect of increased wing area from 7700 to 8400 to 9000 ft². The nacelle location was preserved at the baseline % span location. The larger planform configurations met the necessary performance sizing constraints, and the thumbprints were evaluated at a common engine size of 750 lb/sec. The top-of-climb weights were based on the sized results for the 5000 nm mission.

In going from 7700 to 9000 ft², the boom reduction is about 8.4% (from 2.96 to 2.71 psf), however, most of the benefit comes at wing area larger than 8400 ft². Thus, an over-sized wing (relative to optimum performance sized) gives a reduced wing loading and reduced sonic boom due to lift.

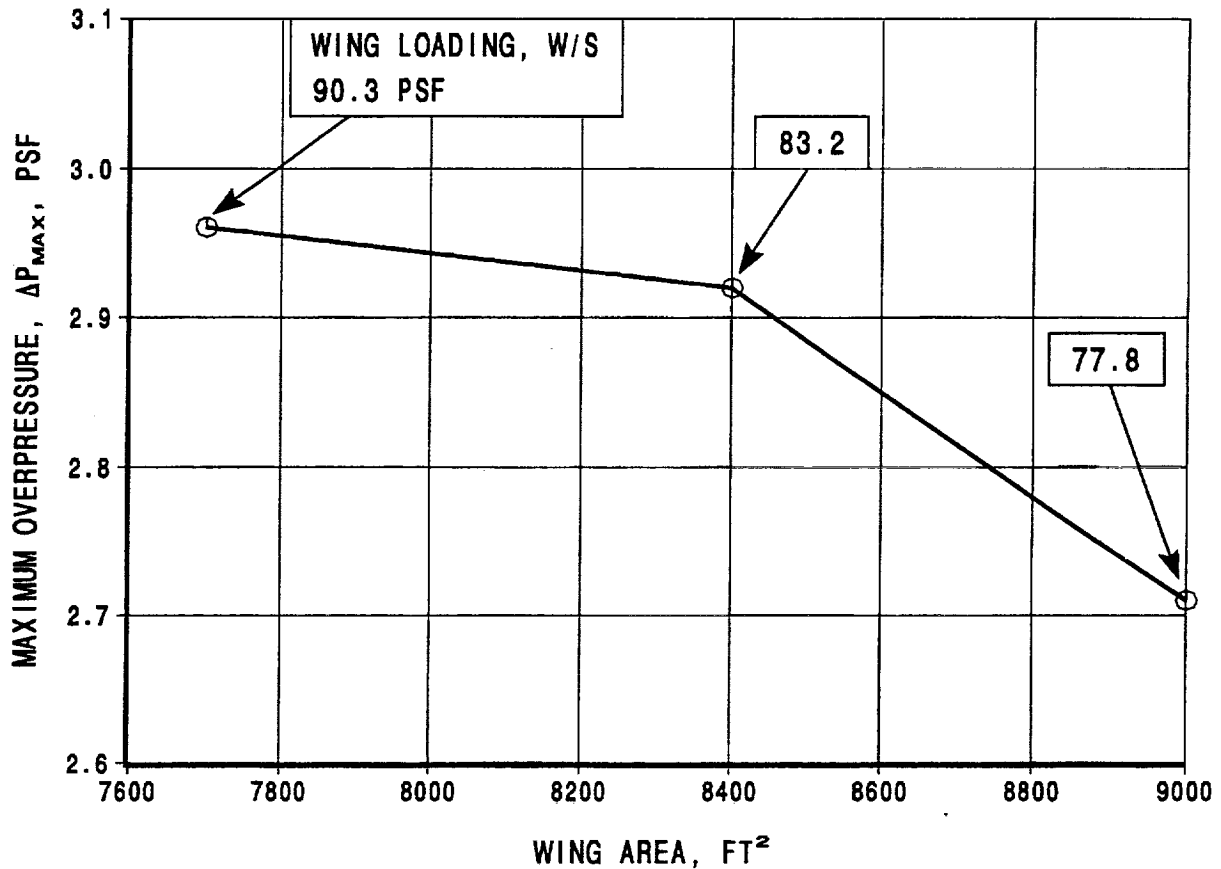


Figure 6. Maximum overpressure variation with wing size.

Effect of Outboard Wing Sweep (A-5)

In this study, the outboard wing was swept from 48.0 deg (baseline) to 55.0, 62.0, and 68.5 deg. No attempt was made to account for performance sizing or for any effect of gross weight or cruise altitude, or to redesign the wing camber and twist.

The results show a significant reduction in maximum overpressure from 2.89 psf at 48 deg sweep to 2.57 at 68.5 deg, which is an 11% boom reduction. Larger sweep on the outboard wing provides a more gentle build-up of lift and a longer lifting length.

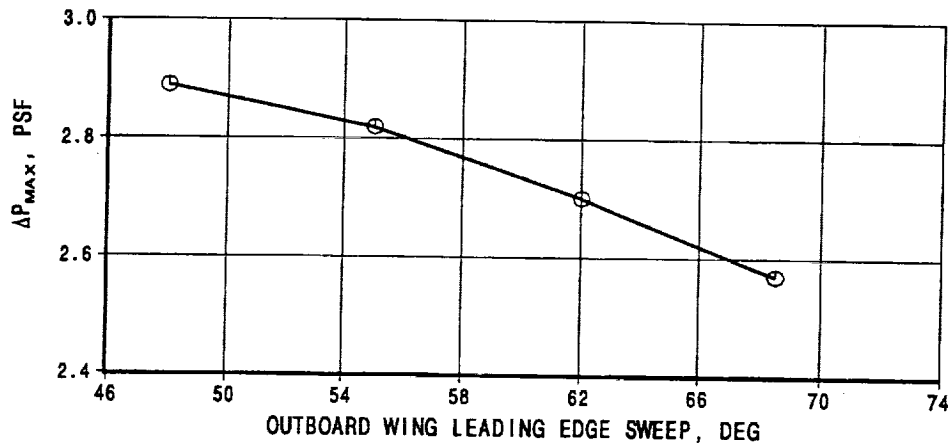


Figure 7. Maximum overpressure variation with outboard wing leading edge sweep.

Effect of Wing Planform (A-9)

A major activity was a wing planform study of ten different planforms, most of which were defined in Task 11. The ten planforms were defined at approximately the same wing size and analyzed for sonic boom at the same flight condition: Mach number 2.4, gross weight of 683,740 lb, altitude of 54850 ft, and a C_L of 0.115. Figure 8 compares the planform shapes and shows the following groupings of planform variations:

- baseline configurations (Boeing Ref. H and Douglas arrow-wing)
- outboard sweep variations (39 to 56 deg)
- wing leading edge break variations (34 to 70% span)
- inboard sweep and strakelet variations (0 to 500 ft² added area).

Leading edge sweep angles are noted on Figure 8.

Figure 9 shows the planform effect on maximum overpressure, with the data presented several ways. The sonic boom lift parameter, K_L , includes the effect of lifting length, L , and lift condition. The K_L parameter and average leading edge sweep are both reasonably good as predictors for the effect of sonic boom, showing similar trends in maximum overpressure. The lowest sonic boom occurs with the largest leading edge sweeps, such as the the planform with the 70% span leading edge break location. The benefit provided by an increase in the inboard leading edge sweep (with a "super" strakelet) is particularly interesting since it is much more feasible compared to an increase in outboard wing sweep.

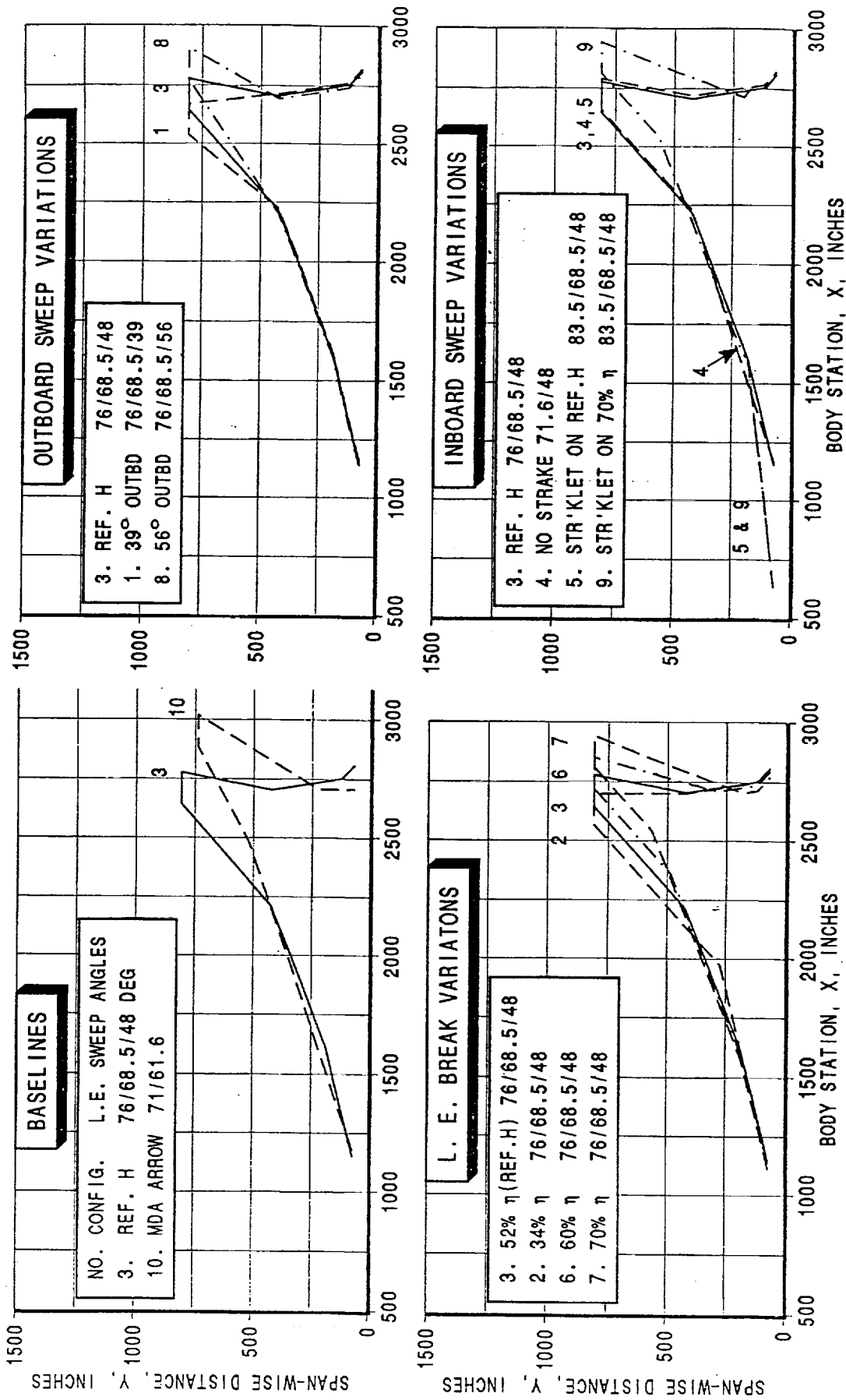


Figure 8. Summary and notation for the ten planforms of the planform study.

START-OF-CRUISE CONDITIONS:
 ALTITUDE = 54,850 FT
 GW = 683,740 LB
 $K_L = \text{Sonic Boom Lift Parameter}$
 $= (\beta/2) C_L S_{REF} / L^2$
 where $L = \text{lifting length}$

SEE PLANFORM DEFINITIONS ON SEPARATE PLOT

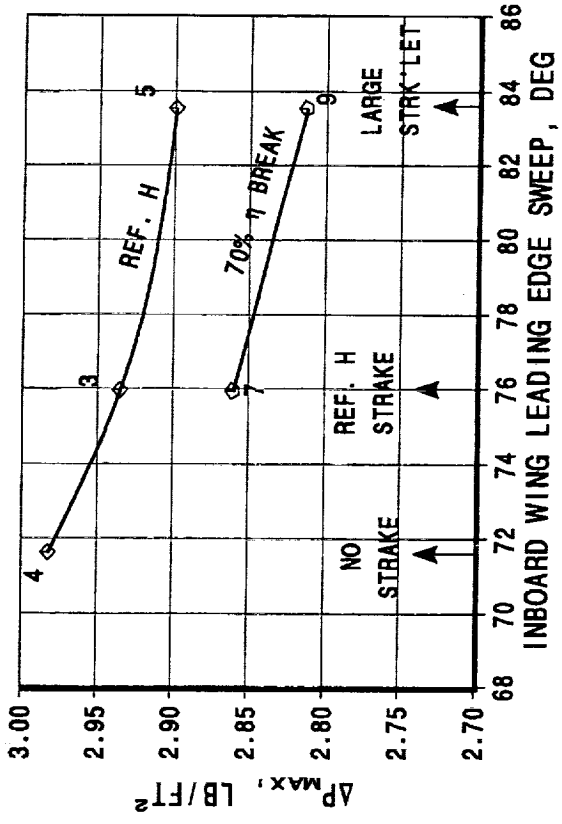
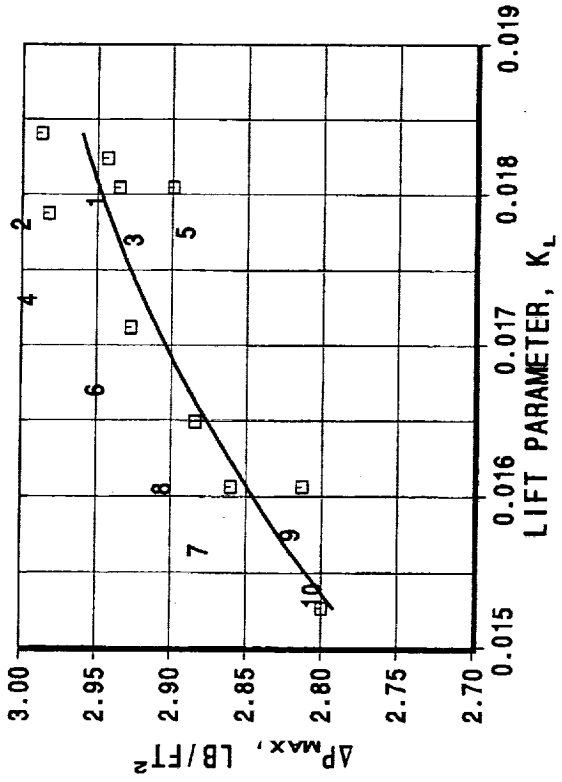
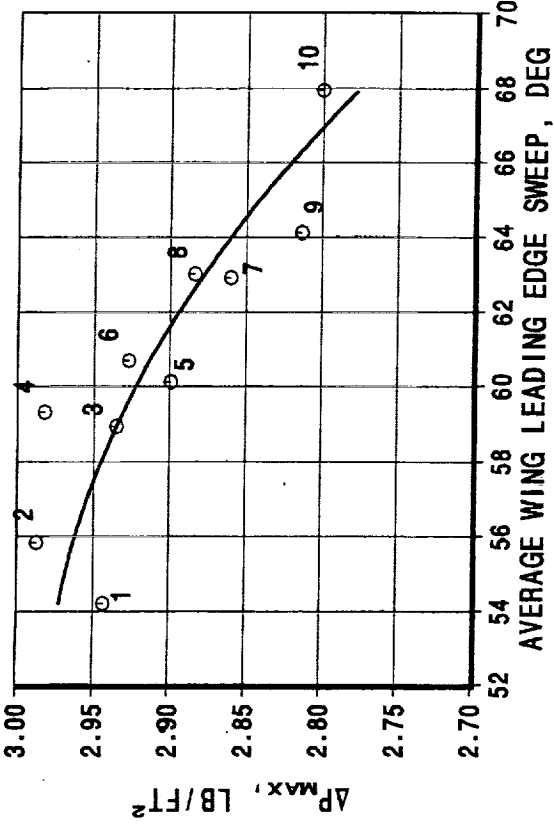


Figure 9. Summary of planform effect on sonic boom.

Effect of Extended Wing Leading Edge Strakelet (A-8)

The baseline Reference H has a small strakelet on the wing leading edge at the side of body, as shown in Figure 10. A bigger strakelet has the potential for providing more lift forward on the configuration and for reducing the strength of the wing shock (and reduced drag, as well). An attempt was made to design such a strakelet, but the result was a higher sonic boom maximum overpressure. An examination of the bigger strakelet showed an increase in drag-due-to-lift, indicating a bad camber and twist design. No further work was done on this concept, but this remains as a candidate for boom reduction.

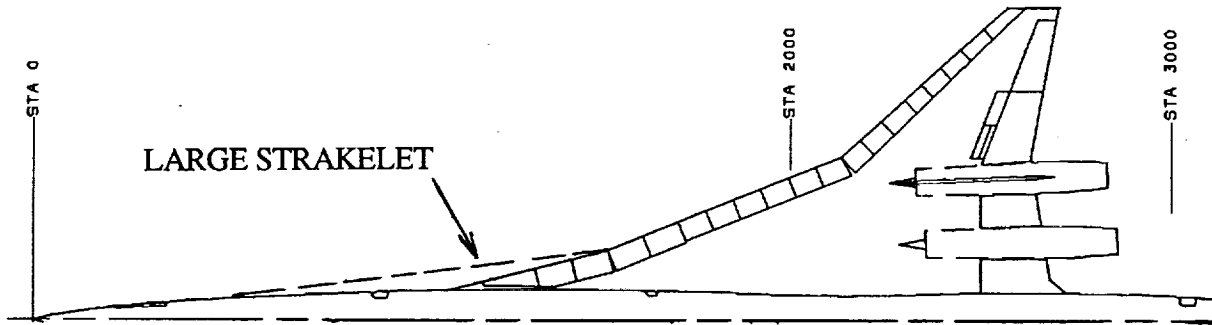


Figure 10. Larger wing leading edge strakelet.

Effect of Smoothed Break in the Outboard Wing Leading Edge (A-11)

At the "break" in the outboard wing leading edge sweep, the sweep changes abruptly from 68.5 deg inboard to 48.0 deg outboard. This is a strong disturbance to the flow; smoothing out this change in sweep may provide some sonic boom reduction. However, an approximate sonic boom analysis with MLT methods showed no benefit. A more detailed analysis is needed, accounting for thinner airfoil sections in the smoothed region due to the longer chords, re-optimized camber and twist, and re-arearuled fuselage.

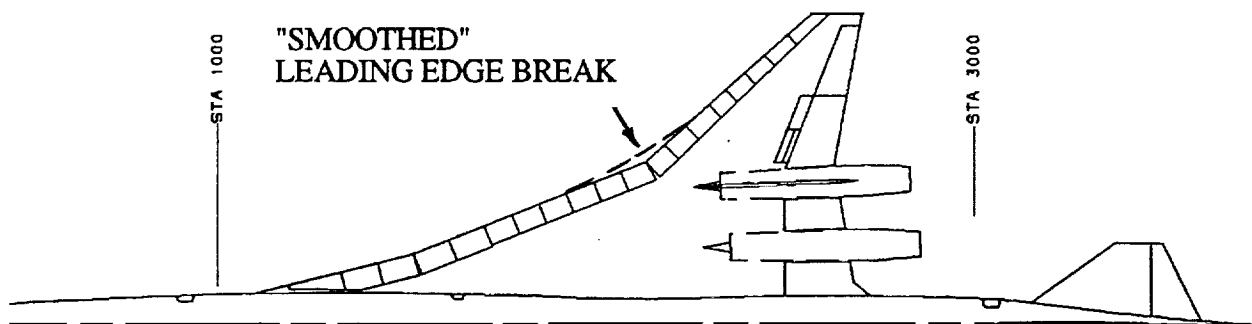


Figure 11. Illustration of "smoothed" leading edge break.

Effect of Modified Nacelle Forecowl (A-6)

The baseline 3770 nacelle forecowl on the baseline -1122 Reference H has a lip angle of about 2.15 deg. While this is not excessive, it produces a shock wave with an intensity of about .031 in C_p and .055 in $F(y)$ for the isolated nacelle. Since all four nacelles are lined up, they produce a significant disturbance in both lift and volume. It was thought that a smaller lip angle and a reduced shock strength had the potential for an accompanying sonic boom reduction. Accordingly, the lip angle was reduced to 1.5 deg, which reduced the shock strength to .022 C_p and the $F(y)$ peak to .037, and gave an essentially constant C_p level on the nacelle forecowl. The effect on sonic boom, however, was only a 0.4% reduction in maximum overpressure. This small effect is probably due to the fact that the average pressure on the forecowl was unchanged (the lip radius and maximum radius were unchanged). This suggests that the maximum radius needs to be reduced for any sonic boom benefit. However, that would reduce the positive lift interference effects for a performance penalty, and also reduce the nacelle volume available for engine accessories.

Effect of Engine Match (A-18)

The 3770 engine is designed to have cruise thrust that is 70% of takeoff thrust, which is close to optimum for the Reference H configuration. However, for an arrow-wing planform with reduced cruise drag and poor low speed performance, the 3765 engine is a better performer. It has cruise thrust that is 65% of takeoff thrust, which is a better match to the airplane characteristics. The effect of the two engines was analyzed on the planform with the leading edge break at 70% span. After performance sizing, the better engine match gives a reduction of 35,000 lb in start-of-cruise gross weight and a boom reduction from 2.90 to 2.87 psf. The boom reduction is smaller than expected (based on the sized TOGW reduction), however, because of slightly lower altitude and the fact that the 3765 is physically shorter in length so that the pressure levels on the nacelle exterior are higher.

Other Studies on the Reference H

Fouladi in Reference 3 describes CFD results for the sonic boom analysis of the two baseline configurations (-1122 and -1405), and also the boom-softened configuration (1444). He also describes CFD optimization results for the optimization of fuselage camber and wing dihedral. Cheung in Reference 4 presents his CFD analysis of the baseline sonic boom (1122) and optimization of wing leading edge sweep and wing dihedral.

As can be seen in Figure 4, many of the potential boom-softening options have not yet been studied. Although 18 items remain untouched, many of them are low priority because of their expected adverse effect on airplane performance. Other options need further study. Wing dihedral is a special case that was given considerable attention, and is reported in the next section.

WING DIHEDRAL

Positive dihedral provides a reduction in sonic boom because of the increase in the virtual length of the lift and volume distributions. A fairly aggressive dihedral design (5 deg) was adopted to fully exploit the boom reduction and explore the effect on performance. Both MLT and CFD methods were used to design the dihedral "shape". The CFD results are reported in References 3 and 4. The MLT far-field wave-drag method results are described here in some detail since they provide some insight into the benefit of wing dihedral, and gave good results compared to the CFD design methods.

Figure 12 shows the D/Q of the equivalent bodies of revolution for the -1405 baseline as cut by the Mach angle for azimuthal angles, θ , from -90 to $+90$ deg. The D/Q value at $\theta = -90$ deg is very large and is precisely the equivalent body used for sonic boom calculation for the boom that propagates directly downward. (The sonic boom at θ values from zero to $+90$ propagate upward and would be of interest only for secondary booms). It appears that conventional designs are inadvertently designed to produce the strongest boom directly below the vehicle! Actually, this will always be the case for a conventional design with a straight wing trailing edge and with the nacelle inlets aligned at the same longitudinal station. Wing dihedral provides a way to reduce the high D/Q for the equivalent body at $\theta = -90$ deg by making the wing appear to be more swept, and also by making the nacelles appear staggered due to the shear between the inboard and outboard nacelles.

Figure 12 also shows the D/Q variation for the -1405 with wing dihedral. The average D/Q is essentially unchanged, but the D/Q for the $\theta = -90$ equivalent body is reduced by one-half, which is directly related to the boom reduction for the downward propagating boom.

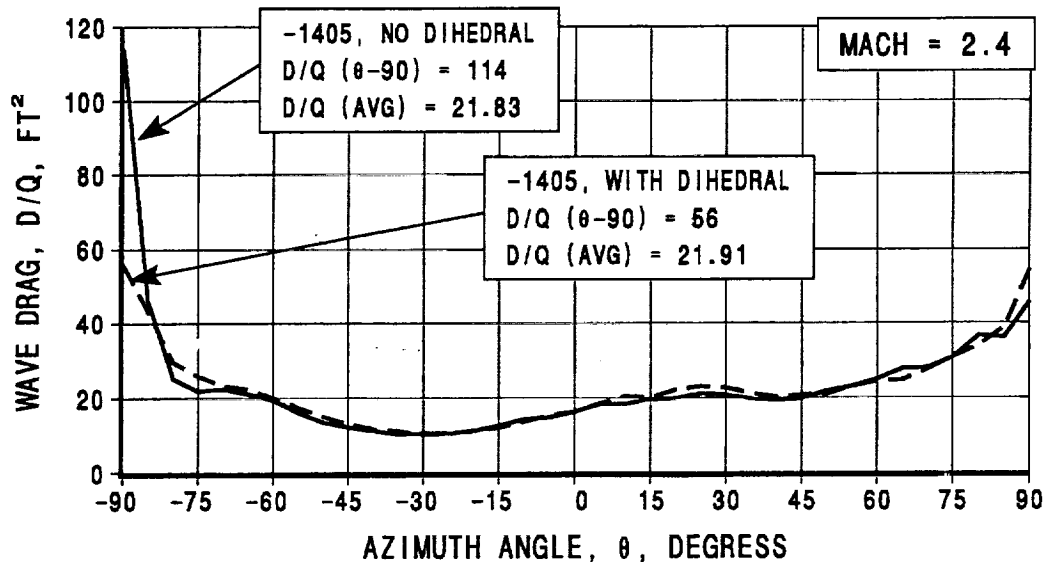


Figure 12. Variation of wave drag D/Q with azimuth angle, θ , with and without dihedral.

Figure 13 below shows the build-up of the equivalent areas of the different airplane components at Mach 2.4 for the θ -90 cuts. The sharp area peak caused by the nacelles and the sudden drop at the wing trailing edge contribute to a very high-drag equivalent-body, with a D/Q of 114. This analysis illustrates a significant sonic boom "problem" of the Reference H planform. The area distributions in Figure 14 show the effect of wing dihedral in reducing the maximum area and adding effective sweep to the wing trailing edge. The D/Q of the θ -90 total equivalent body with dihedral is reduced by one-half to 56. However, the average D/Q (or wave drag) is essentially unchanged.

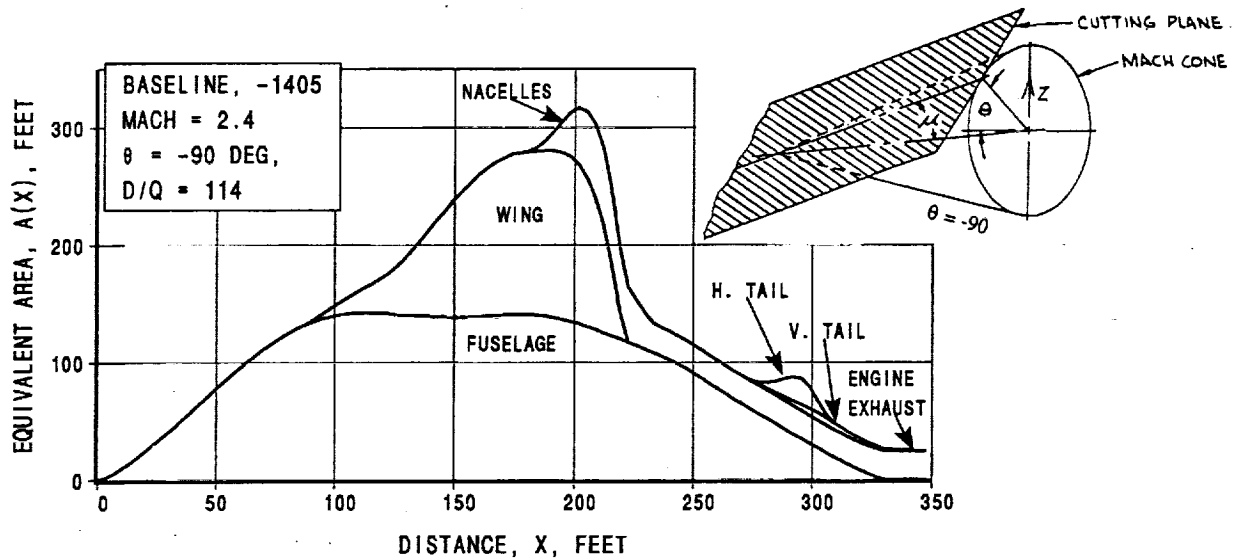


Figure 13. Equivalent body due to volume for θ -90 deg cut at Mach 2.4.

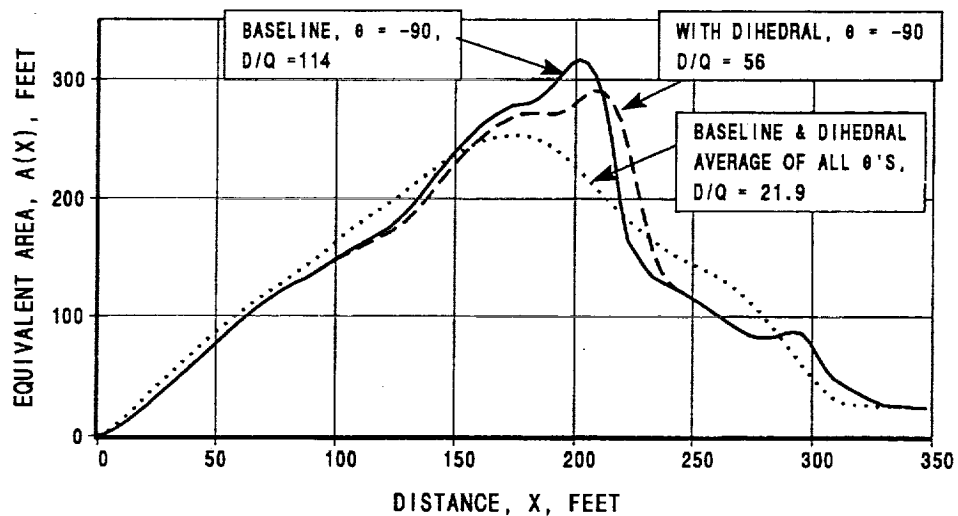


Figure 14. Equivalent-body area distributions for θ -90 cuts at Mach 2.4, with and without dihedral.

The MLT method for designing wing dihedral consisted of using far-field supersonic area rule methods (Ref. 5) to determine an optimum dihedral shape. It was obvious vertical separation of the inboard and outboard nacelles was beneficial and that the wing tip should be as high as possible. However, structural aspects of wing dihedral are a major concern, since any additional wing weight will increase OEW and MTOW, degrading overall airplane performance. The wing tip shear was therefore limited to about +58 inches with respect to a flat wing (and +83 inches from the baseline wing with its small anhedral). CFD optimization results (Refs. 3, 4) also provided some useful insight. The final dihedral design on the boom-softened -1444 reduced the D/Q value at $\theta -90$ to 37.4, with a small decrease in average D/Q. Figure 15 gives a comparison of the span-wise wing shapes with and without dihedral.

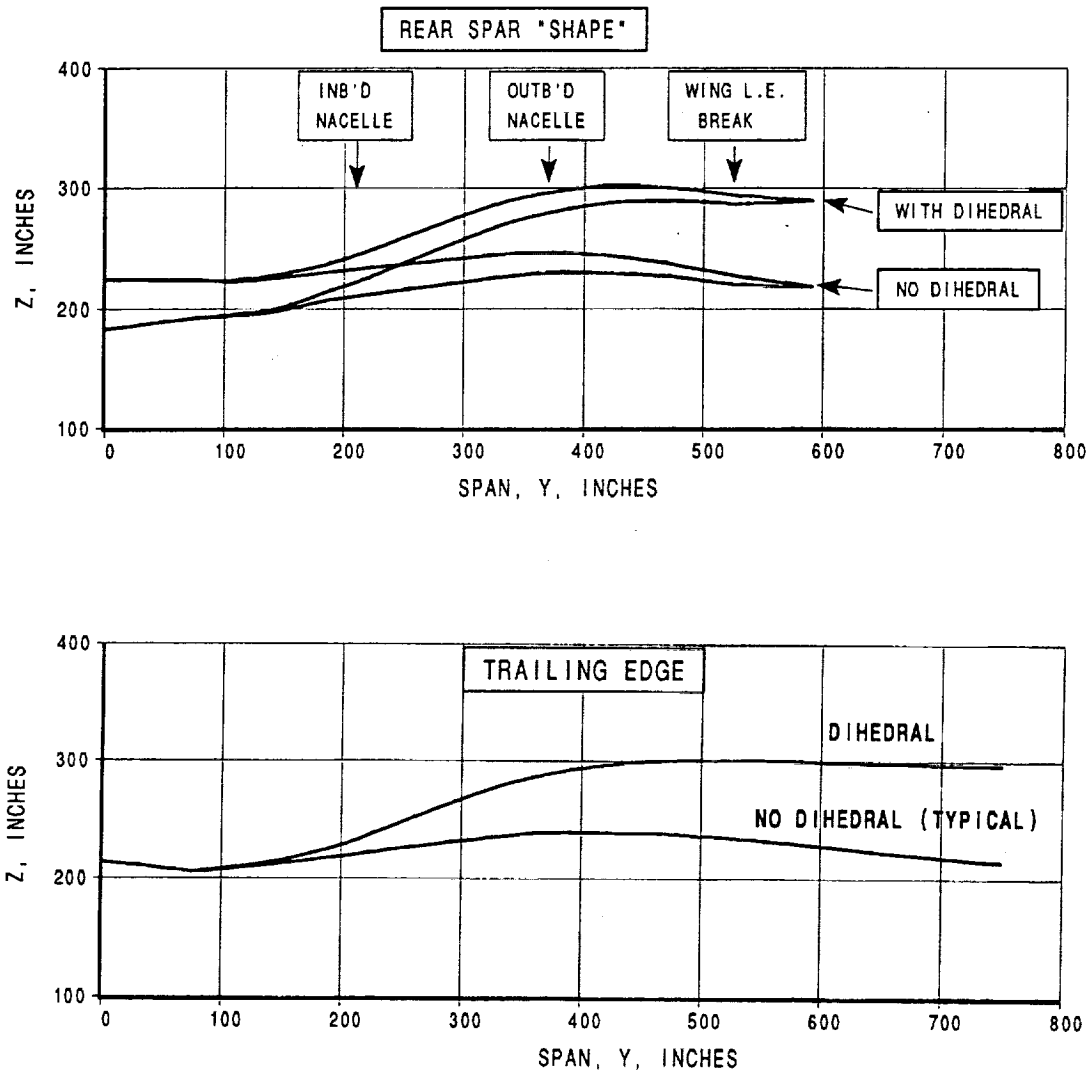


Figure 15. Rear views of trailing edge and rear spar "shapes", with and without dihedral.

While the MLT design method only dealt with volume effects, it appears that the resulting design provides a significant reduction in the lift contribution to sonic boom, as well. The sonic boom reduction is 5% in maximum overpressure for the 5 degrees of dihedral.

The impact of wing dihedral on OEW and MTOW was assessed through structural and performance analyses. A fairly detailed non-linear structural analysis gave a 20% increase in the weight of the wing box. This was offset by a weight decrease because of a shorter landing gear. Wing dihedral places the inboard nacelles higher from the ground, which determines the landing gear length for adequate clearance during takeoff rotation and landing flare. The landing gear of the -1444 was 12 inches shorter than it would have been without wing dihedral.

The weight increments for wing dihedral are as follows:

Unsize Δ OEW	
Wing structure	+3,950
Landing gear	<u>-1,190</u>
Net difference	+2,760 lb
Sized Δ MTOW	
	+13,900 lb

Wing dihedral introduces an additional complexity to the configuration, with good and bad effects, which will need to be studied and understood. Favorable effects include the following:

- 1) Reduced sonic boom because of the increase in virtual lifting length.
- 2) Reduced length (and weight) of the main landing gear. Or, for the same gear length, there would be more touchdown clearance. For the HSCT, "tail strike" is really "nacelle strike", and may be a compelling reason to consider wing dihedral as a way to protect the expensive nacelle-nozzle-engine hardware.

Unfavorable effects of wing dihedral include the following:

- 1) Reduced lateral-directional stability and handling qualities, specifically, reduced lateral control during crosswind landing, and reduced control during high speed engine failure (rolling moment due to sideslip). By one estimate, five degrees of wing dihedral means 20% more lateral control authority will be required.
- 2) Increased wing weight will be required to maintain wing structural requirements.

In conclusion, wing dihedral shows promise for sonic boom reduction, but the adverse effects to the configuration aerodynamics and structure must be minimized.

BOOM-SOFTENED CONFIGURATION, 1080-1444

The result of the parametric trade studies reported in previous sections showed that the most promising boom-softening options are related to changes to the wing. This is consistent with the fact that the HSCT sonic boom is lift dominated. The planform trade study, in particular, indicated that increasing the outboard wing sweep from 48 to 55 deg was beneficial. In addition, the Task 11 (Technology Integration) Planform Study showed a promising configuration with 55 deg outboard sweep, the Planform J (or 1080-1407). This planform has several boom-softening features, such as longer lifting length, increased average wing leading edge sweep, and a further outboard location of the break in the outboard wing leading edge sweep (52% span for the -1405 and 70 % span for the -1407). Accordingly, the -1407 became a candidate boom-softened configuration.

A number of additional boom-softening options were considered (such as fuselage forebody camber and reduced nacelle forecowl angle), but most were rejected because of little or no sonic boom reduction or adverse effects to airplane performance. The one exception was wing dihedral. As described in the previous section, wing dihedral gives an effective increase in wing sweep and a nacelle stagger effect. The boom-softened -1444 configuration, therefore, has the planform of the -1407 with the addition of wing dihedral; it differs from the -1405 in the wing design only. The fuselage area-ruling is slightly different because of the different wing. Empennage, engines, systems, landing gear, etc., are all identical for both configurations. A comparison of the -1405 and -1444 wing parameters and general features are given in Figure 16 below.

Parameter / Feature	units	-1405 Baseline	-1444 Derivative
Wing Parameters*			
Wing Span	ft	137.2	125.1
Wing area (gross)	ft ²	8500	8500
Aspect Ratio	--	2.21	1.84
Wing L.E. Sweep	deg	76/68.5/48	71.0/55.0
Average L.E. Sweep	deg	59.0	65.7
Wing L.E. Break	% span	52	70
Wing Dihedral	deg	-2.5	+4.8
General Features*			
MTOGW	lb	672,700	672,700
Fuselage length	ft	314.0	314.0
Engine size	lb/sec	900	900
Tri-class passengers	--	304	304

* Note: These are the point design values (unsized).

Figure 16. Comparison of key airplane characteristics, -1405 and -1444.

A direct comparison of the two planforms is shown in Figure 17 for the same gross wing area of 8500 ft². This clearly shows the boom-softening features of the -1444 planform: longer lifting length, increased leading edge sweep, and 70% span leading edge break.

Since the aspect ratios are so different for the two wings, the aerodynamics are considerably different also. In particular, the low aspect ratio (1.84) of the -1444 gives high L/D at Mach 2.4 cruise, as shown in Figure 18. However, the higher aspect ratio (2.21) of the -1405 gives better L/D at Mach numbers below Mach 1.5. The wing dihedral design is shown in Figures 15. Figure 19 is a two-view drawing of the -1444.

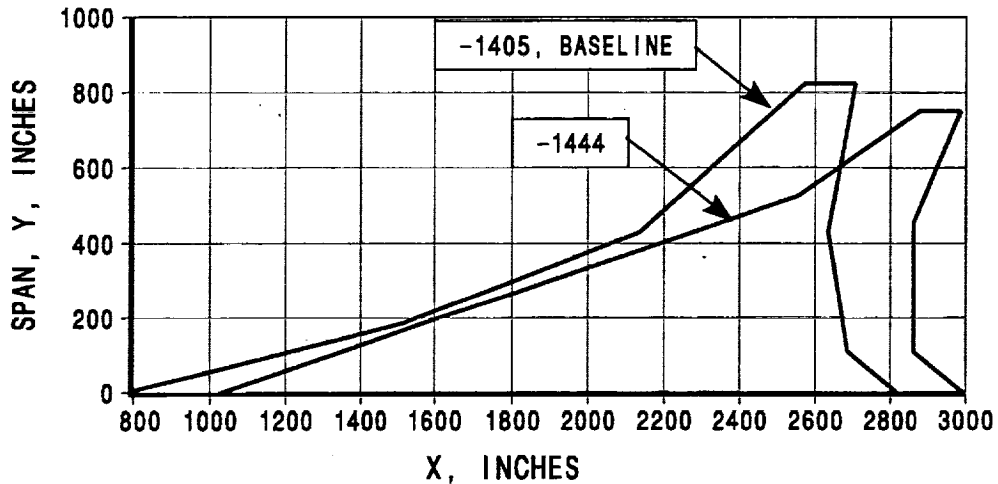


Figure 17. Comparison of the two wing planforms at 8500 ft² gross area.

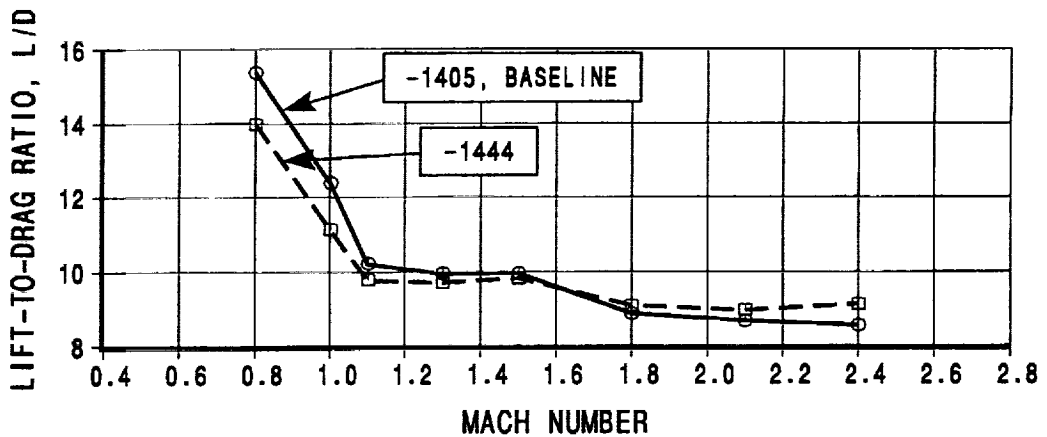


Figure 18. Comparison of L/D with Mach number for the two configurations.

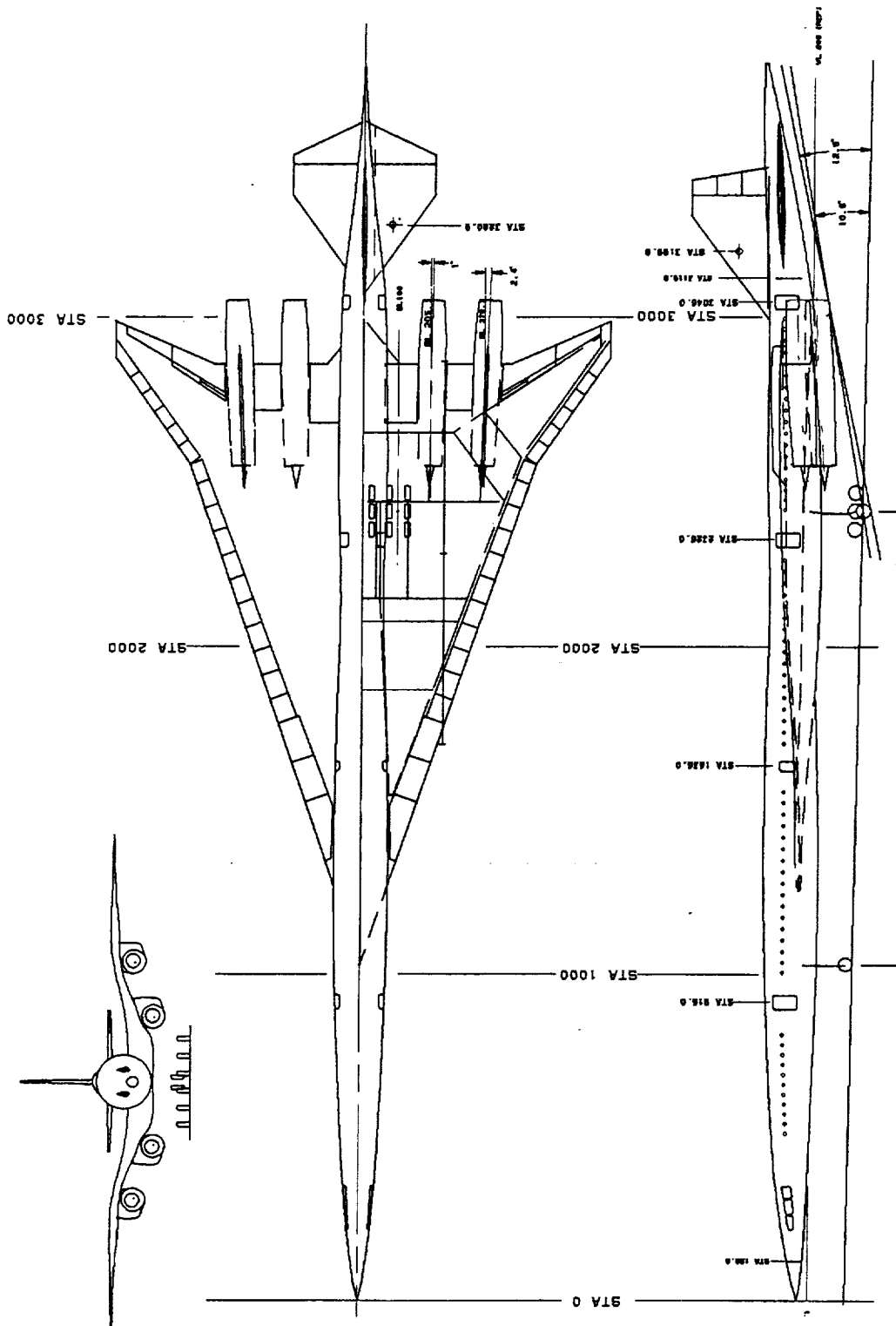


Figure 19. Configuration drawing of the Boom-Softened Configuration, 1080-1444.

The performance sizing of the -1444 is an important result, since it gives a direct measure of the performance gain or loss due to incorporating the boom-softening features. The performance sizing of the baseline -1405 was given in Figure 2. The performance sizing of the -1444 was done with the same sizing rules as for the -1405 (Task 11 rules). The resulting performance-sizing chart (or "thumbprint") is given below in Figure 20.

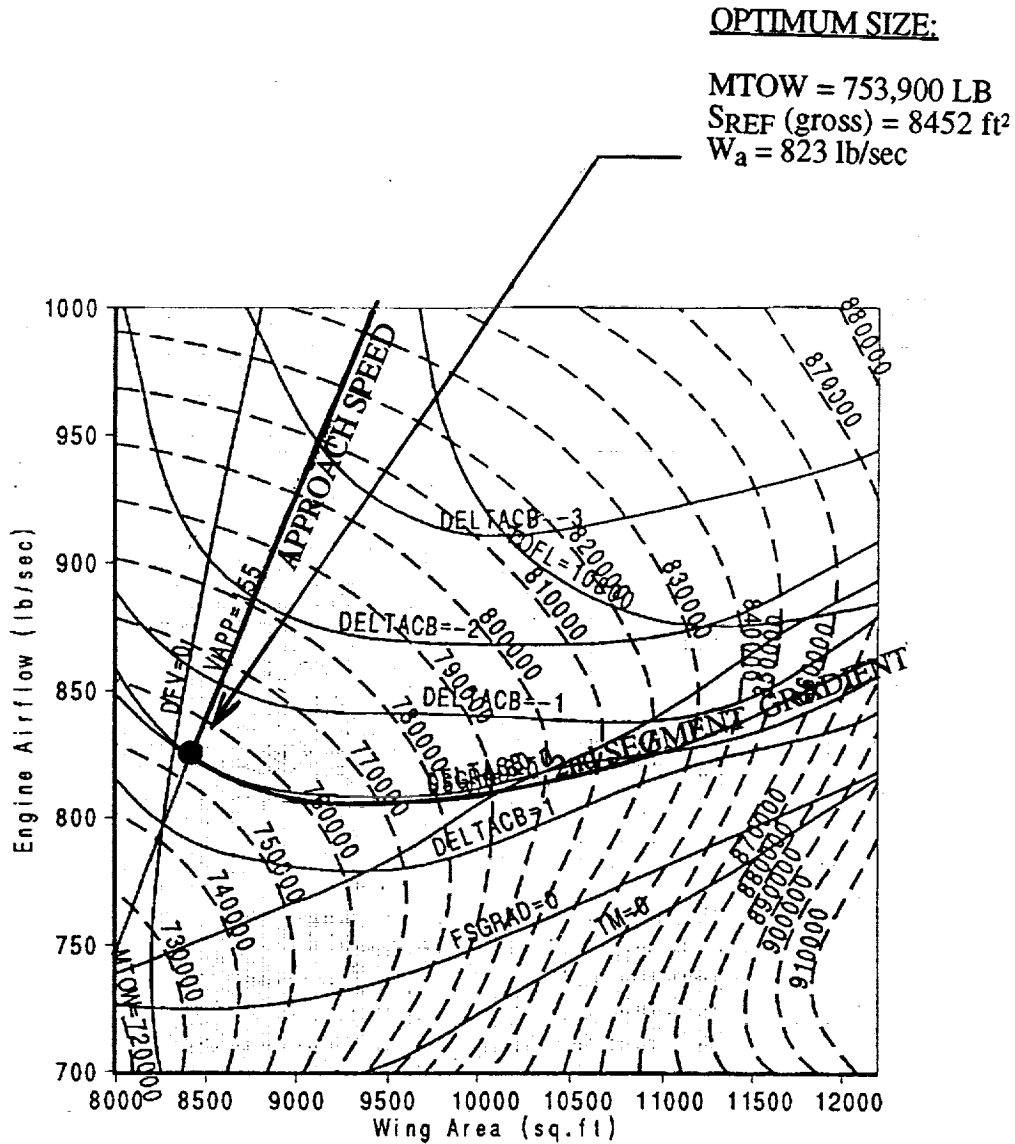


Figure 20. Performance-sizing chart for the Boom-Softened 1080-1444.

Figure 21 below summarizes the two performance-sized airplanes. The thumbprint in Figure 20 shows that the -1444 wing is sized very close to the "design point" size of 8500 ft². This is smaller than the -1405, due to adequate wing volume for fuel at a smaller area. The -1444 sizing point is determined by landing approach speed (155 KEAS) and second segment climb gradient. Low speed issues are most critical for the -1444, while the -1405 the sizing point was determined by fuel volume and climb time. At this -1444 sizing, two low-speed requirements were relaxed somewhat; takoff field length and takeoff noise levels were higher than desired. It was felt that further development and optimization of takeoff leading edge flap setting could eventually provide adequate performance.

Parameter	units	Baseline -1405	Derivative -1444	-1407
MTOW	lb	746,900	753,900	740,000
SREF	ft ²	9,119	8,452	8,293
W _a	lb/sec	774	823	807
OEW	lb	312,163	317,882	309,683
Block Fuel	lb	332,184	330,206	325,250
Block Time	hr	5.29	5.24	5.24
All-engine TOFL	ft	10,730	12,200	12,210
CL _{approach}	--	0.658	0.623	0.623
V _{approach}	KEAS	143.4	154.7	154.5
Start Crz Altitude	ft	53,600	55,335	55,300
Start Crz GW	lb	638,700	665,135	651,700
Start Crz L/D	--	8.54	9.11	9.07

Figure 21. Comparison of -1405 and -1444 Performance Sizing.

The -1407 configuration performance sizing was available from Task 11, which allows a determination of the effect of wing dihedral on performance (the only difference between the -1407 and -1444 is wing dihedral). The performance-sized parameters for the 1407 are shown in Figure 21, and some important increments are summarized as follows:

Configuration	Δ OEW	Δ MTOW	Δ (L/D)
-1405, Baseline	0.0	0.0	0.0
-1407	-2480	-6900	xx
-1444	+5719	+7000	+0.57

The sonic boom analysis of the two configurations was updated after the performance sizing to account for differences in start-of-cruise gross weight and altitude. The standard MLT methods were used (the Boeing version of Ref. 6). Sonic boom was also analyzed with a CFD method and is reported by Fouladi in Ref. 3.

Sonic boom loudness for the two pressure signatures is 108.5 PLdB for the -1405 and 108.2 PLdB for the -1444, for a difference of about 2.3 PLdB.

An approximate build-up of the sources of the sonic boom reduction is as follows:

Configuration	ΔP_{\max} psf	$\Delta(\Delta P_{\max})$ %
Baseline (1405)	2.97	0.0
Increase in wing sweep	2.88	-3.0
plus increase in lifting length	2.70	-9.0
plus wing dihedral (1444)	2.57	-13.5

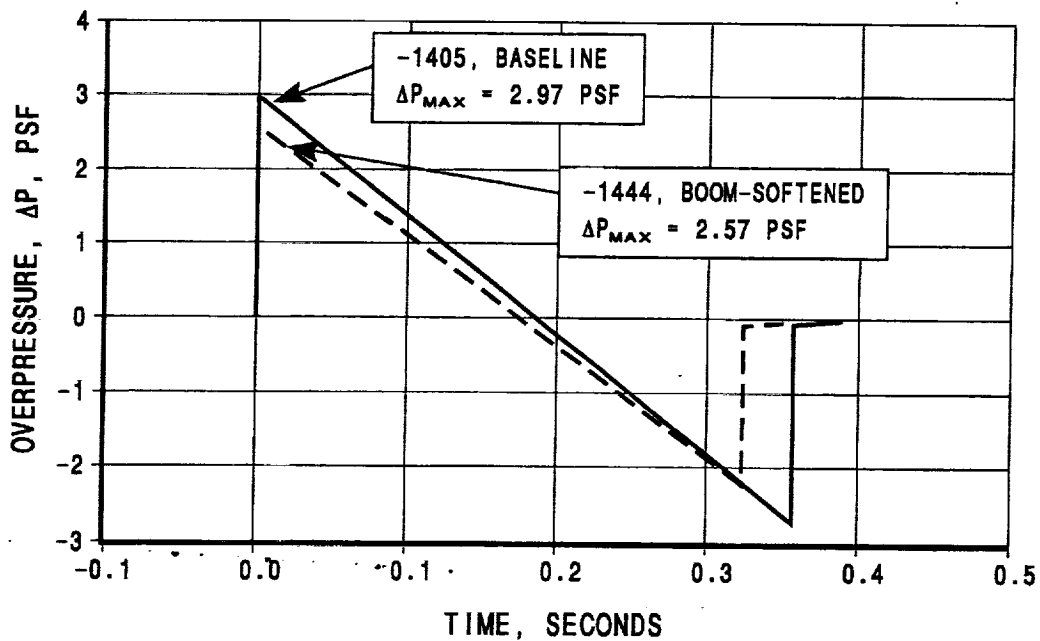


Figure 22. Sonic boom pressure signatures for baseline and modified configurations.

FUTURE DIRECTIONS

The work of Jones (Ref. 7) and Hayes and Weiskopf (Ref. 8) in establishing sonic boom lower bounds is directly applicable to boom-softening efforts, since far-field N-waves are assumed in both cases. The lower bound for typical HSCT cruise conditions indicate about 1.8 psf maximum overpressure. However, we do not have the design freedom to achieve such low overpressures. The results to date indicate 2.5 psf is within range. Areas of further study include the following:

- Only about half of the candidate boom-softening options have been examined, as indicated in Figure 4. More work is certainly warranted.
- Certain boom-softening options deserve further consideration. For example, wing dihedral is a poor man's way to obtain effective wing sweep and nacelle stagger.
- CFD design and optimization methods offer the potential for achieving further reductions in ways that are not obvious or expected.

CONCLUSIONS

- The greatest potential for sonic boom reduction rests on the tailoring of the lift distribution by modifications to the wing planform and size. Promising modifications include increased wing size (decreased wing loading), and increased wing slenderness, which may be achieved through increased wing leading edge sweep and/or reduced span.
- Wing dihedral shows promise for sonic boom reduction, but the adverse effects on the aerodynamics and structure must be understood and minimized.
- The modifications that are most beneficial for reduced sonic boom aggravate the low speed, takeoff field length, and community noise problems.
- The constraint imposed by the need for very small or no performance penalty is a severe one and will limit the range of boom-softening modifications.
- For the -1444 configuration, with aggressive boom-softening and significant wing modifications, about 0.4 psf reduction in maximum overpressure was achieved (from 2.97 to 2.57 psf). However, this is only about 2.3 db reduction in loudness (from 110.5 to 108.2 PLdB). This is at the expense of a 1% penalty in MTOGW.
- Technology advances that result in greater efficiencies in structures and propulsion will translate directly into reduced sonic boom, provided that these advances produce a reduction in wing loading.

ACKNOWLEDGMENTS

I would like to thank the Team for their hard work. The Team members were as follows: Reggie Abel (Boeing), Dan Baize (NASA, LaRC), Samson Cheung (MCAT @ NASA Ames), Kamran Fouladi (Lockheed @ NASA LaRC), George Haglund (Boeing), and Eugene Tu (NASA Ames). Our technical discussions were always stimulating and productive; you made my job as Team Leader easy and fun. Each of you contributed in significant but different ways. Special thanks go to Kamran, Eugene, and Samson for your fine CFD work. You broke new ground with your CFD optimizations of wing dihedral with nacelles.

For the performance sizing, the following Boeing personnel provided expert guidance and analyses: Eric Adamson (High-Speed Aerodynamics), Tom Creighton (Configuration), Jim Fogleman (Stress / Structures), Glenn Parkan and Jim Rams (Weights), Theron Ruff and Jeff Coffey (Performance Sizing), and Satish Samant (Low-Speed Aerodynamics).

REFERENCES

1. Edwards, Thomas A., editor: High-Speed Research: Sonic Boom, Volume II. NASA CP-10113, Feb., 1994.
2. McCrudy, David A., editor: High-Speed Research: 1994 Sonic Boom Workshop, NASA/CP-1999-209699, 1999.
3. Fouladi, Kamran: Langley's Computational Efforts in Sonic-Boom Softening of the Boeing HSCT. High-Speed Research: Sonic Boom, NASA/CP-1999-209520, 1999.
4. Cheung, Samson: Sonic Boom Minimization Efforts on Boeing HSCT Baseline. High Speed Research: Sonic Boom, NASA/CP-1999-209520, 1999.
5. Middleton, W. D., et al: A System for Aerodynamic Design and Analysis of Supersonic Aircraft. Part 1 - General Description and Theoretical Development. NASA CR-3351, December, 1980.
6. Hayes, Wallace D., et al: Sonic Boom Propagation in a Stratified Atmosphere, with Computer Program. NASA CR-1299, 1969.
7. Jones, L. B.: Lower Bounds for Sonic Bangs. J. Royal Aeron. Soc., Vol. 65, June, 1961, pp 433-436.
8. Hayes, Wallace D., and Weiskopf, Francis B.: Optimum Configurations for Bangless Sonic Booms. Quarterly of Applied Mathematics, October, 1972, pp 311-328.

Boom Softening And Nacelle Integration On An Arrow-Wing High-Speed Civil Transport Concept

Robert J. Mack

NASA Langley Research Center

Sonic Boom Workshop

September 12 - 13, 1995

BOOM SOFTENING AND NACELLE INTEGRATION ON AN ARROW-WING HIGH-SPEED CIVIL TRANSPORT CONCEPT

Robert J. Mack

NASA Langley Research Center

Hampton, Virginia

SUMMARY

An arrow-wing High-Speed Civil Transport (HSCT) concept, the HSCT-11C, was designed as a "boom-softened" modification of a McDonnell Douglas baseline conceptual aircraft. Preliminary design estimates indicated that the HSCT-11C had about the same weight as the McDonnell Douglas baseline, had an estimated range of about 5000 nautical miles (n.mi), and at full engine power, could takeoff in less than 11,000 feet. A sonic-boom analysis predicted that the "boom-softened" HSCT-11C would generate an N-wave signature on the ground with a nose-shock strength of about 2.4 psf without nacelles, and about 2.7 psf with nacelles. By mounting the engines further aft under extended inboard-wing sections, the predicted ground overpressure nose-shock strengths of a modified HSCT-11C concept, the HSCT-11E, were about 2.5 psf without nacelles, and about 2.6 psf with nacelles; both pressure signatures having an N-wave shape. A comparison of the HSCT-11C, the HSCT-11E, and their F-functions suggested that both nacelle-off and nacelle-on pressure signatures could be made similar, with pressure signature nose-shock strengths at about 2.4 to 2.5 psf. By reducing engine nacelle volume and nacelle-wing interference-lift disturbances, efforts to soften the sonic boom further could proceed further, with limitations dictated by more practical considerations of structure, drag, and engine performance.

INTRODUCTION

During the last cycle of concept design and wind-tunnel testing, the goal of the low-boom-shaped HSCT concepts (the B-935, the LB-16, and the LB-18) was to meet mission requirements and generate shaped, ground-level pressure signatures with nose shock strengths of 1.0 psf or less. The wind-tunnel tests of these concepts produced results that were partially successful and encouraging although not fully up to expectations. In spite of this, however, these conceptual designs were overly optimistic and not acceptable because: the wing planforms had excessive area; the wing structural aspect ratio was too high; one concept had aft-fuselage rather than under-

the-wing engines; and the gross takeoff weights were unrealistically low because of engines that were early, high-tech versions of later, revised, more-realistic engines.

The need for reducing the ground-level overpressure shock strengths still existed; a need to be met within more restrictive guidelines of mission performance and gross takeoff weight limitations. Therefore, it was decided that the next conceptual design cycle would focus on decreased nose shock strengths, "boom softening," in the signatures of the Boeing and the McDonnell Douglas baseline concepts rather than low-boom concepts with shaped-signature designs.

Overly-optimistic results were not the only problem with these low-sonic-boom concepts. Papers given at the 1994 Sonic-Boom Workshop had demonstrated that the problem of successful nacelle integration on HSCT concepts had only been partially solved. Wind-tunnel pressure-signature data, reference 1, from the HSCT-11B (a.k.a. the LB-18) wind-tunnel model, reference 2, showed that the Langley HSCT design and analysis method had been successful in reducing the nacelle-volume disturbances in the flow field. This was due to the engine nacelles mounted behind the wing trailing-edge on the aft fuselage so that no nacelle-wing interference-lift flow-field disturbances were generated. While acceptable from a sonic-boom research point of view, this concept was unacceptable from several practical and structural considerations.

Preliminary wind-tunnel pressure signature data from the LB-16 wind-tunnel model, reference 3, which had the engine nacelles mounted under the wings (the usual location), indicated that the application of the Langley nacelle-integration method had been only partially successful in the reduction of the nacelle-volume with nacelle-wing interference-lift pressure disturbances. So, "boom softening" had to also address the task of successful integration of the engine nacelles, with the engines in the required under-the-wing location. Unless this problem was solved, low-sonic-boom and low-drag modifications to the wing planform, the airfoil shape, and the fuselage longitudinal area distribution could be nullified if the nacelle disturbances added increments to the nose-shock strengths that were removed through component tailoring.

In this paper, an arrow-wing boom-softened HSCT concept which incorporated modifications to a baseline McDonnell Douglas concept is discussed. The analysis of the concept's characteristics will include estimates of weight, center of gravity, takeoff field length, mission range, and predictions of its ground-level sonic-boom pressure signature. Additional modifications which enhanced the softened-boom performance of this concept are also described as well as estimates of the performance penalties induced by these modifications.

SYMBOLS

A_E	equivalent area, ft^2
C_L	lift coefficient
$C_{L,I}$	nacelle-wing interference-lift coefficient
$C_{L,W}$	wing-alone lift coefficient
$F(y)$	Whitham F-function with parameter y , $\text{ft}^{1/2}$

h	altitude, ft
l_e	effective length along the longitudinal axis, ft
M	Mach number
p	ambient pressure, psf
Δp	overpressure in flow field due to aircraft, psf
W	weight of concept at start of cruise, lb
x	axial distance, ft
x_e	effective distance in the longitudinal direction, ft
y	spanwise distance, ft
y	Whitham F-function effective-length parameter, ft
α	aircraft angle of attack at cruise, deg
β	Mach number parameter defined by $(M^2 - 1.0)^{1/2}$

DESIGN OF THE ARROW-WING HSCT-11C CONCEPT

The preliminary design of the arrow-wing HSCT-11C concept was made using the methods outlined in reference 4 along with the modifications reported in reference 5. It was carried out in the following order: (1) concept layout; (2) calculation of component equivalent areas where these area distributions are smooth and continuous; (3) calculation of F-functions from the smooth and continuous equivalent areas; (4) calculation of F-functions for aircraft components whose equivalent areas are not smooth and continuous; (5) summation of F-functions to predict ground-level pressure signatures; (6) prediction of weights and center of gravity; (7) prediction of takeoff and supersonic-cruise characteristics; and (8) redesign to obtain convergence of results.

Several lessons were learned during the last cycle of low-boom concept design and wind-tunnel model testing. Two of the most important ones emphasized the influence of wing lift (lifting length, center-of-lift location, and local lift gradients) and the importance of careful nacelle integration (diameters, inlet lip slopes, location, and interference lift). Attempts at "boom softening" that ignored these lessons would produce discouraging results due to the repetition of past mistakes. Thus, most of the discussion about design features on the Langley "boom softened" HSCT concept will focus on the treatment given to the concept's wing planform (because lift is the dominant source of flow disturbances) and the nacelle-wing integration techniques (because the inlet-lip shock and the nacelle-wing interference lift are strong secondary sources of the flow-disturbances).

Langley “Boom-Softened” HSCT Layout. The initial baseline McDonnell Douglas conceptual HSCT which served as a starting point for the Langley HSCT-11C is shown in figure 1. It is the M2.4-7A M3765-100D configuration, and the first of three aircraft concepts that were used as baselines in this “boom softening” study. Some characteristics of the McDonnell Douglas baseline concept are presented in Table A-1 of Appendix A.

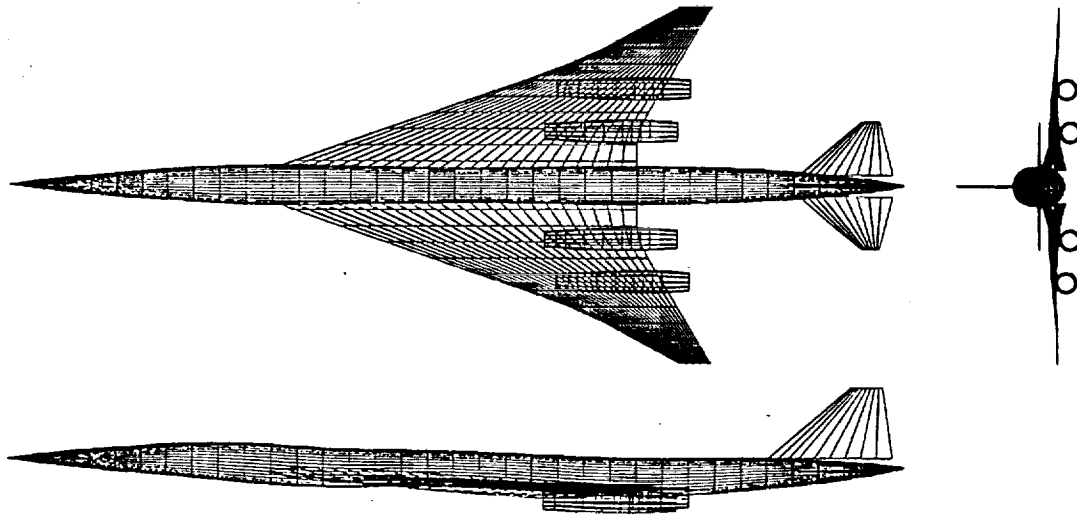


Figure 1. Three-view of the first baseline McDonnell Douglas HSCT concept.

The planform on this baseline concept was designed mainly on the aerodynamic efficiency principle that the lifting length should be no longer than needed for efficient subsonic leading-edge lift growth. A planform designed for low or “softened” boom during cruise, on the other hand, would be lengthened to reduce the lift gradients and decrease the potential for lift-enhanced nose-shock strength. The lengthening of the wing would, of course, be constrained by wing area, wing span, and trailing-edge notching. This was, of course, the main lesson learned from past experience in the design of sonic-boom tailored aircraft concepts.

The planform of the “softened boom” concept, the HSCT-11C, has about the same projected area and span as the McDonnell Douglas baseline, figure 2.

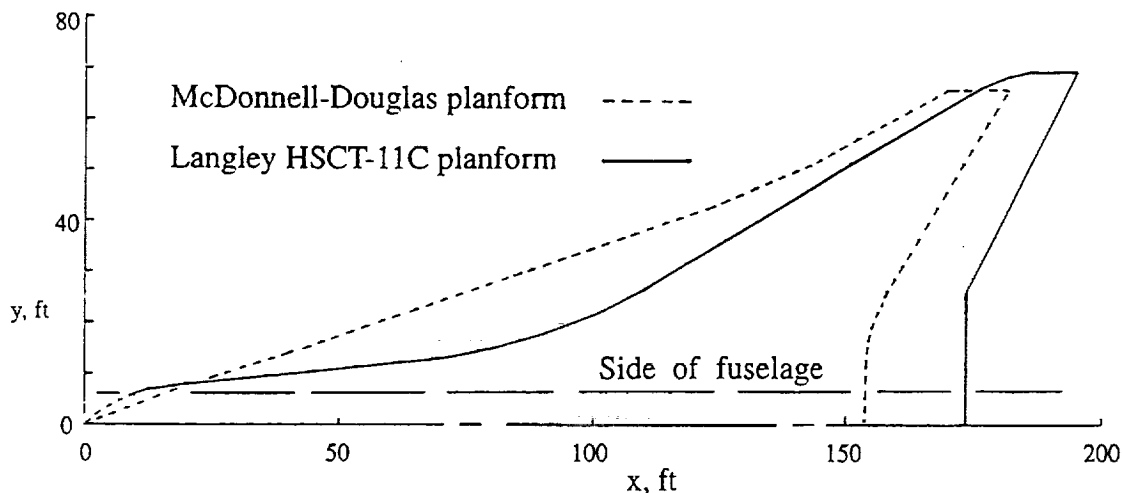


Figure 2. Comparison of the McDonnell Douglas and the HSCT-11C wing planforms.

Notice that the trailing-edge sweep angle on both concepts was the same. However, the trailing-edge break was moved outboard to maintain inboard volume for landing gear and fuel. The leading edge was also changed in a tradeoff between area and lifting length, i.e., a curved strake was added and the span was slightly increased. The outboard panel leading-edge sweep angle was the same on both the HSCT-11C and the McDonnell Douglas baseline. However, the area of this outboard panel was increased on the HSCT-11C. Note the shape of the wing leading edge at the wing-fuselage junction. This feature, used successfully on the HSCT-10B, reference 1, "jump-starts" the wing lift and the wing upwash field that is necessary for efficient utilization of the wing's camber and twist. It mimics the function of the wing apex which is buried in the forward fuselage rather than flying in the free-stream. These modifications preserved most of the aerodynamic efficiency of the wing and lengthened the wing lift, as previously mentioned, to decrease the disturbance gradients that can trigger an increase in the nose-shock strength.

Several other features on the McDonnell Douglas baseline concept were changed or modified on the "boom-softened" HSCT-11C concept. The horizontal tail was replaced with a canard control surface. This was done to ensure that the aircraft could rotate as required during takeoff. These changes can be seen in figure 3, a three view of the HSCT-11C concept. In Table A-2 of Appendix A, some characteristics of the HSCT-11C are presented for comparison with McDonnell Douglas baseline characteristics in Table A-1.

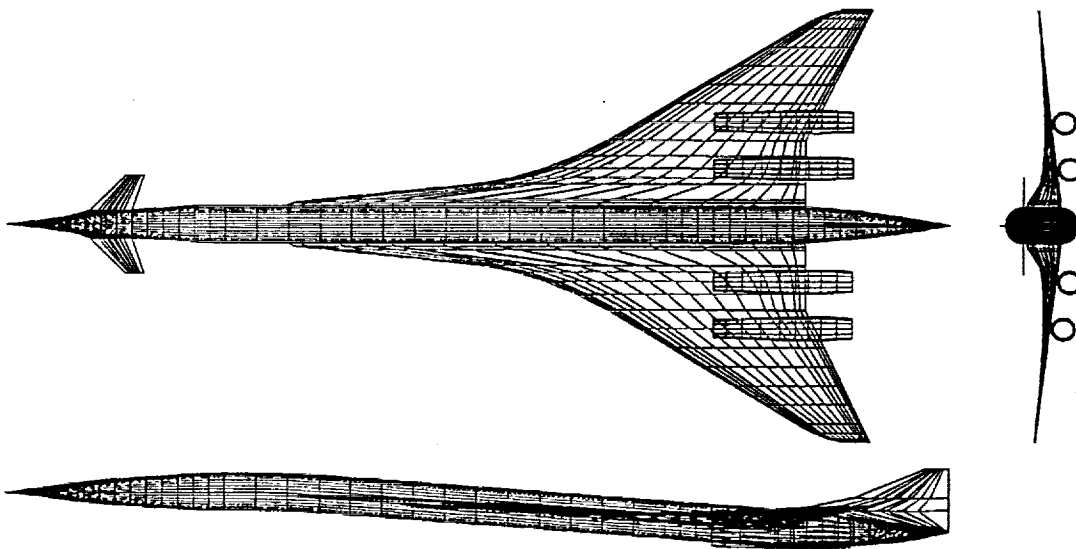


Figure 3. Three view of the arrow-wing "softened-boom" HSCT-11C concept.

As previously mentioned, a noticeable shift in wing area has taken place while the total projected area was kept about the same. The leading-edge sweep angles are very different on these wing planforms with a larger change in sweep angle on the HSCT-11C wing and more of the leading-edge having the outer-panel sweep angle. If the same airfoils and airfoil thicknesses are used, and both wing apices are at the same distance aft of the nose, the center of lift and the center of gravity will be further aft on the "boom-softened" concept. This area shift spreads the lift growth over a somewhat longer distance although there is a local increase of lift gradient across the length where the leading-edge sweep angle decreases dramatically. Moving aftward with the trailing-edge are the engine nacelles which are to be mounted as close to the trailing edge as is structurally feasible. Since the wing area on the McDonnell Douglas baseline and the HSCT-11C

concepts were virtually the same, the floor angle on both concepts could be maintained at 4.0 degrees or less during cruise.

Either a horizontal tail or a canard could control aircraft pitch during takeoff and landing, and if desired, provide lift during cruise. The canard surface could be smaller, since its moment arm was longer than that of the horizontal tail. There would be a tradeoff between canard area, canard moment arm, and wing effectiveness since the wing would be in the canard's downwash field during rotation, lift-off, and climb-out. This canard-wing tradeoff would replace the wing-horizontal tail tradeoff necessitated by the horizontal tail being in the wing's downwash field during the same segments of the mission. Since the canard moves the center of gravity forward while the horizontal tail tends to move it aft, its area and weight could be very mission-sensitive. To simplify the design of the HSCT-11C, the canard was sized to augment the wing control surfaces for takeoff control, and was set at zero-lift during the cruise segment of the mission.

It must be mentioned that HSCT configurations that incorporate sonic-boom reduction technology tend to be nose heavy during the initial stages of preliminary design. Moving the wing forward carries the under-the-wing engine nacelles along with it. However, theory-and-experiment validated sonic-boom methodology usually requires that the engine nacelles be located as far back on the configuration as possible to reduce flow-field disturbances and help with balancing of the configuration. These conflicting points will be more obvious in the discussion on nacelle integration.

Equivalent Areas. The equivalent areas contributed by the fuselage, wing, canard, fin volume, and the wing lift were summed following the method described in reference 5. These equivalent areas could be properly summed because the area distribution of each component was smooth and continuous. At cruise, the canard contributes no lift, so only the area-ruled volume of the canard surface is included in the summation. In figure 4, the longitudinal distribution of the sum of these equivalent areas is shown at the cruise Mach number of 2.4..

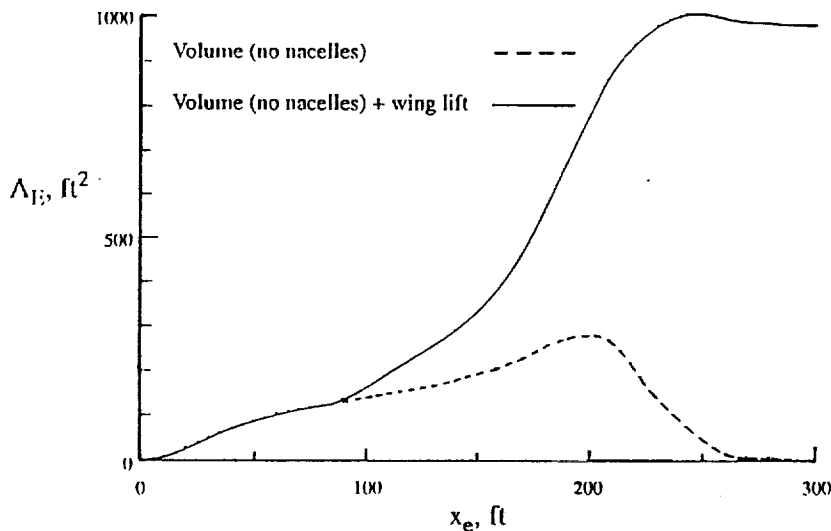


Figure 4. Summed equivalent areas from the wing, wing lift, fuselage, canard, and fin at $M=2.4$ and $\alpha = 0.60$ deg.

Equivalent areas of the engine nacelles and the nacelle-wing interference lift were also calculated, but not added directly to the previous equivalent area sum. This is because the

F-functions of the nacelle volumes have beginning singularities due to the finite-size inlet areas and inlet lip angles. Also, the F-functions of the nacelle-wing interference lift have singularities where the interference zones begin, due to the strong pressure gradients along the shock. So the nacelle-volume and nacelle-wing interference-lift effects were included in the *summation of F-functions* rather than in the summation of equivalent areas.

F-functions And Pressure Signatures. Pressure signatures were predicted from the summed cruise-condition Whitham F-function of the HSCT-11C. This total F-function had three contributions. The first contribution came from the summed wing/fuselage/canard/fin equivalent areas. A second contribution came from each of the engine nacelle volume-alone equivalent areas. The third contribution came from each pair of the nacelle-wing interference lift contributions. Since the second and third F-functions had discontinuities that are inherent in the geometry and nature of their sources, they had to be computed separately, and then summed with the other contributions. The beginning-cruise nacelle-on and nacelle-off F-functions of the HSCT-11C are given in figure 5, and the corresponding calculated ground-level pressures signature are shown in figure 6.

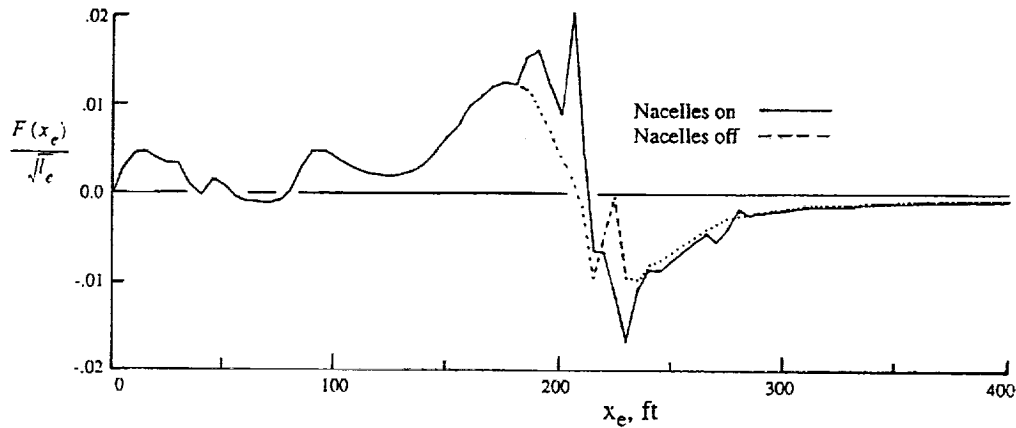


Figure 5. F-function of the HSCT-11C at beginning of cruise, $M=2.4$, and $\alpha = 0.60$ deg.

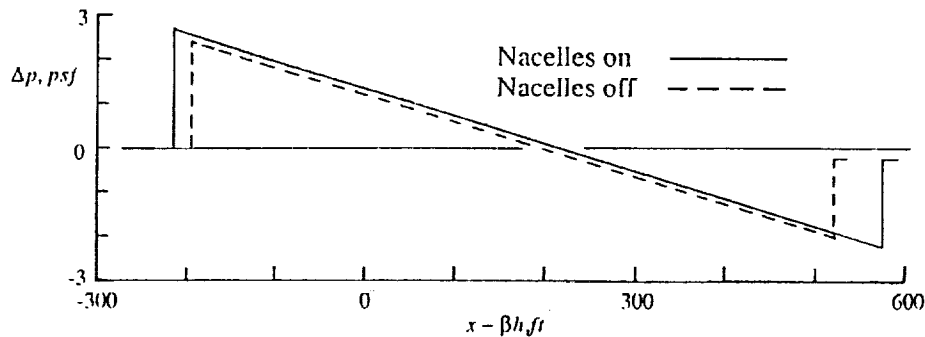


Figure 6. Predicted ground signatures of the HSCT-11C at 56,850 ft, $M=2.4$, and $\alpha = 0.60$ deg.

The McDonnell-Douglas baseline concept generated ground-level nose shocks of about 3.0 psf, so this was used as a reference value. In figure 6, the predicted nose shocks were about 2.4 psf without nacelles, and about 2.7 psf with nacelles. This nacelle-on, nose-shock strength

was about a 10 percent reduction from the baseline concept level. However, a 20 percent reduction in nose-shock strength would be possible if careful nacelle integration could reduce the nacelle-induced disturbances.

Contributions from the engine nacelles have been highlighted in figures 5 and 6 so their effects could be better understood. In figure 5, the nacelle effects, volume, wing lift, and interference lift, can be seen to combine at the most inopportune location, i.e., on the peak of the wing/wing lift/fuselage F-function. So, the extra 0.3 psf of nose-shock strength, i.e., about 10 percent of the reference nose-shock strength, between the nacelles-on and nacelles-off pressure signatures, seen in figure 6, can be attributed to the geometry and placement of the engine nacelles. Engine- nacelle staggering could have been utilized to spread the nacelle disturbances, but since the nacelles are very far aft on the wing, the inboard-nacelle set would have been the logical pair to move in a forward direction. A forward shift in the inboard engine nacelle location would have changed the situation in three ways. First, the volume-only F-function would have moved forward. Second, the interference-lift zone from the inboard nacelle pair would have increased in size, affecting more wing area with the inlet-lip shock spreading over more of the wing. Third, the new interference-lift F-function would have moved forward. The first and the third changes would not have made the situation better and perhaps, would have increased the nose-shock strength more. A different nacelle stagger could have produced more beneficial results. However, the main point is that the conventional nacelle placement under the wings usually adds the nacelle-effects F-function increments at the poorest possible location on the wing/fuselage/canard/fin F-function axis for "boom-softening" purposes. Since this is the most conservative approach of engine-nacelle positioning, it is the most difficult location for achieving significant benefits.

Weight And Center-Of-Gravity Estimate. The weights given in Table A-2 were preliminary estimates that were used to obtain sonic-boom characteristics, supersonic-cruise performance, takeoff field length, and canard surface sizing. Therefore, center-of-gravity calculations made with these weights should be considered approximate. They were still useful, however, in estimating a balance point of the aircraft in cruise, locating the landing gear, and sizing the canard for takeoff.

When fully loaded, the aircraft center of gravity was located at a distance of about 200 feet from the nose, while at the zero-fuel condition, the center of gravity was at a distance of about 196 feet. From this tentative analysis, the main landing gear bogey strut was placed at a distance of 206 feet so that takeoff characteristics could be estimated.

Takeoff And Cruise Performance Estimates. Since the weight estimates were preliminary, takeoff length was calculated with the engines only at full power. With a canard control surface area of about 216 ft² deflected 13 degrees to assist the elevons in rotating the aircraft, the aircraft lifted after a distance of about 9000 ft and at a velocity of about 377 fps (223 kt). Engine-out rudder size and the balanced-field takeoff length were not calculated due to the preliminary nature of takeoff gross weight estimate.

Figure 6 showed the predicted pressure signature at the start of cruise at Mach 2.4, an altitude of 56,850 feet, and a weight of 684,400 pounds. The canard control surface was set at zero-lift, and remained at this zero-lift setting for the duration of the supersonic-cruise segment of the mission. During the cruise segment of the mission, 254,650 pounds of fuel were consumed by the HSCT-11C concept cruising at Mach 2.4 to travel a distance of 4550 nmi.

In this simplified mission, fuel amounting to 10 percent of the gross takeoff weight was allocated to takeoff, climb, and acceleration to cruise Mach number and cruise altitude. This mission segment was estimated to cover a distance of about 200 n.mi. An additional 6,000 pounds of fuel was allocated to descent, deceleration, and landing which was estimated to cover an additional 250 n.mi. At the end of this simplified mission, there were still 46,600 pounds of fuel reserves on board.

DESIGN MODIFICATIONS WITH INTEGRATED NACELLES

The start-of-cruise F-function, figure 5, and the predicted pressure signatures (nacelles on and nacelles off), figure 6, of the HSCT-11C concept indicated that better engine nacelle integration for softened boom as well as high aerodynamic efficiency, low structural weight, etc., had to be achieved in order to remove a nacelle-induced 0.30 psf increment of nose-shock strength. Further attempts at reductions in shock strength ("boom softening") by more subtle techniques such as tailoring of the fuselage shape, carefully-scheduled wing dihedral/anhedral, etc., would then have a chance at making substantial gains.

One method for reducing the nacelle volume and interference-lift effects would be to incorporate the hyperbolic-tangent dihedral schedule proposed by George Haglund of the Boeing Commercial Airplane Company in reference 6. It locally raises the nacelles and wing panels somewhat more rapidly than a constant-angle dihedral, and results in spreading the nacelle-volume and interference-lift effects over a longer length. A three view of the HSCT-11C modified with this hyperbolic-tangent dihedral technique is shown in figure 7.

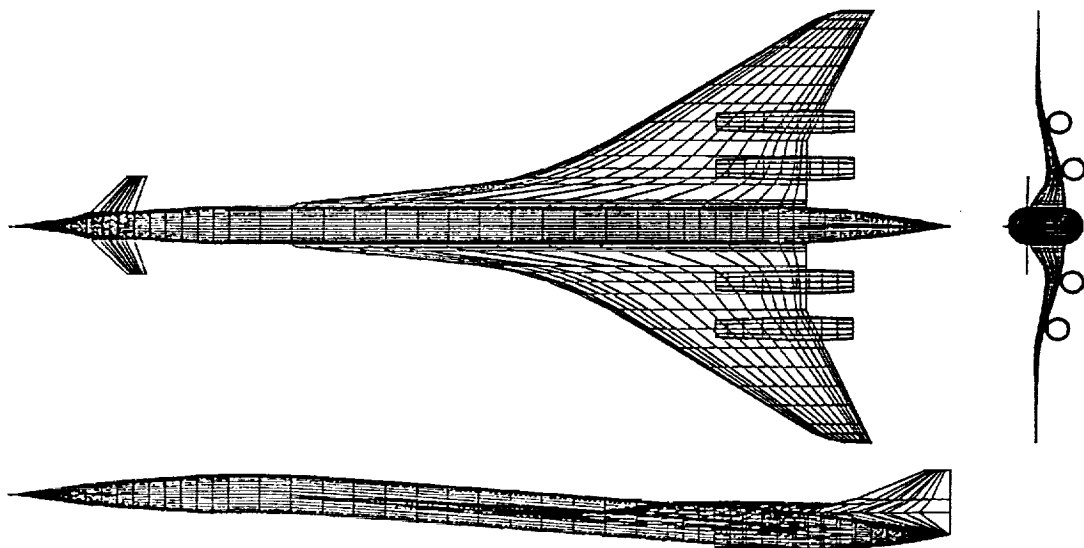


Figure 7. HSCT-11C concept with Boeing-proposed hyperbolic-tangent dihedral.

When applied to the HSCT-11C concept, the nacelle-inlet geometry and interference-lift effects were moved about 6 feet further aft along the F-function axis than is seen in figure 5. Since the local wing dihedral had been altered, the equivalent-area distributions of wing volume and lift

were also modified. Each of these changes was favorable for boom softening, but not to the extent that would make the nacelle-on and nacelle-off nose shock strengths virtually the same. Although it is a promising approach when small changes in the nacelle-effect F-function locations are desired, this application of the hyperbolic-tangent dihedral method did not offer the desired 10 to 20 foot rearward shift in the engine-nacelle volume and interference-lift F-function increments required on the HSCT-11C concept's F-function.

The nacelle-integration difficulties encountered in "boom-softening" the HSCT-11C concept would be much less severe if the nacelle-volume and nacelle-wing interference-lift F-function increments in figure 5 could be shifted by simply moving the nacelles rearward the required distance. Then, it would be possible to obtain the modified F-function shown in figure 8, and the more favorable theoretical pressure signatures shown in figure 9.

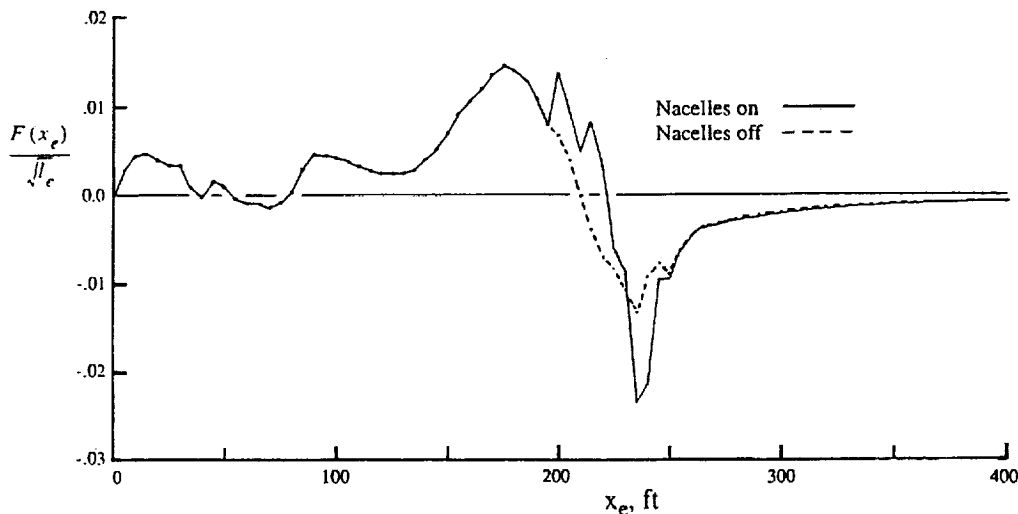


Figure 8. F-function of a modified HSCT-11C concept at $M=2.4$ and $\alpha = 0.60$ deg.

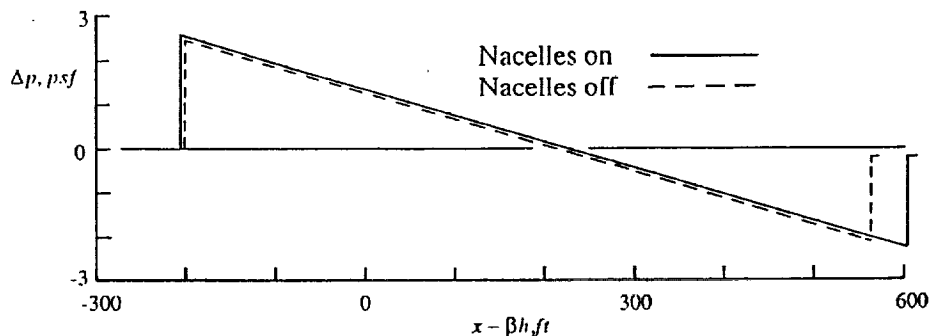


Figure 9. Predicted ground signatures of the modified HSCT-11C at 56,850 ft, $M=2.4$, and $\alpha = 0.60$ deg.

Using 3.0 psf as a reference, the nose-shock strength on the modified HSCT-11C (with nacelles) has been reduced, or "softened", between 15 and 20 percent. To obtain these results, the nacelles had to be shifted 18 feet rearward from their original positions near the trailing-edges of the wing on the HSCT-11C concept. There was no engine support available with the existing wing spars, so new support structure was designed. Since the aft-fuselage-mounted engine nacelles employed

on the HSCT-10B, reference 2, were not accepted by the HSCT community, an idea from the preliminary design of the conceptual Sukhoi/Gulfstream S-21 supersonic business jet and the conceptual Sukhoi S-51 supersonic-cruise passenger airliner, references 7 to 10, was utilized. The wing planform with the modifications required to obtain the results shown in figures 8 and 9 is shown in figure 10. A three view of the modified HSCT-11C, i.e., the HSCT-11E concept, which incorporates these modifications is presented in figure 11, and a table of data describing this modification of the HSCT-11C is given in Table A-3 of Appendix A.

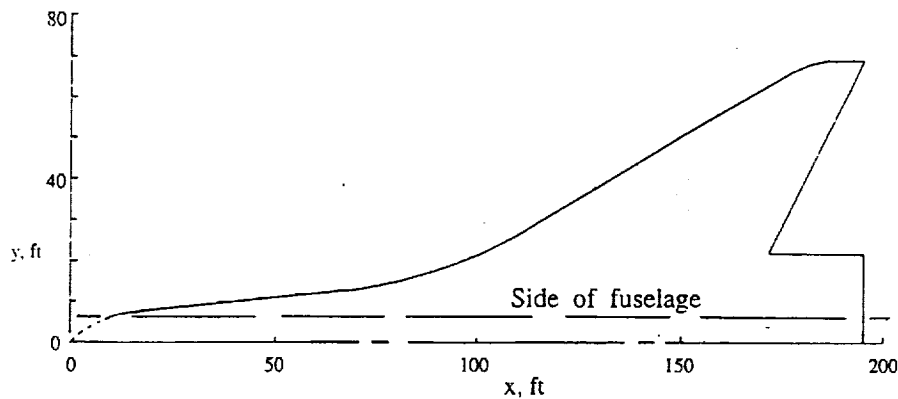


Figure 10. Wing planform of the modified HSCT-11C concept (HSCT-11E).

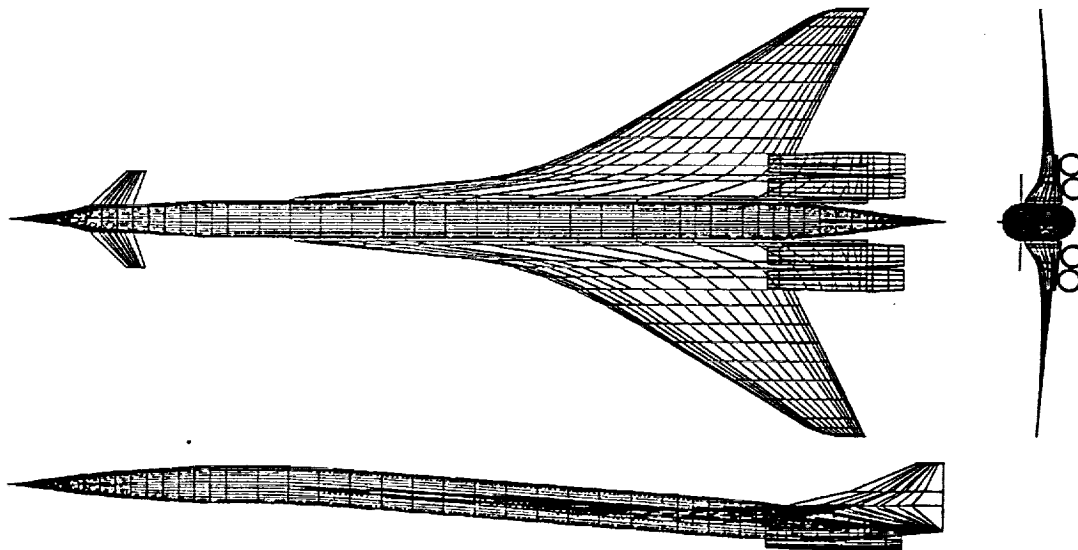


Figure 11. Three view of the Langley HSCT-11E concept.

Inboard-wing panels on the HSCT-11E were extended to function both as engine-nacelle mounts and as additional lifting surface. With these extensions in place, the total wing area increased from 9425 ft² on the HSCT-11C concept to 10,336.5 ft² on the HSCT-11E concept. This modification provided help with the “boom softening” and extra wing volume for fuel. It also increased the wing thickness for landing-gear storage, and decreased the aircraft balancing problems. However, these benefits were obtained at the expense of decreased aerodynamic efficiency, increased landing-gear length, and additional takeoff gross weight.

The problem of increased landing-gear length on the HSCT-11E concept might be solved by mounting the engine nacelles above the upper-wing surface, rather than under the wing, similar to the over-and-under nacelle mounting on the supersonic-cruise concept proposed by the Lockheed-California Company in reference 11. Such a modified HSCT-11E concept would look like the vehicle shown in figure 12, the HSCT-11F.

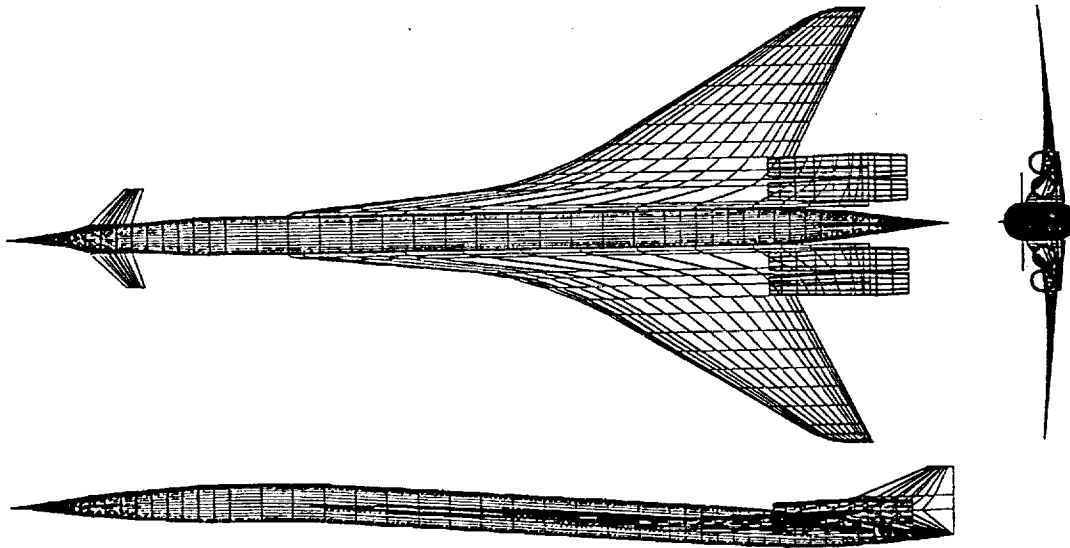


Figure 12. Three view of the modified HSCT-11E concept, the HSCT-11F.

With the engine nacelles above the wing, the landing-gear length and structural weight were reduced but, in this position, the nacelle-wing interference-lift increments were negative. This increased the angle of attack (flat-plate lift) required to meet the cruise lift coefficient, and the result was a nacelle-interference drag-due-to-lift increment not present in the HSCT-11C concept. An incremental interference moment (nose-up) was also induced, but this might be considered favorable because these low-boom or "boom-softened" HSCT concepts tend to be nose-heavy when the wings are positioned aft on the fuselage for maximum sonic-boom alleviation benefits.

By assuming, for preliminary drag comparison purposes only, that the conceptual HSCT-11E and HSCT-11F weighed about the same and had about the same size engine, supersonic-cruise drag penalties could be estimated. The sum of lift-induced, wave, and nacelle-wing interference drag coefficient increments on the HSCT-11F due to mounting the engine nacelles above the wing amounted to an incremental drag increase of 0.0007 or about a 7 percent increase in the net cruise drag coefficient. The corresponding decrease in cruise lift/drag ratio was about 6.6 percent.

There may be other favorable benefits from this above-the-wing nacelle mounting than a nose-up nacelle-wing interference-lift induced moment. With the engine nacelles shifted from the below-the-wing to the above-the-wing position, the nacelle volume effects are moved about 20 feet further aft on the aircraft F-function. Nacelle-wing interference-lift effects were moved very little, but the change in nacelle volume-effects location would help soften the nose shock. Since all these results are preliminary, additional mission performance and weight analyses would need to be done before rejecting either the HSCT-11F or the HSCT-11E, as being structurally impractical although potentially, softened sonic-boom promising.

RESULTS

The change in predicted pressure signatures between figures 6 and 9 indicated that judicious nacelle integration could be used to "soften" or reduce the sonic boom of HSCT concepts, as on the second and third of three recently-designed conceptual configurations. The first concept was the HSCT-10B (a.k.a. the LB-18) which was reported in reference 2. It had aft-fuselage-mounted engine nacelles which generated volume-alone nacelle disturbances. A preliminary sample of experimental results, reference 1, showed a validation of the theoretical predictions with both small and large nacelles, so these results were a partial validation of the Langley nacelle-integration methodology.

The second concept, the HSCT-11C, had engine nacelles mounted in the conventional under-the-wing position. It showed the potential of about a 10 percent reduction, "boom-softening," in nose shock strength with an additional 10 percent possible if nacelle-integration techniques could shift nacelle disturbances further aft.

A third concept, the HSCT-11E which was a modification of the HSCT-11C, showed a potential for about a 20 percent reduction ("boom-softening") in nose-shock strength. However, an unconventional nacelle-integration approach of moving the engine nacelles aft under an extended center-wing section was employed to achieve the desired boom-softened pressure signatures. Since the HSCT-11E would require longer landing-gear struts for takeoff clearance, the option of mounting the engine nacelles above the wing was given a quick evaluation. The estimated drag increment was large enough to suggest that this shift of the nacelles to the above-the-wing position may have significant aerodynamic performance penalties. A more thorough performance and weight analysis would be necessary to determine if this approach held promise since the effect of weight change was not accounted for in the preliminary study.

As with the HSCT-10B, wind-tunnel models and tests are desired to check the validity of the HSCT-11C or HSCT-11E pressure signature predictions. Should these wind-tunnel tests have favorable results, then the full range of applicability of the Langley nacelle-integration method will have been demonstrated. This achievement would make the methodology useful for both the analysis of supersonic-cruise aircraft and the design of low-boom or "softened-boom" conceptual aircraft.

CONCLUDING REMARKS

The arrow-wing HSCT-11C concept, derived from the conceptual McDonnell Douglas baseline aircraft and designed with low sonic-boom technology, achieved a small measure of nose-shock "boom-softening." Preliminary estimates showed that the HSCT-11C had about the same gross take-off weight as the McDonnell Douglas baseline aircraft, had an estimated range of about 5000 n.mi., and at full power, could takeoff in less than 11,000 feet. A sonic-boom analysis predicted that the HSCT-11C would generate a ground overpressure nose shock strength of about *2.4 psf without nacelles*, and about *2.7 psf with nacelles*. While the baseline pressure-signature nose-shock strength was reduced by about 10 percent, it demonstrated that significant progress could be made by a better integration of the nacelles with the airframe. This was achieved by moving the engine nacelles aft under an extended-center-wing section. The predicted ground overpressure nose shock strengths of the modified concept, the HSCT-11E, were about 2.5 psf.

without nacelles, and about 2.6 psf with nacelles. A comparison of HSCT-11C and HSCT-11E F-functions suggested that the nacelle-off and nacelle-on pressure signatures could be made more nearly the same with the signature nose shock strength at about 2.4 to 2.5 psf. This would result in a reduction in nose-shock strength ("boom-softening") of about 15 to 20 percent with more reductions potentially possible.

The HSCT-11E and its predecessor, the HSCT-10B, employed unconventional engine-nacelle locations to achieve the desired goal of either "softened" sonic boom or low sonic boom, respectively. Before either of them could be considered candidates for serious preliminary design studies, they would have to be declared "suitable" or "acceptable" conceptual designs by the United States commercial aircraft companies. From a research point of view, however, these two concepts demonstrated that it was possible to design reduced sonic-boom conceptual aircraft that incorporated realistic aircraft components, could meet reasonable takeoff field length requirements, and could carry 250 to 300 passengers over a 5000 n.mi mission range.

REFERENCES

1. Mack, Robert J.: Wind-Tunnel Overpressure Signatures From A Low-Boom HSCT Concept With Aft-Fuselage-Mounted Engines. High-Speed Research: 1994 Sonic Boom Workshop, *Configuration Design, Analysis, and Testing*, NASA/CP-1999-209699, 1999.
2. Mack, Robert J.: Low-Boom Aircraft Concept With Aft-Fuselage-Mounted Engine Nacelles. High-Speed Research: Sonic Boom, Volume II, NASA Conference Publication 10133, 1993.
3. Darden, Christine M.: Progress In Sonic-Boom Understanding: Lessons Learned and Next Steps. High-Speed Research: 1994 Sonic Boom Workshop, *Configuration Design, Analysis, and Testing*, NASA/CP-1999-209699, 1999.
4. Mack, Robert J.; and Needleman, Kathy E.: A Methodology For Designing Aircraft To Low Sonic Boom Constraints. NASA TM-4246, 1991.
5. Mack, Robert J.: Some Considerations On The Integration Of Engine Nacelles Into Low-Boom Aircraft Concepts. High-Speed Research: Sonic Boom, Volume II, NASA Conference Publication 3173, 1992.
6. Haglund, George T.: Potential For Sonic-Boom Reduction Of The Boeing HSCT. High-Speed Research: 1995 Sonic Boom Workshop, *Configuration Design, Analysis, and Testing*, NASA/CP-1999-209520, 1999.
7. Lambert, Mark, ed.: *Jane's All The World's Aircraft*, 1990-91, 81st Edition, Sentinel House, Surrey UK.
8. Lambert, Mark, ed.: *Jane's All The World's Aircraft*, 1991-92, 82nd Edition, Sentinel House, Surrey UK.

9. Lambert, Mark, ed.: *Jane's All The World's Aircraft*, 1992-93, 83rd Edition, Sentinel House, Surrey UK.
10. Lambert, Mark, ed.: *Jane's All The World's Aircraft*, 1994-95, 85th Edition, Sentinel House, Surrey UK.
11. Bangert, L. H.; Santman, G. H.; and Miller, L. D.: *Effects Of Inlet Technology On Cruise Speed Selection*. Supersonic Cruise Research '79, Part I, NASA Conference Publication 2108, 1979

APPENDIX A

Table A-1. Characteristics of the initial McDonnell Douglas baseline supersonic-cruise concept.

<u>McDonnell Douglas Baseline Concept</u>	
<u>M2.4-7A M3765-100D</u>	
Span, feet	131.9
Length, feet	334.0
Wing Area (reference), square feet	9,450.0
Aspect Ratio	1.84
Number of Passengers	300
Range, nautical miles	5,200.0
Cruise Mach number	2.4
Gross Takeoff Weight, pounds	789,565.0
Beginning Cruise Weight, pounds	690,739.0
Empty Weight, pounds	322,495.0
Payload Weight, pounds	63,000.0
Number of Engines	4
Thrust/engine, pounds	61,200.0

Table A-2. Preliminary design characteristics of the HSCT-11C concept.

<u>HSCT-11C Concept</u>	
Span, feet	138.0
Length, feet	300.0
Wing Area (reference), square feet	9,425.0
Aspect Ratio	2.0
Canard Control Surface Area, square feet	216.4
Number of Passengers	300
Range, nautical miles	5,000.0
Cruise Mach number	2.4
Gross Takeoff Weight, pounds	760,500.0
Beginning Cruise Weight, pounds	684,400.0
Empty Weight, pounds	312,200.0
Payload Weight, pounds	63,000.0
Number of Engines	4
Thrust/engine, pounds	57,000.0

Table A-3. Preliminary design characteristics of the HSCT-11E concept.

<u>HSCT-11E Concept</u>	
Span, feet	138.0
Length, feet	300.0
Wing Area (reference), square feet	10,336.5
Aspect Ratio	1.84
Canard Control Surface Area, square feet	216.4
Number of Passengers	300
Range, nautical miles	5,000.0
Cruise Mach number	2.4
Gross Takeoff Weight, pounds	772,000.0
Beginning Cruise Weight, pounds	696,000.0
Empty Weight, pounds	317,000.0
Payload Weight, pounds	63,000.0
Number of Engines	4
Thrust/engine, pounds	55,000.0

SONIC BOOM PREDICTION AND MINIMIZATION OF THE DOUGLAS REFERENCE OPT5 CONFIGURATION

Michael J. Siclari
Northrop Grumman
Advanced Technology and Development Center
Bethpage, NY

INTRODUCTION

Conventional CFD methods and grids do not yield adequate resolution of the complex shock flow pattern generated by a real aircraft geometry. As a result, a unique grid topology and supersonic flow solver (Ref. 1) was developed at Northrop Grumman based on the characteristic behavior of supersonic wave patterns emanating from the aircraft. Using this approach, it was possible to compute flow fields with adequate resolution several body lengths below the aircraft. In this region, three-dimensional effects are diminished and conventional two-dimensional modified linear theory (MLT) can be applied to estimate ground pressure signatures or sonic booms.

To accommodate real aircraft geometries and alleviate the burdensome grid generation task, an implicit marching multi-block, multi-grid finite-volume Euler code was developed as the basis for the sonic boom prediction methodology. The Thomas two-dimensional extrapolation method of Ref. 2 is built into the Euler code so that ground signatures can be obtained quickly and efficiently with minimum computational effort suitable to the aircraft design environment. The loudness levels of these signatures can then be determined using a NASA generated noise code. Since the Euler code is a three-dimensional flow field solver, the complete circumferential region below the aircraft is computed. The extrapolation of all this field data from a cylinder of constant radius leads to the definition of the entire boom corridor occurring directly below and off to the side of the aircraft's flight path yielding an estimate for the entire noise "annoyance" corridor in miles as well as its magnitude.

An automated multidisciplinary sonic boom design optimization software system was developed during the latter part of HSR Phase I. Using this system, it was found that sonic boom signatures could be reduced through optimization of a variety of geometric aircraft parameters (Ref. 3). This system uses a gradient based nonlinear optimizer (Ref. 4) as the driver in conjunction with a computationally efficient Euler CFD solver (MIM3DSB) for computing the three-dimensional near-field characteristics of the aircraft. The intent of the design system is to identify and optimize geometric design variables that have a beneficial impact on the ground sonic boom. The system uses a simple wave drag data format to specify the aircraft geometry. The geometry is internally enhanced and analytic methods are used to generate marching grids suitable for the multi-block Euler solver. The Thomas extrapolation method is integrated into this system, and hence, the aircraft's centerline ground sonic boom signature is also automatically computed for a specified cruise altitude and yields the parameters necessary to evaluate the design function. The entire design system has been automated since the gradient based optimization software requires many flow analyses in order to obtain the required sensitivity derivatives for each design variable in order to converge on an optimal solution. Hence, once the problem is defined which includes defining the objective function and geometric and aerodynamic constraints, the system will automatically regenerate the perturbed geometry, the necessary grids, the Euler solution, and finally the ground sonic boom signature at the request of the optimizer.

A variety of objective functions and constraints can be specified to minimize the sonic boom ground signature. Simple objective functions such as the minimization of the maximum ground shock pressure magnitude can be specified or more complicated functions that try to shape the signature by minimization of the difference between the current signature and a specified shape. Another aspect or objective of the design system is to maintain aerodynamic efficiency while alleviating the ground sonic boom by maintaining the cruise lift coefficient and lift to drag ratio.

This truly nonlinear design optimization system will be utilized to define candidate modifications to the McDonnell Douglas HSCT 2.4-H5085 "OPT5" reference configuration that have the potential to alleviate or "soften" the sonic boom ground signature. Geometric perturbations to this aircraft geometry involving:

- fuselage volumetric variation
- fuselage camber shapes
- wing thickness or volume
- airfoil shapes
- wing camber & twist distributions
- wing dihedral
- engine nacelles orientation & location
- canard surfaces

will be optimized and/or analyzed to reveal their impact on softening the sonic boom signature and reducing the perceived noise level. Each geometric parameter will be optimized to isolate its individual impact on the sonic boom level and the effect on aerodynamic efficiency. Finally, a combination of geometric perturbations will be utilized to determine the final configuration with limited impact on aerodynamic efficiency and maximum impact on sonic boom reduction.

Even though all of the above geometric parameters were given preliminary scrutiny, only those that were successful in reducing the sonic boom without loss in aerodynamic efficiency will be presented.

ANALYSIS OF THE OPT5 REFERENCE AIRCRAFT

Geometry and Aerodynamic Analysis

Figure 1a shows the wave drag input geometry database used to analyze the OPT5 reference aircraft. The horizontal and vertical tails were not included in the present computations.

The code MIM3DSB is an axial multiblock code that does not require matched block grid interfaces. Hence, as the computation marches downstream, a variety of grid blocks with different grid topologies are used to accommodate the changing geometric requirements such as body, wing-body, wing-body-nacelles, and aft body. In addition, as the distance between the aircraft's longitudinal axis and the outer grid boundary increases, more grid points are added to the blocks as the marching proceeds downstream. For the most part, analytical conformal mappings are used which are very fast and yield reasonably good quality grids. The exception to this is for blocks which contain one or more nacelles. The conformal mappings do not necessarily yield good grids and the series of mappings (i.e. up to 10 transformations) are difficult to manipulate. In these blocks, a two-dimensional elliptic grid generator is used which is fairly reliable and starts with the conformal mapping or analytic grid as an initial guess. The elliptic grid generator can be turned on at any block but requires more computational effort and hence, it is not used for simple body or wing-body cross sections.

Figure 1b shows the basic inviscid drag polar that was computed by MIM3DSB for the baseline wing-body configuration. The cruise design point is at $CL = .105$ and occurs at an angle of attack of 2.0 degrees. The cruise condition corresponds to a inviscid drag of about 73 counts or .0073. Inviscid CD_0 or zero lift drag is about 28 counts or .0028. A single point at the cruise angle of attack is also shown on figure 1b and corresponds to a computation for the wing-body nacelles configuration. The nacelles increase the drag to about 80 counts with a corresponding increase in lift to $CL = .112$.

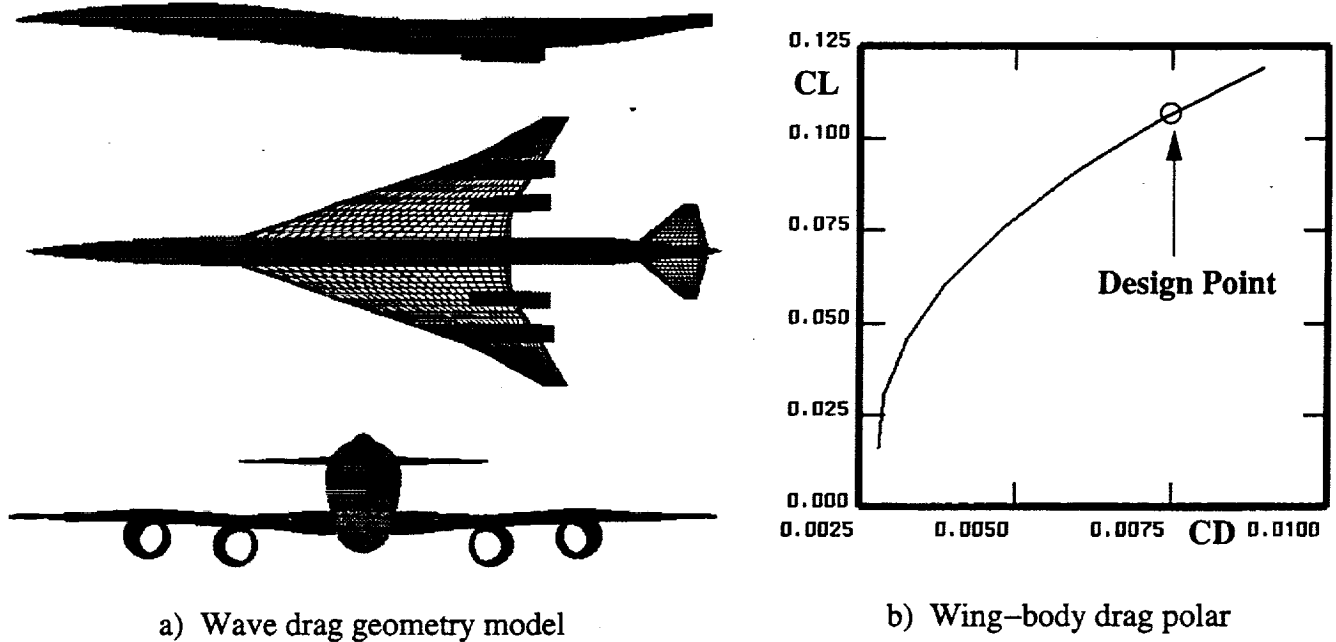


Figure 1 Wave drag geometry input definition and CFD computed aerodynamics for MDC 2.4-H5085 Reference OPT5.

Sonic Boom Analysis

The reference wing-body configuration with and without nacelles was analyzed to determine the baseline ground sonic boom levels. Figure 2 shows a schematic of the computational grid topology used for all the sonic boom computations carried out in this study. Figure 2 illustrates the grid in the lower symmetry plane which mimics the downrunning family of characteristics or wave patterns encountered in supersonic flows. The upstream characteristic is the outer boundary in the crossflow plane. This boundary is adapted automatically to the location of the nose shock. The downstream characteristic corresponds to an artificial inner surface or boundary merely constructed to resolve the flow field of interest. This boundary is taken far enough downstream of the aircraft (i.e. usually with an aft fuselage sting extension) so as not to influence the sonic boom signature, in particular, the tail shock. Figure 2 also indicates the extent of the computational domain necessary to compute the signature 2 body lengths below the aircraft for Mach 2.4 flight. This grid topology concentrates points in the domain of interest and also aligns the grid with the shock waves propagating away from the aircraft. As is well known in the CFD community, grid alignment with shock waves significantly improves the numerical shock capturing accuracy. Also indicated in figure 2 are the 4 extrapolation distances used in the present study. All ground signatures were computed by extrapolating CFD computed signatures from 75, 150, 300, and 600 feet below the aircraft using the Thomas method.

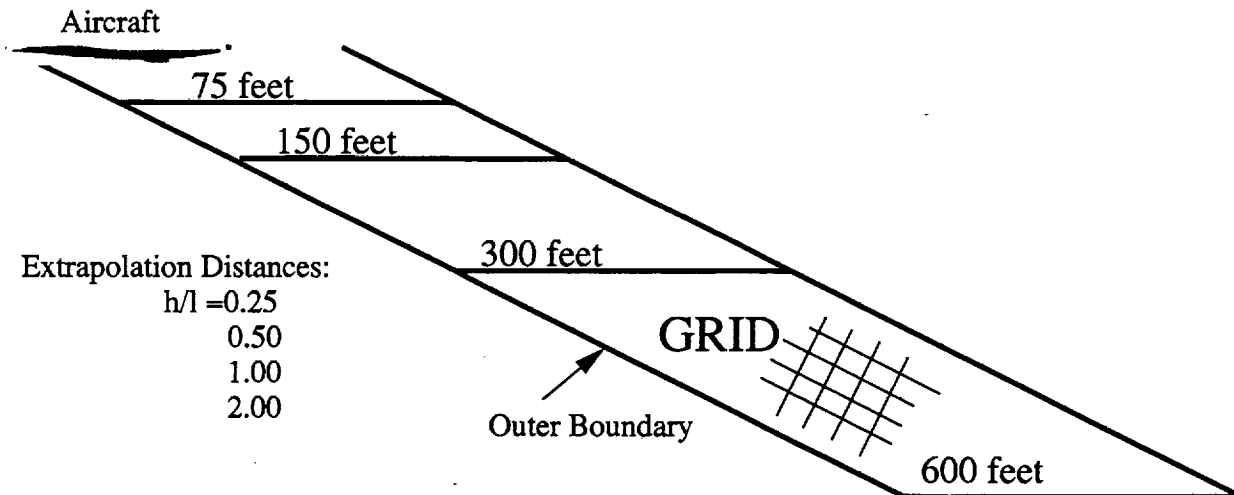
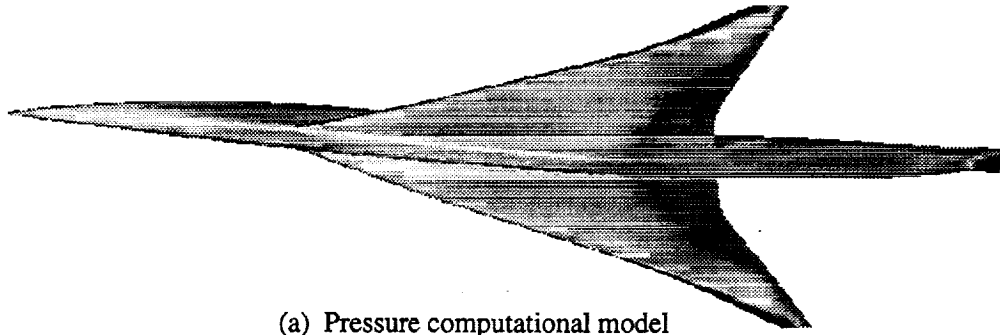


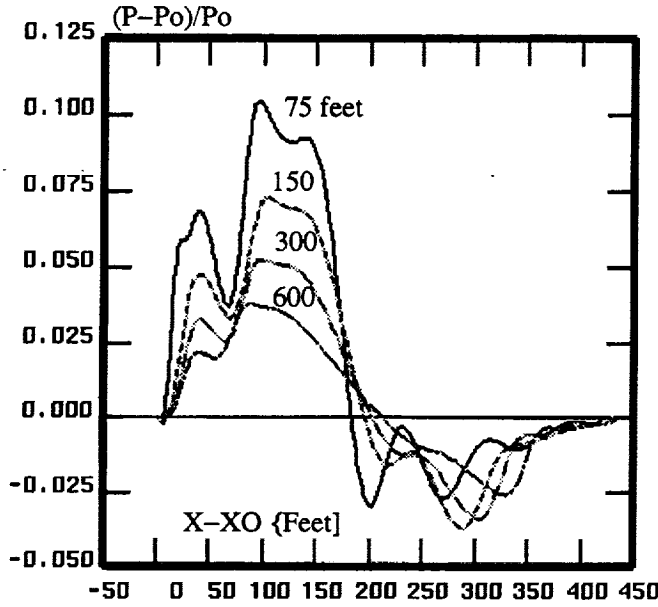
Figure 2 Sonic boom computational grid system (lower symmetry plane) for a Mach 2.4 airplane.

Figure 3 shows a snapshot of the sonic boom analysis for the OPT5 reference wing-body configuration at cruise conditions corresponding to $CL = .105$ and an altitude of 55,045 feet. Figure 3a shows a view of the pressure painted CFD surface model. Figure 3b shows the computed near-field pressure signatures at four distances below the aircraft. The dominance of the strong wing shock is evident in these signatures. Figure 3c shows an image of the pressure footprint 300 feet or one body length below the aircraft. The stronger wing shock can be observed as the broad white band aft of the nose shock. Figure 3d shows the ground track or centerline extrapolated ground pressure signatures using the 4 extrapolation distances mentioned earlier. The signature becomes an N-wave with increasing extrapolation distance. The nose overpressure becomes slightly greater with extrapolation distance and is about 2.6 lbs/ft² at the greatest extrapolation distance of 600 feet or 2 body lengths below the aircraft. The signature becomes longer and the tail shock becomes stronger with extrapolation distance. Figure 3e shows the lateral extent of the boom carpet in miles. The ground carpet signatures were obtained by extrapolating the near field data from a cylinder of constant radius. The maximum shock overpressure is plotted as a function of lateral distance. Significant levels of overpressure (i.e. 1.5 or greater) are propagated 15 miles to the right and left of the aircraft ground centerline track. The levels near the ground track are slightly increased with extrapolation distance while the levels off to the side are somewhat diminished.

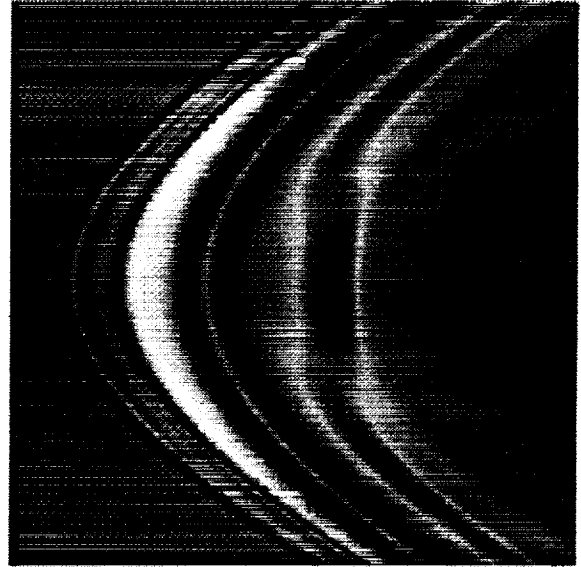
Figure 4 shows a similar snapshot of the sonic boom analysis for the OPT5 reference aircraft with nacelles. Figure 4a shows the CFD pressure painted surface computational model of the configuration. The dark areas are high pressure and indicate shocks propagated due to the nacelle external geometry. MIM3DSB's nacelle model is an idealized one in that only the external geometry is computed and all the flow included in the inlet face area is assumed captured by the engine (i.e. no spillage). In addition, no attempt was made to model the details of the pylons or inlet diverters. They are simply assumed to be thin plates attaching the nacelles to the underside of the wing. Figure 4b shows the near-field signatures. The effect of the nacelles can be seen in the pressure signature at 75 feet below the aircraft as a second small shock at $x \sim 250$ downstream of the wing expansion. This second small shock is absent in the wing-body signature of figure 3b. Figure 4c shows the entire pressure footprint 300 feet below the aircraft. Figure 4d shows the extrapolated ground signatures. Similar behavior is observed in that the nose shock overpressure increases with extrapolation distance and the signature becomes longer and the tail shock becomes stronger. The maximum overpressure with nacelles is about 2.8 lbs/ft² at the largest extrapolation distance of 600 feet or 2 body lengths.



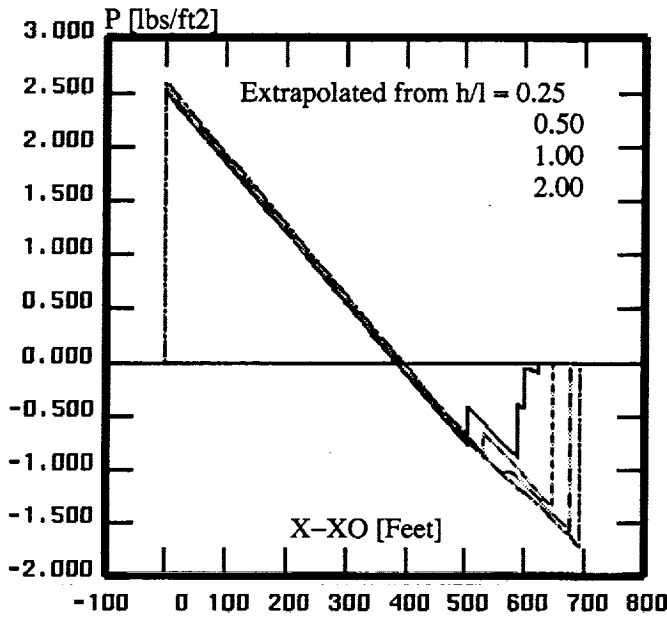
(a) Pressure computational model



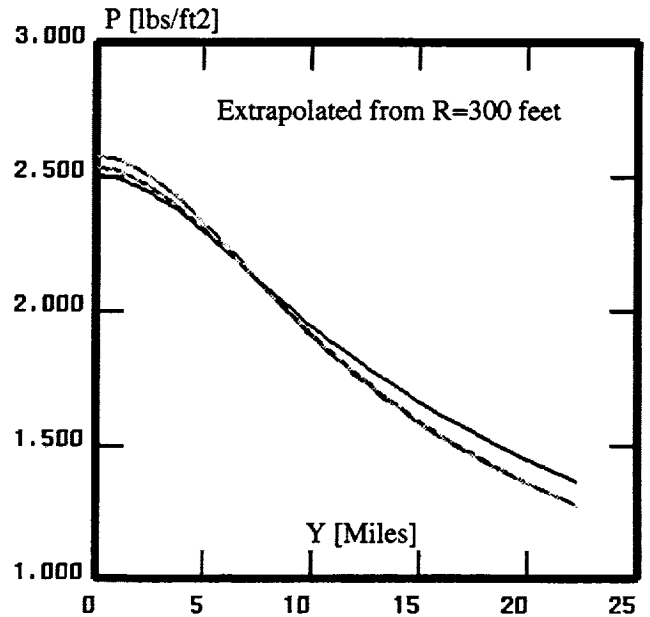
(b) Near-field pressure signatures



(c) Pressure footprint 300 feet below aircraft



(d) Extrapolated ground pressure signatures



(e) Maximum off-track overpressures

Figure 3 Sonic boom analysis of the Reference Douglas OPT5 wing-body configuration, $M = 2.4$, $\alpha = 2.0$ degs., $CL = .105$, $H = 55,045$ feet..

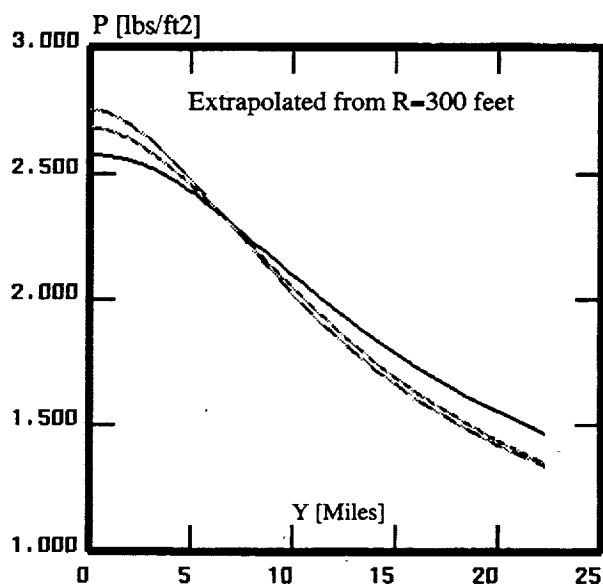
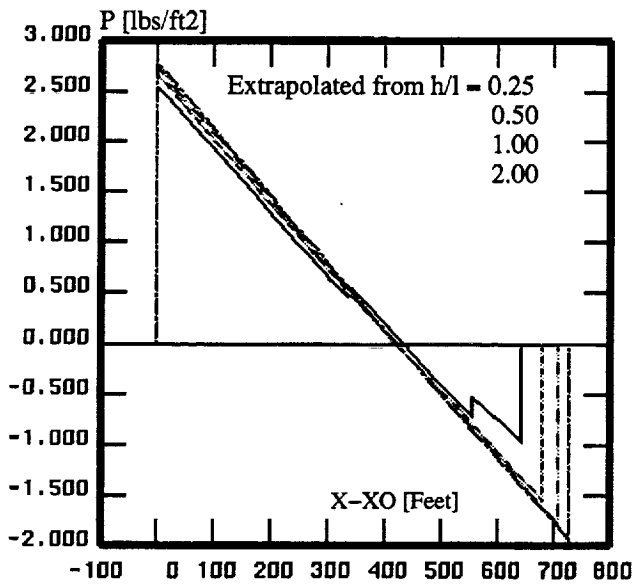
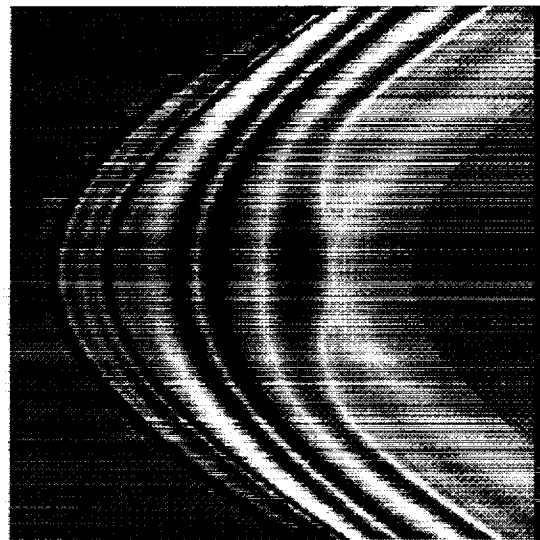
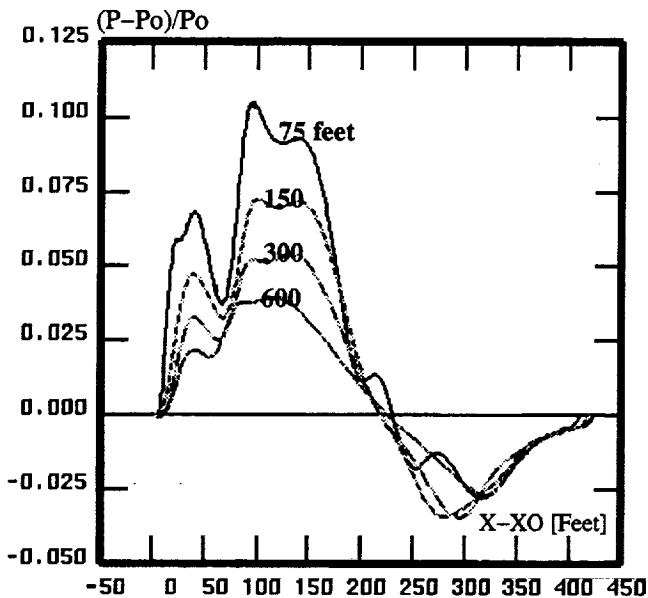
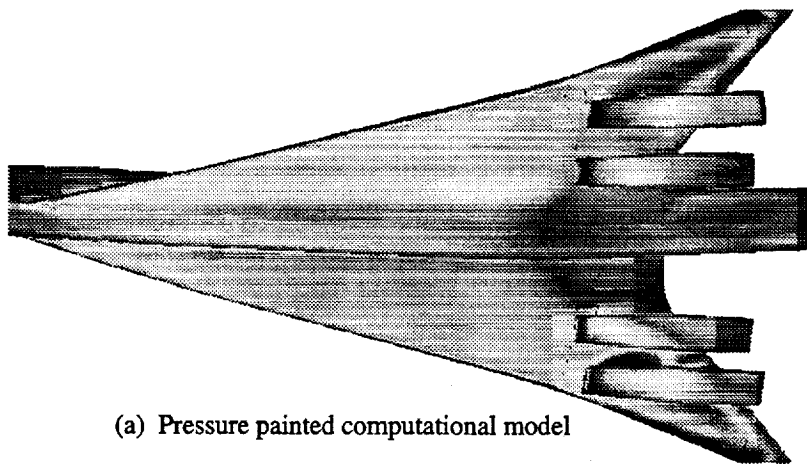


Figure 4 Sonic boom analysis of the Douglas OPT5 wing-body/nacelles, $M = 2.4$, $\alpha = 2.0$ degs., $CL = .112$, $H = 55,045$ feet.

Hence, the addition of nacelles increases the maximum overpressure by about .2 lbs/ft². Figure 4e shows the lateral extent of the ground sonic boom carpet in miles. The ground track or centerline peak overpressure shows a slightly higher increase with extrapolation distance than was observed for the wing-body configuration.

SONIC BOOM MINIMIZATION

It should be mentioned that all the design problems were carried out using an extrapolation distance of 75 feet or $h/l = 0.25$ on a crude computational grid (i.e. in comparison to the fine computational grid used for analysis). This was done primarily due to time constraints and to save computational time. All ground extrapolations were performed with the Thomas ANET code (Ref. 2) All the design optimization computations were carried out using the baseline OPT5 wing-body wave drag geometry data set. The design study was also carried out using a fixed planform corresponding to the reference OPT5 configuration. Hence, optimization of any planform related parameters was not pursued in this preliminary design study. In addition, the effect of nacelles on the optimized geometry was evaluated only by analysis and were not included in the design optimization process.

The NPSOL/MIM3DSB design optimization system reads the baseline wave drag geometry for each evaluation of the objective function and replaces the selected geometric parameter (e.g. wing dihedral, thickness, fuselage camber, etc.) with an analytic description (e.g. user specified functions, cubic splines, etc.) and finally, rewrites the new wave drag data set that is read by MIM3DSB. The new geometry is internally enhanced and a new grid is generated for each evaluation by MIM3DSB. One evaluation of the objective function corresponds to a new geometry and grid generation, a flow analysis, aerodynamic coefficient computation, and ground extrapolation. This is all carried out automatically by MIM3DSB. This is essentially because some design problems may take several hundred evaluations of the objective function to find an optimal solution. Basically, each global iteration of the optimizer will request $2N+1$ evaluations or analyses where N is the number of design variables. For convergence, the optimizer typically takes from 5 to 10 global iterations.

Each design problem requires upper and lower bounds on each of the design variables. In addition, linear constraints can also be imposed on the design variables mainly to insure that the geometry remains well behaved. Nonlinear constraints can also be imposed but were not used in the present study because their use requires even more objective evaluations. Instead, penalty functions were utilized to maintain lift, for example:

$$PCL = CL_{MIN}/CL \quad \text{for } CL < CL_{MIN}$$

$$PCL = 1.0 \quad \text{for } CL > CL_{MIN}$$

$$OBJ = P_{MAX} (PCL)^n \quad \text{where } n = 1 \text{ to } 4.$$

and P_{MAX} is the maximum ground sonic boom overpressure in lbs/ft². If the lift coefficient drops below a minimum value CL_{MIN} , a penalty (PCL) is imposed on the objective function (OBJ). The penalty functions are essential when the problem involves wing twist or camber. Otherwise, the optimal solution will simply be driven towards the lowest lift coefficient in order to reduce the sonic boom.

Wing Dihedral

Several types of wing dihedral were studied. Gull type wings were considered initially but were rejected due to the sharp corner that results in the wing geometry. This was undesirable for both computational and aerodynamic reasons. Aerodynamically, the corner might result in crossflow separation at low angles of attack. As a result, a smooth parabolic dihedral was chosen and is illustrated in figure 5. The dihedral was bi-parabolic or comprised of two parabolas, described by three design variables. The three design variables were: the wing-body juncture slope (θ_1), the span location of zero slope (Y_1), and the tip dihedral slope (θ_2).

The optimization problem was governed by an upper bound of 20 degrees wing-body juncture dihedral and -20 degrees tip angle. The zero slope span station had lower and upper bounds of $y=20$, and $y=50$. Figure 5 shows a table of some intermediate and the final optimal design solution. As will sometimes occur in design optimization problems, the optimal solution is up against one or more design space boundaries. The minimum sonic boom was achieved at 20 degrees wing-body juncture dihedral angle and a zero slope at a span station of $y=50$. Hence, optimum reduction of sonic boom with dihedral will occur with maximum inboard dihedral angle and positive dihedral as far outboard as possible. Evidently, a negative tip dihedral does not alleviate the shock strength or sonic boom. Depending upon the amount of inboard dihedral and the extent, the sonic boom can be reduced by as much as 0.37 lbs/ft² or about 15%.

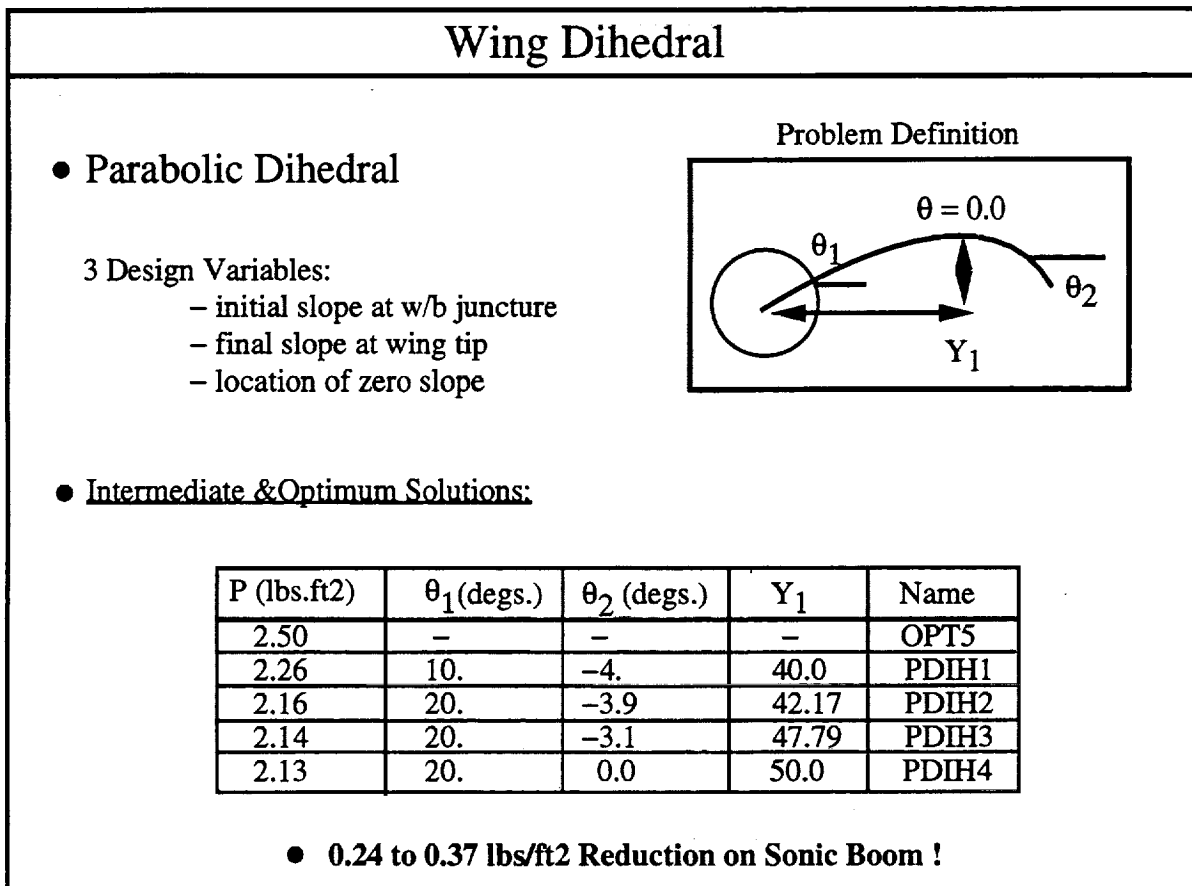


Figure 5 Summary of wing dihedral design problem.

Wing Thickness Variation and Airfoil Shape

The airfoil shape and thickness was allowed to vary as a function of the wing span. Figure 6 shows a summary of the wing airfoil and thickness design problem. Four span stations were defined where the thickness and airfoil shapes would be imposed. At each span station the airfoil shape could be varied by a shape function parameter lambda (λ) which related the airfoil shape at that station to a linear combination of two distinctly different airfoil shapes. In addition, the thickness was also allowed to vary at each of the four span stations. The maximum thickness was bounded by 2% and 6% chord. The shape parameter lambda took on values between 0 and 1. Hence, at each span station, two parameters governed the thickness and airfoil shape. This leads to 8 design variables. The entire wing was then defined given the design variables by using cubic spline fits.

Initially, the two basis airfoil shapes were defined to be a sharp circular arc airfoil and the blunt NASA 0012 scaled airfoil shape. Figure 7 tabulates the optimum solutions found for this problem. Once again, the optimal solution is up against a design boundary. The optimum inboard thickness is the maximum constraint which decreases to the minimum constrained value at the next span station. The optimal airfoil shape parameter defines the inboard airfoil to be blunt and the outboard airfoils to be sharp. The sonic boom overpressure was decreased by a significant .43 lbs/ft² or about 17%. Along with this reduction in sonic boom was a slight increase in drag of about 3 to 5 counts.

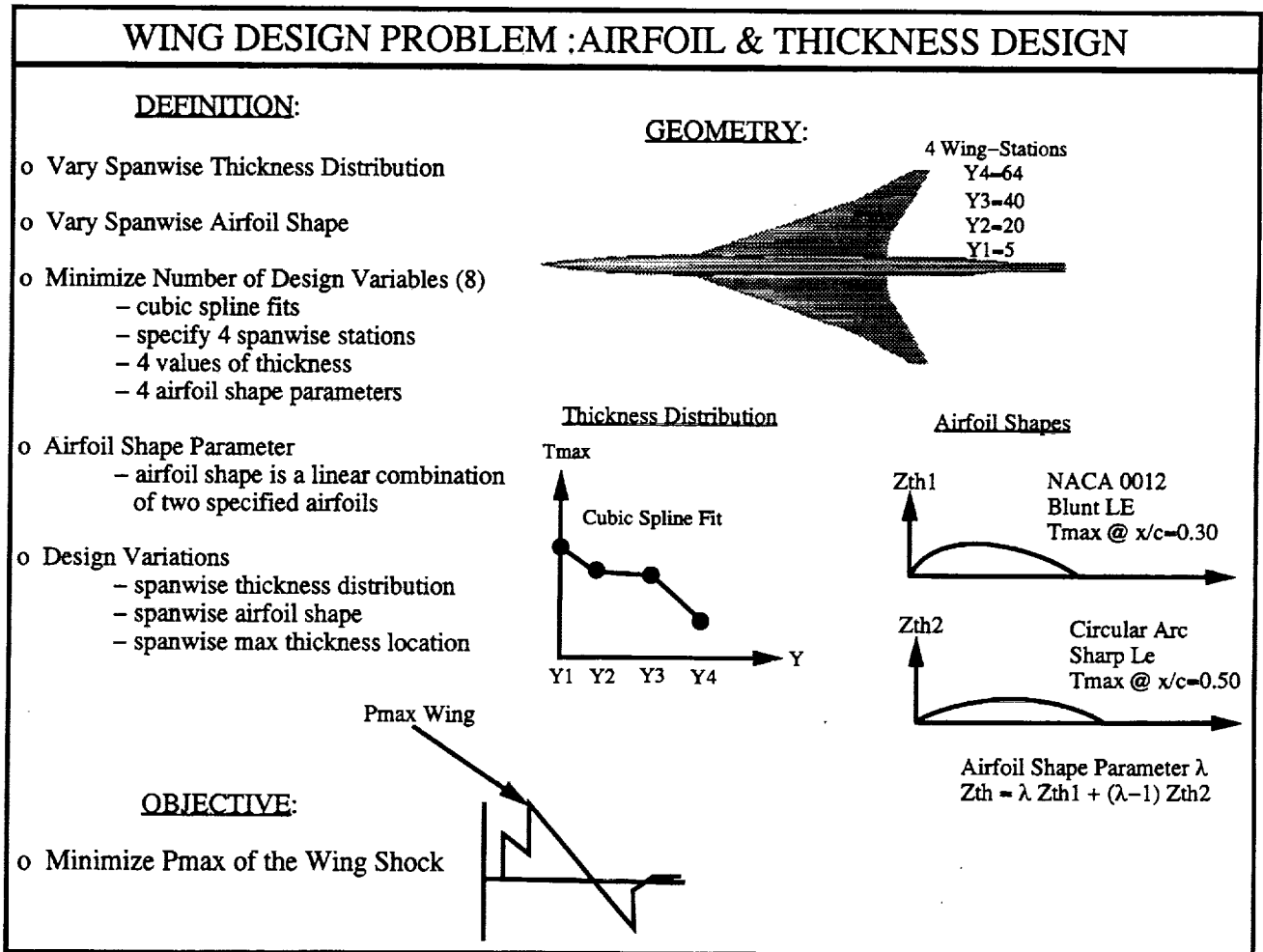


Figure 6 Summary of wing airfoil and thickness design problem.

The more aerodynamically efficient 65A006 scaled airfoil shape was then substituted for the NACA 0012. The optimal solution for these airfoils is also shown in figure 7. Once again, the thickness is at its maximum value at the most inboard station. Unlike the previous problem, the airfoils thicken somewhat on the outboard stations. The airfoil parameter behaves in a similar fashion with blunt inboard and sharp outboard. Slightly more bluntness is added near the tip region. This wing design resulted in 0.32 lbs/ft² or about a 13% reduction in sonic boom overpressure. The sonic boom reduction was not quite as large as in the previous wing design except this design was accompanied by a negligible increase in drag.

The design problem as formulated involves several parameters. The wing thickness, the airfoil shape and sharp versus blunt leading edge. To try to understand the major contributor to reducing the sonic boom, the design problem was reformulated using only thickness or volume. Very little reduction in sonic boom was achieved by varying airfoil thickness alone.

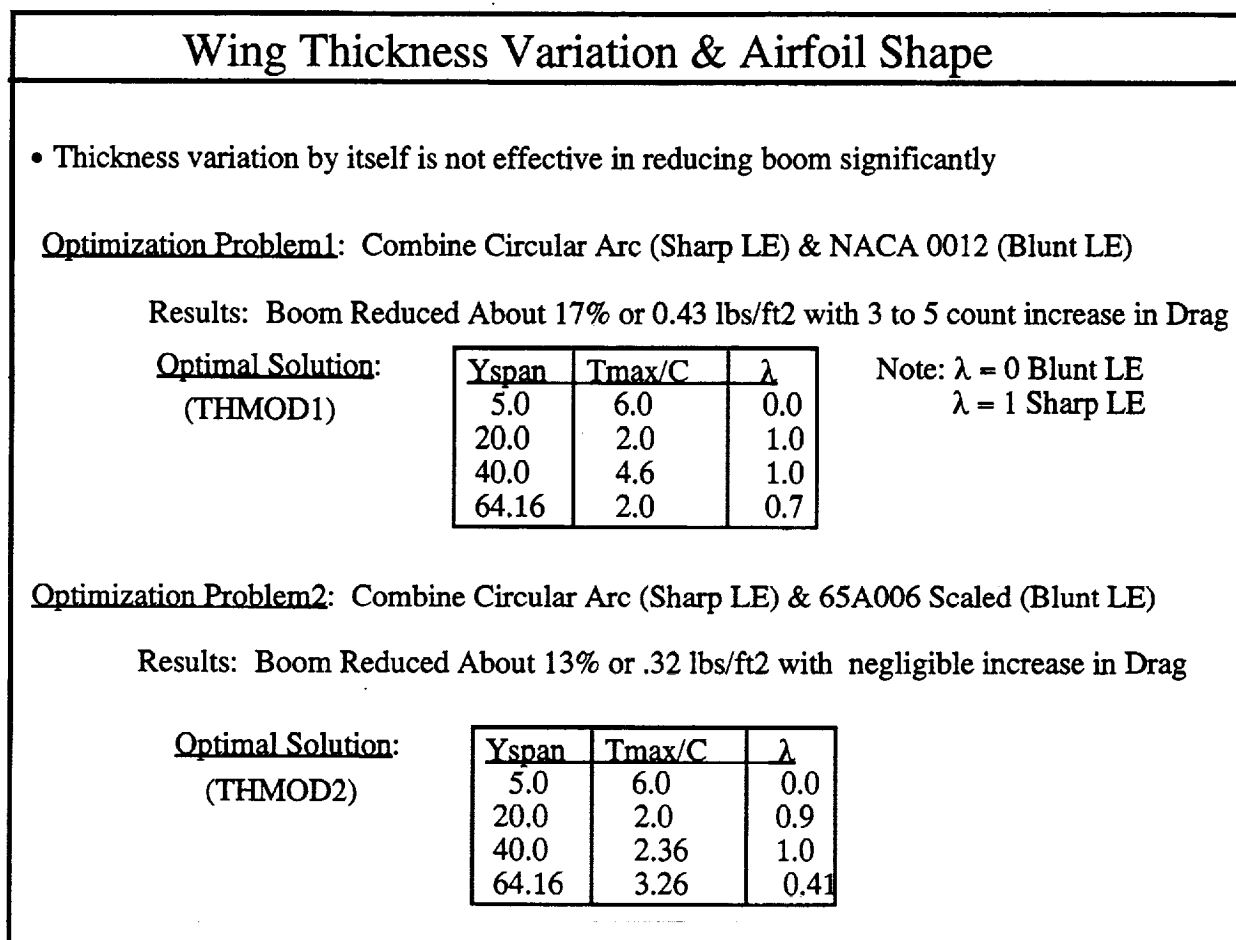


Figure 7 Wing thickness and airfoil shape optimized solutions.

As mentioned earlier, the upper bound on the maximum wing thickness was found to be the optimal solution for the inboard airfoil. The reference OPT5 configuration's maximum thickness is about 2.4% chord for the entire span of the wing. It was felt that 6% thickness with the large inboard chord was too great a thickness to be practical. Hence, a compromise solution was sought. The 65A006 scaled airfoil was chosen due to its beneficial drag characteristics and the inboard airfoil was constrained to 4% thickness. The shape parameters were defined to be those found for the optimal solution. This compromise solution is tabulated in figure 8. Analysis revealed a 0.25 lbs/ft² or about a 10% reduction in sonic boom overpressure. Limiting the thickness variation led to a smaller reduction in sonic boom overpressure. Hence, even though thickness variation alone does not significantly reduce sonic boom, it does have an effect when used in combination with different airfoil shapes.

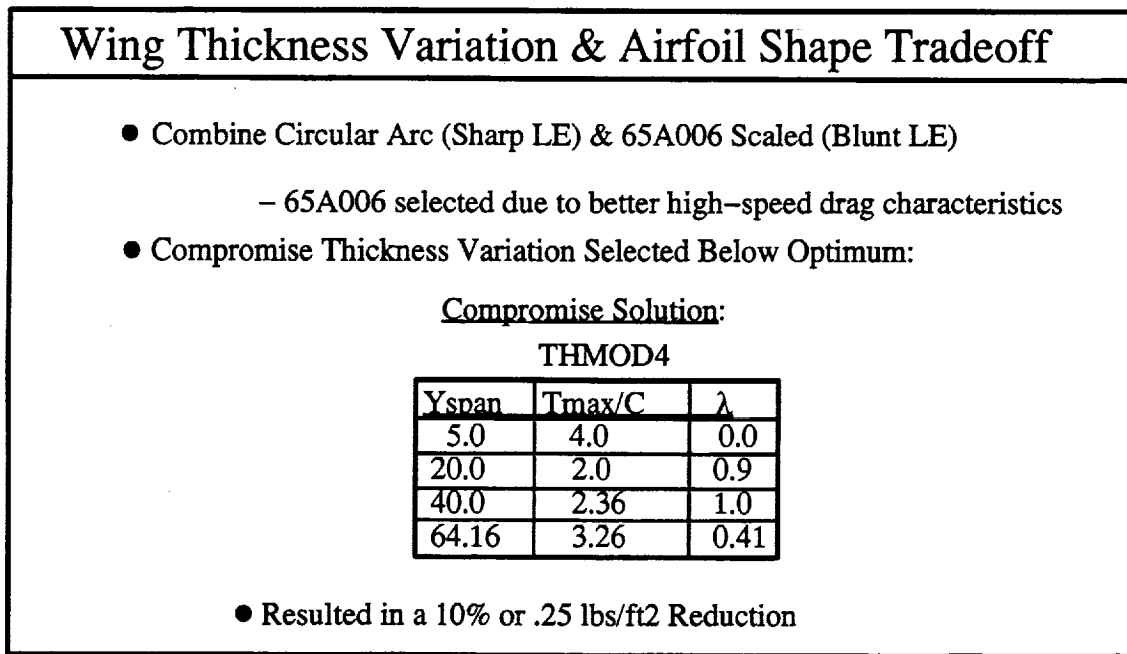


Figure 8 Compromise thickness solution.

Wing Camber and Twist

Wing camber and twist were also given preliminary scrutiny. Wing twist was optimized as a function of wing span. No significant reduction in sonic boom was achieved. Wing camber was also studied using a parabolic camber shape. This also did not lead to a significant reduction in sonic boom. These geometric parameters were optimized using the reference OPT5 geometry. Hence, this does not necessarily mean that wing twist and camber can not be used to reduce the boom but should be further studied in conjunction with the other parameters that were successful such as dihedral, wing thickness and shape, and fuselage camber. Sensitivity to wing twist and camber may become apparent on lower boom or multi-shock configurations. In addition, as is the case with wing camber, only one type of analytic camber shape was tried due to time constraints. Other camber shapes might be more successful and should be studied.

Fuselage Volume

Variation in fuselage volume was also studied. Although fuselage volume could be used to reduce the boom, it could not be accomplished without a significant penalty in drag, hence, it was not pursued further. The use of fuselage volume was also complicated by the complex three-dimensional shape of the OPT5 fuselage.

Fuselage Camber

Figure 9 shows a summary of the fuselage camber design problem. The entire fuselage camber line up to $x = 273$ feet (i.e. just past the trailing edge of the wing) was fitted with cubic splines with camber design variables specified every 20 feet. This resulted in 13 design variables for the cubic spline fitted camber line. An optimum solution was found with the lift constraint that $CL > 0.10$. This optimum solution resulted in a significant decrease in peak overpressure of about 0.30 lbs/ft² or a 12% reduction. Unfortunately, the optimum camber line contained a steep break near the aft end that resulted in a rapid expansion on the lower surface and a strong shock on the upper surface of the fuselage. This optimum fuselage camber shape appeared to be impractical and a variety of smooth hand developed camber shapes were run following the basic behavior of the optimum shape. Figure 9 tabulates the various shapes and the reduction in peak overpressure as well as the lift and drag. Two of these camber shapes, FMOD4 and FMOD6 are shown plotted in figure 9 in comparison to the original fuselage camber line of the reference OPT5 configuration. Basically, both modified camber lines shift the fuselage expansion more forward relative to the wing location. Only a small reduction in peak overpressure was obtained with these smooth shapes on the order of 5%.

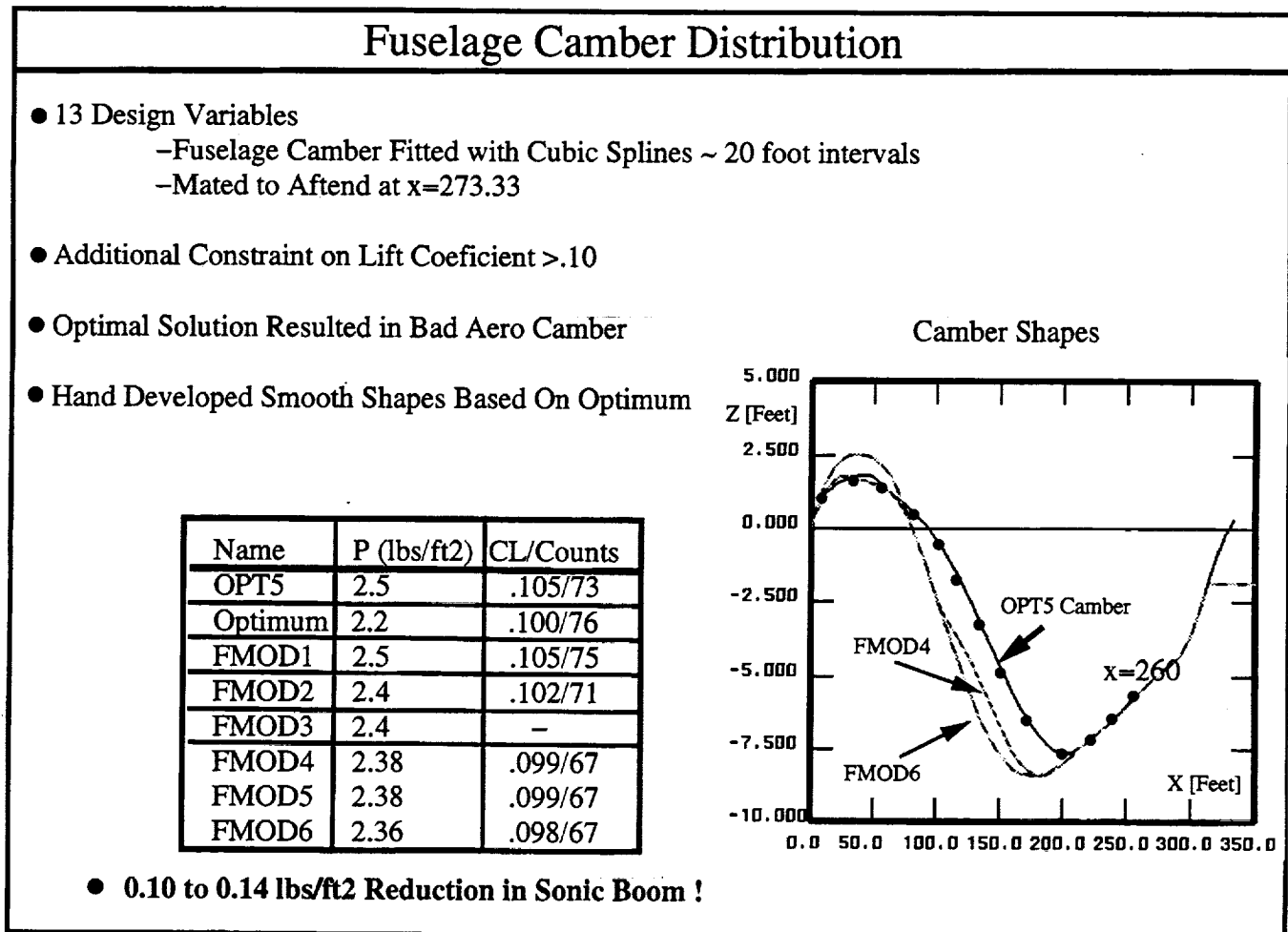


Figure 9 Summary of fuselage camber design problem.

SELECTION AND EVALUATION OF CANDIDATE MODIFICATIONS

A variety of optimum and intermediate modifications were derived during this preliminary design study involving wing dihedral, wing thickness and airfoil shape, and fuselage camber. The next task was to combine these geometric perturbations into an aircraft configuration. There was no way of determining how these geometric perturbations would affect the sonic boom level when combined into a single configuration. As a result, two different geometric configurations were studied. The first configuration was relatively conservative and used a modest dihedral (PDIH1) with a 10 degree wing-body juncture dihedral angle. The thickness and airfoil shape used was that shown in figure 8 (THMOD4). This was used because of the high-speed characteristics of the NACA 65A006 airfoil shape. Lastly, a modest increase in fuselage camber (FCAM4) was utilized. This configuration is designated MOD144. The first digit refers to dihedral, the second digit thickness/airfoil shape mod, and the third digit fuselage camber shape.

The second configuration was more aggressive in dihedral and used somewhat more fuselage camber. The dihedral chosen (PDIH4) has a 20 degree wing-body juncture angle. The same thickness/airfoil shape mod was used (THMOD4) and the fuselage camber was slightly more aggressive (FCAM6). The values associated with these mods are tabulated in figures 5, 8 and 9. This configuration was designated as MOD446.

Figure 10 shows the two modified aircraft in comparison to the OPT5 reference aircraft. Only the front and side views are shown, the plan views are identical since the premise of this preliminary optimization was not to change the wing planform.

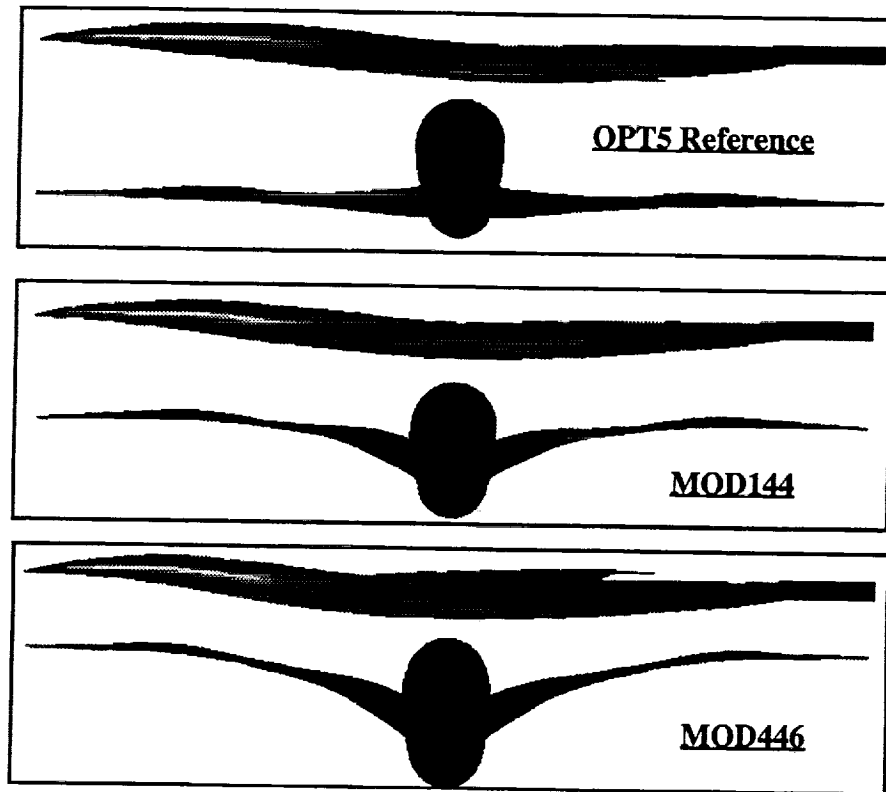


Figure 10 Comparison of reference and optimized geometries.

ANALYSIS OF OPTIMIZED BOOM CONFIGURATIONS

Both MOD144 and MOD446 wing-body configurations were analyzed with respect to aerodynamics and sonic boom. A fine grid analysis was carried out on both configurations. Figure 11 shows the ground sonic boom signatures extrapolated from the four distances below the aircraft of 75, 150, 300, and 600 feet at Mach 2.4 and an altitude of 55,045 feet. All of these signatures were obtained at the same lift coefficient of 0.105. For both MODS, the angle of attack was increased to achieve the same lift coefficient. For MOD446, the angle of attack increased to 2.5 degrees in comparison to 2 degrees for the reference OPT5 aircraft. The ground level signatures of both configurations extrapolated from $h/l = 0.25$ or 75 feet indicate a multi-shock signature. Breaking up the N-wave signature significantly reduces the boom level. For MOD144, both shocks are just under 2 lbs/ft². For MOD446, both shocks exhibit peak pressures under 1.7 lbs/ft² using the same aircraft extrapolation distance of 75 feet. The interesting aspect of these signatures is that the individual effects of the geometric modifications were almost additive if one compares the individual sonic boom level reductions for each of the three geometric parameters to the combined reduction. The extrapolation distance used in the optimization was 75 feet or $h/l = 0.25$. The analysis shows that all target reductions were achieved for this distance.

When the signatures are extrapolated from greater distances below the aircraft, the multi-shock signature has a tendency to coalesce. In the case of MOD144, the signature quickly coalesces into an N-wave. MOD446 maintains a multi-shock signature out to the maximum extrapolation distance of 600 feet. The nose overpressure for MOD446 is about 1.66 lbs/ft² rising to a second shock peak overpressure of about 2.19 lbs/ft². Observations of figure 11 indicate that the signature is converging with extrapolation distance since each distance is twice the previous one and the change to the signature decreases substantially. Hence, the accuracy of the ground extrapolation method and the proper distance for extrapolation will be an important issue for signatures other than N-waves. Evidently, the decay of these shocks as predicted by the CFD computation is significantly different than the decay predicted by the extrapolation method. This explains the sensitivity to extrapolation distance. The difference may also be due to three-dimensional effects not included in the extrapolation method or it may be due to nonlinear effects predicted by the CFD or both. It has been mentioned by other investigators that this sensitivity to the extrapolation distance is being caused by a loss in accuracy in the CFD method (i.e. failure to accurately capture shocks at large distances below the aircraft). This seems unlikely since this usually results in an underprediction or complete smearing of the shock waves, whereas, the shock strengths are increasing in strength with greater extrapolation distance. The ground signatures of the reference OPT5 aircraft do not exhibit this sensitivity mainly because the signatures of figures 2 and 3 are N-waves. The only effect on an N-wave due to extrapolation distance is a slight increase in peak overpressure, signature length, and tail shock.

Figure 12 shows a comparison of the ground signatures of MOD144 and MOD446 in comparison to the OPT5 reference aircraft signature at extrapolation distances of 300 and 600 feet. At 300 feet, the signature of MOD144 has already coalesced into an N-wave. The signature of MOD446 remains multi-shock at an extrapolation of 300 feet with shock levels of 1.64 and 2.08 lbs/ft².

In an effort to understand the effects of the modifications on the signatures, figure 13 shows a plot of the near-field signatures of the OPT5 with MOD446 at distances of 75 and 150 feet below the aircraft. The OPT5 signature has a wing shock that is significantly greater in magnitude in comparison to the nose shock. For MOD446, the situation is completely reversed in that the nose shock is twice the magnitude of the wing shock at 75 feet below the aircraft. This is the main reason why the coalescence into an N-wave was prevented with the MOD446 configuration.

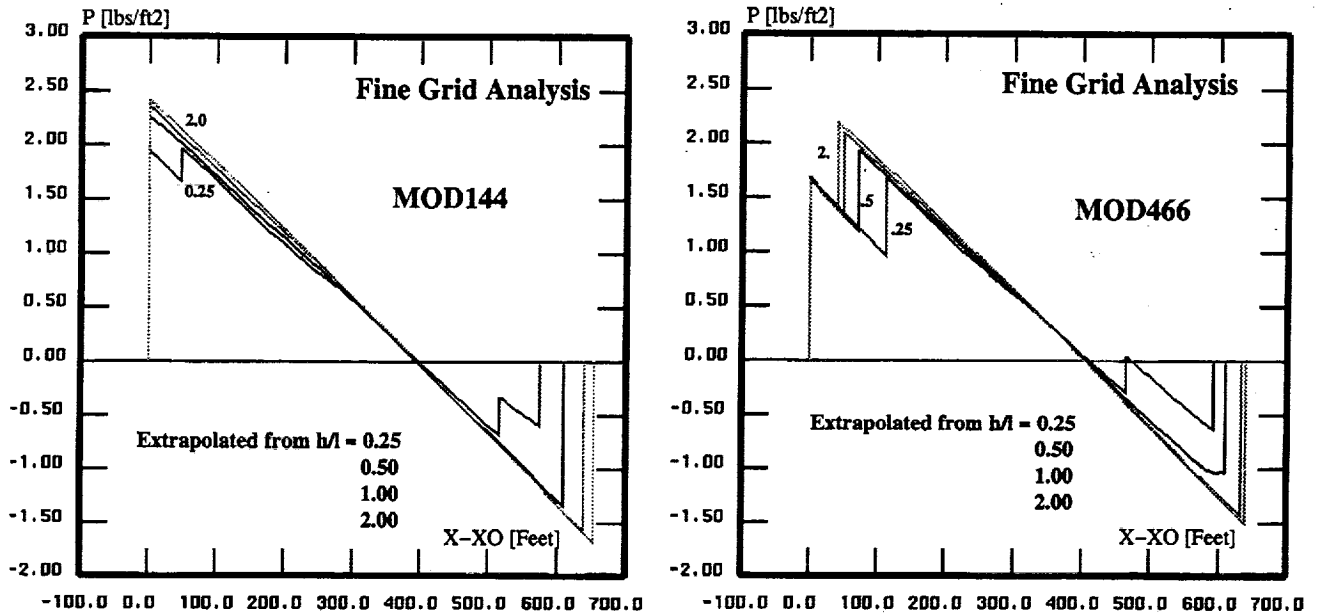
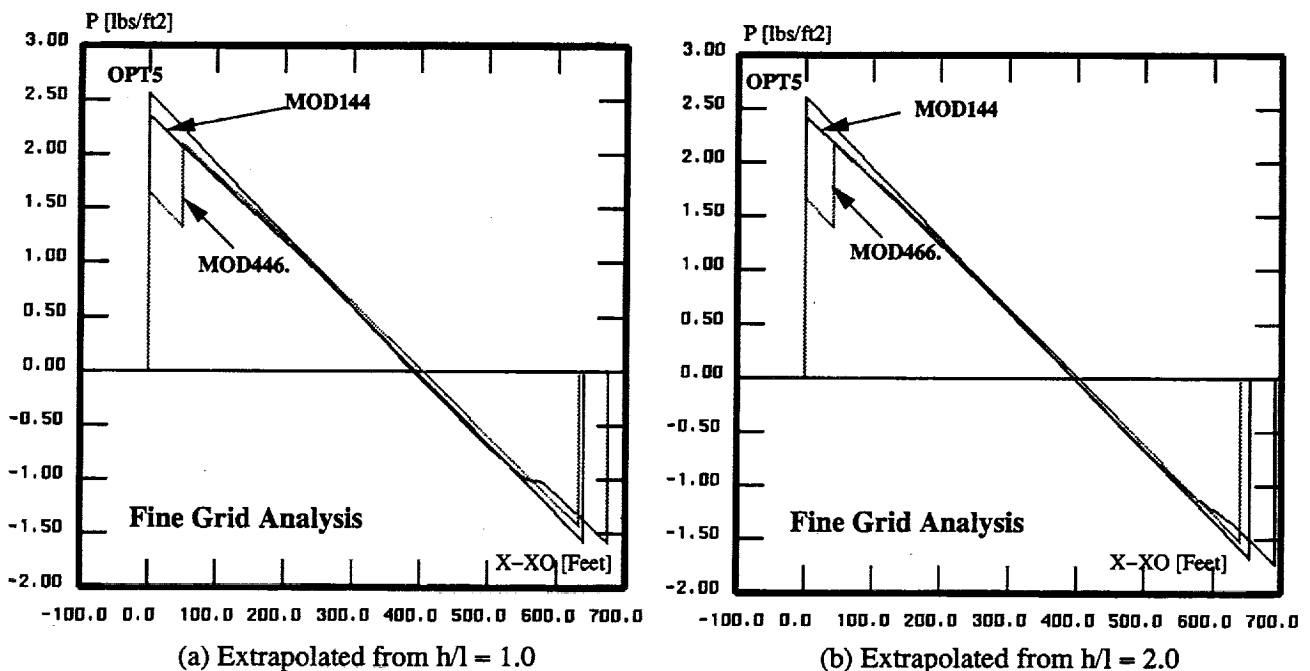


Figure 11 Fine grid analysis of optimized geometries, ground sonic boom signatures, $M = 2.4$, $CL = .105$, $H = 55,045$ feet.



(a) Extrapolated from $h/l = 1.0$

(b) Extrapolated from $h/l = 2.0$

Figure 12 Comparison of OPT5 ground signatures with optimized geometries, $M = 2.4$, $CL = .105$, $H = 55,045$ feet.

Other fine grid analyses were carried out on both MODS at different lift coefficients. Figure 14 shows the results at the design lift coefficient of 0.105 and lower lift coefficients. At a $CL = 0.094$, MOD144 maintains a multi-shock signature with peak overpressures of about 1.6 and 1.7. The peak overpressure levels of MOD446 also decrease significantly with reduced lift coefficient although it appears that MOD144 might perform better than MOD446 at reduced lift coefficients. Hence, it is also extremely important to accurately know the weight of the aircraft and its cruise altitude so that the design lift coefficient can be properly specified for boom minimization. For these designs, a 5 to 10% reduction in weight will have a significant impact on the boom levels.

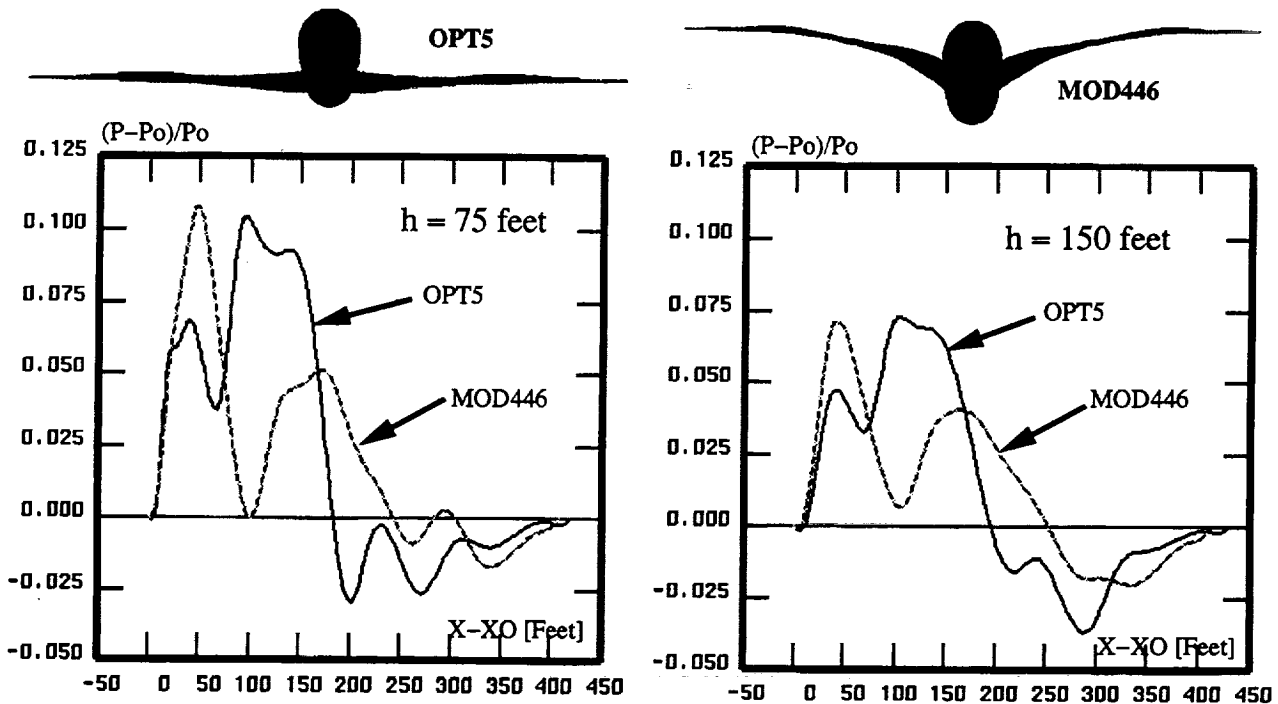


Figure 13 Comparison of near-field signatures for OPT5 Reference and MOD446.

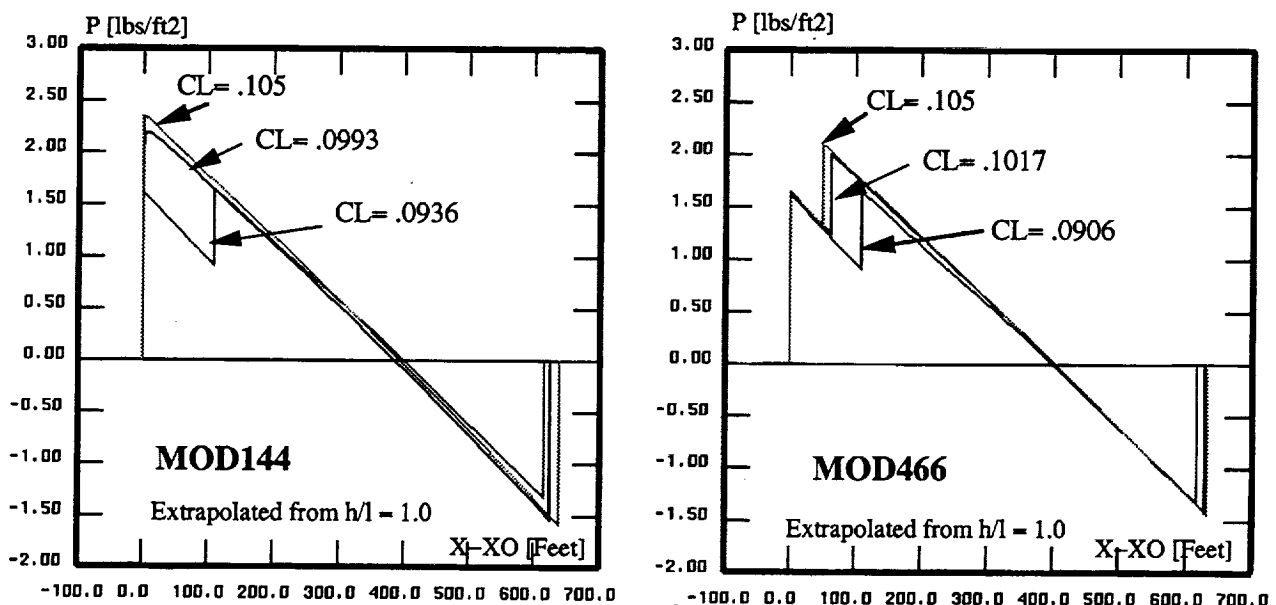


Figure 14 Ground signatures of optimized geometries as a function of lift coefficient.

Figure 15 shows a comparison of the drag polar for all three aircraft enlarged near the cruise lift coefficient. Both MOD144 and MOD466 actually show a slight gain in aerodynamic efficiency in comparison to the reference OPT5 aircraft. The drag of MOD446 is reduced by only about 1 count while MOD144 shows a 2 to 3 count reduction in drag at the cruise lift coefficient.

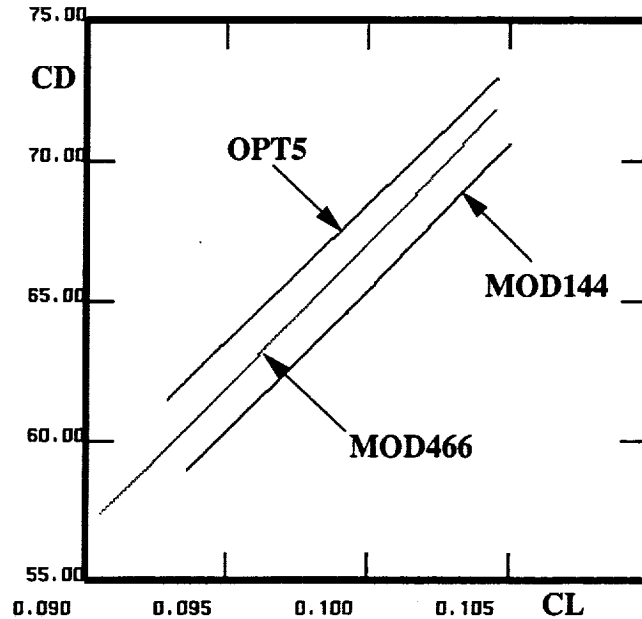
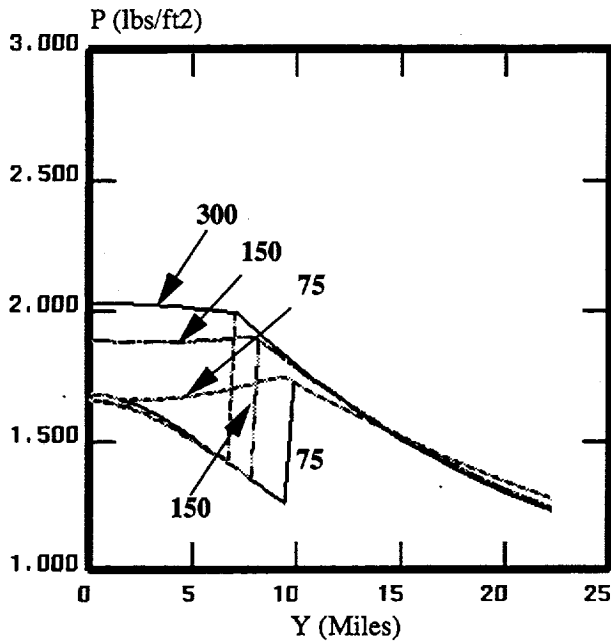
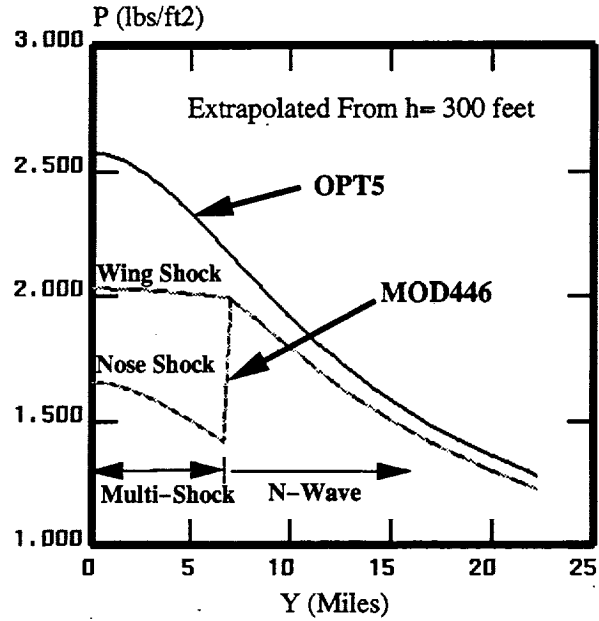


Figure 15 Comparison of drag polars near cruise lift for OPT5 and optimized geometries.

Figure 16 shows the lateral extent of the ground sonic boom carpet for MOD446. Figure 16a shows the changes that occur as a function of extrapolation distance. Overpressure in lbs/ft² is plotted versus lateral distance in miles. For each extrapolation distance, nose shock and maximum overpressure are plotted. Inboard of the jump in overpressure, the signature is comprised of two shocks (i.e. multi-shock). Outboard of the discontinuity, the signature has coalesced into an N-wave, indicative of the single shock overpressure. At an extrapolation distance of 75 feet, a multi-shock signature is maintained out to a lateral distance of almost 10 miles. Beyond 10 miles, the signature becomes an N-wave. The maximum overpressure extrapolated from 75 feet is only about 1.75 lbs/ft² for the entire ground footprint. As the extrapolation distance increases, lateral coalescence into an N-wave occurs closer to the ground track and results in overall higher ground overpressures. Figure 16b shows a comparison of the lateral behavior of the reference OPT5 ground carpet with that of MOD446 using an extrapolation distance of 300 feet. In terms of nose shock overpressure or maximum ground overpressure the sonic boom carpet has been significantly decreased for the MOD446 wing-body configuration.



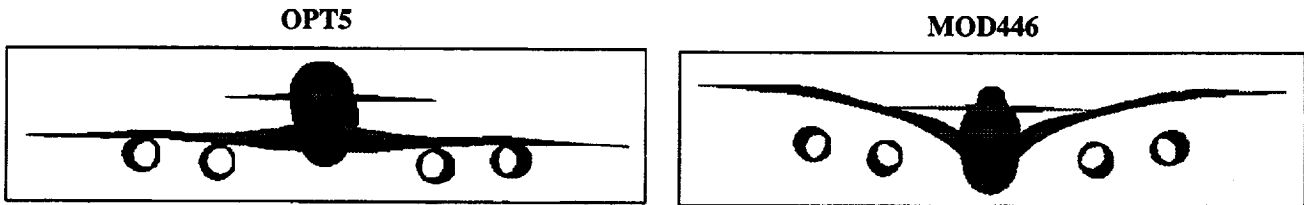
(a) MOD446



(b) OPT5 vs. MOD446

Figure 16 Lateral propagation of sonic boom carpet.

Nacelle Effects



The effects of nacelles were not included in this preliminary design study except by post design analysis. The MOD446 was analyzed with an ad hoc vertical geometric orientation of the original OPT5 nacelles. Figure 17 compares an analysis of the near-field pressure signatures of the MOD446 configuration with and without nacelles. The effect of the nacelles is clearly indicated in the pressure signatures 75 feet below the aircraft. In addition, at 75 feet below the aircraft, both configurations show the nose shock being significantly stronger than the wing shock. In both nacelle-off and nacelle-on configurations, as the distance below the aircraft increases, the relative strength of the nose shock and wing shock become nearly the same pressure level. For nacelles-off, the nose shock maintains slightly higher pressures than the wing shock for all distances plotted below the aircraft. Figure 18 shows the ground signatures computed with/without the nacelles for the MOD446 configuration. The ground signatures of the nacelle-off configuration does not coalesce into an N-wave for all the extrapolation distances. On the other hand, with the nacelles on, the wing and nacelle shocks coalesce to form a single shock with higher pressures in comparison to the nose shock. Hence, the nacelles on ground signature eventually coalesces into an N-wave. If the nose shock has a significantly higher pressure level than the wing shock, the signature will not coalesce because the shock inclination of the nose shock will be greater than the wing shock.

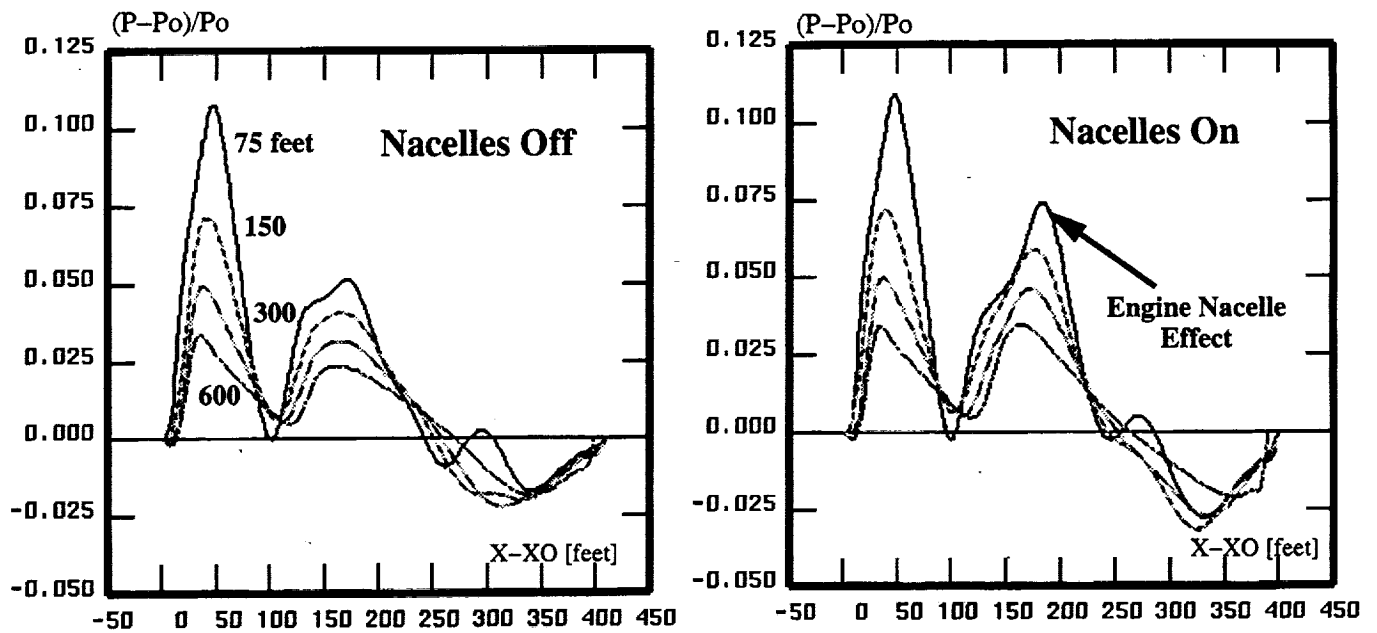


Figure 17 Near-field pressure signatures for MOD446 with/without nacelles.

Hence, this preliminary study of the effect of nacelles points to the importance of proper nacelle integration, in particular, when trying to design a multi-shock signature. For the reference OPT5 configuration (figures 2 and 3), the only effect of the nacelles was to slightly increase the shock overpressure due to its N-wave character. In the future, two possibilities exist. One, to overdesign the wing-body knowing the adverse effect of the nacelles, or two, include the nacelles in the design optimization process. Whether the nacelles can be practically included in the design process will be the focus of a future study. The essential difficulty is that the presence of the nacelles causes grid generation difficulties and increase the computational time by a factor of two to three.

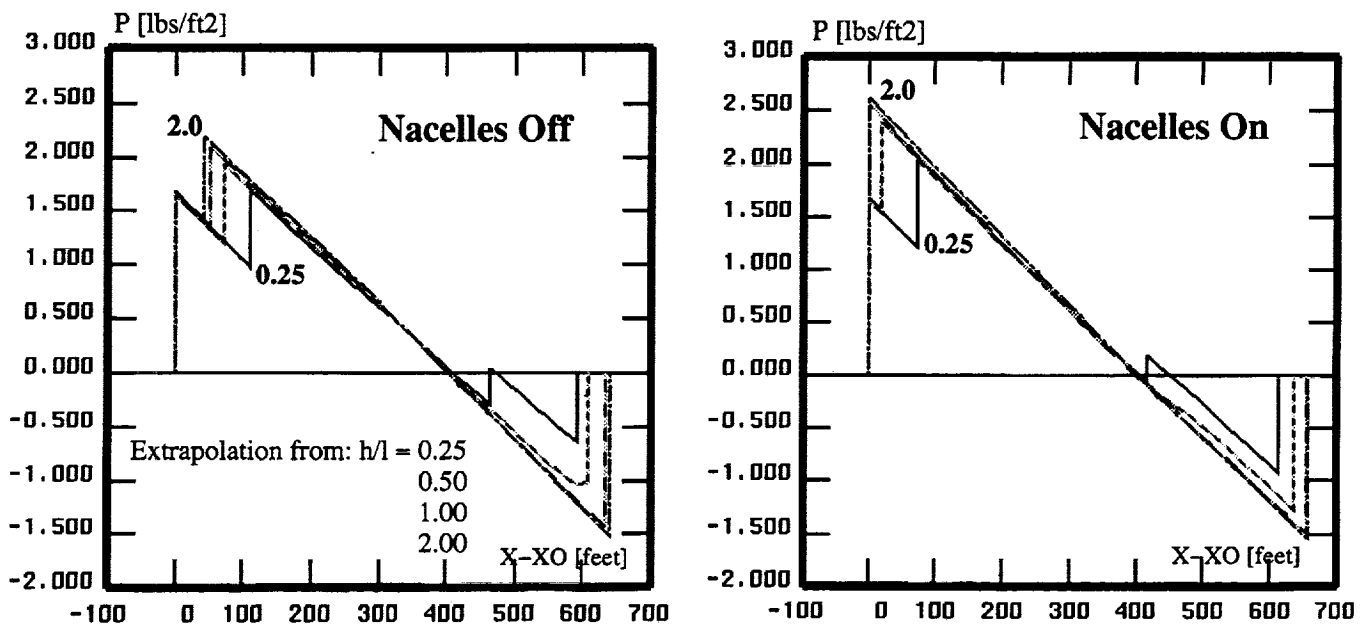


Figure 18 Ground pressure signatures for MOD446 with/without nacelles.

Summary of Optimized Results

Table 1 lists a summary of the fine grid analyses of the ground sonic boom overpressures for the OPT5 reference aircraft, the MOD144, and the MOD466 configurations. The OPT5 and the MOD466 were also analyzed with nacelles. The overpressures are also listed as a function of extrapolation distance. In addition, the lift and drag coefficients (not a function of extrapolation distance) are also listed along with the angles of attack that were used for each analysis. If the signature exhibit a multi-shock pattern, both overpressures are listed. For N-waves, a single overpressure magnitude in lbs/ft² is indicated. The MOD446 wing-body configuration indicates a low boom of 1.68/1.67 lbs/ft² at an extrapolation distance of 75 feet or an h/l = 0.25. This distance corresponds to the design point and the target low boom was indeed achieved. At greater extrapolation distances, the nose shock overpressure is relatively invariant but the wing shock increases in strength due to the increasing tendency towards coalescence as the extrapolation distance increases. The increase in wing overpressure with each doubling of the extrapolation distance is noticeably diminishing, indicating convergence of the ground pressure signature. The MOD446 wing-body configuration indicates about a 35% reduction in nose shock overpressure and about a 15% reduction in maximum overpressure.

Also shown in Table 1 is the effect on the ground signature in the presence of nacelles. The reference OPT5 configuration overpressure shows an increase of 0.18 lbs/ft² at the extrapolation distance of 600 feet or an h/l = 2.0. The effect of nacelles on the MOD466 configuration is to cause coalescence of the multi-shock signature into an N-wave at extrapolation distances greater than 300 feet or h/l = 1.0. With nacelles, the MOD446 configuration shows a reduction of only about 6% at the 600 foot extrapolation distance.

The large sensitivity in ground signature characteristics with extrapolation distance indicates that the methodology for atmospheric extrapolation should be given further scrutiny to judge its accuracy relative to aircraft proximity.

TABLE 1: SUMMARY OF SONIC BOOM AND AERODYNAMICS

h (extrapolation feet)	75 P (lbs/ft ²)	150 P (lbs/ft ²)	300 P (lbs/ft ²)	600 P (lbs/ft ²)		CL	CD	Alpha
Configuration								
OPT5 W/B	2.49	2.52	2.55	2.60		0.105	.0073	2.0
OPT5 W/B/N	2.55	2.66	2.73	2.78		0.112	.0080	2.0
MOD144 W/B	1.95/1.95	2.24	2.41	2.41		0.105	.0071	2.4
MOD144 W/B/N	—	—	—	—		—	—	—
MOD466 W/B	1.68/1.67	1.64/1.92	1.64/2.08	1.66/2.19		0.105	.0072	2.5
MOD466 W/B/N	1.68/2.05	1.64/2.38	2.55	2.59		0.110	.0081	2.5

Note: Two Numbers: Multi-Shock Signature
Single Number: N-Wave

COMPARISON OF EXTRAPOLATION METHODOLOGIES

All of the preceding optimizations and analyses were based on the Thomas atmospheric extrapolation method to obtain the ground sonic boom signatures. A more recently developed methodology contained within the MDBOOM code has been identified by NASA as a possible improvement to the extrapolation methodology. MDBOOM was originally developed by K. Plotkin of Wyle Laboratories (see Ref. 5) and updated or modified by J. Morgenstern of McDonnell Douglas Aerospace. MDBOOM, unlike the Thomas code, uses near-field data on a cylinder of constant radius to obtain extrapolated ground signatures. The Thomas ANET code uses a single two-dimensional near-field signature as input.

Version 2.3 of MDBOOM was preliminarily exercised on some of the near-field CFD flow field data previously described in this paper. Figure 19 shows some MDBOOM ground signatures for both the reference OPT5 and the MOD446 wing-body configurations extrapolated from three cylinders with radii of 75, 150, and 300 feet. For the reference OPT5 configuration, an N-wave results similar to the Thomas prediction. The nose overpressure varies from 2.71 to 2.78 lbs/ft². Unlike the Thomas code where the pressure increases with extrapolation distance, the MDBOOM results indicate no consistent trend. The MDBOOM nose overpressures are higher than those predicted by the Thomas ANET method by about .1 to .2 lbs/ft² (see Fig. 3d). Figure 19b shows a similar plot of MDBOOM ground signatures for the MOD446 wing-body configuration. MDBOOM results show significantly less sensitivity to extrapolation distance in comparison to the Thomas code (Fig. 11).

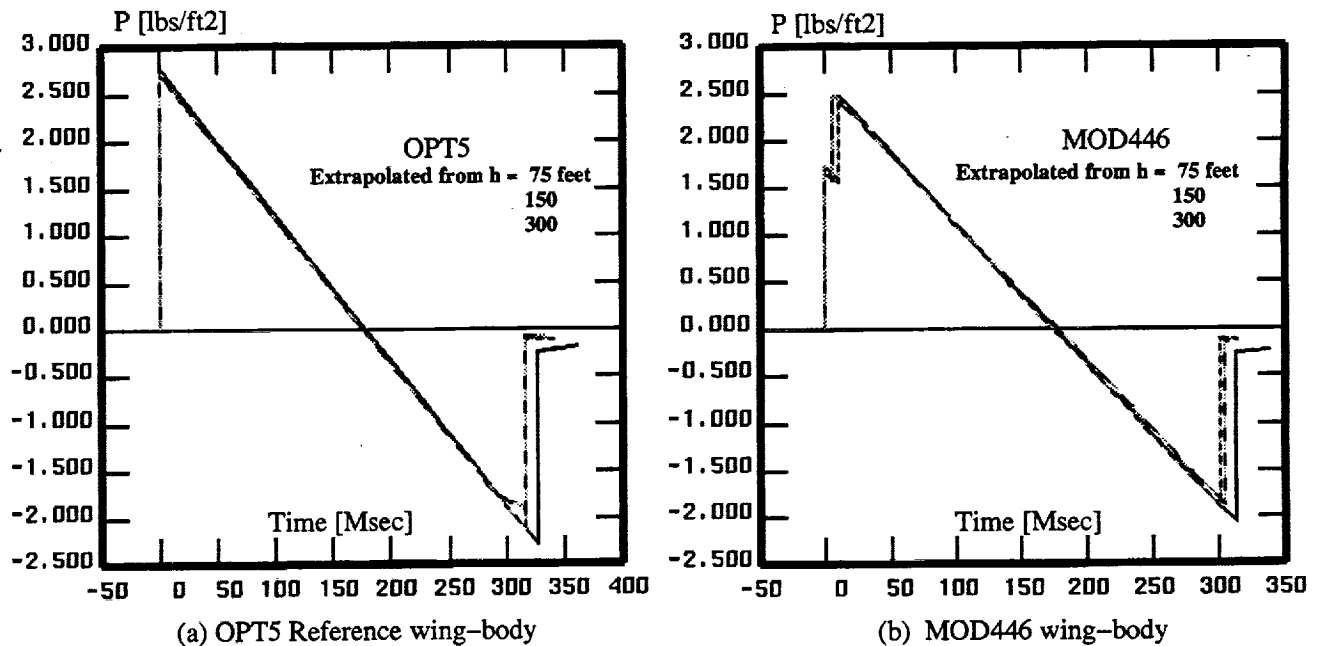


Figure 19 MDBOOM ground signature predictions.

Figure 20 shows a further comparison between the ground signatures predicted by MDBOOM and the ANET codes. These signatures were all extrapolated using a distance of 300 feet. Figure 20a shows a comparison for the reference OPT5 wing-body configuration. The MDBOOM nose overpressure is higher than that predicted by the Thomas ANET method. Figure 20b shows a similar comparison for the MOD446 wing-body configuration. MDBOOM predicts higher pressures and more coalescence than the Thomas ANET code. A 10% reduction in maximum sonic boom overpressure is predicted by MDBOOM for the MOD446 wing-body configuration in comparison to the 15% reduction predicted by the Thomas method.

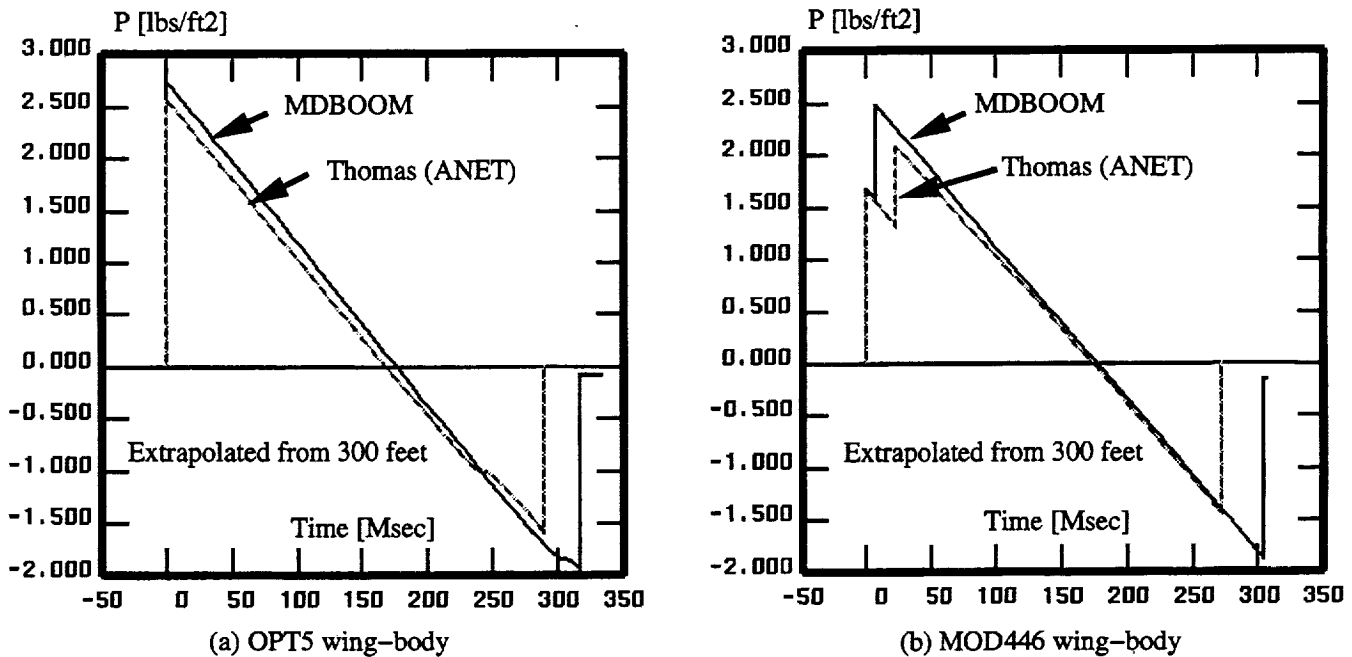


Figure 20 Comparison of MDBOOM and Thomas ANET predictions of ground pressure signatures.

CONCLUSIONS

The figure below lists the conclusions and lessons learned in this preliminary design study aimed at reducing the ground sonic boom of the Douglas OPT5 configuration.

Preliminary Conclusions & Future Work

- Sonic Boom of OPT5 Douglas Wing–Body Configuration Reduced More Than 15% by:
 - Wing Dihedral
 - Wing Thickness Distribution & Airfoil Shape (LE)
 - Fuselage Camber
- Aerodynamic Efficiency Retained If Not Slightly Improved
- Two Ways to Reduce Boom:
 - 1) Reduce Shock Strength
 - 2) Prevent Coalescence
- Preventing Coalescence will Depend on Accuracy of Atmospheric Propagation Method
 - highly sensitive to Lift Coefficient
- Thomas ANET code:
 - results highly dependent on extrapolation distance
- MDBOOM:
 - less dependency on extrapolation distance
 - more difficult to use and implement in design process
 - predicts higher pressures and more coalescence
 - reduced boom reduction from 15 to 10%
- Future Improvements:
 - Carry out design optimization at $h/l > 0.25$ (e.g. 0.50 or 1.0) or
 - Replace Thomas ANET extrapolation with MDBOOM
- Future Studies:
 - Compare Atmospheric Propagation Methods on These Configurations
 - Thomas, MDBOOM, & others

REFERENCES

1. Siclari, M.J. and Fouladi, K., "A CFD Study of Component Configuration Effects on the Sonic Boom of Several High-Speed Civil Transport Concepts," presented at the NASA HSR Sonic Boom Workshop, pp 227-299, Volume II, held at Ames Research Center, Moffett Field, CA, May 12-14, 1993.
2. Thomas, C.L., "Extrapolation of Sonic Boom Pressure Signatures by the Waveform Parameter Method". NASA TN D-6832, 1972.
3. Siclari, M.J., "The Analysis and Design of Low Boom Configurations Using CFD and Numerical Optimization Techniques," presented at the NASA HSR Sonic Boom Workshop, 1994.
4. Gill, P.E., Murray, W., Saunders, M.A., and Wright, M.H., "User's Guide for NPSOL (Version 4.0): A Fortran Package for Nonlinear Programming," Technical Report SOL 86-2, January 1986, Department of Operations Research, Stanford University.
5. Plotkin, K.J., "Calculation of Sonic Boom from Numerical Flowfield Solutions: MDBOOM Version 2.2", Wyle Research Report WR 92-14, July 1992

POTENTIAL FOR SONIC BOOM REDUCTION OF THE 2.4-H5085 ARROW WING HSCT

John M. Morgenstern
McDonnell Douglas Aerospace
Long Beach, CA

INTRODUCTION

Preliminary human acceptability studies of sonic booms indicate that supersonic flight is unlikely to be acceptable even at noise levels significantly below 1994 low boom designs (reference 1, p. 288). Further, these low boom designs represent considerable changes to baseline configurations, and changes translate into additional effort and uncertain structural weight penalties that may provide no annoyance benefit, increasing the risk of including low boom technology. Since over land sonic boom designs were so risky (and yet the acceptability studies highlight how annoying sonic booms are), boom softening studies were undertaken to reduce the boom of baseline configurations using minor modifications that would not significantly change the designs. The goal of this work is to reduce boom levels over water. Even though Concorde over water boom has not been found to have any adverse environmental impact, boom levels for baseline HSCT designs are 50% higher in overpressure than the Concorde (due to a doubling in configuration weight with only a 50% increase in length).

The objective of FY95 softening studies was to determine the potential for sonic boom softening of Technology Concept baseline candidates to determine if there is a preference from boom softening technology that needs to be considered in candidate selection. Brainstorming on ways to reduce the sonic boom without major configuration changes lead to the following list of options to investigate:

BOOM SOFTENING OPTIONS

Small Modifications

- Different trim/tail loading

- Wing dihedral

- Fuselage camber

- Outboard wing sweep (also in planform study)

- Increased wing area

Moderate Modifications

- Planform variations from planform study

- Canard/3-surface

- Fuselage length

- Shaping of front shock using area/lift distribution

With many trade studies to perform, a method was needed to rapidly design and optimize many different configuration variations. In order to make fair comparisons, configurations would need to be brought to the same level of optimization and refinement as the baseline. For example, re-area ruling to insure that both baseline and softened designs have an optimized drag increment, and increasing dihedral wing t/c in the z-direction by 1/cosine of the dihedral angle to insure that the thickness of the rotated wing remains the same. Rapid design optimization and sonic boom assessments were done by integrating the latest modified-linear theory sonic boom prediction improvements, including 3-D lift and volume integration and Euler CFD nacelle interference lift, into a highly automated method. The automated method links linear theory lift, volume, and trim optimization to produce final aerodynamic and sonic boom levels from simple inputs such as sweep, t/c, wing area, and fuselage area constraints. This method has been validated and calibrated as the standard design tool at McDonnell Douglas. The efficiency of this method allows through refinement of softening trades.

Planforms A, B, and J (from HSR's Technology Integration Planform Study, figure 1) were analyzed for sonic boom with the results summarized in table 1 below.

PLANFORM	P _{MAX}	PL _{dB}	MTOGW (lb.)
A	2.9	107.9	754,900
B	3.1	108.8	795,800
J	2.9	108.1	720,500

Table 1

Since the Arrow wing Planform A had the lowest noise, it's planform was kept as the baseline for boom softening trades.

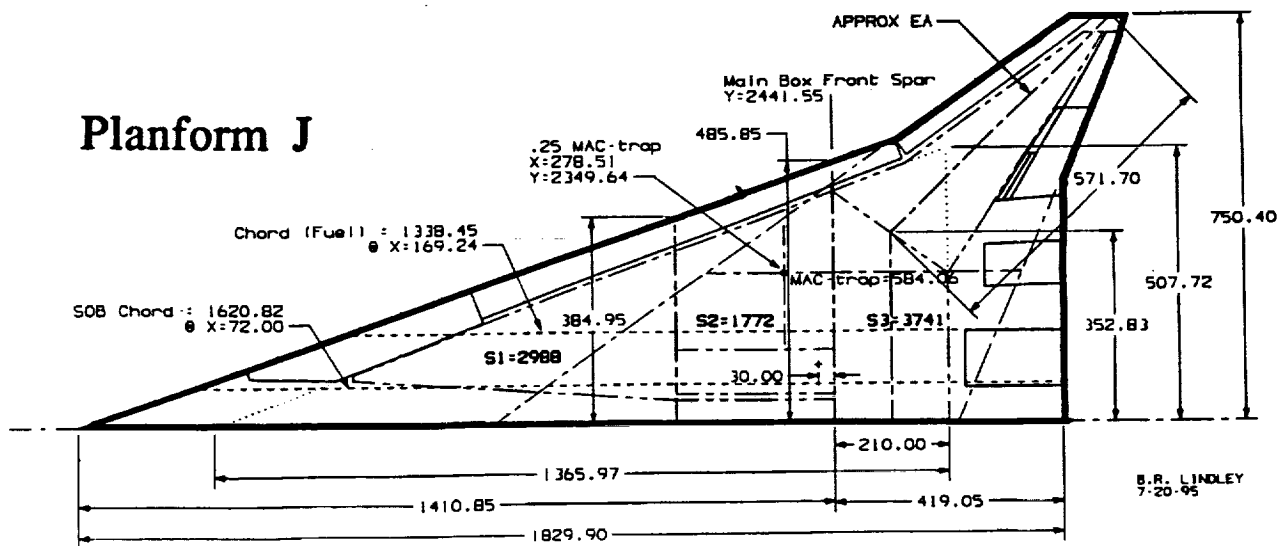
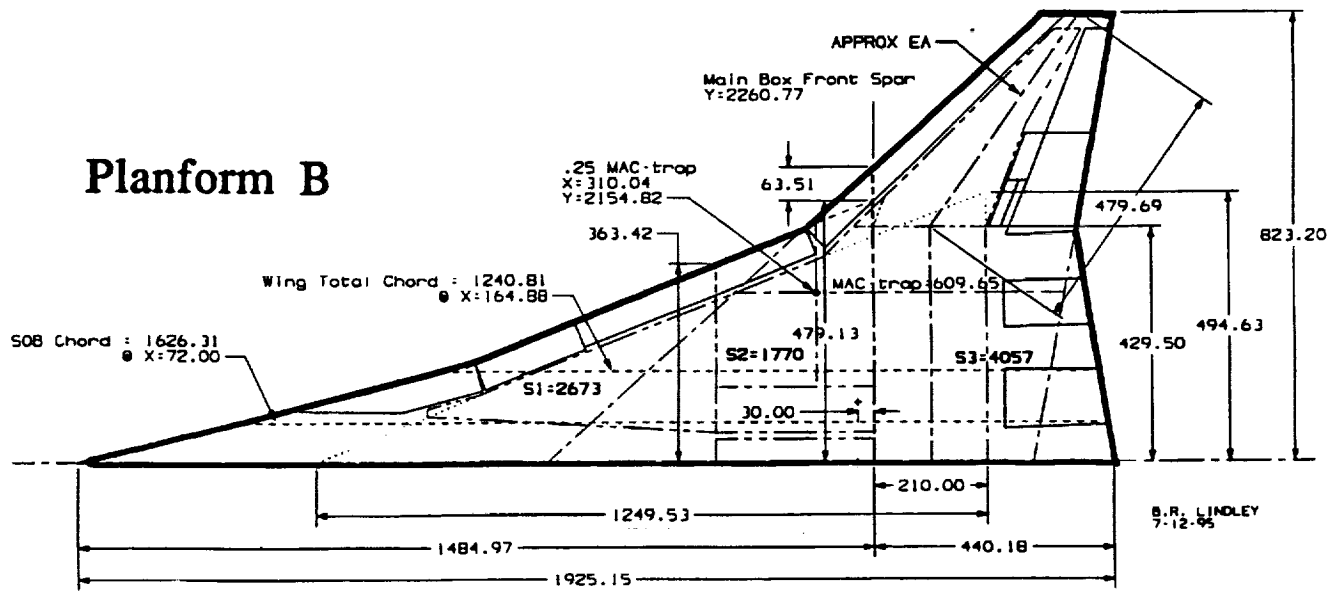
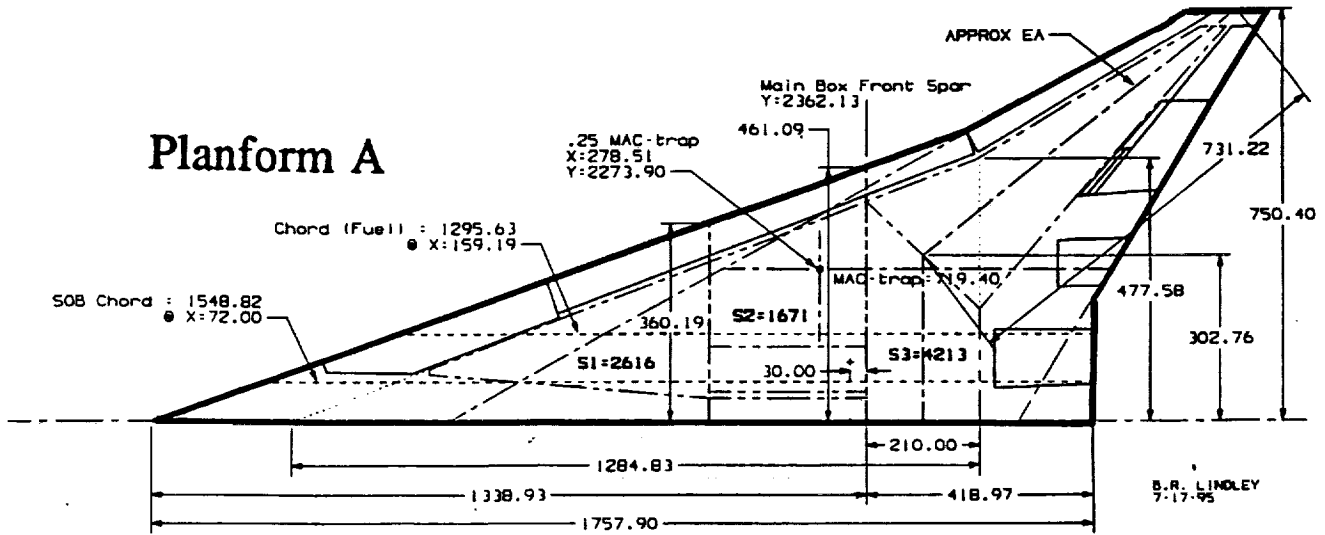


Figure 1

After analyzing the proposed boom softening configuration changes the following options were found to be effective at reducing boom and were selected for integration into a final softened configuration: shaping, dihedral, wing area increase, and alternate trimming.

To begin the boom softening process, the 'F' function [F(x)] of the baseline, figure 2, was examined to see where improvements could be made. For the initial "No Shaping" case below, a large nacelle shock can be seen at 180 feet. An update in the nacelle pylon weight equation allowed the nacelles to be moved aft to reduce the shock they generate with less of a weight penalty. This substantially reduces the nacelle shock as seen in the "Nacelles Aft" F(x) data. Additionally, the nacelle shaping was employed by reducing the cowl lip angle to 3 degrees, further reducing the nacelle shock strength and lowering drag 1.4 counts. Both of the changes were found to improve overall performance in addition to sonic boom, so they were incorporated as a baseline update and used as a starting point for the following trades. Boom changes in psf are shown in table 2 and in figure 3.

Phi (degrees)	56°	45°	30°	15°	0°
No Shaping (psf)	1.20	1.72	2.29	2.71	3.00
Nacelle Aft	1.16	1.65	2.24	2.69	2.89
Nacelles Shaped (baseline)	1.16	1.65	2.23	2.64	2.83

Table 2

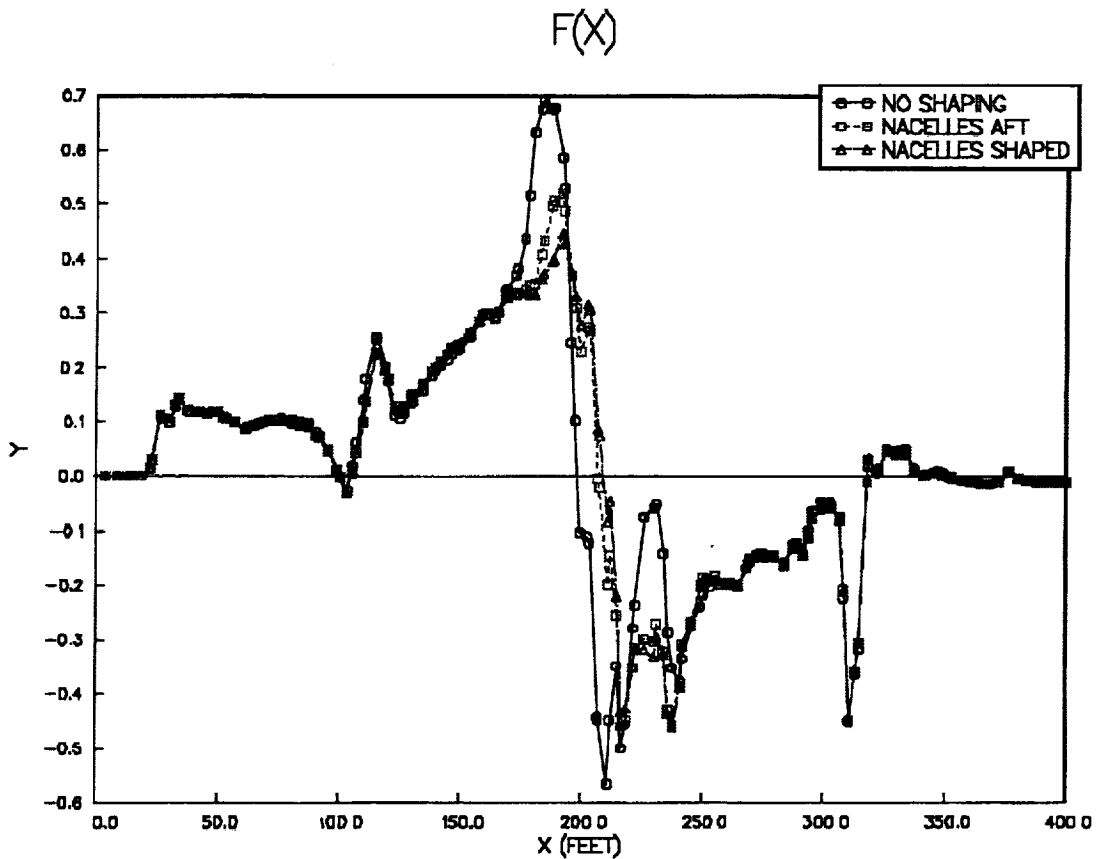


Figure 2

Sonic Boom Carpet - Shaping Trade

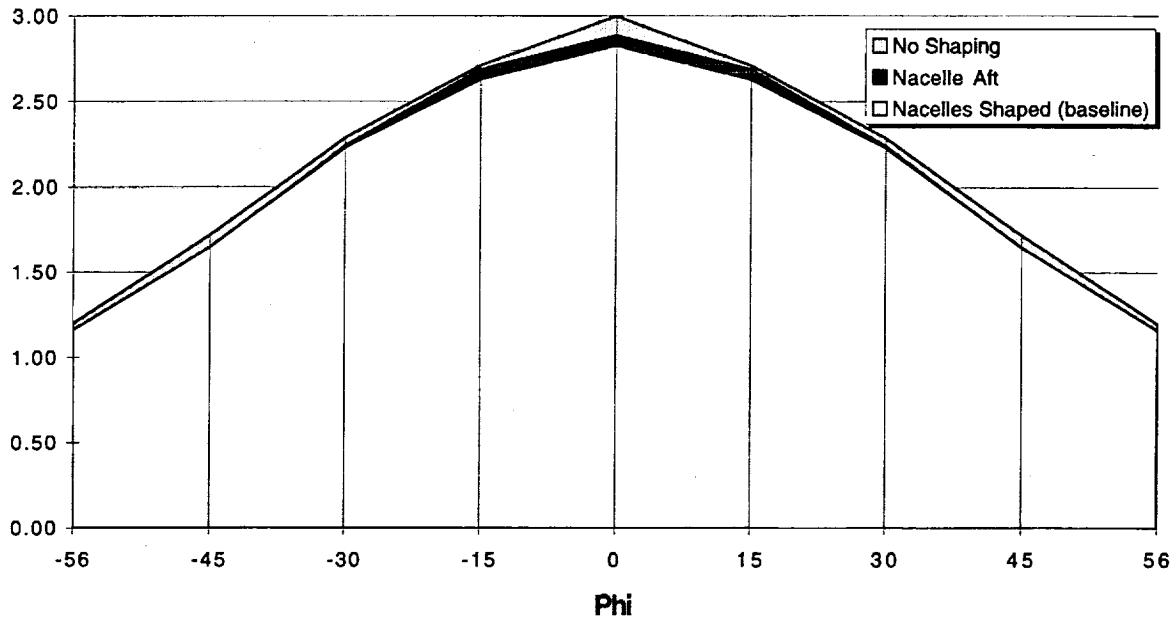


Figure 3

8/29/95

Dihedral had shown potential for reducing the nacelle and wing shock strength. However, the improved starting point from shaping did not yield the boom reductions with dihedral seen before shaping was applied. The dihedral numbers describe, in order, the average angle from the wing root to the inboard engine span station, inboard engine to the outboard engine span station, and outboard engine to wing tip. (Note that dihedral wing thickness and lift were maintained, requiring a slight increase in span and lift in the dihedral plane.) Figure 4 shows a little improvement was gained undertrack and almost nothing off-track with these or other dihedral options, so the baseline dihedral was retained.

Phi	56°	45°	30°	15°	0°
5°,5°,-2°(baseline)	1.16	1.65	2.23	2.64	2.83
5°,10°,-2°	1.14	1.63	2.25	2.62	2.80
5°,15°,-2°	1.13	1.64	2.24	2.61	2.72

Table 3

Boom Carpet Chart 1

Sonic Boom Carpet - Dihedral Trade

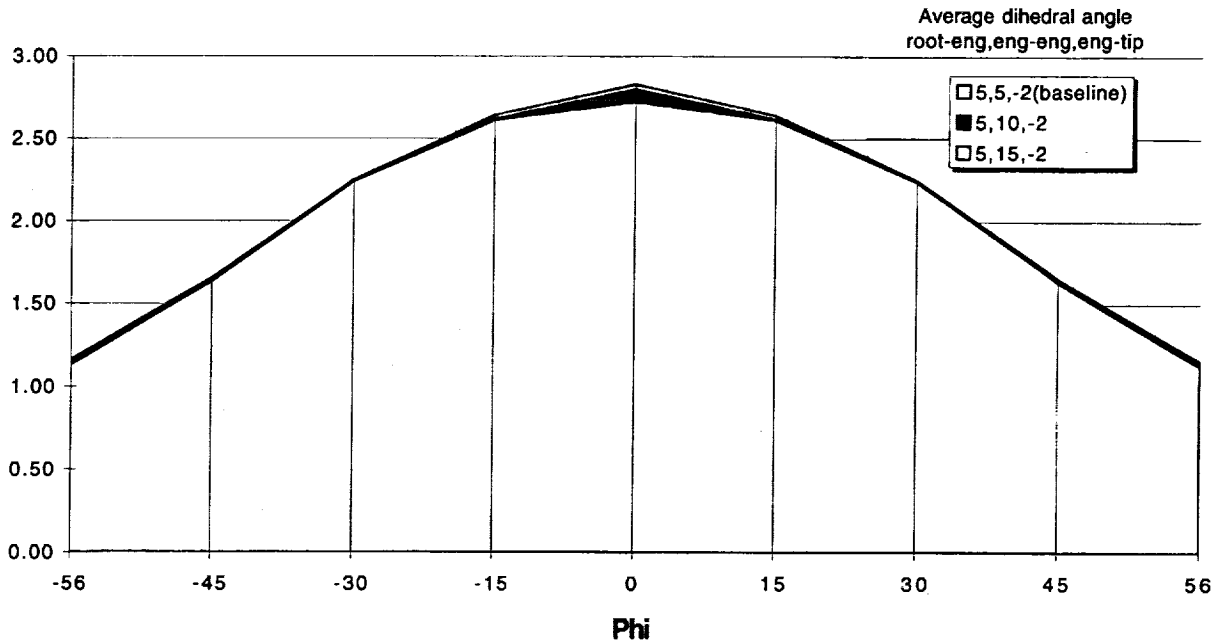


Figure 4

8/29/95

The poor results with dihedral, relative to other studies, motivated further investigation. It was found that while dihedral stretched out the lift distribution reducing lift-per-foot and lift shock strength (figure 5), holding t/c actually increased shock strength due to area (as seen by the F function due to area) shown in figure 6 lessening the softening due to dihedral. Additionally, off-track lift distribution actually became more compressed due to dihedral.

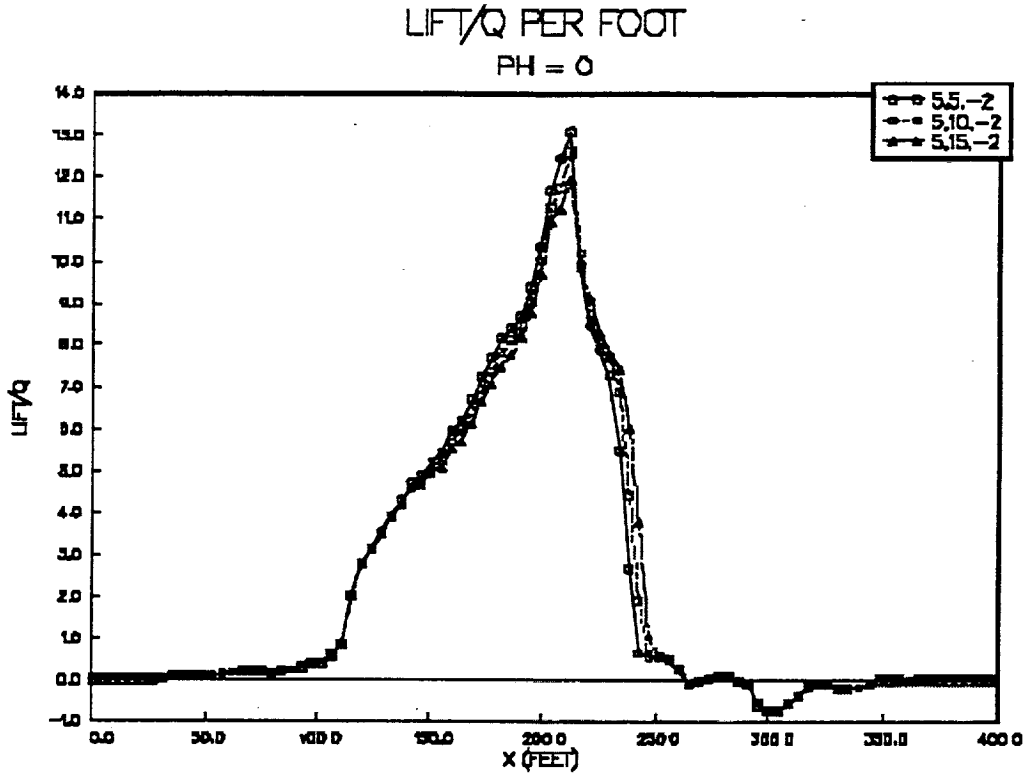
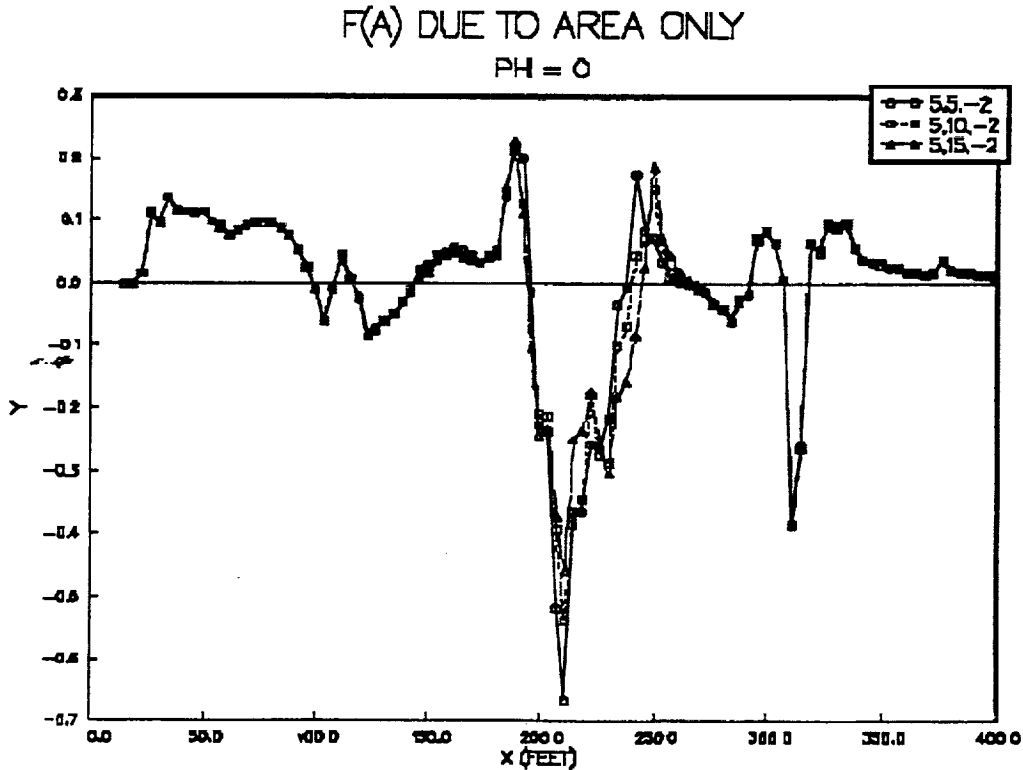


Figure 5 above, and 6 below



Additionally, off-track distribution actually became more compressed due to dihedral (figure 7).

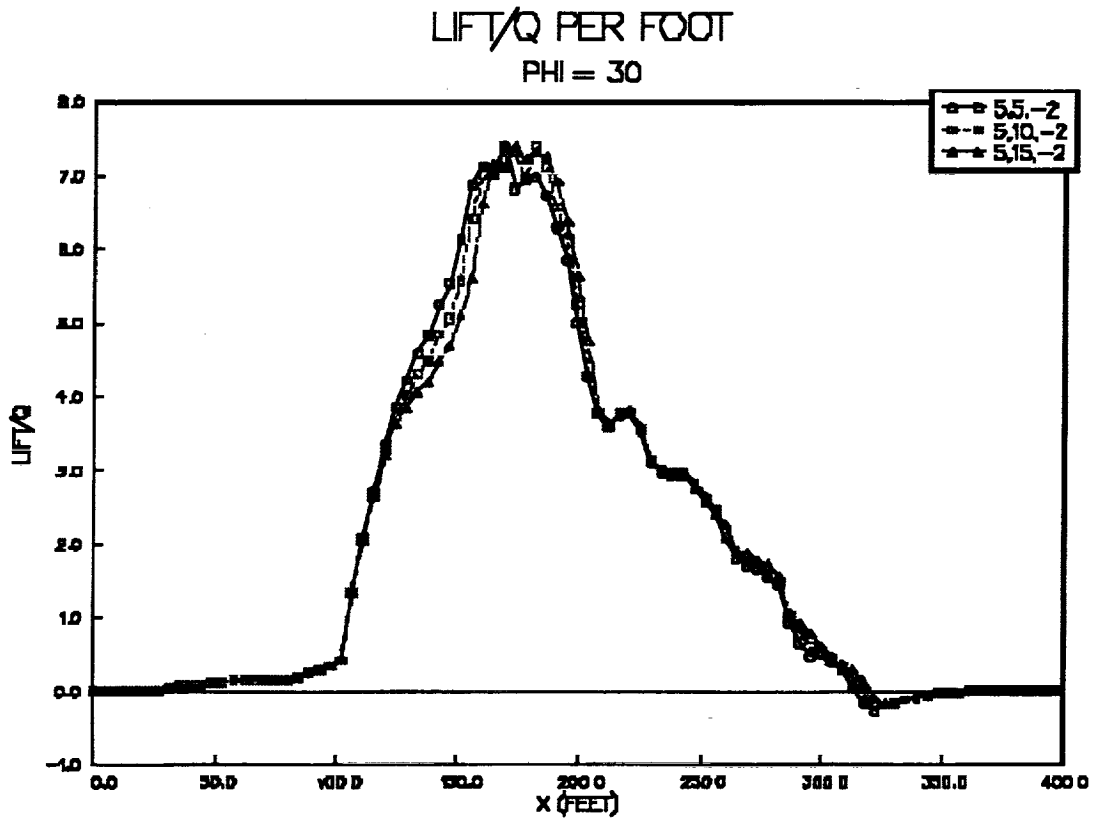


Figure 7

Wing area changes also produced no improvement in sonic boom, figure 8, for this Arrow Wing design, so the integrated configuration wing area was sized for best performance. Increasing the wing area did not result in a lower cruise CL; rather, mission performance optimization has the airplane fly higher to maintain maximum L/D. Further, this fuselage's area constraints seemed to make unfavorable area changes with larger wing areas, especially at 8,950 sq. ft. Multivariable optimization of fuselage area and camber coupled with increases in wing area may find a more favorable trend for increasing wing area.

Phi	56°	45°	30°	15°	0°
9500 sq. ft.	1.18	1.66	2.24	2.67	2.86
8950 sq. ft.	1.17	1.65	2.10	2.64	2.88
8500 sq. ft.	1.16	1.65	2.23	2.64	2.83

Table 4

Boom Carpets Chart 2

Sonic Boom Carpet - Wing Area Trade

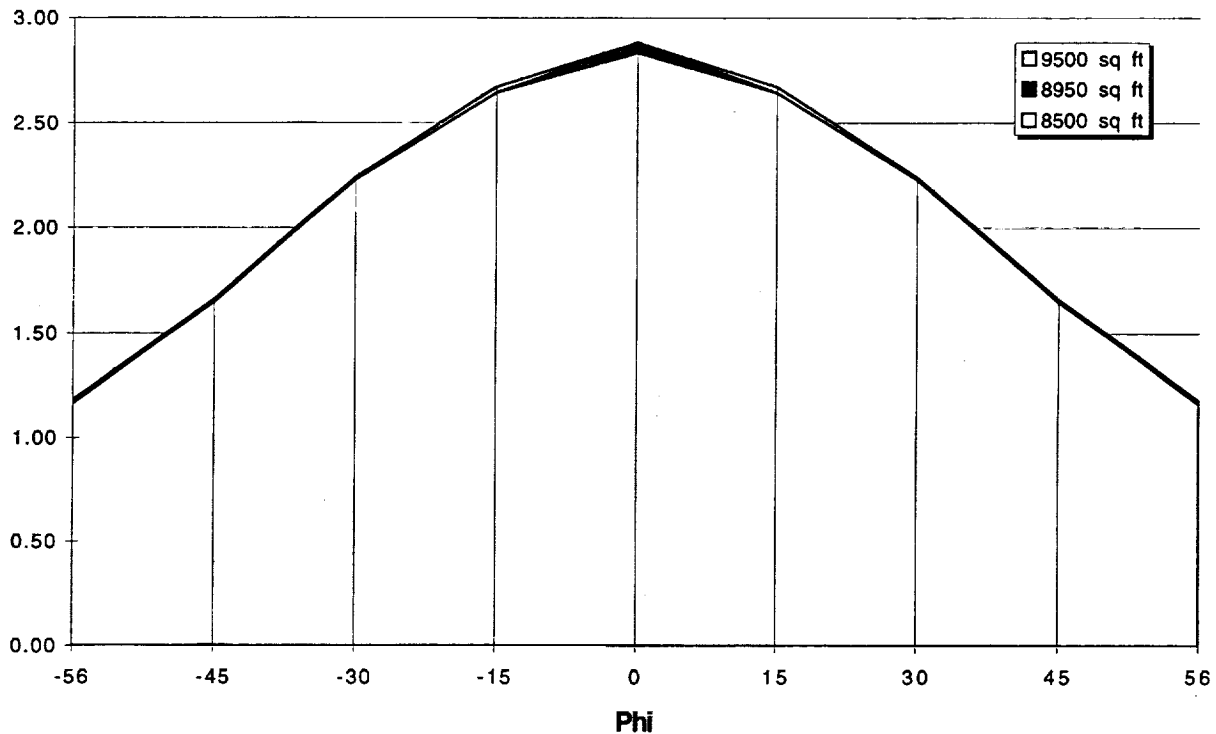


Figure 8

8/29/95

Alternate trimming proved beneficial at reducing boom off-track as well as maintaining its improvement in combination with other options, figure 9. In contrast with dihedral, the canard seemed especially effective at reducing boom off-track where the wing shock is weaker. The 3-surface seemed to just further spread out the lift and allow a slightly higher load on the canard.

Phi	56°	45°	30°	15°	0°
Baseline	1.16	1.65	2.23	2.64	2.83
Canard	1.14	1.59	2.13	2.56	2.78
3-Surface	1.11	1.54	2.06	2.46	2.64

Table 5

Boom Carpet Chart 3

Sonic Boom Carpet - Alternate Trim Trade

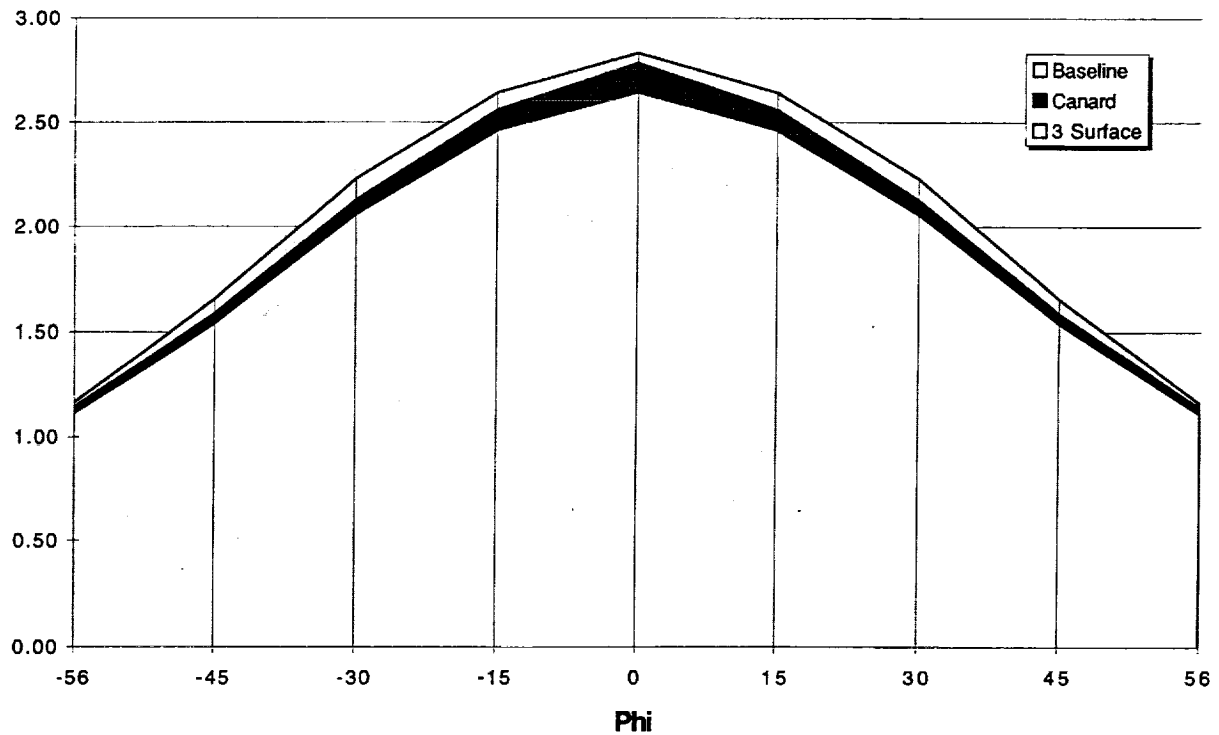


Figure 9

8/29/95

The F function below (figure 10) shows how the canard adds a spike on the front of the signature and shifts some of the wing lift from the apex to the outboard wing. Both of these changes help to reduce the front shock strength. The 3-surface F function illustrates how the extra lift from the horizontal tail has reduced the lift on the wing, further reducing the front shock and angle-of-attack, and spreading the signature out.

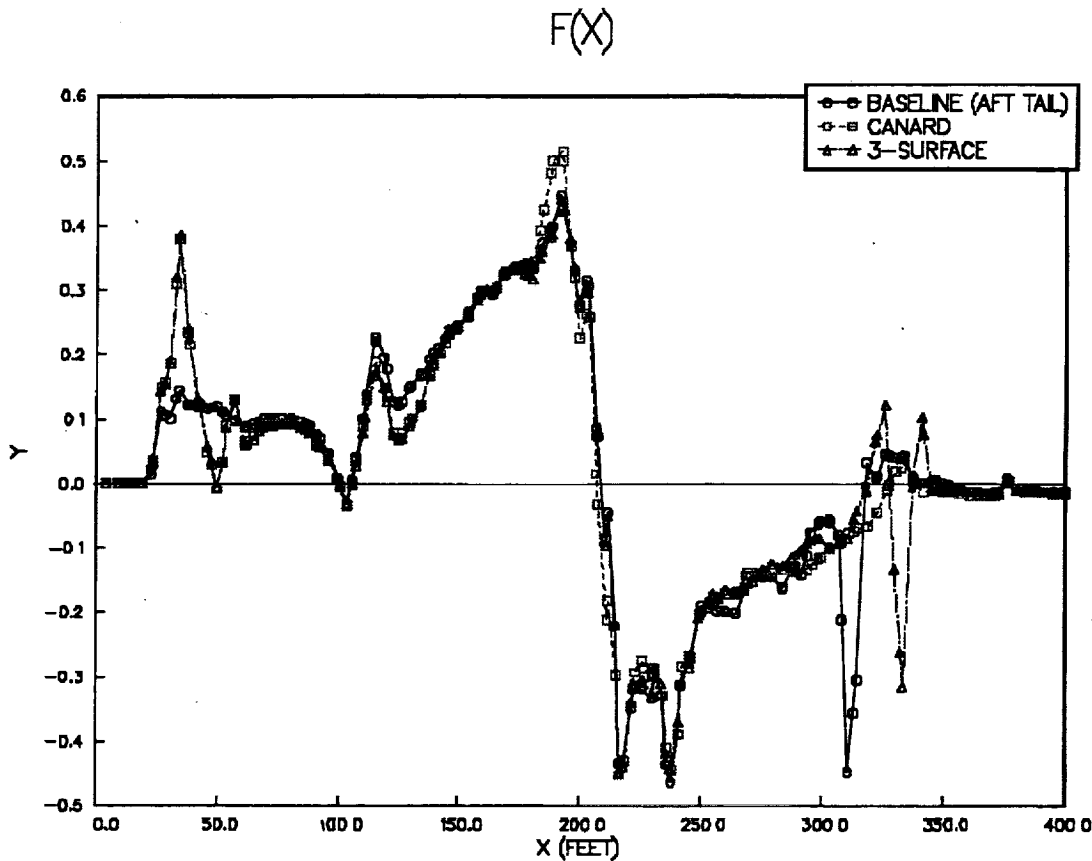


Figure 10

The final softened configuration integrates shaping and 3-surface trimming yielding an 8% reduction from the baseline in the final, sized numbers shown below. Boom levels are listed for the whole sonic boom carpet (about 47 miles wide cutoff to cutoff) from near cutoff at phi of 56 to undertrack at phi of 0.

SONIC BOOM

Phi (degrees)	56°	45°	30°	15°	0°
Baseline Plan A (psf)	1.2	1.7	2.2	2.6	2.8
Final Softened	1.1	1.5	2.0	2.4	2.6

Table 6

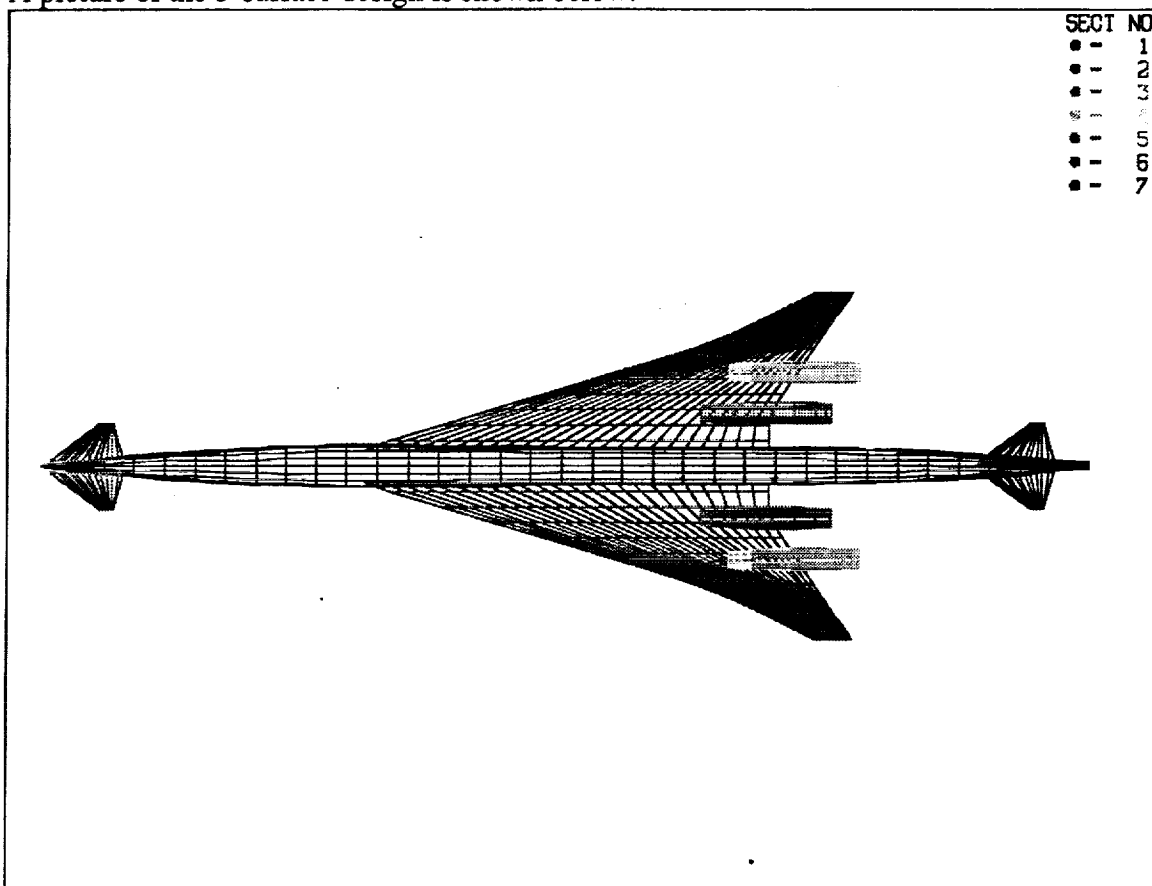
The performance of the softened configuration is very similar to the baseline. The major change with the switch to a 3-surface trim concept carries a little load at the nose and tail. Trim deflections were optimized for maximum trimmed L/D but the wing twist and camber were not changed to account for the canard downwash. The 3-surface trimmed L/D at the Mach 2.4 cruise condition was just 0.5% lower resulting in about 80% of the 7,000 lb. MTOGW increase shown below.

PERFORMANCE

	Baseline Plan A	Final Softened
MTOGW (lb.)	749,000	756,000
OEW	323,000	323,500
Δ L/D	base	-0.5%

Table 7

A picture of the 3-surface design is shown below:



SUMMARY

- **Shaping and alternate trimming were used to reduce the 2.4-H5085 (Planform A) Arrow Wing baseline sonic boom overpressures 10% across the entire boom carpet.**
- **Performance analysis of the softened design resulted in less than a 1% increase in MTOGW.**
- **2.6 psf overpressure is still much higher than the 2.0 psf Concorde. To go much lower is likely to require multiple front shock signatures.**

REFERENCES

1. Darden, Christine M., "Progress in Sonic-Boom Understanding: Lessons Learned and Next Steps." NASA CDCP-1001, October 1994, pp. 269-292.

REPORT DOCUMENTATION PAGE			Form Approved OMB No. 0704-0188	
Public reporting burden for this collection of information is estimated to average 1 hour per response, including the time for reviewing instructions, searching existing data sources, gathering and maintaining the data needed, and completing and reviewing the collection of information. Send comments regarding this burden estimate or any other aspect of this collection of information, including suggestions for reducing this burden, to Washington Headquarters Services, Directorate for Information Operations and Reports, 1215 Jefferson Davis Highway, Suite 1204, Arlington, VA 22202-4302, and to the Office of Management and Budget, Paperwork Reduction Project (0704-0188), Washington, DC 20503.				
1. AGENCY USE ONLY (Leave blank)	2. REPORT DATE December 1999	3. REPORT TYPE AND DATES COVERED Conference Publication		
4. TITLE AND SUBTITLE 1995 NASA High-Speed Research Program Sonic Boom Workshop <i>Volume II—Configuration Design, Analysis, and Testing</i>			5. FUNDING NUMBERS WU 537-07-21-21	
6. AUTHOR(S) Daniel G. Baize, Editor				
7. PERFORMING ORGANIZATION NAME(S) AND ADDRESS(ES) NASA Langley Research Center Hampton, VA 23681-2199			8. PERFORMING ORGANIZATION REPORT NUMBER L-17573	
9. SPONSORING/MONITORING AGENCY NAME(S) AND ADDRESS(ES) National Aeronautics and Space Administration Washington, DC 20546-0001			10. SPONSORING/MONITORING AGENCY REPORT NUMBER NASA/CP-1999-209520	
11. SUPPLEMENTARY NOTES				
12a. DISTRIBUTION/AVAILABILITY STATEMENT Unclassified—Unlimited Subject Category 02 Distribution: Nonstandard Availability: NASA CASI (301) 621-0390			12b. DISTRIBUTION CODE	
13. ABSTRACT (Maximum 200 words) The High-Speed Research Program and NASA Langley Research Center sponsored the NASA High-Speed Research Program Sonic Boom Workshop on September 12–13, 1995. The workshop was designed to bring together NASA's scientists and engineers and their counterparts in industry, other Government agencies, and academia working together in the sonic boom element of NASA's High-Speed Research Program. Specific objectives of this workshop were to (1) report the progress and status of research in sonic boom propagation, acceptability, and design; (2) promote and disseminate this technology within the appropriate technical communities; (3) help promote synergy among the scientists working in the Program; and (4) identify technology pacing the development of viable reduced-boom High-Speed Civil Transport concepts. The Workshop was organized in four sessions; Sessions I—Sonic Boom Propagation (Theoretical); Session II—Sonic Boom Propagation (Experimental); Session III—Acceptability Studies—Human and Animal; and Session IV—Configuration Design, Analysis, and Testing.				
14. SUBJECT TERMS High-speed research; High-speed civil transport; Sonic boom propagation (theoretical and experimental)			15. NUMBER OF PAGES 187	
			16. PRICE CODE A09	
17. SECURITY CLASSIFICATION OF REPORT Unclassified	18. SECURITY CLASSIFICATION OF THIS PAGE Unclassified	19. SECURITY CLASSIFICATION OF ABSTRACT Unclassified	20. LIMITATION OF ABSTRACT UL	